Consortium for Small-Scale Modelling

Newsletter

February 2004

No. 4

www.cosmo-model.org

Editors: Günther Doms (DWD), Ulrich Schättler (DWD) and Andrea Montani (ARPA-SIM)
Printed at Deutscher Wetterdienst, PO. Box 100465, 63004 Offenbach am Main, Germany

Table of Contents

1 Introduction

This is the fourth Newsletter of the Consortium for Small-Scale Modelling (COSMO). Currently, the Newsletter is prepared once a year in January/February, with the opportunity to add special issues at irregular intervals if required.

The basic purpose of the Newsletter is threefold:

- to review the present state of the model system and its operational application and to give information on recent changes;
- to present the principal events concerning COSMO during the last year and to summarize recent research and development work as well as results from the model verification and diagnostic evaluation;
- to provide the meteorological community and especially all external users of the model system with information on COSMO's activities and with new information on the model system and its current forecast quality.

The present Newsletter is organized as follows. Section 2 gives a general overview of the current organizational structure of the COSMO consortium. The present state of the model system, i.e. the LM-package, is summarized in Section 3, including a short description of the model and its data assimilation system, information on the preprocessor programs to provide initial and boundary conditions, and finally remarks on postprocessing utilities and hints on the available model documentation.

Operational and pre-operational applications of the LM-package at the COSMO meteorological centres are described in Section 4. Information about the recent changes to the model system as well as changes in the model set-up at the meteorological centres are outlined in Section 5. Section 6 gives you an overview of the six COSMO Working Groups and their recent research and development activities.

Section 7 provides short information on the main COSMO meetings and events during the last year. Other activities such as internal visits and guest scientist programs are also included. Finally, some forthcoming events planned for this year are announced.

Recent results from the verification of the operational models, both for surface parameters and for vertical profiles, are summarized in Section 8. This section also includes contributions related to the development of new methodologies for model verification as well as results from the verification of new model components.

Section 9 is devoted to reports on various research topics related to model development and application, including data assimilation, numerics, physics, interpretation, and technical aspects. Finally, all COSMO activities related to the LM-system within international and national projects of the member meteorological services are listed in Section 10. This list will be updated in the forthcoming issues.

The Appendices concern the use of the GRIB binary data format for the output and input analyses and forecast fields. These lists will also be updated, and we hope they will be helpful, especially for new users of the LM and its forecast products.

Information about COSMO and the LM can also be obtained from our web-site ***www.cosmo-model.org*** or the mirror site ***cosmo-model.cscs.ch***. Many thanks to Theodore Andreadis from HNMS for running, updating and supervising the web-sites.

The present organization of the Newsletter may change in future. Please contact the editors for any comments and suggestions as well as proposals for items to be included or excluded in the next issue. The editors recognize that typographical and other errors or inconsistencies may be present. We apologize for this, and your assistance in correcting them will be welcome.

We would also like to encourage all the scientists in the COSMO Working Groups to document their work, e.g. in form of a short progress summary or a longer report, to be included in the next Newsletter. Special thanks to all who provided contributions and graphical material for the present issue:

Marco Arpagaus (MeteoSwiss)
Euripides Avgoustoglou (HNMS)
Michael Baldauf (DWD)
F. Boccanera (ARPA-SIM)
Heinz-Werner Bitzer (AWGeophys)
Davide Cesari (ARPA-SIM)
Ulrich Damrath (DWD)
Pierre Eckert (MeteoSwiss)
Patrizio Emiliani (UGM)
Massimo Ferri (UGM)
Jochen Förstner (DWD)
Thomas Frisius (Univ. Frankfurt)
Alessandro Galliani (UGM)
Almut Gassmann (Univ. Bonn)
Thomas Hanisch (DWD)
Zavisa Janjic (NCEP)
Pirmin Kaufmann (MeteoSwiss)
Stefan Klink (DWD)
Detlev Majewski (DWD)
Chiara Marsigli (ARPA-SIM)
Andrzej Mazur (IMGW)
Malgorzata Mierkiewicz (IMWG)
Guy de Morsier (MeteoSwiss)
Aurelia Müller (DWD)
Fabrizio Nerozzi (ARPA-SIM)
Iannis Papageorgiou (HNMS)
Jan Parfiniewicz (IMGW)
Tiziana Paccagnella (ARPA-SIM)
Paolo Patruno (ARPA-SIM)
Marjorie Perroud (MeteoSwiss)
Ulrich Pflüger (DWD)
Peter Prohl (DWD)
Bodo Ritter (DWD)
Dominique Rouffieux (MeteoSwiss)
Christoph Schraff (DWD)
Francis Schubiger (MeteoSwiss)
Klaus Stephan (DWD)
Jürgen Steppeler (DWD))
Katarzyna Starosta (IMGW)
Jan-Peter Schulz (DWD)
Ermanno Veccia (UGM)
Emanuele Zala (MeteoSwiss)

To run a complex NWP system at a COSMO meteorological centre requires the continuous effort of many people. Thanks to all of them, especially to those implementing new model versions, maintaining the operations, and organizing the data transfer between the centres:

– Michael Gertz and Thomas Hanisch at DWD,
– Jean-Marie Bettems and Emanuele Zala at MeteoSwiss,
– Theodore Andreadis and Euripides Avgoustoglou at HNMS,
– Davide Cesari and Paolo Patruno at ARPA-SIM and
– Jan Parfiniewicz and Marek Lazanowicz at IMGW.

Finally, thanks to all who supported us concerning technical problems during the editorial work. For any comments, suggestions and questions please contact the editors:

Günther Doms
guenther.doms@dwd.de

Ulrich Schättler
ulrich.schaettler@dwd.de

Andrea Montani
andrea.montani@smr.arpa.emr.it

2 Organizational Structure of COSMO

2.1 General

The ***Consortium for Small-Scale Modelling*** (COSMO) was formed in October 1998 at the regular annual DWD/MeteoSwiss meeting. At present, the following national, regional and military meteorological services are participating:

DWD	Deutscher Wetterdienst, Offenbach, Germany
HNMS	Hellenic National Meteorological Service, Athens, Greece
IMGW	Institute for Meteorology and Water Management, Warsaw, Poland
MeteoSwiss	MeteoSchweiz, Zürich, Switzerland
UGM	Ufficio Generale per la Meteorologia, Roma, Italy
ARPA-SIM	Servizio Idro Meteorologico di ARPA, Bologna, Italy
AWGeophys	Amt für Wehrgeophysik, Traben-Trarbach, Germany

The general goal of COSMO is to develop, improve and maintain a non-hydrostatic limited-area modelling system to be used both for operational and for research applications by the members of COSMO. The emphasis is on high-resolution numerical weather prediction by small-scale modelling. COSMO is initially based on the "Lokal-Modell" (LM) of DWD with its corresponding data assimilation system.

A Memorandum of Understanding (MoU) on the scientific collaboration in the field of non-hydrostatic modelling was signed by the Directors of DWD, HNMS, MeteoSwiss and UGM in March/April 1999. Meanwhile, the MoU has been replaced by an Agreement between the participating National Meteorological Services. The national weather service IMGW of Poland joined the consortium in 2002.

2.2 Agreement

The structure of the cooperation and both internal and external relationships of COSMO are defined and further detailed in an Agreement between the National Meteorological Services of the participating countries On 3 October 2001, the final version of the COSMO Agreement has been signed by the representatives of the National Meteorological Services (DWD, HNMS, MeteoSwiss and UGM). The Director of the national weather service of Poland (IMGW) signed the Agreement on 4 July 2002.

There is no direct financial funding from or to either member. However, the partners have the responsibility to contribute actively to the model development by providing staff resources, by making use of research cooperations and by seeking for national funding whenever possible. A minimum of 2 scientists working in COSMO research and development areas is required from each member. In general, the group is open for collaboration with other NWP groups, research institutes and universities as well as for new members. For more details on the COSMO Agreement, please contact the present Chairman of the Steering Committee, Dieter Frühwald (dieter.fruehwald@dwd.de).

2.3 Organizational Structure

COSMO's organization consists of a Steering Committee (composed of one representative from each National Meteorological Service), a Scientific Project Manager, Work-package Coordinators and Scientists from the member institutes performing research and develop-

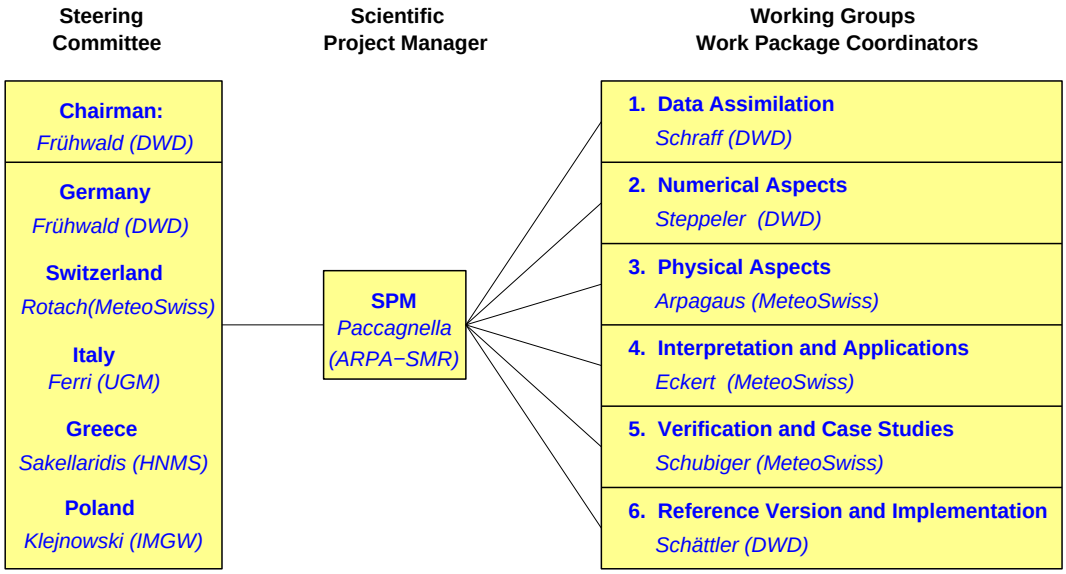

Figure 1: Organizational structure of COSMO as of January 2004

ment activities in the COSMO working groups. At present, six working groups covering the following areas are active: Data assimilation, numerical aspects, physical aspects, interpretation and applications, verification and case studies, reference version and implementation. The current organizational structure is sketched in Fig. 1 (see Section 7 for changes in the Steering Committee and WP-Coordinators).

COSMO's activities are developed through extensive and continuous contacts among scientists, work-package coordinators, scientific project manager and steering committee members via electronic mail, special meetings and internal workshops. Once a year there is a General Meeting of the COSMO group in order to present results, deliverables and progress reports of the working groups and to elaborate a research plan with new projects for the next annual period. Following this meeting, a final work plan for each working group is set up. The recent 5th COSMO General Meeting was held on 24-26 September 2003 in Langen (Germany). The 6th General Meeting is scheduled for 22-24 September 2004 in Rome (Italy).

3 Model System Overview

The limited-area model LM is designed as a flexible tool for numerical weather prediction on the meso-β and on the meso-γ scale as well as for various scientific applications using grid spacings from 50 km down to about 50 m. Besides the forecast model itself, a number of additional components such as data assimilation, interpolation of boundary conditions from a driving host model and postprocessing is required to run a NWP-system at a meteorological service. In the following sections, the components of the LM-package - as available to the COSMO group - are shortly described.

3.1 Short Description of the LM

This section gives only a brief overview of the Lokal-Modell. For a comprehensive description, the reader is referred to the documentation of the LM package (see section 3.6). An overview is given by Steppeler et al. (2003).

3.1.1 Dynamics and Numerics

The regional model LM is based on the primitive hydro-thermodynamical equations describing compressible nonhydrostatic flow in a moist atmosphere without any scale approximations. A basic state is subtracted from the equations to reduce numerical errors associated with the calculation of the pressure gradient force in case of sloping coordinate surfaces. The basic state represents a time-independent dry atmosphere at rest which is prescribed to be horizontally homogeneous, vertically stratified and in hydrostatic balance. The basic equations are written in advection form and the continuity equation is replaced by a prognostic equation for the perturbation pressure, i.e. the deviation of pressure from the reference state.

The model equations are formulated with respect to a rotated lat/lon-grid with coordinates (λ, φ). The rotated coordinate system results from the geographical (λ_g, φ_g) coordinates by tilting the north pole. In the vertical, we use a generalized terrain-following height coordinate ζ, where any unique function of geometrical height can be used for transformation. Since ζ doesn't depend on time, the $(\lambda, \varphi, \zeta)$-system represents a non-deformable coordinate system, where surfaces of constant ζ are fixed in space - in contrast to the pressure based coordinate system of most hydrostatic models, where the surfaces of constant vertical coordinate move in space with changing surface pressure. By default, a hybrid sigma-type (formulated with respect to the base-state pressure) vertical coordinate is used.

The model equations are solved numerically using the traditional Eulerian finite difference method. In this technique, spatial differential operators are simply replaced by suitable finite difference operators and the time integration is by discrete stepping using a fixed timestep Δt. The model variables are staggered on an Arakawa-C/Lorenz grid with scalars (temperature, pressure and humidity variables) defined at the centre of a grid box and the normal velocity components defined on the corresponding box faces. For a given grid spacing, this staggering allows for a more accurate representation of differential operators than in the A-grid, where all variables are defined at the same point. In general, we use second order centered finite difference operators for horizontal and vertical differencing.

Because the governing nonhydrostatic equations describe a compressible model atmosphere, meteorologically unimportant sound waves are also part of the solution. As acoustic waves are very fast, their presence severely limits the time step of explicit time integration schemes. In order to improve the numerical efficiency, the prognostic equations are separated into terms

Table 1: LM Model Formulation: Dynamics and Numerics

Model Equations:	Basic hydro-thermodynamical equations for the atmosphere: – advection form, – non-hydrostatic, fully compressible, no scale approximations, – subtraction of horizontally homogeneous basic state at rest.
Prognostic Variables:	Horizontal and vertical Cartesian wind components, temperature, pressure perturbation, specific humidity, cloud water content. Options for additional prognostic variables: – cloud ice, turbulent kinetic energy, rain and snow water content.
Diagnostic Variables:	Total air density, precipitation fluxes of rain and snow.
Coordinate System:	Rotated geographical (lat/lon) coordinate system horizontally; generalized terrain-following height-coordinate vertically. Built-in options for the vertical coordinate are: – hybrid reference pressure based σ-type coordinate (default), – hybrid version of the Gal-Chen coordinate, – hybrid version of the SLEVE coordinate (Schär et al., 2002).
Grid Structure:	Arakawa C-grid, Lorenz vertical grid staggering.
Spatial Discretization:	Second order horizontal and vertical differencing.
Time Integration:	Leapfrog HE-VI (horizontally explicit, vertically implicit) time-split integration scheme by default; includes extensions proposed by Skamarock and Klemp (1992). Additional options for: – a two time-level split-explicit scheme Gassmann (2002), – a three time-level 3-d semi-implicit scheme (Thomas et al., 2000), – a two time level 3rd-order Runge-Kutta scheme (regular or TVD) with various options for high-order spatial discretization. (Förstner and Doms, 2004).
Numerical Smoothing:	4th order linear horizontal diffusion with option for a monotonic version including an orographic limiter (Doms, 2001); Rayleigh-damping in upper layers; 3-d divergence damping and off-centering in split steps.
Lateral Boundaries:	1-way nesting using the lateral boundary formulation according to Davies (1976). Options for: – boundary data defined on lateral frames only, – periodic boundary conditions.

which are directly related to acoustic and gravity wave modes and into terms which refer to comparatively slowly varying modes of motion. This mode-splitting can formally be written in the symbolic form

$$\frac{\partial \psi}{\partial t} = s_\psi + f_\psi \,, \tag{1}$$

where ψ denotes a prognostic model variable, s_ψ the forcing terms due to the slow modes and f_ψ the source terms related to the fast acoustic and gravity wave modes. f_ψ is made up of the pressure gradient terms in the momentum equations, the temperature and pressure contributions to the buoyancy term in the equation for the vertical velocity, and the divergence term in the pressure and the temperature equation. The subset of equations containing the f_ψ-terms is then integrated with a special numerical scheme.

The default time integration method used in LM is a variant of the Klemp and Wilhelmson

(1978) scheme including extensions proposed by Skamarock and Klemp (1992). It is based on a Leapfrog integration for the slow modes from time level $n-1$ to time level $n+1$ using an integration interval of $2\Delta t$. The slow mode tendencies are evaluated at time level n for horizontal advection and at time level $n-1$ for most physical forcings. Tendencies from vertical advection and diffusion are calculated by a quasi-implicit scheme. The integration step is then subdivided into a number N_s of small time steps $\Delta\tau_s$ according to $2\Delta t = N_s\Delta\tau$ and the prognostic equations (1) are stepped forward according to

$$\psi^{\nu+1} = \psi^{\nu} + f_{\psi}^{\nu}\Delta\tau + s_{\psi}^{n}\Delta\tau\,. \tag{2}$$

In the integration of (2), sound waves are treated explicitly for horizontal directions using the forward-backward method while implicitly for the vertical direction (HE-VI scheme). Thus, the small time step $\Delta\tau$ is limited by the CFL stability criterion for horizontal but not for vertical sound wave propagation. This makes the HE-VI scheme numerically very efficient for large grid aspect ratios, i.e. $\Delta x/\Delta z >> 1$, which are typically used in meso-β and meso-γ applications. An additional 3-D divergence damping as well a slight time off-centering in the vertical implicit formulation is applied to damp acoustic modes. On the big time step, the Asselin time filter and a 4th-order horizontal diffusion are used for numerical smoothing.

Three alternative time integration schemes have also been implemented for optional use: a two time-level time-split method based on the work of Gassmann (2002), a three-timelevel Leapfrog-based Eulerian 3-D semi-implicit scheme according to Thomas et al. (2000) and recently a new two time-level scheme based on 3rd-order Runge-Kutta integration with total variation diminishing (TVD) option (Förstner and Doms, 2004). The latter scheme is intended to be used for high-resolution applications of LM in near future. Table 1 summarizes the dynamical and numerical key features of the LM.

3.1.2 Initial and Boundary Conditions

For operational applications and real data simulations, LM is driven by the new global model GME of DWD using the traditional boundary relaxation technique (see Section 3.3). Information on the GME as well as on recent changes to the global model are summarized in the *Quarterly Report of the Operational NWP-Models of the Deutscher Wetterdienst*. This report series is available online at the DWD web-site (*www.dwd.de*). Optionally, initial and boundary data may also be provided from the IFS global model at ECMWF. In this context, a new option for using boundary data which are defined on lateral frames only (by default, the boundary conditions are defined on the full 3-d model domain) has been introduced.

A four-dimensional data assimilation cycle based on a nudging analysis scheme (see Section 3.2) can be installed for operational NWP with the LM at COSMO meteorological services. In this case, the initial conditions come from the continuous LM assimilation stream and only boundary data have to be provided by GME forecasts. However, an operational NWP-system can also be set-up without a data assimilation cycle by relying on pure dynamical adaption of large-scale initial fields. In this case, the initial conditions come from interpolated (and initialized) GME analyses. To reduce noise generation and spin-up effects resulting from non-balanced interpolated data, a diabatic digital filtering initialization (DFI) scheme (Lynch et al., 1997) has been implemented. By default, the DFI initialization consists of a 1-h adiabatic backward integration followed by a 1-h diabatic forward integration of the model.

For various research applications as well as for model testing and evaluation, the LM provides a capability to handle idealized cases using user-defined artificial initial and boundary data. For these types of application, periodic lateral boundary conditions can be specified optionally. Additionally, a 2-dimensional model configuration can be used.

3.1.3 Parameterization of Physical Processes

A variety of subgrid-scale physical processes is taken into account by parameterization schemes. Initially, the physics package of LM has been adapted from the former operational hydrostatic models EM/DM. Meanwhile, a number of additional schemes have been developed and implemented for optional use: a new scheme for vertical diffusion based on prognostic turbulent kinetic energy, a new diagnostic scheme for surface layer transports, a new grid-scale cloud and precipitation scheme including cloud ice as a prognostic variable, a new multi-layer soil model, and the Kain-Fritsch scheme for deep moist convection. Work on a new lake model, a revised version of the surface layer scheme, a new scheme for moist convection and a cloud microphysics scheme including graupel is in progress.

Table 2 gives a short overview on the parameterization schemes used by default and on additional options implemented so far.

Table 2: LM Model Formulation: Physical Parameterizations

Grid-scale Clouds and Precipitation:	Cloud water condensation/evaporation by saturation adjustment. Precipitation formation by a bulk parameterization including water vapour, cloud water, rain and snow (scheme HYDOR), where rain and snow are treated diagnostically by assuming column equilibrium (default). Further options are: – the LM cloud ice scheme HYDCI (Doms, 2002), – a warm rain scheme following Kessler(1969), – prognostic treatment of rain and snow (Gassmann, 2002; and Baldauf and Schulz, 2004, for the Leapfrog integration scheme).
Subgrid-scale Clouds:	Subgrid-scale cloudiness is interpreted by an empirical function depending on relative humidity and height. A corresponding cloud water content is also interpreted.
Moist Convection:	Mass-flux convection scheme (Tiedtke, 1989) with closure based on moisture convergence (default). Further Options: – a modified closure based on CAPE within the Tiedtke scheme. – the Kain-Fritsch convection scheme.
Radiation:	δ-two stream radiation scheme after Ritter and Geleyn (1992) for short and longwave fluxes; full cloud-radiation feedback.
Vertical Diffusion:	Diagnostic K-closure at hierarchy level 2 by default.Optional: – a new level 2.5 scheme with prognostic treatment of turbulent kinetic energy; effects of subgrid-scale condensation and evaporation are included and the impact from subgrid-scale thermal circulations is taken into account.
Surface Layer:	Constant flux layer parameterization based on the Louis (1979) scheme (default). Optional: – a new surface scheme including a laminar-turbulent roughness sublayer.
Soil Processes:	Soil model after Jacobsen and Heise (1982) with 2 soil moisture layers and Penman-Monteith transpiration; snow and interception storage are included. Climate values changing monthly (but fixed during forecast) in third layer. Optional: – a new multi-layer soil model including freezing of soil water (Schrodin and Heise, 2001).

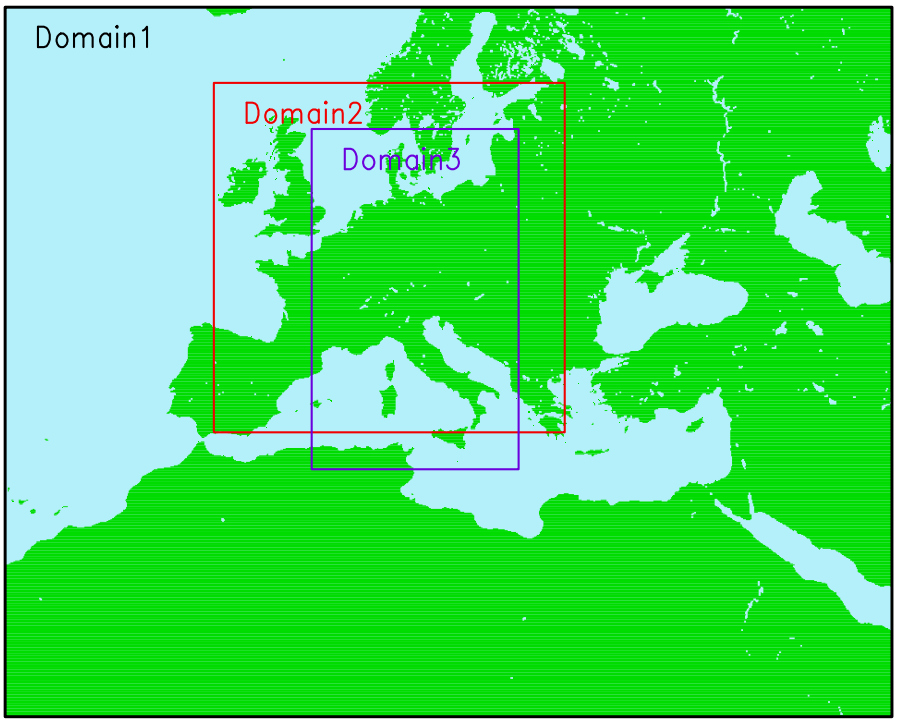

Figure 2: Domains of external parameter datasets used by COSMO partners

3.1.4 External Parameters

The parameterization of physical processes, but also the adiabatic model part requires some parameters which are not derived by data assimilation or by interpolation from a driving model. These so-called external parameters are defined in additional data sets. The LM requires the following external parameters: mean topographical height, roughness length, soil type, vegetation cover, land fraction, root depth and leaf area index. The sources for these data are indicated below.

- Mean orography:
  derived from the GTOPO30 data set (30"x30") from USGS.
- Prevailing soil type:
  derived from the DSM data set (5'x5') of FAO.
- Land fraction, vegetation cover, root depth and leaf area index:
  derived from the CORINE data set of ETC/LC.
- Roughness length:
  derived from the GTOPO30 and CORINE datasets.

External parameters for LM can be derived by a preprocessor program for any domain on the globe at any required spatial resolution. However, this is very time consuming because of the size of the high-resolution global data sets. Within the COSMO group, we thus have prepared some predefined data sets with external parameters on three different domains. These domains are shown in Fig. 2.

Domain 1 covers Europe and surrounding countries; data sets for this domain are available at 28 km, 21 km, 14 km and 7 km grid spacing. The smaller Domain 2 covers Germany

and surrounding countries; the corresponding data set gives the external parameters at 7 km resolution. Domain 2 is only used at DWD. Finally, Domain 3 covers central and southern parts of Europe. For this domain, the external parameters are given at 2.8 km resolution. The LM can then be very easily positioned anywhere within these domains.

Details on the location of the three domains are shown in Table 3, where longitude (λ) and latitude (ϕ) of the rotated coordinates and those of the geographical lat-lon grid (λ_g, ϕ_g) are given in degree. The resolution and the corresponding file names (these are required for the interpolation programs to generate initial and boundary data from a host model) are indicated in Table 4. The specifications refer to a rotated lat-lon grid of LM with the north-pole at geographical latitude 32.5° (N) and longitude -170.0° (W).

Table 3: Location of Domains in rotated and in geographical coordinates

Name	Domain corners	λ	ϕ	λ_g	ϕ_g
Domain 1	upper left	- 26.75	9.25	- 42.74	56.07
	upper right	33.25	9.25	70.36	51.49
	lower left	- 26.75	- 38.75	- 11.26	14.54
	lower right:	33.25	- 38.75	35.96	12.34
Domain 2	upper left	- 12.625	4.125	- 15.25	59.26
	upper right	11.125	4.125	32.48	59.77
	lower left	- 12.625	-19.50	- 4.87	36.62
	lower right:	11.125	-19.50	23.15	36.92
Domain 3	upper left	- 6.00	1.00	- 1.37	58.00
	upper right	8.00	1.00	25.06	57.61
	lower left	- 6.00	-22.00	3.19	35.20
	lower right:	8.00	-22.00	19.06	34.97

Table 4: Grid spacing $\Delta\lambda$ (= $\Delta\phi$) in degrees, approximate resolution Δs in m, number of gridpoints and file name of the datasets for the domains

Name	$\Delta\lambda, \Delta\phi$ (°)	Δs (m)	no. of grid points	Filename
Domain 1	0.2500	28000	241 x 193	lm_d1_28000_241x193.g1
	0.1875	21000	321 x 257	lm_d1_21000_321x257.g1
	0.1250	14000	481 x 385	lm_d1_14000_481x385.g1
	0.0625	07000	961 x 769	lm_d1_07000_961x769.g1
Domain 2	0.0625	07000	381 x 379	lm_d2_07000_381x379.g1
Domain 3	0.0250	02800	561 x 921	lm_d3_02800_561x921.g1

3.1.5 Coding and Parallelization

To meet the computational requirements of the model, the program has been coded in Standard Fortran 90 and parallelized using the MPI library for message passing on distributed memory machines. Thus it is portable and can run on any parallel machine providing MPI. Also it can still be executed on conventional single-processor computers without MPI.

The parallelization strategy is the two dimensional domain decomposition which is well suited for grid point models using finite differences (see Fig. 3). Each processor gets an appropriate part of the data to solve the model equations on its own subdomain. This subdomain is surrounded by halo grid-lines which belong to the neighboring processors. At present, we use 2 grid-lines for the halo. However, as the number of halo grid-lines is soft-coded, this can be easily changed whenever necessary (e.g., in case of high order advection schemes). During the integration step each processor updates the values of its local subdomain; grid points belonging to the halo are exchanged using explicit message passing. The number of processors in longitudinal and latitudinal direction can be specified by the user to fit optimal to the hardware architecture (vector, scalar, cache-size, etc).

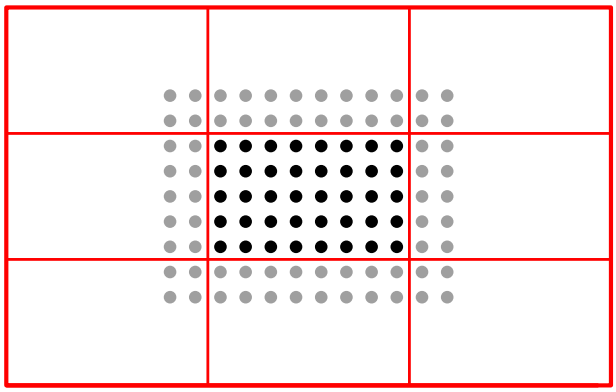

Figure 3: 2-D domain decomposition with a 2 gridline halo

Table 5 shows the timings of the LM for a one-hour full-physics simulation on a 325×325×35 gridpoints domain using 7km grid spacing and a 40 sec time step for various numbers of processors on an IBM SP3. Starting with 15 processors - which are required to fit the model into core memory - the number of processors has been doubled up to 240. The speedup behaviour of the LM shows an almost ideal scaling (half the CPU-time for twice the number of processors) up to 120 processors. With 240 processors, the execution time becomes larger than expected from ideal scaling. Here, the subdomain treated by a processor is so small that the ratio between physics-dynamics calculations – which scale superlinear – and the time for communication (data exchange and wait times due to load imbalances) and I/O – which both scales sub-linear – becomes disadvantageous.

Table 5: Timings for a 1-h LM forecast for various number of processors on an IMB-SP3

Number of Processors	15	30	60	120	240
Total CP-Time	571.53	284.04	136.34	67.61	38.10
Dynamics, Physics, Diagnostics	541.13	261.39	118.25	51.59	22.96
Communication	22.05	16.69	12.81	11.25	9.23
Input and Output	8.35	5.96	5.28	4.77	5.91

3.2 Data Assimilation

The requirements for the data assimilation system for the operational LM are mainly determined by the very high resolution of the model and by the task to employ it also for nowcasting purposes in the future. Hence, detailed high-resolution analyses have to be able to be produced frequently, and this requires a thorough use of asynoptic and high-frequency observations such as aircraft data and remote sensing data. Note that the synoptic scales are largely determined by the lateral boundary conditions provided by the steering model, and the main purpose of the assimilation scheme is to analyze the meso scales.

By design, 3-dimensional analysis methods tend to be less appropriate for this purpose. They do not allow to account for the exact observation time of asynoptic data, and they make it necessary to neglect most of the high-frequent data unless the analysis scheme is applied very frequently at significant computational costs. Moreover, the geostrophic approximation, usually a key ingredient of such schemes, is of limited validity in the meso scale. Therefore, 4-dimensional methods offer potential advantages since they include the model dynamics in the assimilation process directly. Yet, the 4-dimensional variational (4DVAR) method is too expensive for operational application of the LM considering the small amount of time available to produce the analyses and forecasts.

As a result, a scheme based on the observation nudging technique has been developed to define the atmospheric fields. It is based on an experimental nudging analysis scheme which had been developed for DM and the Swiss model version SM (Schraff, 1996; 1997) and which compared favorably with the operational OI-analysis of the DM in various case studies. The new LM-scheme, however, has been adapted to the nonhydrostatic modelling framework and runs on distributed memory machines using domain decomposition. To compute the analysis increments locally for the grid points of each sub-domain, the observational information of the total domain is previously distributed to the sub-domains.

For some of the surface and soil fields, a set of 2-dimensional intermittent analysis schemes is applied in addition. This comprises of the snow analysis, the sea surface temperature (SST) analysis, and the variational soil moisture analysis scheme.

3.2.1 Nudging-Based Assimilation Scheme

Nudging or Newtonian relaxation consists of relaxing the model's prognostic variables towards prescribed values within a predetermined time window (see e.g. Davies and Turner (1977), Stauffer and Seaman (1990)). In the present scheme, nudging is performed towards direct observations which is more appropriate for high-resolution applications than nudging towards 3-dimensional analyses (Stauffer and Seaman, 1994). A relaxation term is introduced into the model equations, and the tendency for the prognostic variable $\psi(\mathbf{x}, t)$ is given by

$$\frac{\partial}{\partial t}\psi(\mathbf{x},t) \quad = \quad F(\boldsymbol{\psi},\mathbf{x},t) \quad + \quad G_\psi \cdot \sum_{k_{(obs)}} W_k \cdot [\psi_k - \psi(\mathbf{x}_k, t)] \tag{3}$$

F denotes the model dynamics and physical parameterizations, ψ_k the value of the k^{th} observation influencing the grid point $\mathbf{x}$ at time t, $\mathbf{x}_k$ the observation location, G_ψ the constant so-called nudging coefficient and W_k an observation-dependent weight which usually varies between 0 and 1. Neglecting the dynamics and physics and assuming a single observation with a constant weight W_k equal 1, the model value at the observation location relaxes exponentially towards the observed value with an e-folding decay rate of $1/G_\psi$ corresponding to about half an hour.

In practical applications, the nudging term usually remains smaller than the largest term of the dynamics so that the dynamic balance of the model is not strongly disturbed. The coupling between the mass and wind field innovations is primarily induced implicitly by the model dynamics. If the assimilation process is successful the model fields will be close to dynamic balance at the beginning of the forecast, and an initialization step is not required.

The factors W_k determine the relative weights given to the different observations at a specific grid point. For a single observation, this weight (w_k) comprises of the quality (and representiveness) of the observation (ϵ_k) and of weights which depend on the horizontal (w_{xy}) or vertical (w_z) distance respectively temporal (w_t) difference between the observation and the target grid point. If an increasing number of observations influence the grid point the total nudging weight should be limited to avoid the nudging term to become dominant over the dynamics. This is achieved by complementing the individual weight w_t by a relative weight (Benjamin and Seaman, 1985):

$$W_k = \frac{w_k}{\sum_j w_j} \cdot w_k \tag{4}$$

$$w_k = w_t \cdot w_{xy} \cdot w_z \cdot \epsilon_k \tag{5}$$

Currently, only conventional observations are used, namely from TEMP and PILOT (temperature and wind, including the significant levels; humidity up to 300 hPa; geopotential only to derive one pressure increment at the lowest model level), AIRCRAFT (all data), and SYNOP, SHIP and DRIBU reports (station pressure; wind for stations below 100 m above msl; humidity; 2-m temperature is used only for the soil moisture analysis). Note that given a cut-off time of 2.5 hours, observations from up to about 2 hours after the actual analysis time can still be assimilated in the first hours of the operational forecast runs. As a quality control, the observed values are compared with the model fields of the assimilating run itself. For multi-level temperature data, a hydrostatic height and thickness check is included, and a spatial consistency check is performed for the station pressure data.

Equation (3) indicates that in principle the scheme consists of two main steps, i.e. the determination of the observation increments and the computation of the weights. With respect to the vertical interpolation required for the first step, the vertical scale of multi-level temperature and wind observations is adjusted to the vertical model resolution by averaging the observed profile over the thickness of model layers. As a result, the simulated thickness between two pressure levels is automatically relaxed towards the observed thickness when nudging temperature data. In contrast, humidity data are interpolated without averaging in order to capture thin layers of clouds as well as possible. Note that the increments are determined as differences in relative humidity which implies that relative rather than specific humidity is relaxed towards the observed humidity. In this sense, the analyzed quantities are horizontal wind, potential temperature, relative humidity, and pressure at the lowest model level.

Related to the second step, incomplete profiles and single-level increments are vertically extended and provided with vertical weights w_z according to a Gaussian (approx.) in log pressure (correlation scale is $1/\sqrt{3}$ for upper-air wind and 0.2 for upper-air temperature and humidity, and the cut-off is 850 m for surface-level wind resp. the lowest model layer for surface-level humidity). Thereafter, upper-air increments are spread laterally along horizontal surfaces since spreading along the terrain-following model levels as usually applied in nudging-type schemes has disadvantages near steep orography particularly in cases with low stratus (Schraff, 1997). In contrast, surface-level increments are spread along the model levels to limit the area of influence to close to the ground. The spreading includes the computation of the horizontal weights w_{xy} using the function $(1 + \Delta r/s) \cdot e^{-\Delta r/s}$ for the scalar

quantities (Δr being the horizontal distance between observation and target grid point). The wind correlations are split into a longitudinal and transverse part, and this allows to specify the degree of divergence (γ) of the resulting wind analysis increment field (Lorenc et al., 1991). Both the correlation scales s and the non-divergence factor γ increase with height and with distance to the observation time and vary between about 60 km and 160 km resp. 0.4 and 0.7 . The function used for the temporal weights w_t is 1 at the observation time and decreases linearly to zero at 3 hours (for radiosonde data) resp. 1.5 hours (for other data) before and 1 resp. 0.5 hours after the observation time. Hourly or more frequent data are linearly interpolated in time.

Table 6: Data Assimilation for LM

Method	Nudging towards observations
Implementation	continuous cycle of 3-hour assimilation runs
Realization	identical analysis increments used during 6 advection time steps
Balance	1. hydrostatic temperature increments (up to 400 hPa) balancing 'near-surface' pressure analysis increments 2. geostrophic wind increments balancing 'near-surface' pressure analysis increments 3. upper-air pressure increments balancing total analysis increments hydrostatically
Nudging coefficient	$6 \cdot 10^{-4} s^{-1}$ for all analyzed variables except pressure $1.2 \cdot 10^{-3} s^{-1}$ for 'near-surface' pressure
Analyzed variables	horizontal wind vector, potential temperature, relative humidity 'near-surface' pressure (i.e. at the lowest model level)
Spatial analysis	Data are analyzed vertically first, and then spread laterally along horizontal surfaces. vertical weighting: approximately Gaussian in log(p) horizontal weighting: isotropic as function of distance
Temporal weighting	1.0 at observation time, decreasing linearly to 0.0 at 3 hours (upper air) resp. 1.5 hours (surface-level data) before and 1.0 resp. 0.5 hours after observation time; linear temporal interpolation of frequent data.
Observations	SYNOP, SHIP, DRIBU: - station pressure, wind (stations below 100 m above msl) - humidity TEMP, PILOT: - wind, temperature: all standard levels, significant levels up to 150 hPa - humidity: all levels up to 300 hPa - geopotential used for one 'near-surface' pressure increment AIRCRAFT: - all wind and temperature data
Quality control	Comparison with the model fields from assimilation run itself

In the current scheme, the resulting analysis increment fields are partly balanced explicitly in a third major step before being added to the model fields. Three types of balancing are applied. First, a hydrostatic upper-air temperature correction balances the pressure analysis increments at the lowest model layer. It is nearly constant within the lowest 1500 m (therefore

hardly modifies the stability within the boundary layer) and decreases rapidly further above such that the geopotential above 400 hPa is not directly modified by the surface pressure nudging (for hydrostatic conditions). This significantly reduces the vertical extent of the mass field disturbance imposed by the pressure nudging and results in a better adjustment of the wind field and a greatly improved assimilation of the pressure data. Secondly, a geostrophic wind correction partly balances the wind field with respect to the mass field increments imposed by the surface pressure nudging including the temperature correction. Finally, an upper-air pressure correction balances the total analysis increments of the mass field hydrostatically. This is the only feature directly related to the fact that the model is non-hydrostatic. Note that it does not change the non-hydrostatic properties of the full model fields. The correction prevents the introduction of direct sources of vertical wind for which there is no direct control without vertical wind observations being available to be assimilated. This is important since the vertical velocity is still small on the scales to be analyzed with the current scheme and observations (in contrast e.g. to a latent heat nudging scheme). Table 6 summarizes the main features of the LM nudging scheme.

3.2.2 Sea Surface Temperature Analysis

Since the latent and sensible heat fluxes over water depend crucially on the surface temperature, a sea surface temperature (SST) analysis is performed once per day (00 UTC). Starting from the previous analysis as first guess, all the ship and buoy observations from the previous 6 days are used in a correction scheme based on Cressman-type weighting. In data-poor areas, this is blended (via the global SST analysis) with a daily 1° x 1° SST analysis from NCEP which also incorporates satellite data. For the sea-ice cover in the Baltic Sea, an external analysis (from the Bundesamt fuer Seeschiffahrt und Hydrologie) is used.

3.2.3 Snow Depth Analysis

The occurrence of a snow cover strongly influences the radiative absorption and reflection properties of the land surface and therefore the screen-level temperature. The snow water content is a prognostic quantity of the model, and is analyzed once every 6 hours. The method is based on a simple weighted averaging of SYNOP snow depth observations. The weighting depends both on the horizontal and vertical distances to the target grid points. In areas, where the density of these data is not sufficient, an average of snow depth increments derived from SYNOP precipitation, temperature, and weather reports as well as the model prediction are also included.

3.2.4 Soil Moisture Analysis

In land areas without snow, screen-level temperature (and humidity) is significantly influenced by the soil water content on clear-sky days. An inadequate specification of soil moisture can lead to forecast temperature errors of several degrees. The variational analysis scheme (Hess, 2001) derives improved moisture contents once per day by minimizing a cost functional J which depends on the deviations of the forecast temperature $T(\eta)$ from the observed (resp. analyzed) temperature T^o and of the soil moisture η from a given background state η^b:

$$J(\eta) = \frac{1}{2}\Big(T^o - T(\eta)\Big)^T \mathbf{R}^{-1}\Big(T^o - T(\eta)\Big) + \frac{1}{2}\Big(\eta - \eta^b\Big)^T \mathbf{B}^{-1}\Big(\eta - \eta^b\Big) \qquad (6)$$

The observation error covariance $\mathbf{R}$ and background error covariance $\mathbf{B}$ reflect the trust in the observations resp. the background. To solve the minimization problem, two assumptions are made. Firstly, since the 2-m temperature mainly depends on the soil moisture at the same location, the problem can be decoupled horizontally, and a low-dimensional (equal to the number of analyzed soil layers) minimization can be performed for each grid point individually. Secondly, (moderate) changes of soil moisture are assumed to lead to linear changes in temperature. This allows to derive the linear relationships $\mathbf{\Gamma}$ by means of one additional forecast run per analyzed soil layer where each of these forecasts has slightly different values for the initial soil moisture. The minimum of J can then be found by solving $\nabla J(\eta) = 0$ directly without using the adjoint method.

In the current implementation, two additional 15-hour forecasts are required to analyze two (sets of) soil layers for 0 UTC of the previous day by comparing forecast and observed temperature at 12 and 15 UTC. The analysis increments are then added to the soil moisture of the 0 UTC nudging analysis of the current day. The resulting soil moisture is used both as initial state for the operational LM forecast of the current day and as background state for the next soil moisture analysis. This background state η^b is important in order to reduce the daily variation of the soil moisture contents and to stabilize the minimization in cases of weak soil-atmosphere coupling (i.e. cloudy situations). Together with η^b (see above), the background error covariance $\mathbf{B}$ for the following day is provided in a Kalman-filter cycled analysis:

$$(\mathbf{B})^{next} \;=\; \mathbf{A} \;+\; \mathbf{Q} \quad , \quad where \;\; \mathbf{A} = (\nabla^2 J)^{-1} = \left(\mathbf{\Gamma}^T \mathbf{R}^{-1} \mathbf{\Gamma} + \mathbf{B}^{-1} \right)^{-1} \tag{7}$$

This takes into account both an increase of confidence in the retrieved soil moisture values due to the utilized screen-level observations (as part of the analysis error covariance $\mathbf{A}$) and a decrease of confidence due to the model error $\mathbf{Q}$ of the soil model. While $\mathbf{A}$ can be computed explicitly, $\mathbf{Q}$ is the main tuning parameter of the scheme. It influences the relative weight given to the past and the present observations and has an impact on the temporal variability of the soil moisture. The scheme has been successfully tested in various case studies and it is operated at DWD since March 2000.

3.3 Boundary Conditions from Driving Models

The LM can be nested in the global model GME of DWD (Majewski, 1998; Majewski et al., 2002) or the ECMWF global spectral model IFS. The lateral boundary formulation is by the Davies (1976) relaxation technique, where the internal model solution is nudged against an externally specified solution within a narrow boundary zone by adding a relaxation forcing term to the equations.

The external solution is obtained by interpolation from the driving host model at discrete time intervals. The interpolated fields are hydrostatically balanced, i.e. a hydrostatic pressure is prescribed for the nonhydrostatic pressure variable in LM at the lateral boundaries. Within these specified time intervals, the boundary data are interpolated linearly in time (which is done inside the model). Normally the boundary update interval is chosen to be one hour for meso-β scale applications of the LM. The boundary values (and initial values, if no data assimilation suite is operated) are obtained by a preprocessing program from the host model.

- ***GME2LM:***
  interpolation from the new triangular mesh global model GME of DWD.
- ***IFS2LM:***
  interpolation from the global spectral model IFS of ECMWF.

A documentation of the GME2LM preprocessor program is available at the COSMO Website. An additional interpolation program LM2LM for one-way self-nesting of LM is in preparation. It is planned to combine all pre-processor routines into a single interpolation program INT2LM.

3.4 Postprocessing

Postprocessing includes all applications that use the direct model output of LM runs. In general, there is a wide range of such applications at each meteorological service, ranging from simple graphical display of weather charts or meteograms for single grid points, or statistical correction of near surface weather elements by Kalman filtering, to more complex derived products supplying information on environment and health, transportation, agriculture and media presentation. Most of these postprocessing tools are very specific to the computer platform, data base system and visualization software of each service and thus cannot be shared within the COSMO group. There is, however, a number of postprocessing programs available within COSMO.

(a) Graphics
Work on two common plotting packages has been completed. The first has been developed at MeteoSwiss and uses Metview with an interface to the GRIB1 LM output data; the other one has been developed at ARPA-SMR and is based on the public domain VIS5D packages; a special routine converts the GRIB1 binary format to the VIS5D data format.

(b) Models
A *Lagrangian Particle Dispersion Model* (LPDM) may be used operationally in case of radioactive accidental releases to predict long-range transport, dispersion, and wet and dry deposition of radioactive material. The calculation of about $10^5 - 10^6$ trajectories of tracer particles is based on wind fields from LM (at hourly intervals) and superimposed turbulent fluctuations (TKE, Monte Carlo method). Radioactive decay and convective mixing are included. The concentration is calculated by counting the particle masses in arbitrary grids.

A *Trajectory Model* may provide guidance on transport routes. The meteorological input is derived from LM at hourly intervals.

An integral part of the NWP-system at DWD is a *Wave Prediction Suite* comprising two models, namely the global model GSM (global sea state model), and a local one (LSM) which covers the Baltic Sea, the North Sea and the Adriatic Sea with a high-resolution mesh. GSM and LSM have been developed by research institute GKSS in Geesthacht (Germany).

(c) Interpretation
An objective weather interpretation scheme (developed at DWD) derives the forecasted 'weather', i.e. the WMO weather code, based on LM output fields. Pressure, temperature, dew point temperature, liquid water content, cloud cover, precipitation and wind speed values are used as input parameters to define the present weather.

3.5 Data Flow of the LM-Package

The various components of the LM Package and the corresponding data flow are illustrated in Figure 4. In case of a set-up without data assimilation (right part of Figure 4), the interpolation programs (GME2LM, IFS2LM or LM2LM) provide initial and boundary conditions for the LM forecast runs (LM-FCT) from the corresponding driving models. This step involves the data set of the external parameters (see Section 3.1.4).

With a system set-up using the LM nudging analysis (left part of Figure 4), the GME2LM provides boundary conditions (LM-BC) from the GME assimilation cycle for the LM runs in nudging analysis mode (LM-NUD) within the assimilation stream. The LM-NUD runs start from a given LM analysis (LM-ANA) to generate an analysis for the next analysis time. The forecasts then start from these LM-ANA initial data using boundary condition from the GME forecast.

To run the LM in nudging mode, a preprocessor program is required which provides the observational data in a special data file format (AOF). The LM analysis file may be modified by incremental analyses of sea surface temperature, snow depth and soil moisture (see Section 3.2). All these programs use GTS and non-GTS observation data, which are archived in a local data base system. The interface to these data is usually not portable as it depends on the data base system of each meteorological centre.

The LM runs in forecast mode generate direct model output, which includes also fields from the LM internal postprocessing (see Appendix B). These data are then subject to various visualization tools, external postprocessing and other applications such as follow-up models at COSMO Met Services.

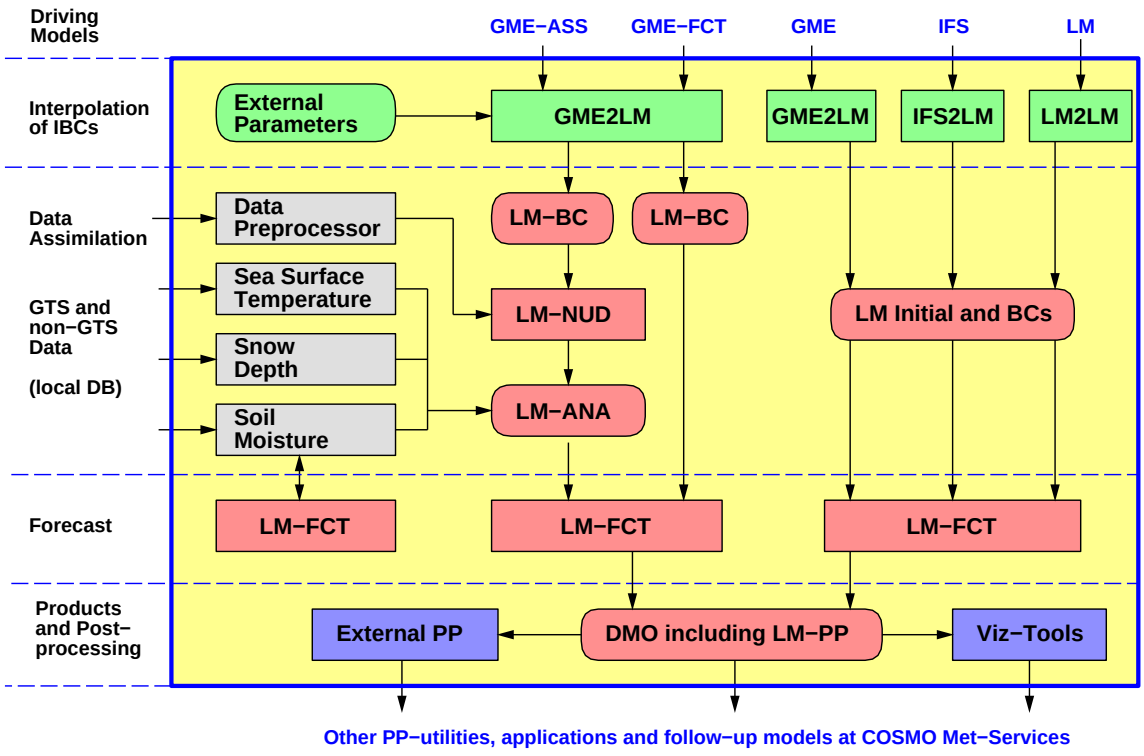

Figure 4: Process and data flowchart of the LM Package for a set-up using data assimilation (left part) and a set-up without data assimilation (right part). Rectangular boxes indicate components of the Package (programs), rounded boxes indicate data files generated by the components.

3.6 Documentation

The following parts of the model documentation are available at the COSMO web-site.

(a) The Nonhydrostatic Limited-Area Model LM of DWD

Part I: *Scientific Documentation*
Part II: *Implementation Documentation*
Part III: *User's Guide*
Part X: *Soil Moisture Analysis*

(b) The Interpolation Program GME2LM

Unfortunately, this documentation is not up to date and a new release is in preparation. The new documentation of the LM-package will be split in seven parts.

A Description of the Nonhydrostatic Regional Model LM

Part I: *Dynamics and Numerics*
Part II: *Physical Parameterization*
Part III: *Data Assimilation*
Part IV: *Implementation Documentation*
Part V: *Preprocessing*
Part VI: *Postprocessing*
Part VII: *User's Guide*

Parts I - III form the scientific documentation, which provides information about the theoretical and numerical formulation of the model, the parameterization of physical processes and the four-dimensional data assimilation including soil moisture analysis. The scientific documentation is independent of (i.e. does not refer to) the code itself. Part IV describes the particular implementation of the methods and algorithms as presented in Parts I - III, including information on the basic code design and on the strategy for parallelization using the MPI library for message passing on distributed memory machines. The generation of initial and boundary conditions from coarse grid driving models is described in Part V. Available internal and external postprocessing utilities are described in Part VI. Finally, the User's Guide (Part VII) provides information on code access and how to install, compile, configure and run the model. The User's Guide contains also a detailed description of various control parameters in the model input file (in NAMELIST format) which allow for a flexible model set-up for various applications. All parts of the new documentation will be made available at the COSMO web-site *www.cosmo-model.org* during 2004. Part I (Doms and Schättler, 2002) and Part III (Schraff and Hess, 2003) are already available.

4 Operational Applications

The LM is operated in five centres of the COSMO members (ARPA-SIM, DWD, HNMS, IMGW, MeteoSwiss). Following a 1-year preoperational trial from October 1998 to November 1999, the model became operational at DWD in December 1999. At MeteoSwiss the LM was integrated in a preoperational mode two times a day since July 2000. The model became fully operational in February 2001. In Italy the model runs operational twice a day at ARPA-SIM. The HNMS in Greece integrates the LM once a day in parallel to their old operational system. IMGW integrated the LM twice a day since October 2001 in a preoperational mode and switched to an operational schedule when they officially joined the COSMO group in July 2002. Figure 5 shows the integration domains of the model runs at the COSMO meteorological centres.

ARPA-SIM, HNMS and IMGW use interpolated boundary conditions from forecasts of the global model GME of DWD. Only a subset of GME data covering the respective LM-domain of a COSMO meteorological centre are transmitted from DWD via the Internet. HNMS and IMGW start the LM from interpolated GME analyses. In this case it is possible to smooth the initial fields using the digital filtering scheme of Lynch et al. (1997). At DWD, a comprehensive data assimilation system for LM has been installed, comprising the LM nudging analysis for atmospheric fields, a sea surface temperature (SST) analysis, a snow depth analysis and the soil moisture analysis according to Hess (2001). A data assimilation system based on the LM nudging scheme is now also used at MeteoSwiss (since November 2001) and at ARPA-SIM (since October 2003). Since September 2003, MeteoSwiss uses lateral boundaries from interpolated IFS-forecasts.

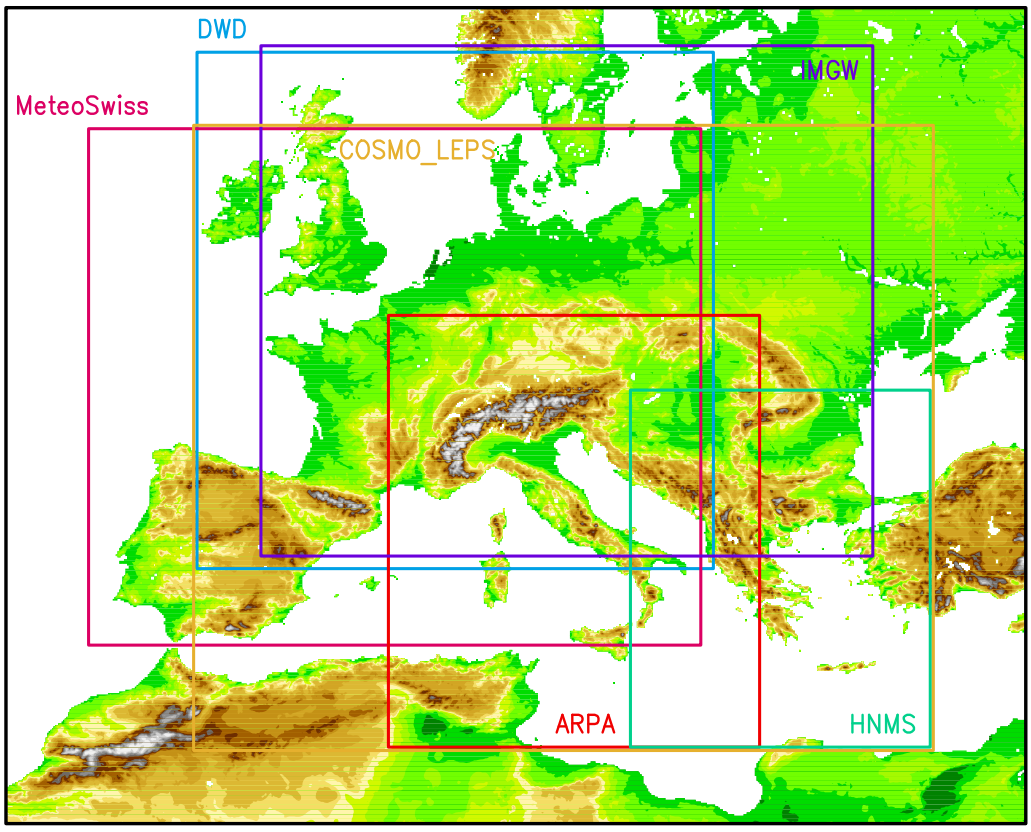

Figure 5: LM integration domains used at DWD, MeteoSwiss, ARPA-SIM, HNMS, IMGW and for the COSMO-LEPS

ARPA-SIM installed the COSMO-LEPS (Limited Area Ensemble Prediction System) based on LM and ECMWF ensemble forecasts at the ECMWF computing centre. 5 operational LM runs are performed (10 km grid spacing, 32 levels) starting at 12 UTC on initial and boundary conditions for 5 representative members of an ECMWF-EPS superensemble.

In addition, the national weather service of Italy, UGM in Rome, runs the LM at the ECMWF computing centre for the same domain as ARPA-SIM and also for a bigger domain comparable to the COSMO-LEPS domain. The lateral boundaries for these runs are taken from the IFS.

The following sections give a brief overview on the configurations of the operational LM systems in the COSMO meteorological centres. MeteoSwiss, ARPA-SIM and UGM have renamed the model within their services: the LM application in Switzerland is called ***aLMo*** (Alpine Model), the LM application in Italy is called ***LAMI*** (Limited Area Model Italy).

4.1 ARPA-SIM (Bologna)

Basic Set-Up of LM
The regional meteorological service ARPA-SIM in Bologna operates the LM (as LAMI) at 7 km grid spacing. The rotated lat-lon coordinates of the lower left and the upper right corner of the integration domain are $(\lambda = -5°, \varphi = -24.0°)$ and $(\lambda = 9.5625°, \varphi = -7.0625°)$, respectively. See Figure 5 for this model domain. The main features of the model set-up are summarized in Table 7.

Table 7: **Configuration of the LAMI at ARPA-SIM**

Domain Size	234 x 272 gridpoints
Horizontal Grid Spacing	0.0625° (∼ 7 km)
Number of Layers	35, base-state pressure based hybrid
Time Step and Integration Scheme	40 sec, 3 time-level split-explicit
Forecast Range	72 h
Initial Time of Model Runs	00 UTC and 12 UTC
Lateral Boundary Conditions	Interpolated from GME at 1-h intervals
Initial State	Nudging data assimilation cycle, no initialization
External Analyses	None
Special Features	Use of filtered topography, new TKE scheme, new surface-layer scheme, cloud-ice scheme
Model Version Running	lm_f90 3.5
Hardware	IBM SP pwr4 (using 32 of 512 processors)

Changes in the last year
The most important changes in the last year were the introduction of an operational data assimilation suite (see below) and the treatment of cloud ice in the LM.

Data assimilation
Since October 2003 the assimilation suite has become the main operational suite and the run initialized directly from GME is not performed anymore. As during the experimental period, the assimilation suite includes two 12-h cycles with AOF-file provided by UGM Rome with SYNOPs, AIREPs, TEMPs and PILOTs. Two forecasts up to 72 hours, at 00 and 12 UTC,

are performed daily starting from the analyses provided by the assimilation cycles. Figure 6 illustrates the scheme of the assimilation suite.

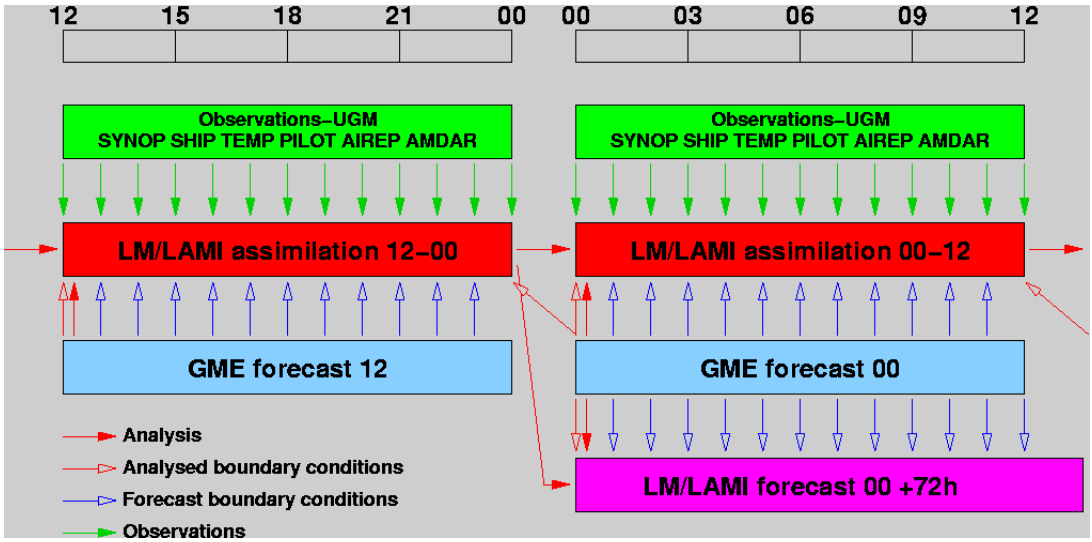

Figure 6: The assimilation suite at ARPA-SIM

Computer system
Since autumn 2003, an experimental backup suite is being set up at ARPA on a cluster of i386 computers with a total of 32 processors INTEL Xeon 2.4Ghz, connected by Gigabit ethernet network and running the Linux/GNU operating system. The setup is the same as the one on IBM at Cineca and the suite is controlled by ECMWF SMS software.

4.2 DWD (Offenbach)

Basic Set-Up of LM
The LM runs operationally at DWD using a 7 km grid spacing and 35 vertical levels. The rotated lat-lon coordinates of the lower left and the upper right corner of the integration domain are $(\lambda = -12.5°, \varphi = -17.0°)$ and $(\lambda = 7.75°, \varphi = 3.25°)$, respectively. See Figure 5 for this model domain. The main features of the model set-up are summarized in Table 8.

Changes in the last year
These are the main changes in the operational setup in the last year:

- The computation of the maximal wind gusts: now also the convective gusts created by downdrafts are considered for determining the maximal gusts in the LM.
- The parameterization of moist convection: to avoid convective drizzle, new thresholds for the minimal moisture convergence and the minimal vertical motion were set in the Tiedtke convection scheme.
- The introduction of cloud ice in GME and LM.

Data Assimilation
At DWD, a comprehensive data assimilation system for LM has been installed. Besides the analysis by observational nudging, three external analyses are run: a sea surface temperature

Table 8: **Configuration of the LM at DWD**

Domain Size	325 x 325 gridpoints
Horizontal Grid Spacing	0.0625° (~ 7 km)
Number of Layers	35, base-state pressure based hybrid
Time Step and Integration Scheme	40 sec, 3 time-level split-explicit
Forecast Range	48 h
Initial Time of Model Runs	00 UTC, 12 UTC, 18 UTC
Lateral Boundary Conditions	Interpolated from GME at 1-h intervals
Initial State	Nudging data assimilation cycle, no initialization
External Analyses	Sea surface temperature (00 UTC) Snow depth (00, 06, 12, 18 UTC) Variational soil moisture analysis (00 UTC)
Special Features	Use of filtered topography, new TKE-scheme new surface-layer scheme, cloud-ice scheme
Model Version Running	lm_f90 3.1
Hardware	IBM SP3 (using 165 of 1280 processors)

(SST) analysis (00 UTC), a snow depth analysis (00, 06, 12 and 18 UTC) and a variational soil moisture analysis (00 UTC).

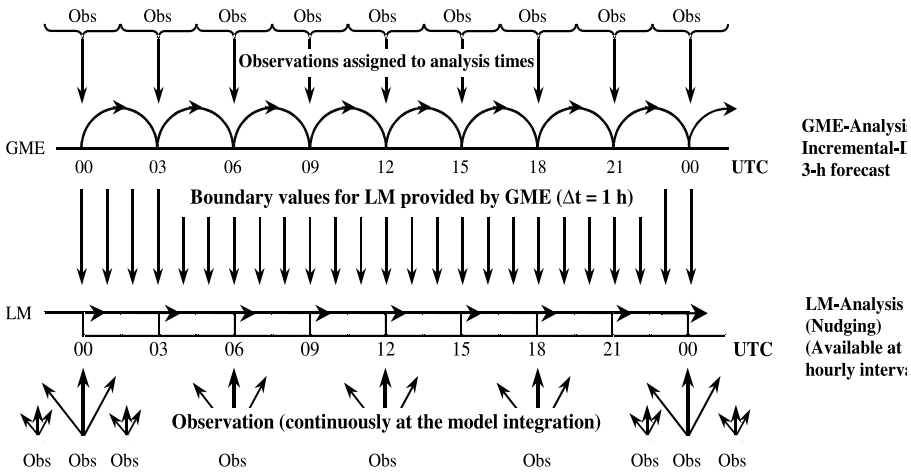

Figure 7: 4-D data assimilation for GME and LM

The data assimilations for the models GME and LM proceed as parallel streams which are coupled only via the boundary data. (see Fig. 7). The GME analysis is based on a 3-D multivariate optimum interpolation (OI) of deviations of observations from 3-h forecasts (first guess), generating an intermittent assimilation cycle with 3-h analysis frequency. All observations within a time window of ± 1.5 hours are considered as instantaneous, i.e. to be valid at analysis time.

The 3-h GME forecasts to produce the first guess are used to generate boundary data at 1-h intervals for the LM assimilation cycle. The nudging scheme produces a continuous analysis stream, where data are assimilated at the time they are observed - but using a time-weighting function to spread the information in time. For practical reasons, 3-hour LM assimilation

runs are done. LM analysis files are written every hour.

Operational Schedule
The operational schedule is structured by data assimilation for GME and LM every three hours, i.e. for 00, 03, 06, 09, 12, 15, 18 and 21 UTC. The data cut-off time for the 00 UTC and 12 UTC model runs of both GME and LM is 2 h 14 min. Based on this analyses, GME performs a 174-h forecast, and LM performs a 48-h forecast. Another 48-h prediction of both models is performed starting at 18 UTC with a data cut-off time of 4 hours. Besides the forecast models, a wave prediction suite comprising a global and a local sea state model (GSM and LSM) is run operationally.

4.3 HNMS (Athens)

Basic Set-Up of LM
The national meteorological service of Greece, HNMS in Athens, operates the LM in a pre-operational mode at 14 km grid spacing. The rotated lat-lon coordinates of the lower left and of the upper right corner of the integration domain are $(\lambda = 4.5°, \varphi = -24.0°)$ and $(\lambda = 16.25°, \varphi = -10.0°)$, respectively. See Figure 5 for this model domain.

Since August 2002, HNMS has utilized its computational resources at ECMWF and operates the LM at the IBM SP on a daily basis at 00 and 12 UTC. The domain is the same as in the one used for the local operation but the grid spacing has been reduced to 7 km. In addition to their regular operational use at the National Meteorological Center, the results were used for the partial support of the first Olympic test event that was held in August 2002 at the Saronic Gulf, South of the Athens Metropolitan area. Table 9 shows the main features of both model set-ups for the greek runs.

Table 9: **Configuration of the LM at HNMS and at ECMWF**

Domain Size	95 x 113 grid points	189 x 225 gridpoints
Horizontal Grid Spacing	0.125° (∼ 14 km)	0.0625° (∼ 7 km)
Number of Layers	35, base-state pressure based hybrid	
Time Step	80 sec	30 sec
Integration Scheme	3 time-level split-explicit	
Forecast Range	48 h	48 h
Initial Time of Model Runs	00 UTC	00, 12 UTC
Lateral Boundary Conditions	Interpolated from GME at 1-h intervals	
Initial State	Interpolated from GME	
External Analyses	None	
Special Features	Use of filtered topography	
Model Version Running	lm_f90 3.5	
Hardware	HP	IBM SP

Figure 8 shows the results for 10 meter winds for a sample of dates where strong winds were prevailing over almost all of Greece and in particular over the sea area.

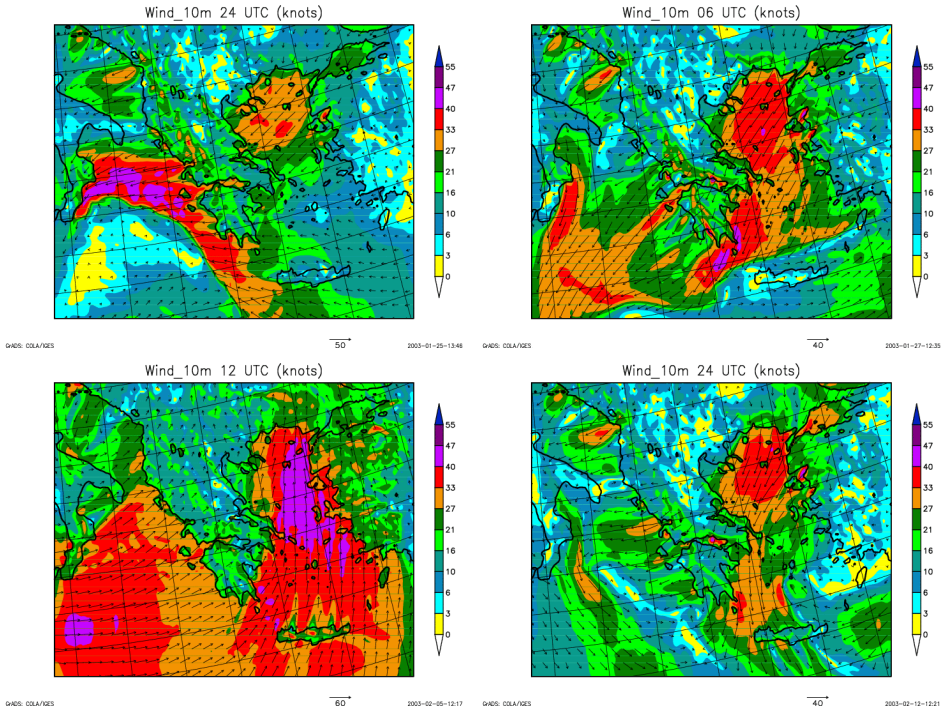

Figure 8: Forecast products used at HNMS, Athens

4.4 IMGW (Warsaw)

Basic Set-Up of LM

The national meteorological service of Poland, IMGW in Warsaw, operates the LM in an operational mode at 14 km grid spacing twice a day (00 UTC and 12 UTC). The rotated lat-lon coordinates of the lower left and of the upper right corner of the integration domain are $(\lambda = -10.0°, \varphi = -16.5°)$ and $(\lambda = 14.0°, \varphi = 3.5°)$, respectively. See Figure 5 for this model domain. The main features of the model set-up are summarized in Table 10.

Table 10: **Configuration of the LM at IMGW**

Domain Size	193 x 161 gridpoints
Horizontal Grid Spacing	0.125° (∼ 14 km)
Number of Layers	35, base-state pressure based hybrid
Time Step and Integration Scheme	80 sec, 3 time-level split-explicit
Forecast Range	72 h
Initial Time of Model Runs	00 UTC and 12 UTC
Lateral Boundary Conditions	Interpolated from GME at 1-h intervals
Initial State	Interpolated from GME
External Analyses	None
Special Features	Use of filtered topography, new TKE-scheme new surface-layer scheme, cloud-ice scheme
Model Version Running	lm_f90 3.5
Hardware	SGI 3800 (using 88 of 100 processors)

The results of the LM forecasts are provided to the Weather Offices and to the RADAR

and HYDRO units of IMGW (also for verification). Figure 9 shows some of these forecast products.

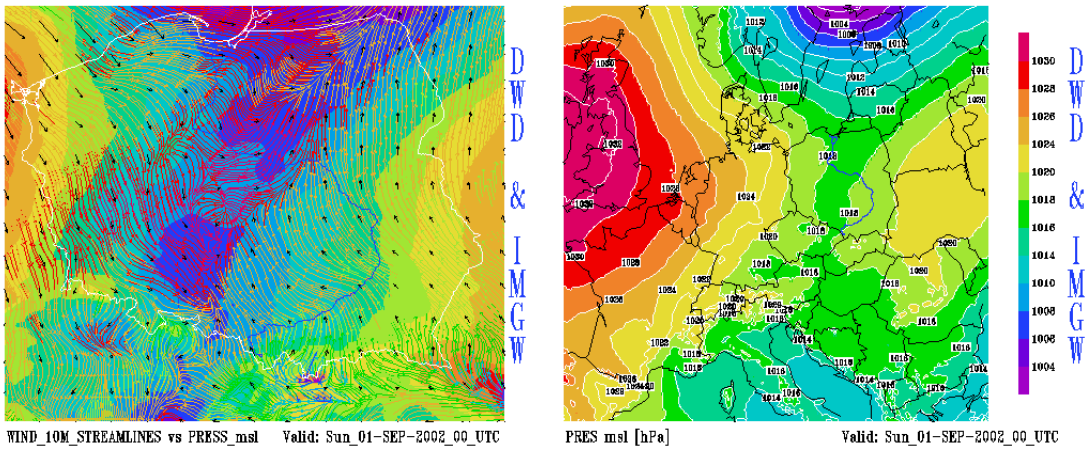

Figure 9: Forecast products used at IMGW, Warsaw

In addition to the operational runs with dx=14 km the LM also runs with a resolution of 7 km, but only for a forecast range of 30 hours.

4.5 MeteoSwiss (Zürich)

The Alpine Model (aLMo) is the operational 7km version of the LM at MeteoSwiss. The model is computed on a NEC SX-5 operated by the Swiss Centre for Scientific Computing (CSCS) in Manno (Tessin). During the operational forecasting slots the SX-5 enters near-dedicated mode: 14 CPUs are then reserved for the model integration and 1 CPU is left for the interpolation of the lateral boundary fields provided by the driving global model. From the global model (Integrated Forecast System, IFS, from ECMWF) only frames are used. The operational suite is controlled by the LM Package. This is a set of shell scripts running on SGI Origin 3000.

Basic Set-Up of aLMo

The aLMo domain extends from 35.11 N, 9.33 E (lower left) to 57.03 N, 23.41 E (upper right). This domain is covered by a grid of 385×325 points with a horizontal resolution of 7 km (see Figure 5). The borders are placed over sea in order to reduce negative interferences generated in the transition zone of the orographies of the driving model (IFS) and aLMo. The main features of the model set-up are summarized in Table 11.

Vertical Coordinates

In operational mode the model runs with 45 levels vertically distributed as shown in Fig. 10.

Hardware and Communications

The computational work of the aLMo suite is managed by 3 systems:

- SUN Enterprise 3000	at MeteoSwiss	(dissemination)
- SGI Origin 3000	at CSCS	(control, pre- and postprocessing, trajectories)
- NEC SX5	at CSCS	(IFS2LM, aLMo, LPDM)

Table 11: **Configuration of the aLMo at MeteoSwiss**

Domain Size	385 x 325 gridpoints
Horizontal Grid Spacing	0.0625° (∼ 7 km)
Number of Layers	45, base-state pressure based hybrid
Time Step and Integration Scheme	40 sec, 3 time-level split-explicit
Forecast Range	72 h
Initial Time of Model Runs	00 UTC and 12 UTC
Lateral Boundary Conditions	Interpolated from IFS at 3-h intervals
Initial State	Nudging data assimilation cycle, no initialization
External Analyses	Merging of LM-DWD snow analysis
Special Features	Use of filtered topography
Model Version Running	lm_f90 3.5+
Hardware	NEC SX5 (using 14 of 16 processors)

Figure 11 shows the present configuration of hardware and communication used for the operational application of aLMo.

Data Flow
All the operational processes are illustrated in the flow diagram of Figure 12. The format of the different products is shown by the different colours of the connections.

LM Package
The operational suite is driven by "LM Package", a software developed at Meteo Swiss. It has a modular structure and is composed by 50 shell scripts. It can be executed in three different modes: operational, test and personal mode. In operational mode preprocessing, aLMo and postprocessing are running concurrently; warnings and exits are transmitted to the permanently on-duty operators, who have the possibility to do manual interventions.

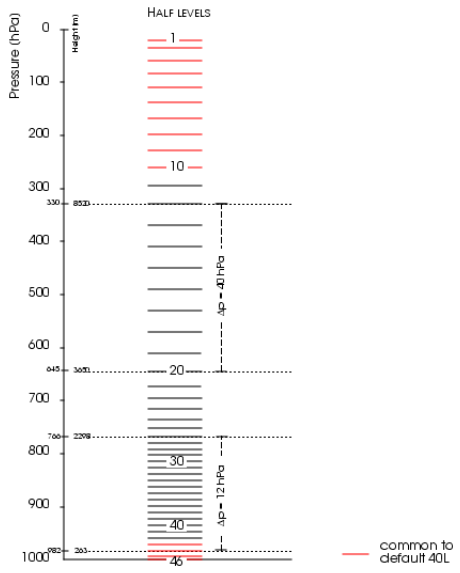

Figure 10: Vertical distribution of levels used at MeteoSwiss

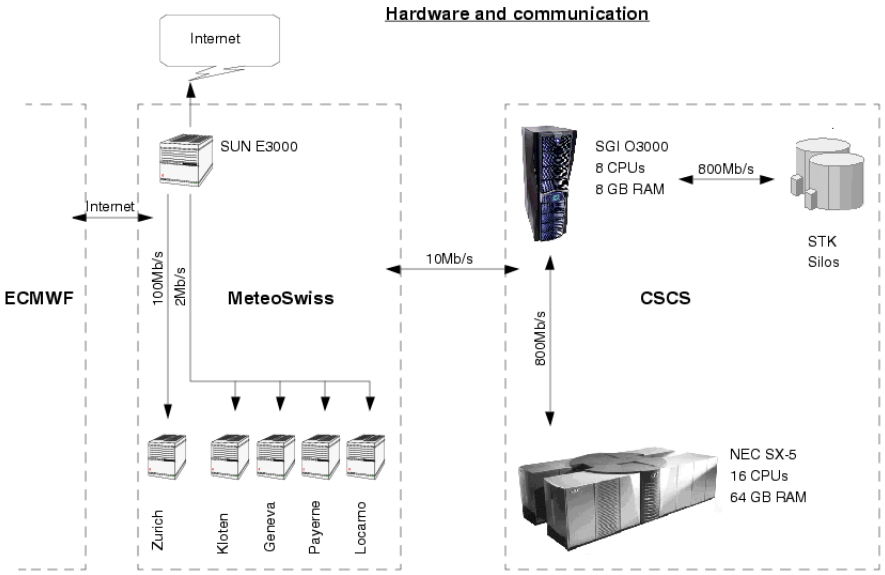

Figure 11: Present configuration of hardware and communications at MeteoSwiss

Products

- 2-D plots: produced by MetView every 3 or 6 hours
- Animations: Hourly loops produced with IDL and AVS
- Tables and extracts of the model output in different formats
- Trajectories
- Concentrations calculated by the LPDM module

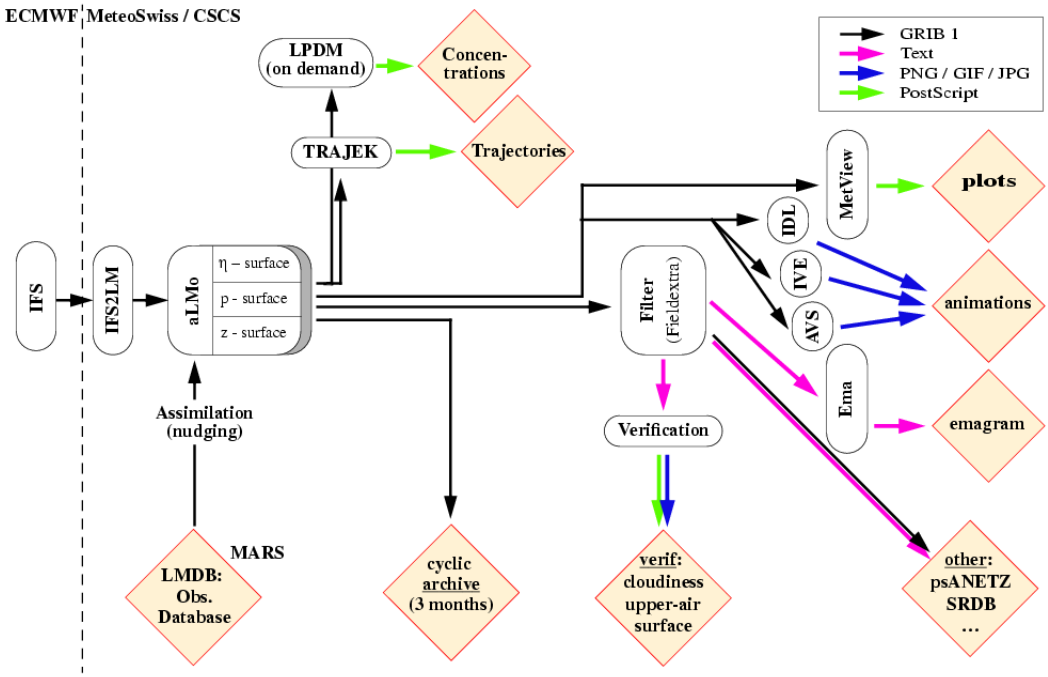

Figure 12: Dataflow of the current operational system at MeteoSwiss

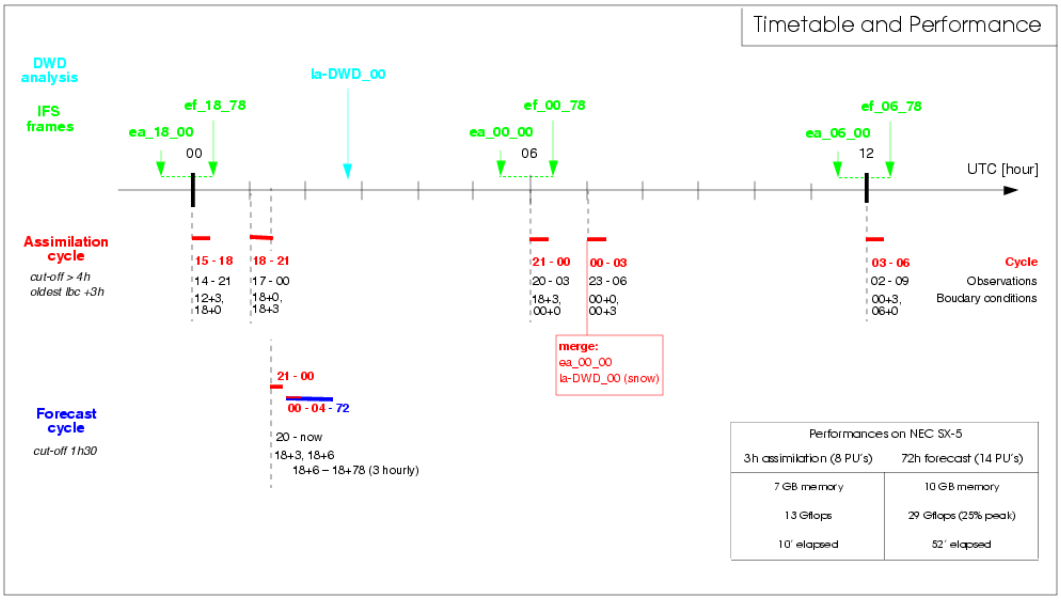

Figure 13: Time table of the aLMo assimilation cycle at MeteoSwiss

Assimilation Cycle

The data assimilation at MeteoSwiss is implemented with 3-hour assimilation runs. aLMo files are written every hour. The cut off time is at least 4 hours. The observations are taken from the aLMo data base, basically a copy of the ECMWF message/report data base. At the beginning of the 00-03 UTC and 12-15 UTC assimilation runs the soil parameters are updated from the IFS analysis. In a similar way the LM snow analysis from DWD is merged into aLMo initial conditions. The schedule for half a day is displayed in Fig. 13.

Time Table

The analysis used by the main 72h forecasts is produced just ahead of the main runs (aLMo forecast) with a 3h run of aLMo in assimilation mode with the IFS frames from 6h earlier (18 or 06 UTC). The boundary conditions in the frames are updated every 3 hours. During the main forecast runs assimilation continues during the first 4 hours. The postprocessing is divided into a time critical and a non time critical part. During the first part the crucial products for Meteo Swiss internal clients (mainly forecasters) are generated and disseminated. During the second part the remaining products for internal and external clients are created. Archiving and statistics take place at the very end of the task. The concurrent processes of the operational production are illustrated in Fig. 14.

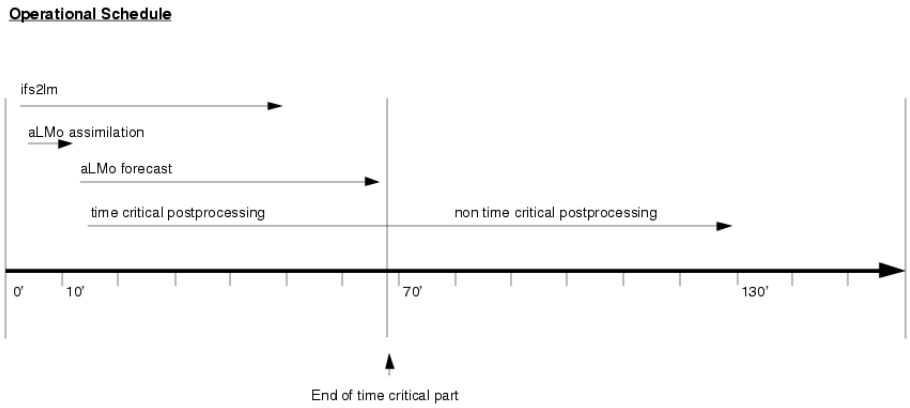

Figure 14: Time table of the operational suite at MeteoSwiss

Verification
The output of the Model undergoes four different types of verification:

- Surface verification: The surface parameters are compared to measurements taken by synoptical and automatic stations.
- Upper air verification: verification of the model against measured radiosonde ascents;
- Cloud verification: verification of the model cloudiness based on METEOSAT visible images.
- Radar verification: verification of the precipitation against swiss radar network measurements.

4.6 COSMO Limited-Area Ensemble Prediction System

The COSMO limited area ensemble prediction system (COSMO-LEPS) based on LM and ECMWF ensemble forecasts has been installed at ECMWF by our colleagues at ARPA-SIM in Bologna (Montani et al., 2003) The system is ready for a quasi-operational trial since November 2002, using 120-h forecasts of 5 LM runs starting at 12 UTC on initial and boundary conditions for 5 representative members of an ECMWF-EPS superensemble. Supervision and scheduling of the suite is done by ARPA-SIM. COSMO-LEPS probability products (derived and processed by the group in Bologna) are ready at about 7.30 GMT. The dissemination to COSMO centres is by GRIB-files.

Basic Set–Up of COSMO–LEPS
Within COSMO–LEPS framework, LM runs operationally at ECMWF using a 10 km grid spacing and 32 vertical layers. The rotated lon–lat coordinates of the lower left and upper right corner of the integration domain are ($\lambda = -12.5^o$, $\varphi = -16.0^o$) and ($\lambda = 14.95^o$, $\varphi = 11.13^o$), respectively. The main features of the model set–up are summarised in Table 12.

Table 12: **Configuration of COSMO–LEPS, run at ECMWF by ARPA-SIM**

Domain size	306 × 258 gridpoints
Horizontal grid spacing	0.09^o ($\sim$ 10 km)
Number of layers	32, basic-state presure based hybrid
Time Step and Integration Scheme	60 sec, 3 time–level split–explicit
Forecast Range	120 h
Initial Time of Model Runs	12 UTC
Lateral Boundary Conditions	Interpolated from EPS members at 6-h intervals
Initial State	Interpolated from EPS members' analyses
Special Features	Use of filtered topography
Model version running	lm_f90 3.5 (since 1/10/2003)
Hardware	IBM p690 clusters (using 84 processors)

Changes in the last year
Since 1/9/2003, a 10–member suite is being experimented. In addition to the 5 LM integrations with the operational convection scheme ("Tiedke runs"), 5 more runs are performed using the recently–implemented Kain–Fritsche convection scheme ("KF runs"). In order to

minimize modifications to the operational suite and to test properly the impact of the new scheme, the 5 KF integrations use the same boundary and initial conditions as the Tiedke runs. Rainfall probability maps using the 10–member suite are being produced and disseminated in addition to the operational ones. The skill of the KF runs as well as the usefulness of a 10–member suite will be evaluated during 2004.

Two test suites started on 1/10/2003 to assess the impact of the clustering–selection technique when either the most recent EPS or the two most recent EPSs are used to select the representative members (when compared to the operational suite when 3 successive EPS sets are employed). The verification will be performed **only** on EPS runs by assessing the performance of the "reduced" EPS, that is the 5–member EPS obtained after the clustering–selection technique.

COSMOE-LEPS Products
A number of probabilistic products have been added in 2003 and some thresholds values and cumulation periods have been changed. At present, the following products are available.

- Probability of 24-h precipitation amount exceeding 1, 20, 50, 100 and 150 mm thresholds.
- Probability of 72-h precipitation amount exceeding 50, 100, 150 and 250 mm thresholds.
- Probability of maximum 2m-temperature above 20, 30, 35 and 40 Celsius thresholds.
- Probability of minimum 2m-temperature below 5, 0, -5 and -10 Celsius thresholds.
- Probability of maximum 10m wind speed above 10, 15, 20 and 25 m/s thresholds.
- Probability of maximum CAPE (in 24 hours) exceeding 2000., 2500., 3000. and 3500. J/kg thresholds.
- Probability of minimum SHOWALTER INDEX (in 24 hours) below 0, -2, -4 and -6 thresholds.
- Probability of minimum 'height of 0 °C isotherm' (HZEROCL) over 24 hours below 1500, 1000, 700 and 300 m thresholds.
- Mean sea level pressure and accumulated precipitation from 5 deterministic LM runs (every 24 hours).
- Geopotential at 700 hPa and temperature at 850 hPa from 5 deterministic LM runs (every 24 hours).

5 Changes to the Model System

In this section, important changes to the LM-system which have been introduced during the last year are briefly described, and the possible impact on the forecast products are summarized. Of course, changes in the host model GME can also have a significant impact on the LM forecasts. Important changes to GME and its data assimilation are summarized below.

- The global analysis is now using PAOB data to improve the GME analysis and forecast in the southern hemisphere. PAOBs (bogus data of sea surface pressure) are provided by the Australian Met. Service based on surface observations and images of polar orbiting satellites. The data are available for 00 and 12 UTC and consist of about 400 "observations" daily. PAOBs are used by the GME data assimilation scheme over the oceans and in extratropical regions only (December 2002).
- An improved quality check for humidity observations of SATEM data has been introduced in the global data assimilation. Before, almost all observations, even "out-layer" were able to enter the humidity analysis of GME. Flagging those observations which differ from the 3-h first guess by more than 40% improved the global analysis and forecasts by up to 6 hours beyond day 5 (March 2003).
- Some modifications have been introduced to the snow depth analysis and the SST analysis schemes. For the new (planned) prognostic treatment of sea ice in the GME, the SST now allows to modify the predicted values of sea ice cover, ice thickness and ice surface temperature according to analyzed values. The global snow depth analysis now uses the NOAA snow cover analysis once a day to adapt the first-guess snow depth in regions with no measurements. For a more realistic estimate of the snow albedo, a new variable has been introduced, the "fresh snow factor" (September 2003).
- Cloud ice content is introduced as a new prognostic variable (in both GME and LM) allowing for a better description of upper-air atmospheric humidity and of the cloud–radiation feedback (September 2003).
- The operational global data assimilation now uses also MODIS data. These are wind vectors in polar regions which are derived from measurements of the "Moderate Resolution Imaging Spectroradiometer" instrument of the polar orbiting Terra and Aqua satellites. An impact study has shown a neutral impact of these data for the northern hemisphere, but a noticeable positive impact for the southern hemisphere (December 2003).
- Since 17 December 2003, the GME data assimilation runs with Pseudo-Temps derived from ECMWF IFS-fields. Pseudo-Temps are vertical profiles of temperature, wind and humidity, which are calculated over sea (at about 9150 points) and over the antarctic region (350 points) from ECMWF analyses at 00 UTC. The spatial distance of this "observations" is about 190 km, and they are assimilated similar to radiosonde data. In the GME data assimilation cycle, Pseudo-Temps are included once a day in the final 00 UTC analysis to improve the first guess for the main runs. Parallel assimilation experiments for the spring period 2003 and for the autumn/winter period 2002/2003 revealed a significant positive impact on GME forecasts.

For more detailed information on changes to GME and its data assimilation, please refer to the *Quarterly Report of the Operational NWP-Models of the Deutscher Wetterdienst* (available at `www.dwd.de`).

5.1 Major Changes to LM

Cycle 3 of the LM software library lm_f90 was introduced in February 2003. The model version 3.1 was defined as the latest reference version, containing a number of new features and significant changes to the model code as e.g. the implementation of a new multi-layer soil model, the Kain-Fritsch convection scheme, the SLEVE vertical coordinate, frames as lateral boundary conditions, a scheme for prognostic treatment of the precipitation phases for optional use within the 2 time-level integration scheme, and extensions in both the nudging analysis scheme and the model diagnostic output.

During 2003/04 a number of updates have been introduced. The changes up to version 3.7 are described below. The main features are – besides code optimization and bug corrections – a new option to assimilate GPS data, a new version of the multi-layer soil model with modified organization and data handling, the implementation of prognostic precipitation within the Leapfrog time integration scheme, the introduction of a new dynamical core using 3rd-order Runge-Kutta time integration, and the generation of synthetic satellite images using the RTTOV library.

Notes on lm_f90 Version 3.1

This version was created on 3 February 2003. It is formal identical to the version 2.19 from October 2002.

Notes on lm_f90 Version 3.2

This version was created on 7 February 2003. The cloud ice threshold for autoconversion is set to 0 (in subroutine `hydci` of module `src_gscp.f90`), to improve the performance of the cloud ice scheme (analogous to changes made for the global model GME).

Besides, some optimizations have been performed in the communications. The computations for the horizontal diffusion, which are identical in the leapfrog-scheme and the 2timelevel scheme have been put to a new external subroutine `hori_diffusion.f90`.

Also, it is now possible to work with boundary data defined on frames and with Rayleigh damping. For that, a new NAMELIST variable `ilevbotnoframe` has been introduced. For the first `ilevbotnoframe` levels, the boundary data has to be specified for the full grid. (These changes are based on the work of Lucio Torrisi, UGM Rome).

Notes on lm_f90 Version 3.3

This version was created on 22 April 2003. It introduces the option to assimilate GPS data, the possibility to use bias-corrected radiosonde humidity, and a bug correction on output fields used for operational postprocessing.

- Nudging of GPS data:
  Introduction of an option to assimilate integrated water vapour (TQV) from ground-based GPS data. The GPS observations are read from a dedicated ASCII file named 'gps' in COST 716 format. 'Observed' humidity profiles derived from TQV by scaling model humidity profiles are nudged like radiosonde humidity profiles. (The horizontal correlation scale is set to a fixed value of 0.45 of that used for radiosondes.) The following new NAMELIST variable have been defined.

Parameter	Definition / Purpose
gnudggp	Nudging coefficient for GPS data
maxgpo	Maximum number of GPS data
lgps	Data of observation type GPS used in exclusion area
lcd096	Data of code type GPS used in exclusion area
lgpsbias	Bias correction applied to GPS data

Note that the NAMELIST of previous versions does not need to be changed as long as GPS data are not used.

- Nudging:
  Additional code number in instrument specification for reports with bias-corrected (Vaisala RS80) radiosonde humidity. The bias correction itself is done in MAKEAOF / BUFR2AOF.

- Bug corrections:
  An error in the routine `calclmod` of module `pp_utilities` to calculate a modified cloud cover being used for operational graphical presentations was corrected.

Notes on lm_f90 Version 3.4

This version was created on 25 June 2003. It contains small changes in the Tiedtke convection scheme (`src_conv_tiedtke.f90`) to suppress "convective drizzle". A minimum moisture convergence and a minimum grid-scale lifting are now used to initiate moist convection and the formulation of precipitation formation in the updraft has been changed.

Notes on lm_f90 Version 3.5

This version was created on 2 September 2003. It contains changes to the interpretation of cloud cover and to the model diagnostics, an implementation of the total zenith delay (for GPS assimilation) and a number of optimizations for the communications.

- Interpretation of cloudiness:
  A modification in the radiation scheme related to the interpretation of cloud cover when running with the cloud ice scheme has been introduced. The formulation has also been adapted to the global model GME.

- Restructuring of the diagnostics (the YU* files):
  The modules `src_diagnosis.f90` and `src_differences.f90` have been eliminated from the source code, because the corresponding options have not been applied by most of the users. Note:
  All NAMELIST variables for these routines have to be removed from the NAMELIST group `/DIACTL/`. These are `ldia`, `n0dia`, `h0dia`, `nincdia`, `hincdia`, `istartdia_tot`, `jstartdia_tot`, `ienddia_tot`, `jenddia_tot`, `ldiffdia`, `n0diffdia`, `h0diffdia`, `nincdiffdia`, and `hincdiffdia`.

- Gridpoint output:
  The grid point output (long and short form) has been adapted to include cloud ice and to use new (English) variable names. Note that the format of the short and long grid point output forms has also been changed.

- Implementation of zenith total delay:
  A routine `calztd` has been added to the module `pp_utilities.f90` to compute the total (ZTD), the wet (ZWD) and the hydrostatic (ZHD) zenith delay for the GPS signal through the atmosphere (ZTD = ZWD + ZHD). All 3 variables can be chosen as additional GRIB output fields. They are implemented in the DWD GRIB table 202 as element numbers
  121: ZTD, 122: ZWD, 123: ZHD
  with level type = 1 (two-dimensional fields).

- Optimizations for the communications:

  – The global communication in the radiation scheme for computing the maximum of `zmaxmu0` has been eliminated by computing `zmaxmu0` for a whole latitude in every processor.

  – The two global communications in routine `org_leapfrog` have been combined into one call.

  – The boundary exchange for the surface pressure in the main program `lmorg.f90` and in routine `dfi_initialization.f90` has been eliminated. The surface pressure is now computed in routine `near_surface.f90` for the whole domain (before it was computed in `src_relaxation.f90` for the interior domain).

  – In routine `dfi_initialization`, a bug has been corrected for the communication of variables for the convection scheme.

- Optimizations for the boundary exchange:
  Several kinds of performing the communication for the processor boundary data exchange have been implemented.

  – Up to now only an explicit buffering of the data to a sending buffer (`sendbuf`: using routines `putbuf` and `getbuf`) and an immediate send (MPI_Isend) together with a blocking receive (MPI_Recv) has been realized.

    Now there is the choice of the explicit buffering or an implicit buffering by using MPI-datatypes. For every boundary exchange an MPI-datatype is defined and the buffering can then be done implicitly by the system (and at least on the IBM more efficiently).

    The buffering can be chosen with the new NAMELIST parameter `ldatatypes` in the group `/RUNCTL/`:

Parameter	Value	Definition / Purpose
`ldatatypes`	.TRUE.	implicit buffering
	.FALSE.	explicit buffering (this is the default)

  – The exchange can then be done using one of the three kinds:
    1) immediate send, blocking receive and wait on the sender side
    2) immediate receive, blocking send and wait on the receiver side
    3) using MPI_Sendrecv
    The type of communication for the boundary exchange can be chosen by the new NAMELIST parameter `ncomm_type` in the group `/RUNCTL/`, which can be 1, 2 or 3. The default is `ncomm_type` = 1.

  – In addition, most barriers for the time-measurement can now be switched off by setting the new NAMELIST parameter `ltime_barrier` to .FALSE. The default is `ltime_barrier` = .TRUE. (as it was up to now).

The defaults of the three new NAMELIST parameters are set in a way that the boundary exchange is done in the same way as before:
(`ldatatypes` = .FALSE., `ltime_barrier` = .TRUE. and `ncomm_type` = 1).

The new options can be tested on every machine to check if a gain in runtime performance can be achieved. On the IBM we see a gain in forecast mode of up to 10 percent by setting
`ldatatypes` = .TRUE., `ltime_barrier` = .FALSE., `ncomm_type` = 3.

Notes on lm_f90 Version 3.6

This version was created on 11 December 2003. It contains changes to the new soil model, the digital filtering algorithm, the data assimilation and a number of optimizations for vector computers.

- New multi-layer soil model:
  Besides an updated version of `src_soil_multlay.f90`, the whole organization and data handling for the new multi-layer soil model has been changed.
  - The new variables `T_SO`, `W_SO` and `W_ICE` are coded with leveltyp 111 and octet(8) of the product definition section (is pds(10)) gives the depth of the layer in centimeters.
    NOTE: At DWD the first layer is chosen to be in the depth of 0.5 cm. This cannot be coded correctly, so it will be coded with 1 cm.
  - The multi-layer soil model can be switched on by setting the following NAMELIST variables (in group `/PHYCTL/`):
    `lmulti_layer` =.TRUE.,
    `ke_soil` = 7,
    `czml_soil` = 0.005, 0.02, 0.06, 0.18, 0.54, 1.62, 4.86, 14.58.
    The values for `ke_soil` and `czml_soil` are the default values chosen for the global model GME at DWD. The LM must run with the same layers, because there is no vertical interpolation of soil layers yet.
    NOTE: The values for `czml_soil` are given in meters!

- Digital filtering:
  Some bug corrections in routine `dfi_initialization.f90` have been done. When setting the boundary values for the adiabatic backward integration, there was no check, whether the moisture variables (qv, qc, qi) remain positive definite. With cloud ice (qi) switched on, it could happen that negative values of qi occurred. This is avoided now.

  Also, the possibility to use frames for the boundary values has now been introduced.

- Changes in the data assimilation:
  A new option to assimilate single SATOB winds similarly to aircraft winds has been introduced. Also, modifications to assimilation of GPS-derived Integrated Water Vapour (TQV) have been implemented:
  - new NAMELIST variable `rhfgps` for horizontal correlation scale,
  - extrapolation below orography for determination of TQV increments,
  - revised ice-to-water correction of TQV (for model version without cloud ice),
  - revised GPS observation error flag in the VOF.

Additionally, some minor bug corrections and modifications within the nudging scheme have been done:

- no further bias correction of Vaisala RS80 bias-corrected humidity data,
- default for NAMELIST variable `tconbox` doubled,
- improved general, statistical, warning, and error messages (and ensuring the printing of error messages at calls of routine `model_abort`).

- Checks of the IOSTAT-values:
  Checks of the IOSTAT-values when reading the NAMELIST-groups have been introduced. These values have not been checked before, but the IBM does not abort when errors occur while reading a NAMELIST group. So the IOSTAT-values are now checked and the program is aborted by routine `model_abort` in case of errors.

  NOTE: For that reason the handling of reading the different groups for `/GRIBOUT/` had to changed! To know how many different groups have to be read by the program, a new NAMELIST parameter `ngribout` (number of different groups `/GRIBOUT/` for GRIB output has been introduced in the group `/IOCTL/`. The default is `ngribout` = 1. If you want to have more groups for `/GRIBOUT/`, you have to change this value.

- Optimizations for vector computers:
  There were some suggestions by NEC (Switzerland and Germany) for optimizations of the LM code when running on vector processors.

  - `src_gscp.f90`
    Most of the power-functions (a**b) have been replaced by EXP-LOG calls (since $a^b = \exp(b \ln a)$). This is faster also on the IBM.
  - `src_sing_spread.f90`
    A loop has been splitted into 2 single loops for better vectorization.
  - `turbtran.incf`
    Modification of 2 DO-WHILE loops in order to enable vectorization of DO-loops contained.
  - `coe_so.incf` and `coe_th.incf`
    In both routines all the loops contained are combined into one single loop. This reduces the number of temporary arrays and memory traffic.

Notes on lm_f90 Version 3.7

This version was created on 18 February 2004. It contains three new features and a number of modifications in the existing code.

The three new features are:

- Prognostic treatment of rain and snow in the default 3 timelevel Leapfrog scheme.
- Additional options for the 2 timelevel Runge-Kutta integration scheme.
- Computation of synthetic satellite images (for Meteosat7 and MSG).

And the modified features are:

- Renaming of some GRIB names (important for NAMELIST input and GRIB I/O).

- Adaptations in the TKE-scheme.
- Choice of precipitation scheme (NAMELIST variable `itype_gscp`).
- Check of humidity variables and setting to zero, if they are too small.

The new NAMELIST input parameters related to these changes are listed in the following table.

Group	Parameter	Default	Definition / Purpose
RUNCTL	luse_rttov	.FALSE.	to switch on/off the synthetic satellite images
PHYCTL	rat_sea	1.0	laminar scaling factor for heat over sea and land
	lprogprec	.FALSE.	prognostic treatment of rain and snow for 3-timelevel and 2-timelevel integration schemes
	ltrans_prec	.TRUE.	to switch on/off the 3-d transport of rain and snow (if prognostic treatment of precipitation is switched on)
DYNCTL	irunge_kutta	0	for choosing the type of Runge-Kutta scheme
	irk_order	2	choosing the order of the scheme
	iadv_order	3	choosing the order for the horizontal advection
	hd_corr_u	1.0	correction factor for horizontal diffusion flux of u,v,w
	xkd	0.1	coefficient for divergence damping
	lvertad_impl	.TRUE.	for switching on/off implicit vertical advection in the Runge-Kutta-scheme

To be consistent with GME and other models, some GRIB variable names have been changed. This affects the NAMELIST Group `GRIBOUT`.

Old name	New Name	Meaning
GPH	FI	Geopotential height
IWV	TQV	Total column water vapour
IQI	TQI	Total column cloud ice
IQC	TQC	Total column cloud water
IWATER	TWATER	Total column water
IDIV_HUM	TDIV_HUM	Total column humidity convergence
GZ0	Z0	Dynamical roughness length
ALB	ALB_RAD	Surface albedo
PHI	RLAT	Geographical latitude
RLA	RLON	Geographical longitude

Also some internal variable names dealing with values for latitudes and/or longitudes have been changed for the same reason (rla → rlon, phi → rlat, tgphi → tgrlat, cphi → crlat, acphir → acrlat). In the following, we describe the new features and the modifications in more detail.

- Prognostic treatment of rain and snow
  A Prognostic treatment of rain and snow for use in the 3 timelevel Leapfrog scheme has been implemented. The corresponding budget equations are solved by time-splitting: First, 3-d transport with the wind field is done by a semi-Lagrangian advection scheme (over a $2\Delta t$ time interval); a corresponding transport routine has been implemented in the dynamics. In a second step, the transported variables are then updated due to microphysics and fallout; a corresponding precipitation scheme `hydci_pp` has been added in the module `src_gscp.f90`. The time integration for cloud ice has also been changed: To avoid inconsistencies in the thermodynamic feedback, cloud ice is also advected over a $2\Delta t$ interval from time level $n-1$ to $n+1$ by applying the positive advection scheme twice (this replaces the former hybrid integration, where cloud ice is integrated from n to $n+1$).

  The new scheme can be switched on with the new NAMELIST parameter `lprogprec` (in the group `PHYCTL`). The only possible choice for the microphysics scheme is then `itype_gscp = 3` (see below: treatment of `itype_gscp`). Optionally, the 3-d transport can be switched off by setting `ltrans_prec` to `.FALSE.`. In this case, only fallout and microphysical sources and sinks are treated prognostically.

- New Runge-Kutta options in the 2-timelevel integration scheme
  In addition to the existing 2-timelevel scheme in the module `src_2timelevel.f90` (by Almut Gassmann), normal Runge-Kutta variants of 2nd- and 3rd-order in time as well as a slightly more sophisticated 3rd-order TVD-Runge-Kutta (total variation diminishing) scheme have been implemented in the new module `src_runge_kutta.f90`. In contrary to the scheme by Almut Gassmann, the Runge-Kutta time-loop contains the effects of the complete slow tendencies (especially the full 3-d advection is computed in each Runge-Kutta-step). The integration of the small time steps is done in the new routine `fast_waves_rk.f90`. The type of scheme is set with the new NAMELIST-Parameter `irunge_kutta`:

  0: Scheme by Almut Gassmann,
  1: Normal Runge-Kutta scheme,
  2: TVD Runge-Kutta scheme.

  In case of the normal Runge-Kutta scheme (i.e. only for `irunge_kutta=1`, the order in time can be chosen from 1st, 2nd and 3rd order by setting the new NAMELIST-Parameter `irk_order` correspondingly (value: 1, 2 or 3). For the TVD-scheme, only the 3rd-order in time variant is possible.

  In addition, the order in space of the operator for the horizontal advection of the variables u, v, w, pp and T can be chosen from 3rd, 4th, 5th and 6th order space discretization by setting the NAMELIST-Parameter `iadv_order` correspondingly (value: 3, 4, 5 or 6).

  At the moment, we recommend the use of the 3rd-order Runge-Kutta TVD-scheme with 5th-order horizontal advection. This scheme is activated by switching the 2-timelevel integration scheme on (with `l2tls=.TRUE.`) and setting `irunge_kutta=2`, `irk_order=3`, `iadv_order=5`.

- Computation of synthetic satellite images (for Meteosat and MSG)
  An interface to the RTTOV7-library (the Radiative Transfer Model) has been introduced into the LM. This interface has been developed at the DLR Institute for Atmospheric Physics in Oberpfaffenhofen. With this interface and the RTTOV7-library it is possible to compute "synthetic" satellite images (brightness temperatures and radiances) derived from model variables for Meteosat5-7 and Meteosat Second Generation. The RTTOV7-library has been developed by UKMO et.al. in the framework

of the ESA NWP-SAF. To use the RTTOV7 library, a license is necessary. To switch on/off the computation of the synthetic satellite images, a new NAMELIST Variable `luse_rttov` has been introduced (in group `RUNCTL`). If `luse_rttov=.TRUE.`, an additional NAMELIST group `SATCTL` is read in, in which additional control variables can be set. For a detailed description of the interface and the NAMELIST parameters, see the User Guide (not yet ready).

Besides these new features, some modifications were introduced in the existing schemes. These are described below.

- A NAMELIST variable `rat_sea` has been introduced to set the ratio of the laminar scaling factor for the heat and moisture surface fluxes over sea and land. Default for this variable is `rat_sea = 1.0`. A factor in the computation of the stability-function "sm" (in the file `stab_funct.incf`) has also been changed.
- The treatment of the NAMELIST variable `itype_gscp` to select a specific parameterization scheme for precipitation formation has been changed. Up to now it was as follows.

itype_gscp	Selection	Subroutine	Valid for integration scheme
1	Warm Rain Scheme (diagnostic rain)	`kessler`	2 and 3 timelevels
2	Rain/Snow Scheme (diagnostic rain and snow)	`hydor`	2 and 3 timelevels
3	Cloud Ice Scheme (diagnostic rain and snow)	`hydci`	2 and 3 timelevels
4	As 2, but with prognostic rain and snow	`hydorprog`	2 timelevels only
5	As 3, but with prognostic rain and snow	`hydciprog`	2 timelevels only

In order to be more flexible later on and to avoid too many numbers for `itype_gscp` applying for different model set-ups, some new parameters have been introduced. Now the treatment is as follows: Valid values for `itype_gscp` are 1, 2 and 3. Prognostic treatment of rain and snow can be switched on/off with the new NAMELIST parameter `lprogprec`. Depending on the value for `l2tls` (to choose between 2- and 3-timelevel integration scheme), `lprogprec` and `itype_gscp`, the following routines are called:

	l2tls = .FALSE.		l2tls = .TRUE.	
lprogprec:	.FALSE.	.TRUE.	.FALSE.	.TRUE.
itype_gscp				
1	kessler	–	kessler	–
2	hydor	–	hydor	hydorprog (if irunge-kutta = 0)
3	hydci	hydci_pp	hydci	hydciprog (if irunge-kutta = 0) hydor_pp (if irunge-kutta > 0)

Depending on `itype_gscp`, an internal logical switch `lprog_qi` is set, with which the LM will determine, whether cloud-ice treatment is switched on or off.

- In the main program `lmorg.f90`, a check of all humidity variables (qv, qc, qi, qr, qs, qrs) has been introduced: if these variables become too small (< 1.0E-15), they are set to zero.
- A new NAMELIST parameter `hd_corr_u` to control the horizontal diffusion of the wind speeds (default 1.0) has been introduced in the group `DYNCTL`.

In addition, some technical changes have been implemented.

- The optimization of the power functions in `src_gscp` (replaced by EXP(... * LOG(..)) had to be modified. This must only be done, if the argument for the LOG-function is not zero.
- The routine for the boundary exchange (`exchg_boundaries`) has been enlarged to exchange up to 24 variables at the same time.
- A consistent treatment of unit-numbers for ASCII-files has been introduced to avoid that the same unit number is used twice in the model. For that purpose, 2 new routines have been introduced in the module `environment.f90`.

  `get_free_unit(iunit)`: returns a unit-number (between 21 and 100), which is not yet used. If `iunit` < 0, no more free unit number is available.

  `release_unit(iunit)`: sets the unit-number free again.
- The routine `model_abort` (in the module `environment.f90`) has been changed, so that now also processors with id $\neq 0$ can write error messages. But still, if an error in processor 0 occurs, this is the first and only processor that will report the error. All processors with id $\neq 0$ first sleep for 30 seconds. Their processes are either killed by processor 0 or they will report their errors then. If processor 0 gets an error, it will close all files with unit numbers determined by the new routine `get_free_unit`.

Planned Releases

Also in 2004, there will be a number of new model versions – not only due to error corrections and optimizations, but also due to the changes in the new physics packages and changes in the model dynamics. By now, the following releases are planned.

- Code modifications (mainly organizational) to run LM in climate mode
- Optimizations for the new RK3 time integration scheme
- Implementation of new physics for the high-resolution LM
- Code re-organization and optimization of the TKE-scheme
- Code re-organization and optimization of the asynchronous I/0.

5.2 Major Changes to GME2LM

The interpolation program GME2LM has been changed only once in 2003 to modify variables related to the new multi-layer soil model, to do some additional security checks and to optimize the data exchange between processors.

Notes on GME2LM Version 1.18

This version of GME2LM was created on 21 October 2003. It contains changes in the calculation of the new multi-layer soil variables. These variables are now defined on the main levels (half levels before).

More checks when reading the NAMELIST variables have been implemented. When the specified file for the LM external parameters cannot be found, the program aborts now (before, the external parameters have then been interpolated from GME external parameters). Only when the specified file name is 'interpolate', and such a file does not exist, the external parameters still are interpolated from GME.

The boundary exchange for the parallel program has been re-written in the same way as in LM version 3.6. There now is the choice between an implicit data buffering using MPI Datatypes (new NAMELIST variable `ldatatypes` =.TRUE.) or the (old) explicit buffering (`ldatatypes`=.FALSE.)

The exchange can then be done using one of the three kinds:
1) immediate send, blocking receive and wait on the sender side
2) immediate receive, blocking send and wait on the receiver side
3) using MPI_Sendrecv

The type of communication for the boundary exchange can be chosen by the new NAMELIST parameter `ncomm_type` in the group `/CONTRL/`, which can be 1, 2 or 3. The default is `ncomm_type` = 1. (see also LM Version 3.5)

6 Working Groups

COSMO's scientific and technical activities are organized in *Working Groups* (WG) which cover the main research areas related to a NWP-system. Each Working Group is headed by a *Work Package Coordinator* (WPC), who is responsible for the consistency of the execution of the work packages and for the coordination, planning, and supervision of the scientific and technical activities related to the work packages in his group.

This section gives an overview on the current personnel composition of the WGs. All scientists contributing actively to the work packages are included in the lists, also those from outside COSMO member institutions. For each WG, the main research activities from the recent COSMO period (Oct 2002 - Oct 2003) are briefly summarized and a short note on the planned activities for the present period (Oct 2003 - Oct 2004) is given. The work plan lists as well as a detailed description of each work package within a WG, are available at the member area of our web-site.

6.1 Working Group 1: Data Assimilation

This working group considers various aspects of 4-dimensional assimilation of observation data using the nudging analysis technique. For soil moisture and some surface fields, a set of 2-dimensional intermittent analysis schemes is applied in addition. The group is headed by Christoph Schraff (DWD) as WPC. The following scientists are members of this group.

Name	Institution	e-mail
Jerzy Achimowicz	IMGW	jerzy.achimowicz@imgw.pl
Jean-Marie Bettems	MeteoSwiss	jean-marie.bettems@meteoswiss.ch
Massimo Bonavita	CNMCA	bonavita@meteoam.it
Michael Buchhold	DWD	michael.buchhold@dwd.de
Davide Cesari	ARPA-SMR	dcesari@smr.arpa.emr.it
Francesca di Giuseppe	ARPA-SMR	fdigiuseppe@smr.arpa.emr.it
Reinhold Hess	DWD	reinhold.hess@dwd.de
Stefan Klink	DWD	stefan.klink@dwd.de
Blazej Krzeminski	IMGW	blazej.krzeminski@imgw.pl
Martin Lange	DWD	martin.lange@dwd.de
Daniel Leuenberger	MeteoSwiss	daniel.leunenberger@meteoswiss.ch
Joanna Linkowska	IMGW	joanna.linkowska@imgw.pl
Fabrizio Nerozzi	ARPA-SMR	fnerozzi@smr.arpa.emr.it
Andrea Rossa	MeteoSwiss	andrea.rossa@meteoswiss.ch
Christoph Schraff	DWD	christoph.schraff@dwd.de
Klaus Stephan	DWD	klaus.stephan@dwd.de
Friedrich Theunert	AWGeophys	friedrichtheunert@awg.dwd.de
Antonio Vocino	CNMCA	vocino@meteoam.it

- A main focus was on the assimilation of radar-derived precipitation by means of latent heat nudging (LHN). Sensitivity experiments have been performed both in an OSSE framework for an idealised supercell storm and in real-case studies on a 7 km and 2.8 km resolution. Better results are obtained when convection is simulated explicitly rather than parameterised, and when the humidity is also adjusted (see *Assimilation of Radar Data in the LM at DWD* by S. Klink and K. Stephan in Section 9). In the real cases, the positive impact of LHN disappears after 3 to 6 hours of free forecast.

- The work on the assimilation of ground-based GPS-derived total precipitable water (PW) ceased in early 2003. It included the conduction of parallel assimilation cycle and forecast experiments for several periods. In one period, a bias correction was applied to account for a summerly diurnal wet bias of the observed PW relative to the model forecasts. This decreased a tendency to overestimate precipitation. While the statistical impact of the GPS data was found to be neutral to positive, except for cloud cover in low status periods, there were also individual cases with distinct negative impact on precipitation forecasts. A key factor to these problems is the vertical distribution of the PW information. It requires further efforts (or imposing restrictions) before operational use of the GPS data.
- Work has started to derive retrievals of temperature and humidity profiles from NOAA polar orbiting satellite data by means of a 1DVAR package from NWP SAF. Yet in the first place, this is done to be used in a 3D-PSAS data assimilation for lower-resolution HRM applications.
- Work has also started to derive statistically based vertical and horizontal correlation or weight functions for the nudging-type scheme by means of radiosonde observations.

In 2004, the development work to use satellite data will be intensified, partly with some delay to original plans. The 1DVAR approach will be applied also to MSG data and in the framework of the nudging-type scheme for the LM. Cloud information based on satellite data as well as conventional data will also be striven to be assimilated. Some effort can be redirected to the use of GPS-derived PW, and the other work packages mentioned above will be continued. Furthermore, the variational soil moisture analysis scheme will be extended, the temporal nudging weights tuned, and the snow analysis improved.

(Christoph Schraff, DWD)

6.2 Working Group 2: Numerical Aspects

The WG on numerical methods and basic model dynamics is headed by Jürgen Steppeler (DWD) as WPC. Currently, the following scientists are members of this group.

Name	Institution	e-mail
Michael Baldauf	DWD	michael.baldauf@dwd.de
Heinz-Werner Bitzer	AWGeophys	heinz-werner.bitzer@dwd.de
Davide Cesari	ARPA-SMR	dcesari@srm.arpa.emr.it
Günther Doms	DWD	guenther.doms@dwd.de
Jochen Förstner	DWD	jochen.foerstner@dwd.de
Almut Gassmann	DWD	almut.gassmann@dwd.de
Guy de Morsier	MeteoSwiss	guy.demorsier@meteoswiss.ch
Tiziana Paccagnella	ARPA-SMR	tpaccagnella@smr.arpa.emr.it
Jan Parfiniewicz	IMWG	jan.parfiniewicz@imgw.pl
Peter Prohl	DWD	peter.prohl@dwd.de
Georgios Sakellaridis	HNMS	sak@hnms.gr
Ulrich Schättler	DWD	ulrich.schättler@dwd.de
Jürgen Steppeler	DWD	juergen.steppeler@dwd.de
Lucio Torrisi	UGM	torrisi@ecmwf.int

The main research activities of WG 2 for the period Oct 2002 - Sep 2003 and the planned activities for the current year are summarized below.

- Experiments done using the two time level Version of LM indicate that the introduction of a prognostic precipitation scheme, which takes account of the horizontal advection, reduces the systematic error of the precipitation forecast considerable. It is planned to use the prognostic precipitation within the current three time-level scheme. In order to be useful it is planned to develop the operational scheme rather fast, in order that it has a useful production time before the LM will change to a high order two time level scheme.

- It is planned to develop a high order discretization scheme for LM. Order 3 in time and probably order 5 in space are planned. This development will be based on the third order Runge Kutta time discretization scheme. With high resolution applications of LM this scheme is expected to give a sufficient amount of accuracy in order to be able to forecast the interesting scales with enough reliability.

- The Z-coordinate version of LM is expected to give better forecasts of a horizontally stratified atmosphere. High fog and orographically induced winds should be forecasted better than with terrain following models. For the current year key developments are the harmonising of the semi Lagangian and Euler Z-LM as well as the beginning of realistic tests of the z-concept. The aim of these tests is to show that the Z-LM has advantages and no disadvantage as compared to the terrain following LM. Questions of operational efficiency will be followed in a large time frame. For these the semi-Lagrangian version could turn out to be essential.

- Questions of the performance of LM in the tropics are still open and will be followed in the current year.

- Further questions to be investigated are the LM performance on large domain size, questions of vertical discretization abd alternative formulations of the dynamic equations.

(Jürgen Steppeler, DWD)

6.3 Working Group 3: Physical Aspects

The main effort of this working group is to develop new physics packages for future operational applications and to improve existing parameterisations. The WG on physical processes, which is coordinated by Marco Arpagaus (MeteoSwiss), has grown substantially since the publication of the last Newsletter and currently consists of the following scientists:

Name	Institution	e-mail
Euripides Avgoustoglou	HNMS	euri@hnms.gr
Marco Arpagaus	MeteoSwiss	marco.arpagaus@meteoswiss.ch
Giovanni Bonafè	SMR Emilia-Romagna	gbonafe@smr.arpa.emr.it
Claudio Cassardo	Università di Torino	cassardo@ph.unito.it
Günther Doms	DWD	guenther.doms@dwd.de
Grzegorz Duniec	IMGW	grzegorz_duniec@imgw.pl
Marco Elementi	SMR Emilia-Romagna	melementi@smr.arpa.emr.it
Almut Gassmann	Universität Bonn	almut.gassmann@uni-bonn.de
Erdmann Heise	DWD	erdmann.heise@dwd.de
Hans-Joachim Herzog	DWD	hans-joachim.herzog@dwd.de
Witek Interewicz	IMGW	witold_interewicz@imgw.pl
Nicola Loglisci	SMR Piemonte	nicola.loglisci@csi.it
Chiara Marsigli	SMR Emilia-Romagna	cmarsigli@smr.arpa.emr.it
Massimo Milelli	SMR Piemonte	massimo.milelli@csi.it
Dmitrii Mironov	DWD	dmitrii.mironov@dwd.de
David Oesch	Universität Bern	oesch@giub.unibe.ch
Tiziana Paccagnella	SMR Emilia-Romagna	tpaccagnella@smr.arpa.emr.it
Antonio Parodi	CIMA, Genova	antonio@cima.unige.it
Renata Pelosini	SMR Piemonte	renata.pelosini@csi.it
Matthias Raschendorfer	DWD	matthias.raschendorfer@dwd.de
Thorsten Reinhardt	DWD	thorsten.reinhardt@dwd.de
Reinhold Schrodin	DWD	reinhold.schrodin@dwd.de
Jan-Peter Schulz	DWD	jan-peter.schulz@dwd.de
Linda Smoydzin	Universität Bonn	linda.smoydzin@uni-bonn.de
Gerd Vogel	DWD	gerd.vogel@dwd.de

During the last COSMO period, the following topics were of major importance:

- Work continued on the new turbulence scheme based on a prognostic treatment of turbulent kinetic energy (TKE) as well as on the new surface layer scheme. Both schemes are operational at DWD, ARPA-SMR, and IMGW, and are expected to become operational at MeteoSwiss soon. A technical report on parts of this work package ("Evaluation of Empirical Parameters of the New LM Surface-Layer Parameterisation Scheme") can be obtained on the COSMO web-site at http://www.cosmo-model.org/cosmoPublic/technicalReports.htm.

- The new multi-layer version of the soil model TERRA, which includes freezing and melting of soil layers and a revised formulation of the snow model, has been thoroughly tested and is currently undergoing final pre-operational testing. A technical report describing the changes to TERRA ("The Multi-Layer Version of the DWD Soil Model TERRA_LM") is available on the COSMO web-site at http://www.cosmo-model.org/cosmoPublic/technicalReports.htm. Additionally, work has started on the development of a new lake model, which is expected to lead to first experimental results by the end of the current working period.

- Implementation work on the Kain-Fritsch convection scheme continued. Tests show promising results, but rigorous validation is still pending and the code eventually needs substantial re-writing to improve the performance on vector machines. Therefore, alternative implementations of the Kain-Fritsch scheme are also being looked at.

- A cloud-ice scheme has been developed and implemented into both LM and GME. The scheme is running operationally at all member states except MeteoSwiss since September 2003, and is planned to become operational in Switzerland in the first half of 2004.

- Implementation and adaptation of a 3D turbulence formulation is under way, and will be followed by extensive testing, especially at higher resolutions.

The plan for 2004 includes further work on most of the schemes mentioned above. For the new turbulence scheme, this consists of parameter tuning, further extension of the scheme as well as writing up a documentation. The soil model mainly awaits operational implementation, and the implementation of the Kain-Fritsch convection scheme is "work in progress".

New packages for the work plan of 2004 include the parameterisation of boundary layer clouds (either within the new turbulence scheme or an entirely new package) and sub-grid scale cloudiness, inclusion of graupel in the microphysics scheme as well as testing of different aspects of LM runs at 2.8 km or even smaller grid-spacing.

(Marco Arpagaus, MeteoSwiss)

6.4 Working Group 4: Interpretation and Applications

The main effort of this working group is to develop methodologies and tools for the interpretation of high-resolution direct model output, including model applications to limited area ensemble prediction and various postprocessing methods. The WG on interpretation and applications is coordinated by Pierre Eckert (MeteoSwiss). The following scientists are members of the group:

Name	Institution	e-mail
M. Anadranistakis	HNMS	anad@hnms.gr
Marco Arpagaus	MeteoSwiss	marco.arpagaus@meteoswiss.ch
Carlo Cacciamani	ARPA-SMR	ccaciamani@arpa.emr.it
Daniel Cattani	MeteoSwiss	cat@meteoswiss.ch
Günter Doms	DWD	guenther.doms@dwd.de
Pierre Eckert	MeteoSwiss	pierre.eckert.@meteoswiss.ch
R. Kretzschmar	MeteoSwiss	krr@meteoswiss.ch
Andre-Charles Letestu	MeteoSwiss	acl@meteoswiss.ch
Chiara Marsigli	ARPA-SMR	cmarsigli@smr.arpa.emr.it
Andrea Montani	ARPA-SMR	amontani@smr.arpa.emr.it
Andrzej Mazur	IMGW	andrzej.mazur@imgw.pl
Tiziana Paccagnella	ARPA-SMR	tpaccagnella@smr.arpa.emr.it
Volker Renner	DWD	volker.renner@dwd.de
Susanne Theis	Universität Bonn	susanne.theis@uni-bonn.de
Andrea Walser	MeteoSwiss	andrea.walser@meteoswiss.ch

The efforts of WG4 have one side been devoted to the COSMO LEPS. This technique consisting of a downscaling of the ECMWF ensemble with the help of the LM has been implemented semi-operationally and runs on a daily basis since November 2003. Several probabilistic products are disseminated to the member states. New parameters like instability indices and zero degree level have been proposed. The verification based on the Italian high density precipitation network has been carried out, but the statistics for the time being is to poor to draw conclusions. Benchmark verifications based on statistical methods (pattern recognition by artificial neural networks) and the ECMWF EFI (Extreme Forecast Index) are available.

Two workshops have been organised, one in May together with WG5 and the other in September, in which decisions on future operations and research have been taken. The ensemble should be raised to 10 members, alternative clustering regions and parameters

should be tested, a set of test cases should be defined to be used not only by the COSMO LEPS project, but also to test new versions of the LM code.

As regards the LM postprocessing, the following activities have been carried out at DWD. Implementation of the neighbourhood method, probabilistic verification of this method, calibration, tests with stochastic physics on the LM. On the other side, computation and evaluation of various instability indices is in development at MeteoSwiss, the results should be available in 2004. Finally, links to dispersion models, ozone models and hydrology have been investigated at the polish meteorological service.

(Pierre Eckert, MeteoSwiss)

6.5 Working Group 5: Verification and Case Studies

This Working Group takes care for the verification of operational model forecasts, for the development of new verification methods and diagnostical tools as well as for case studies with the LM. The WG was coordinated till September 2003 by Carlo Cacciamani (ARPA-SMR) and since then ad interim by Francis Schubiger (MeteoSwiss).

The following scientists are members of this group:

Name	Institution	e-mail
Theodore Andreadis	HNMS	andrea@hnms.gr
Marco Arpagaus	MeteoSwiss	marco.arpagaus@meteoswiss.ch
Jean-Marie Bettems	MeteoSwiss	jean-marie.bettems@meteoswiss.ch
Carlo Cacciamani	ARPA-SMR	ccacciamani@smr.arpa.emr.it
Theagenis Charantonis	HNMS	tchara@hnms.gr
Ulrich Damrath	DWD	ulrich.damrath@dwd.de
Patrizio Emiliani	UGM-CNMCA	p.emiliani@meteoam.it
Massimo Ferri	UGM	m.ferri@meteoam.it
Alessandro Galliani	UGM	galliani@meteoam.it
Pirmin Kaufmann	MeteoSwiss	pirmin.kaufmann@meteoswiss.ch
Chiara Marsigli	ARPA-SMR	cmarsigli@smr.arpa.emr.it
Andrezj Mazur	IMGW	andrzej.mazur@imgw.pl
Malgorzata Mierkiewicz	IMGW	malgorzata.mierkiewicz@imgw.pl
Massimo Milelli	CSI Piedmont	massimo.milelli@csi.it
Guy de Morsier	MeteoSwiss	guy.de.morsier@meteoswiss.ch
Elena Oberto	CSI Piedmont	elena.oberto@csi.it
Jan Parfiniewicz	IMGW	jan.parfiniewicz@imgw.pl
Renata Pelosini	CSI Piedmont	renata.pelosini@csi.it
Ulrich Pflüger	DWD	ulrich.pflueger@dwd.de
Andrea Rossa	MeteoSwiss	andrea.rossa@meteoswiss.ch
Dominique Ruffieux	MeteoSwiss	dominique.ruffieux@meteoswiss.ch
Francis Schubiger	MeteoSwiss	francis.schubiger@meteoswiss.ch
Katarzyna Starosta	IMGW	katarzyna.starosta@imgw.pl
Ermanno Veccia	UGM-CNMCA	e.veccia@meteoam.it
Emanuele Zala	MeteoSwiss	emanuele.zala@meteoswiss.ch

The main activities of WG 5 for the period Oct 2002 - Sep 2003 covered the following points.

- Operational verification of surface parameters, using SYNOP stations and also regional high resolution networks. Results are summarised in verification reports which are distributed on a quarterly basis on the COSMO website.

- Operational verification of upper-air parameters, using TEMP stations. As in the case of surface verification, results are summarised in reports distributed on a quarterly basis on the COSMO website.
- High resolution verification of precipitation, using available high resolution dense non-GTS surface data. Consolidation of a common data set of non-GTS daily precipitation data.
- Verification of precipitation using radar composites.
- Verification of model cloudiness with Meteosat VIS channel at 12 UTC.
- Verification of integrated water vapour content using GPS data.
- Weather regime verification of vertical profiles and precipitation using radar composites.
- Verification of radiation budget with measurements at Payerne (shortwave and longwave radiation, sensible heat and albedo).
- Verification of runoff over river basins in Poland.
- Verification at MeteoSwiss of aLMo with IFS boundary conditions (instead of GME; results presented at COSMO General Meeting 2003).
- Exchange of two charts per day (precipitation and sea surface pressure) of each operational LM running on the COSMO website for subjective verification (comparison) purposes.

An internal meeting on the verification was held on 26-27 May 2003 in Geneva (CH) together with the the Working Group 4. The presentations covered (1) the COSMO LEPS project, especially the verification aspects of these ensemble forecasts and (2) the actual state of the verification developments at the different centres, namely at DWD a verification of (a) wind gusts and (b) multi-level aircraft measurements vs TEMPs and LM-vertical profiles and at MeteoSwiss the verification of a test chain with IFS lateral bounday conditions.

The major workpackages for 2004 include a continuation of the current operational verification of surface and upper air using SYNOP and TEMP stations. High-resolution dense non GTS-data as well as radar composite data will be used for verification of QPF. Cloudiness will be verified using Meteosat VIS data, integrated water vapour content using GPS data. At ECMWF a common verification package will be installed for the verification of new LM versions.

(Francis Schubiger, MeteoSwiss)

6.6 Working Group 6: Reference Version and Implementation

The WG on code maintenance, reference version, documentation and implementation is headed by Ulrich Schättler (DWD) as WPC. The following scientists contribute to the work of this group:

Name	Institution	e-mail
Theodore Andreadis	HNMS	andreadis@hnms.gr
Euripides Avgoustoglou	HNMS	euri@hnms.gr
Jean-Marie Bettems	MeteoSwiss	jean-marie.bettems@meteoswiss.ch
Davide Cesari	ARPA-SIM	dcesari@srm.arpa.emr.it
Marco Consoli	CSCS / MeteoSwiss	mconsoli@cscs.ch
Guy de Morsier	MeteoSwiss	guy.demorsier@meteoswiss.ch
Günther Doms	DWD	guenther.doms@dwd.de
Marek Lazanowicz	IMGW	marek.lazanowicz@imgw.pl
Jakub Madejak	IMGW	jakub.madejak@imgw.pl
Jan Parfiniewicz	IMGW	jan.parfiniewicz@imgw.pl
Paolo Patruno	ARPA-SIM	p.patruno@smr.arpa.emr.it
Ulrich Schättler	DWD	ulrich.schaettler@dwd.de
Jan-Peter Schulz	DWD	jan-peter.schulz@dwd.de
Lucio Torrisi	UGM	torrisi@meteoam.it
Emanuele Zala	MeteoSwiss	emanuele.zala@meteoswiss.ch

In the period Oct. 2002 - Oct. 2003 the following work was done by WG 6:

- Updates of the GME2LM and LM have been programmed, tested and implemented at all sites. See Section 5 for the program updates and Section 4 for the changes in the operational applications in the COSMO centres.
- A working group on code optimization and portability has been formed and guidelines for the work have been set up. This working group should be a platform to exchange and centralize information. Most important for the work is the "portable optimization".
- A template for describing the operational applications of all COSMO partners has been developed and a first prototype web page has been implemented.
- A page with the list of available software tools for exchange within COSMO has been set up on the private pages of the Web Site.
- Two parts of the restructured documentation have been released (I: Numerics and Dynamics; III: Data Assimilation).
- For the LM Nesting and the different interpolation programs (IFS2LM, LM2LM) only further tests could be made. No activities for an operational coding could be started.

Ongoing activities of WG 6 are the maintenance and the update of the COSMO software and the web site. New versions of the programs will be implemented and tested at all sites. The update procedure for the Reference Version will be installed and the Common Verification Package will be used for testing the new Reference Version. More documentation has to be put to the Web-Site (Update histories of COSMO software; description of the Working Groups) and work on restructuring the (offline) documentation has to go on.

(Ulrich Schättler, DWD)

7 COSMO Meetings and Events

This section summarizes the main meetings, workshops and seminars as well as management decisions from the previous year. Other COSMO activities such as guest scientists and internal visits are also considered. Finally, an overview of the forthcoming activities in the present COSMO working period is given.

7.1 Meetings in 2003

(1) LM User Seminar

This seminar on scientific applications of the LM was organized by Jürgen Steppeler and was held at DWD in Langen, 31 March - 2 April 2003. It was dedicated to research activities with the LM at various universities and covered various scientific topics. Central issues have been physical processes, high-resolution experiments and climate applications of the LM. The 2003 User Seminar included also tutorials on the LM Package and on numerical methods. Proceedings of the seminar have not been published.

(2) COSMO WG4-WG5 Joint Meeting

The members of Working Group 4 for Physical Aspects and of Working Group 5 for Verification and Case Studies met on 26 - 28 May 2003 at MeteoSwiss in Geneva (Switzerland) for a joint internal COSMO workshop (organized by Pierre Eckert). The first day was dedicated to presentations concerning the present status, evaluation, verification and further development of COSMO-LEPS system. The second day continued with presentations related to recent verification results of the operational systems and to high-resolution verification methods, followed by parallel workshop sessions of the two groups. More detailed information about the workshop and plenum discussion results on the third day is available on the private pages of our web-site.

(3) Meeting of the Work Package Coordinators

The work package coordinators (WPCs, i.e. C. Schraff, J. Steppeler, M. Arpagaus, P. Eckert, C. Cacciamani and U. Schättler), the Scientific Project Manager (SPM, T. Paccagnella) and the Chairman of the Steering Committee (M. Capaldo) met at MeteoSwiss in Zürich on 5 June 2003. The first part of the meeting was dedicated to review the progress in the work packages, to identify problems and delays in specific WPs and to set up a list with model deficiencies and technical problems. The second part concerned some preparations for the next General Meeting at DWD in Langen: set-up of the agenda, proposals for new work packages, interdependencies and priorities of WPs, discussion on goals for 2004 and items for the strategic discussion. The minutes of this meeting are available on the private pages of our web-site.

(4) COSMO WG2 Meeting on Numerical Methods

Members of the COSMO numerics group (WG2) met one day before the General Meeting on 23 September 2003 in Langen. The participants discussed the current state of dynamics and numerics in European NWP models. J. Steppeler gave an overview on numerical activities within SRNWP and within COSMO. Finally, the current state of the z-coordinate developments at DWD and ARPA-SIM have been reviewed and the strategy for the future work has been discussed. Especially, the question of including the physics parameterization

by an interpolating interface to the terrain-following model was addressed. The minutes of this internal workshop will be made available on our web-site.

(5) 5th COSMO General Meeting

The recent COSMO general meeting was held in Langen (Germany) on 24-26 September 2003 and was hosted by DWD. With about 60 participants (see Fig. 15), the meeting was well attended. It was a very stimulating meeting with many interesting presentations, with many discussions on various subjects, and with much organizational work related to concrete work packages. The Vice-President of DWD, S. Mildner, opened the meeting by a welcome address and D. Frühwald informed about further details on organization of the meeting. The Chairman of the STC, M. Capaldo presented an account of the work of the Steering Committee and T. Paccagnella summarized the activities of the SPM and the WPCs during the year.

Figure 15: Participants at the 5th COSMO General Meeting 24-26 September 2003, held at the BTZ in Langen, Germany. A part of the crew is still in the coffee break.

The first (public) part was organized in six main sessions according to our working group structure. The work package coordinators gave an overview on progress in the various research and development activities of the working groups, followed by presentations on selected issues by the responsible scientists. Each session was closed by a general discussion on central topics. Summaries of the talks including the slides are available on our web-site. Section 8 and 9 of this Newsletter contains a number of contributions which emerged from the presentations in Langen.

The second (internal part) of the meeting was dedicated to formulate the research plan for the next period (Oct 2003 - Oct 2004). Delayed work packages and proposals for new ones

have been presented by the WPCs and discussed in the plenum. Allowing time for this plenum discussion on future work packages was found to be a good idea and useful, not only for a cross-checking of interdependencies but also for more scientific input and ideas to the following workshops of the WGs. The proposals for work packages were oriented along some basic guidelines for the next working period, which were presented by the Chairman of the STC.

- Consolidation, Documentation and Upgrade of the LM
  - Quality of precipitation forecasts: Increase efforts on the parameterization scheme
  - Assimilation of remote sensing data
  - Multi-national assessment of COSMO-LEPS products
- Application and Interpretation
  - statistical interpretation of high resolution forecasts
- Paving the way for Meso-γ Scale
  - Acceleration of Z-coordinate model versions
  - New parameterization schemes
  - Forefront verification and case studies

Detailed work plans have then been set-up by the working groups in separate workshops, which afterwards were presented to the plenum. The last part of the meeting was dedicated to presentations on future plans and on external collaborations of COSMO member services by national and international projects (see also Section 10), and a general discussion on further perspectives of work in our group. The following main items have been formulated:

- Variational methods for estimating local parameters,
- Quality certification of the LM-system,
- Increase COSMO members participation to EU projects as a group.

The final version of the work plans and a short description of each work package is available on the member area of our web-site.

(6) 10th Meeting of the COSMO Steering Committee

The 10th Meeting of the STC was held on 26 September 2003 during the COSMO General Meeting in Langen (participants: M. Capaldo, G. Sakellaridis, D. Frühwald and J. Ambühl). The Chairman of the STC (M. Capaldo) will leave the Committee due to other duties at UGM. Dieter Frühwald from DWD was elected as the new Chairman for the next two COSMO periods. Massimo Ferri from UGM was assigned as the new Italian representative in the STC. UGM offered to organize the next COSMO General Meeting in Milano (Italy) from 22-24 September 2004. The minutes of this STC meeting are available on the member pages of our web-site.

(7) 11th Meeting of the COSMO Steering Committee

The 11th meeting of the COSMO Steering Committee was held in Athens at HNMS on 28 November 2003 (participants: M. Ferri, G. Sakellaridis, D. Frühwald, J. Ambühl, R.

Klejnowski, M. Rotach and T. Paccagnella). The SPM (T. Paccagnella) presented the draft work plans for the upcoming COSMO period as prepared by the WPCs. All work packages have been approved. The final version of the work plans are available at the member area of our web-site. Further points of discussion have been computer resources for COSMO LEPS and the exchange of non-GTS observational data between COSMO members.

The Swiss representative in the STC, J. Ambühl will leave the Committee by the end of 2003. Mathias Rotach, the head of research and development at MeteoSwiss was assigned as his successor and already attended the meeting.

C. Cacciamani had finished his activities as WG5 work package coordinator due to other duties. The STC assigned Francis Schubiger from MeteoSwiss to take over the responsibilities as coordinator of WG5 for the next COSMO period. Minutes of this meeting will be available on the member area of our web-site.

7.2 Guest Scientists

Jürgen Steppeler from DWD visited the research group of J. Klemp and B. Skamarock at NCAR in Boulder (USA) and stayed from 25 April - 25 May 2003 as a guest scientist. Various numerical aspects, especially higher-order spatial disretizations and implicit methods, have been investigated.

7.3 Internal Visits

G. Doms and U. Schättler from DWD, and A. Walser from MeteoSwiss visited the Numerical Modelling Group at ARPA-SIM in Bologna from 10-11 February. Various technical aspects and the model set-up of the COSMO-LEPS system running at ECMWF have been discussed.

On 11 March, U. Schättler from DWD visited MeteoSwiss for a workshop on code optimization and portability. Various items from WP 6.1.2 have been discussed.

Marco Arpagaus visited the DWD physics group from 28-31 July. Various topics and problems in WG3 have been discussed. A central aspect that has been worked on was the Kain-Fritsch convection scheme, including implementation details and questions related to further testing and evaluation.

Andrzej Mazur from IMGW visited DWD from 18-19 December. Six new staff members at the IMGW Centre for Development of Numerical Weather Forecasts have started their work. Two of them, Witold Interewicz and Grzegorz Duniec, will support the COSMO physics group in 2004.

Giovanni Bonafe from ARPA-SIM visited M. Raschendorfer from the DWD physics group from 12-16 January 2004 to discuss and define further work in WP 3.1.1.6 (on extended parameter tuning).

7.4 Upcoming COSMO Meetings

The following COSMO workshops and meetings are planned for 2004.

8-10 March 2004: LM User Seminar
at DWD, Langen (D)
This seminar is dedicated to research activities and scientific applications of the LM at various

universities and research institutes. This years seminar will also include tutorials on numerics and on the LM Package. Information on the program, registration and accommodation can be found at *www.dwd.de/en/FundE/Analyse/Modellierung/Tagungen*.

5-6 May 2004: COSMO WG4-WG5 Workshop
at MeteoSwiss Geneva, Geneva (CH)
One day workshop with forecasters on the use of LM products. Discussion of guide lines for forecasters. This workshop will be organized by P. Eckert and F. Schubiger.

6-7 May 2004: Meeting of the Work-Package Coordinators
at MeteoSwiss Geneva, Geneva (CH)
Assessment of the progress of WPs, identification of problems and delays, and some preparations for the next General Meeting. The SPM will invite for this meeting during spring.

6-7 September 2004: Meeting of the Work-Package Coordinators
at ARPA-SIM, Bologna (I).
Assessment of the progress and work done and preparation of the next General Meeting.

21 September 2004: COSMO WG2 Meeting on Numerical Methods
UGM, Milano (I)
Discussion on new numerics and dynamical cores. J. Steppeler will invite for this workshop during the year.

22-24 September 2004: 6th COSMO General Meeting
UGM, Milano (I)
Progress Reports from the Working Groups and presentation of results from the work packages; discussion and set-up of a scientific work plan for 2005.

November 2004: Meeting of the Steering Committee
DWD, Offenbach (D)
Regular business meeting, revision of work packages and definition of the final COSMO work plan for 2005.

7.5 Announcements

This section lists a number of meetings which are of specific interest for active participation. Of course, this list is by no means complete.

EGU 1st General Assembly
25-30 April 2004, Nice, France (*www.copernicus.org.egu2004*).

2nd SRNWP Workshop on Verification
April 2004, KNMI, De Bilt, Netherlands. Date is still to be defined.

Joint HIRLAM/SRNWP Workshop on Soil Analysis and Processes
Spring 2004, SMHI, Norrköping, Sweden. The date is still to be defined.

14th ALADIN Workshop
1-5 June 2004, Innsbruck, Austria (*www.cnrm.meteo.fr/aladin/*).

14th International Conference on Clouds and Precipitation
18-23 July 2004, Bologna, Italy (*www.isac.cnr.it/ iccp*).

ECMWF Seminar on Recent developments on numerical methods for atmosphere and ocean modelling
6-10 September 2004, Reading, UK (*www.ecmwf.int/newsevents/calendar*).

3rd European Conference on Radar in Meteorology and Hydrology
6-10 September 2004, Visby, Sweden (Gotland).

DACH 2004 (in German only)
7-10 September 2004, Karlsruhe, Germany (*www-imk.fzk.de/dach2004/*).

26th EWGLAM and 11th SRNWP meeting
4-7 October 2004, Oslo, Norway. The special topic of this year EWGLAM session will be *High resolution modelling in mountainous regions*, the meeting will also include a MAP session.

11th Workshop on High-Performance Computing in Meteorology
25-29 October 2004, Reading, UK (*www.ecmwf.int/newsevents/calendar/*).

Joint HIRLAM/SRNWP Workshop on Variational Methods
November 2004, UK Met Office, Exeter, UK. The date is still to be defined.

ECMWF/ELDAS Workshop on Land Surface Assimilation
8-11 November 2004, Reading, UK (*www.ecmwf.int/newsevents/calendar/*).

3rd European Conference on Severe Storms
9-12 November 2004, Leon, Spain (*www3.unileon.es/congresos/ecss2004/principal.htm*).

SRNWP Workshop on Numerical Techniques
December 2004, date and place still to be defined.

8 Results and Methods of Model Verification

This section summarizes some of the operational verification results for the LM forecasts at various COSMO meteorological centres, both for near-surface and upper-air parameters. More detailed verification results are presented on a quarterly basis at the COSMO website. We also include research oriented contributions related to the development and test of new methods of model verification, including the use of high-resolution non-GTS data, and remote sensing data from GPS-satellites. Verification results using radar composite data have been published in COSMO Newsletter 3 (p. 123-139).

Most of the papers included in this section are write-ups from the COSMO annual meeting 2003 in Langen (D). Many thanks to all of you who provided contributions for the present issue of the Newsletter. The numbering of equations and figures in this section refers to each paper.

Before continuing with the contributions, we summarize shortly some conclusions on model deficiencies from the recent verification results as well as from diagnostic evaluations and from case studies.

Model Deficiencies

From the verification results for the last year, we can summarize some basic problems:

- During evening and nighttime, the 2m-temperature has a quite large cold bias, especially during winter. This effect is less pronounced when the new TKE turbulence and surface layer scheme is used, together with the soil moisture analysis.
- The mean diurnal cycle of 2m-temperature is represented with a too large amplitude (for both the old and new turbulence schemes). The maximum is achieved too early (at noon) and the temperature starts to decrease too early in the afternoon.
- The diurnal cycle of the 2m-dewpoint-temperature is not well captured. With the new TKE and surface layer scheme the diurnal cycle is somewhat better represented by the model.
- 10-m winds appear to be underestimated both in winter and summer, however over the Swiss Middleland (below 800 m asl) there is an overestimation, (especially during night-time) and on the mountain gridpoints there is strong underestimation.
- In summer, the mean daily cycle of both total cloudiness and precipitation is not well represented. Especially, the precipitation peaks too early (at noon) by about 4-6h.
- Low precipitation amounts appear to be overestimated by the model. This may result from convective drizzle or from a too slow evaporation of rain below stratiform clouds.
- Over regions with complex and steep topography (especially over the Alps), the simulated precipitation patterns are still not very satisfactory. However, some progress has been made by introducing the filtered topography and the new scheme for horizontal diffusion.
- A long-standing problem is the windward shift of maximum precipitation over mountain ranges and too less precipitation over the leeside. This effect is much more pronounced in winter than in summer. A test period in winter 2002/2003 showed the potential of the 2-timelevel scheme and prognostic precipitation (see COSMO Newsletter 3, 173-176).

- The cloud cover is overestimated (as compared to SYNOP observations or also to METEOSAT VIS channel): it seems to be due to an overestimation of high clouds (but these high cloud are perhaps not always well observed or not well analysed with satellite data).
- The integrated water vapor content is underestimated (as verified with GPS data) and shows a seasonal cycle with a greater negative bias in summer.
- The vertical profiles (as verified with TEMP soundings) show a cold bias from surface up to 750 hPa (mainly caused during summer season). The mean error in wind speed is small, with a positive bias in the boundary layer and a small negative bias above 800 hPa.
- When starting from interpolated GME analyses, there is a quite strong spin-down of precipitation during the first 12-24h of integration, indicating a too intense dynamical adaption of the initial fields. The nudging assimilation scheme corrects these errors.

At the recent COSMO meeting, several new work packages have been defined to investigate these problems and to find short-term remedies.

High Resolution Verification of Daily Cycle over Switzerland

Francis Schubiger

MeteoSwiss, Krähbühlstrasse 58, 8044 Zürich, Switzerland

The following nomenclature for LM is used in the text below: aLMo means "Alpine Model", the LM version operational at MeteoSwiss and LMD means the operational LM version at DWD.

Results of aLMo and LMD have been computed monthly and seasonally for 2m-temperature, 2m-dewpoint and 2m-dewpoint depression, 10m-wind, precipitation (hourly sums for daily cycle and 6h sums for scores) and for cloud cover (3-hourly intervals).

Two of the main differences between aLMo and LMD are the prognostic TKE-scheme and the soil-moisture analysis (operational at DWD, but not at MeteoSwiss). Since 16 September 2003 aLMo runs with boundary conditions from ECMWF (IFS-frames) and it renders the interpretation of the differences with LMD (boundary conditions from GME) more difficult.

The following points are of main interest:

(1) The 2m-temperature cooling in the evening is too pronounced and there is a negative bias in Winter and Spring during night-time (up to 1.5-2.0 K in the late evening). The diurnal amplitude is too large (with the exception of Summer for gridpoints < 800m) and is a little bit larger in LMD than in aLMo. The daily maxima is reached ~ 1.5 hour too early. In LMD (with prognostic TKE and soil moisture analysis) the daily maxima is $\sim$ 1K higher than in aLMo (i.e the bias was littler in LMD especially in the hot Summer 2003 where aLMo's maxima was too low). See Figure 1 (left side) for results of Winter 2002/2003 and Summer 2003 for gridpoints < 800 m.

(2) The daily cycle of 2m-dewpoint depression is not well reproduced and especially in Winter much too little (aLMo too moist during daytime and too dry during night-time). The TKE scheme, operational for LMD, corrects partly (in Summer and Autumn mostly) this cycle but the values are too low in Winter and Spring (constant negative bias, i.e. too moist). See Figure 1 (right side) for results of Winter 2002/2003 and Summer 2003 for gridpoints < 800 m.

(3) The results for precipitation are summarized in Table 1 with the scores for the frequency bias of the four seasons for the thresholds 0.1, 2, 10 and 30 mm/6h for aLMo and LMD. It shows an overestimation for low amounts (0.1 mm/6h) of 50-80% (except in Autumn only 30%): this overestimation is most pronounced in the Prealps (altitude range 800-1500m). The high amounts (10 mm/6h) are slightly underestimated by 10% (except during last Summer). In Summer there is a too strong diurnal cycle on the mountain gridpoints (due to a too pronounced convection at daytime) and the daily maxima are forecasted about 4h too early (see Figure 4). Differences between aLMo and LMD are little in Winter and Spring; during the hot and dry Summer 2003 aLMo gave $\sim$ 30% more precipitation (overestimation) than LMD, probably due to the missing of the soil-moisture analysis operational at DWD. Since Autumn 2003 the differences between aLMo and LMD are partly due to the different lateral boundary conditions (aLMo runs with IFS-frames) and the comparison between aLMo and LMD is not obvious. Table 1 shows also the scores for the test period (23.05-31.08.03) where aLMo run both with boundary conditions from GME and IFS (each with an own assimilation cycle). The overestimation of precipitation in aLMo is partly removed with the IFS-frames.

Table 1: Frequency bias (%) of predicted precipitation over Switzerland. For all 6-h sums from + 6h till + 48h of all 00 UTC and 12 UTC forecasts, compared to 69 ANETZ stations. The LM precipitation is the mean over 5 gridpoints. For the high amounts (10 and 30 mm/6h) the percentage of occurrences (%) is given. The columns give the values for the four seasons and (on the right part) for the period where aLMo run both with GME- and IFS-boundary conditions.

Threshold	**Winter 2002/3**	**Spring 2003**	**Summer 2003**	**Autumn 2003**	23.05 - 31.08.03 **aLMo-opr**	**aLMo-IFS**
0.1 mm / 6 h						
aLMo	157	168	189	129	198	181
LMD	154	162	150	129	162	–
2.0 mm / 6 h						
aLMo	127	128	144	101	158	143
LMD	124	121	112	109	123	–
10 mm / 6 h	0.94	0.88	1.82	1.88	1.79	–
aLMo	91	89	110	81	118	100
LMD	87	83	77	115	84	–
30 mm / 6 h	0.021	0.038	0.126	0.143	0.117	–
aLMo	77	47	245	94	263	223
LMD	59	53	140	178	132	–

(4) Verification of 10m-wind (for representative stations corresponding to a gridpoint < 800m) gave an overestimation of the wind speed of $\sim$ 0.5-0.8 m/s both in aLMo and LMD (except in Summer daytime with almost no overestimation). The diurnal cycle is qualitatively better in LMD (due to TKE-scheme) but the daytime values are even higher, i.e. positive bias greater (see also COSMO Newsletter 2, page 201). For the gridpoints > 1500m the wind speed is strongly underestimated, due to the same PBL-parametrization over mountains than over flat terrain. See Figure 2 for results of Winter 2002/2003 and Summer 2003 for gridpoints < 800 m.

The mean error in 10m-wind direction (verified for observed wind speed > 3 m/s) is very little, in the range of +5 to +10 degrees (i.e. a little bit biased in clockwise direction). During Summer the errors are a bit larger (up to 15 degrees during night-time).

(5) The diurnal cycle of total cloudiness is not well reproduced in Spring and Summer: there is a positive bias during the night (up to 0.5-1.0 octa). Results in aLMo and LMD are very similar. See Figure 3 for results of Winter 2002/2003 and Summer 2003 for gridpoints < 800 m and > 1500m. In Winter the low cloud amount (stratus) seems quite well reproduced at analysis time in aLMo and LMD (due to the nudging assimilation scheme): the cloud amount for gridpoints < 800 is 1 octa higher than for those > 1500 m (in the observation even 2.3 octa). It is interesting to compare the following two behaviours on the diurnal cycle for mountain gridpoints in Summer: missing of the cycle for cloud cover and much too exaggerated cycle for precipitation (See Figure 4). It could suggest that cloud amount in convective situations is too low.

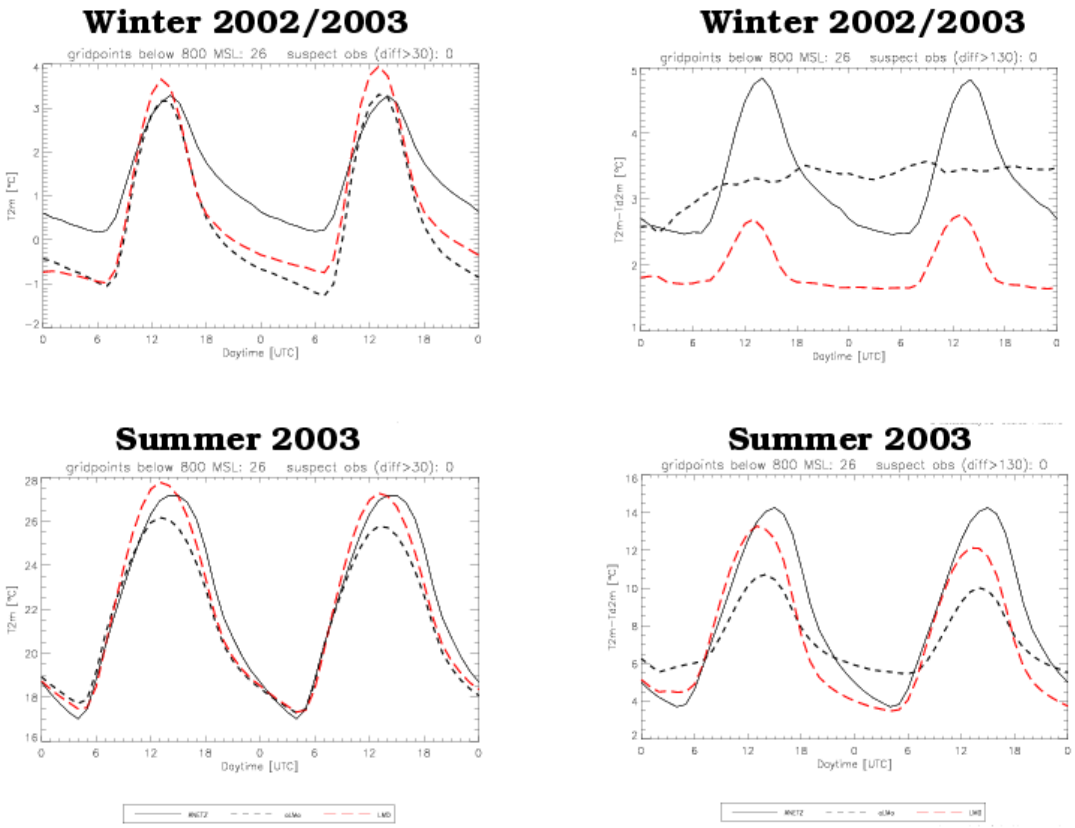

Figure 1: Verification of the daily cycle of 2m-temperature (left) and 2m-dewpoint depression (right) for gridpoints < 800m over Switzerland in Winter 2002/2003 (upper part) and Summer 2003 (lower part). Observations (ANETZ): full line black; aLMo: black dashed; LMD: red long dashes.

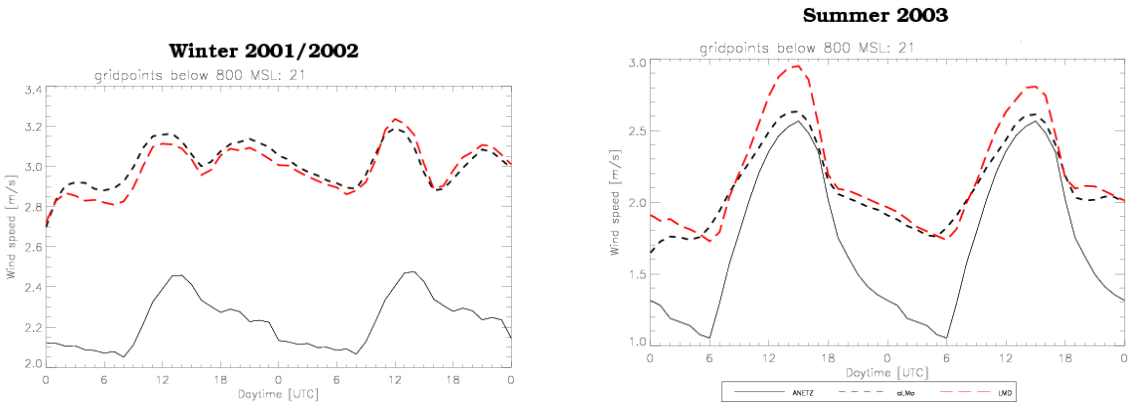

Figure 2: Verification of the daily cycle of 10m-wind speed for gridpoints < 800m over Switzerland in Winter 2002/2003 (upper part) and Summer 2003 (lower part). Observations (ANETZ): full line black; aLMo: black dashed; LMD: red long dashes.

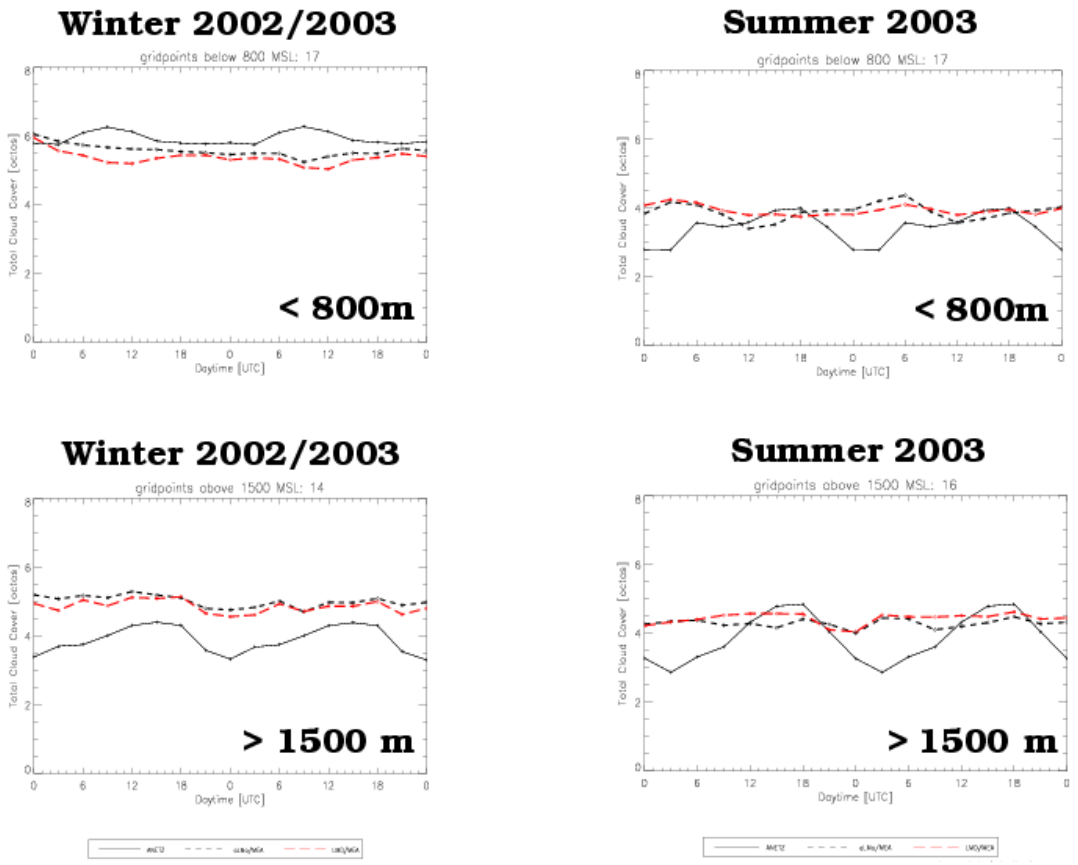

Figure 3: Verification of the daily cycle of total cloud cover over Switzerland in Winter 2002/2003 (left) and Summer 2003 (right) for gridpoints < 800m (upper part, 17 locations) and for gridpoints > 1500m (lower part, 16 locations). Observations (ANETZ): full line black; aLMo: black dashed; LMD: red long dashes. The LM total cloud cover is the mean of 41 gridpoints around the observation station and for three hours, to take in account that an observer sees in the mean a sky radius of ∼ 30 km.

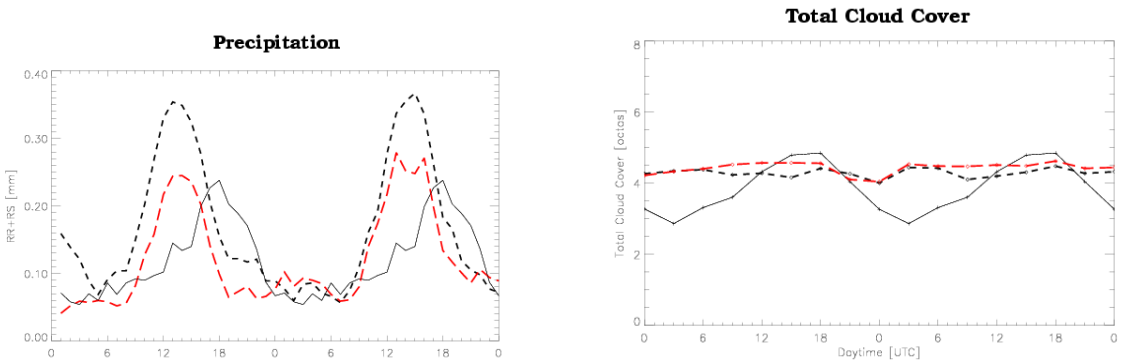

Figure 4: Verification of the daily cycle of precipitation (upper part) and total cloud cover (lower part) for gridpoints > 1500m over Switzerland in Summer 2003. Observations (ANETZ): full line black; aLMo: black dashed; LMD: red long dashes.

Verification of aLMo Runs with European SYNOP and GPS Data

Pirmin Kaufmann

MeteoSwiss, Krähbühlstrasse 58, 8044 Zürich, Switzerland

Abstract

A seasonal verification of all aLMo forecasts back to the beginning of the LM pre-operational phase in summer 2000 has now been completed with consistent settings and scaling, and the results are available at http://www.cosmo-model.org in the member area. A new verification of integrated water vapour (IWV) with remote sensing data derived from the Global Positioning System (GPS) zenith total delay (ZTD) measurements has been completed last year and will be made available on the web page. It currently relies on data provided by KNMI in the framework of COST-716 and the TOUGH project.

1 Introduction

In 2002, the verification of the Alpine Model (aLMo) surface fields has been extended to cover the whole model domain, using all available European SYNOP stations (Kaufmann 2003). During 2003, the verification package has been improved and the shortcomings that were described in the last COSMO Newsletter have been eliminated. The following configuration changes and improvements were made:

- The height difference between station and model elevation is now limited to 100 m instead of 500 m.
- The model elevation of the nearest four grid points is now compared to the altitude of each station to minimize vertical discrepancy.
- Station pressure and 2 m-temperature are now interpolated vertically to compensate for remaining altitude difference.
- The error magnitude is limited to exclude observational errors.
- A requirement for the availability has been introduced, it is set to 80 % of the verified time range and to 33 % of the stations.
- The lower limit for the data quality coded in BUFR as confidence level can be chosen freely.

With this configuration, all seasons since summer 2000 have been verified. MeteoSwiss started running the LM in pre-operational mode on a regular basis at the beginning of July 2000. During the first two month (July and August), only the 00 UTC integrations were carried out. In November 2000, the original unfiltered orography was replaced by a filtered orography. These changes in the model setup have to be considered when comparing the first two seasons (summer and autumn 2000) of the aLMo verification to the seasons thereafter. Due to this limited comparability, the results of these two seasons are not available on the COSMO web page.

The mean error (ME), mean absolute error (MAE), standard deviation of the error (STDE), and root mean square error (RMSE) are computed for the following parameters: Pressure

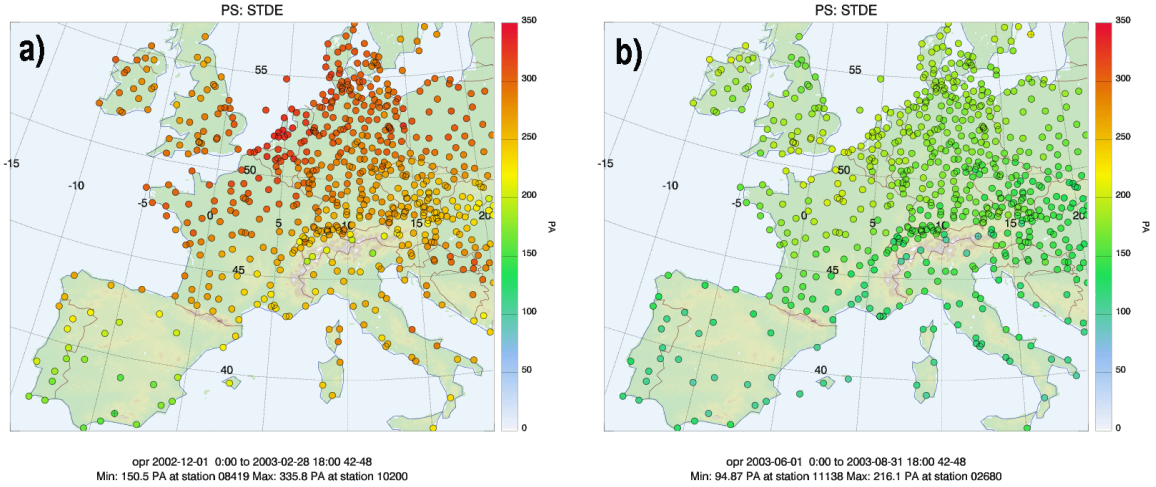

Figure 1: Standard deviation of errors for surface pressure for the forecast range +42 and +48 h of the 00 UTC and 12 UTC aLMo integrations; (a) winter 2002/3, (b) summer 2003.

reduced to mean sea level (PMSL), pressure at station height (PS), temperature at 2 m (T_2M), and dewpoint temperature at 2 m (TD_2M). The verification of integrated water vapour (IWV) has been added in 2003. Three types of verification are made: A temporal verification, a spatial verification and a verification totalling the spatial and temporal scores.

2 Temporal and Spatial Verification

The temporal verification calculates a verification score for series of verification times. Currently, a three month span of 6-hourly SYNOP observations are used. The resulting time series of scores can be used to determine the times at which the aLMo performed well, and those at which the forecast errors where considerable. The latter are prime candidates for case studies aiming towards model improvement. An example for this verification was presented in the last newsletter (Kaufmann 2003).

The spatial verification yields a score at each available SYNOP station. Two examples for winter 2002/3 and summer 2003 are shown in Fig. 1. The STDE of the surface pressure is much larger in winter than in summer. Especially the stations in the northern half of the model domain have a relatively large error of approximately 3 hPa. The seasonal dependence of this error is the same for all years, as will be seen below.

3 Total Scores

A spatial and temporal aggregation of the model errors is calculated and results in one total verification score for all stations and the whole season. This value is calculated for each forecast range separately. In Fig. 2, the mean error of the surface pressure for the same seasons as in Fig. 1 is shown. With increasing forecast range, the mean error slightly increases in winter (Fig. 2 a) and strongly decreases in summer (Fig. 2 b). The strong decrease in summer has already been shown for the summer 2002 in the last Newsletter (Kaufmann 2003) and is a consistent feature of aLMo during the warm season.

The evolution of the scores since the beginning of the pre-operational phase in summer 2000 until autumn 2003 is shown in Fig. 3. The results are valid for the forecast range +42 h to +48 h. In all parameters, a clear seasonal cycle is present, and a large inter-annual

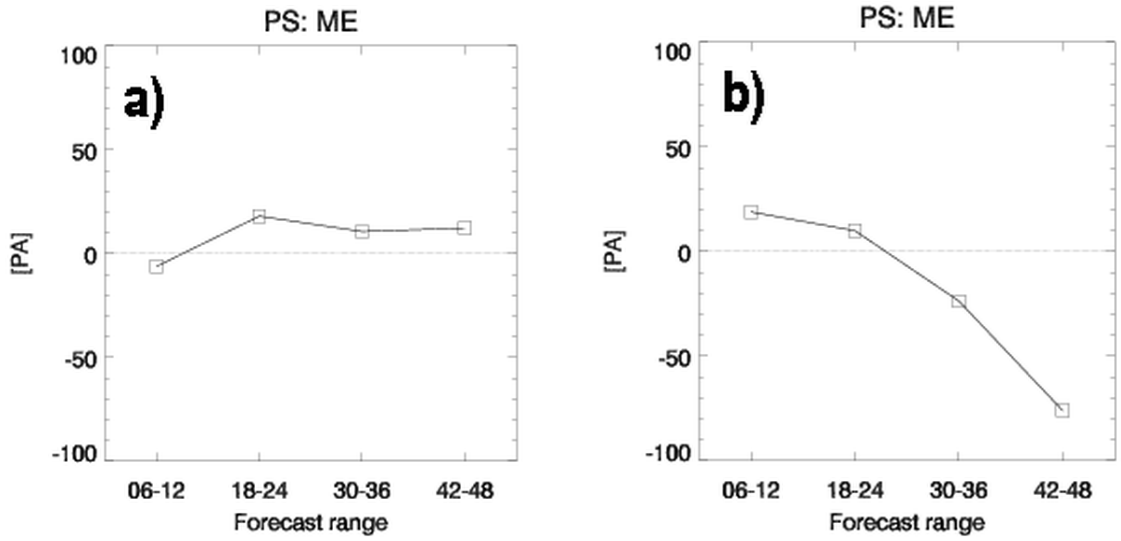

Figure 2: Dependence of the model bias (mean error) on forecast range; (a) winter 2002/3, (b) summer 2003.

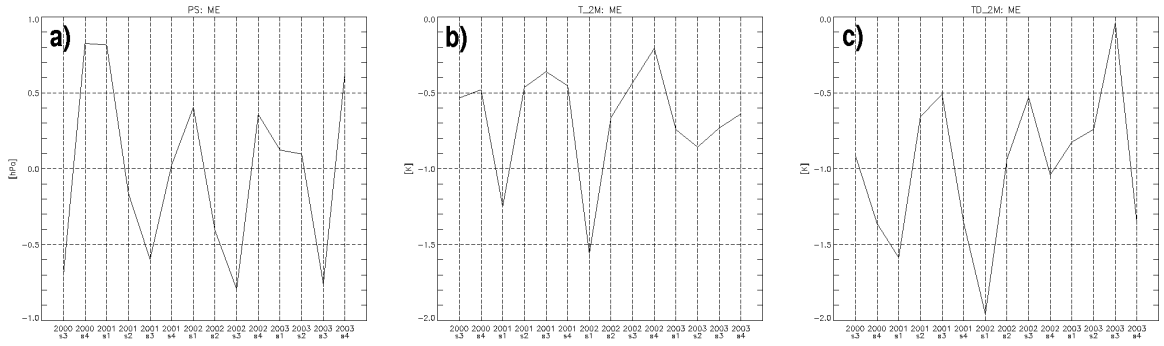

Figure 3: Evolution of seasonal model bias for the forecast range +42 to +48 h since summer 2000 (2000s3); (a) surface pressure, (b) 2 m temperature, (c) 2 m dewpoint.

variability is evident. The surface pressure (Fig. 3a) and the pressure reduced to mean sea level (not shown) both have a positive bias of about 0.5 hPa in winter and a negative bias of about 0.7 hPa in summer. The 2 m-temperature (Fig. 3b) is about 1 K too low in winter and 0.5 K too low in summer, and the dewpoint temperature (Fig. 3c) is about 1.5 K too low in winter and 0.5 K too low in summer. A too low dewpoint temperature is equivalent with an underestimated water vapour content.

A systematic bias of the model can be removed in post-processing or in the interpretation process by an informed forecaster. A more important figure of the model quality is the STDE, giving a reliability measure of the model after compensating for the systematic bias. In Fig. 4, the STDE of PS shows like the bias a seasonal cycle and no clear trend. The last season however, autumn 2003(2003s4), is exceptionally low compared to all three previous autumns, possibly indicating an improving quality of the model forecast due to the use of ECMWF-IFS boundary values. An evaluation of the ECMWF-IFS instead of the GME boundary conditions during summer 2003 has shown a decreased STDE for all parameters. It remains to be seen if the lower STDE values in autumn 2003 is a positive quality signal that persists into the future.

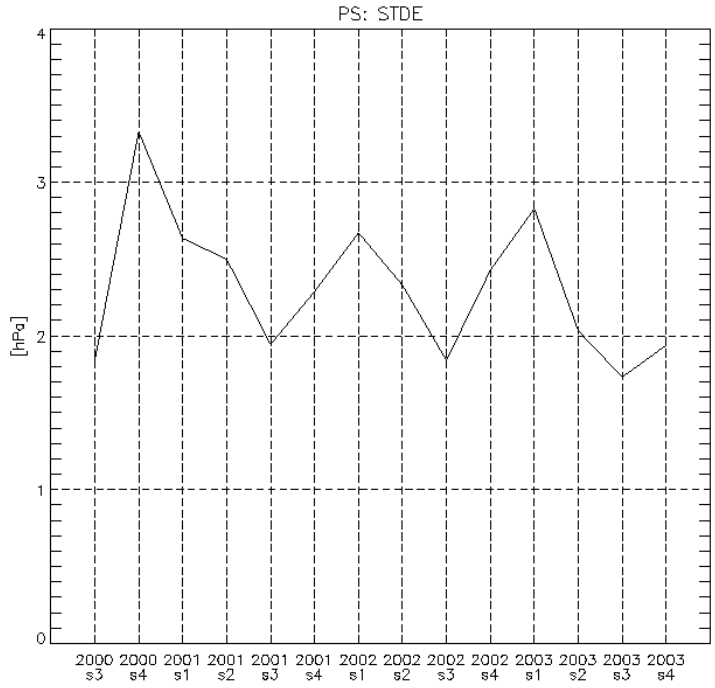

Figure 4: Evolution of standard deviation of errors for the forecast range +42 to +48 h since summer 2000 (2000s3) for surface pressure.

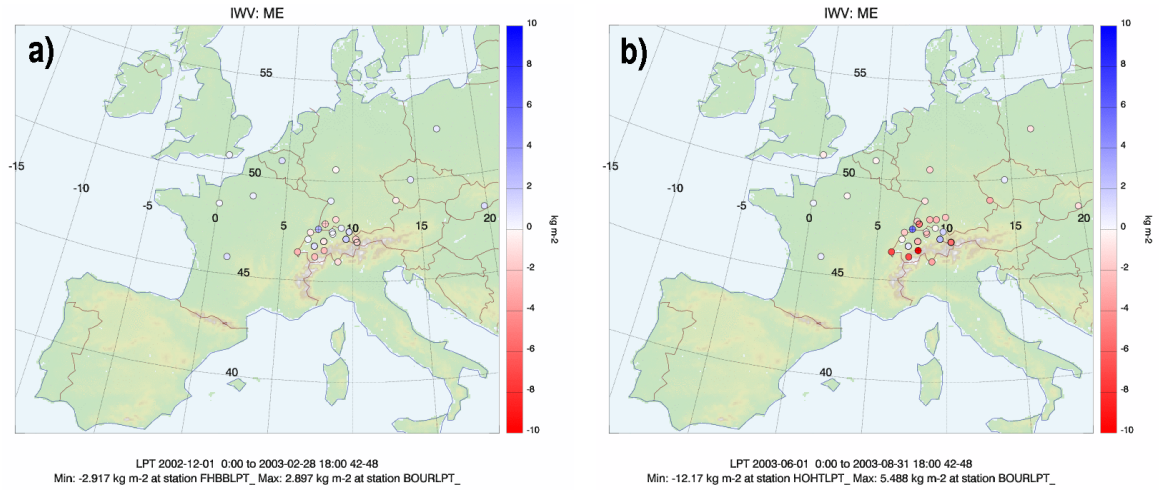

Figure 5: Model bias (mean error) of integrated water vapour for the forecast range +42 and +48 h of the 00 UTC and 12 UTC aLMo integrations; (a) winter 2002/3, (b) summer 2003.

4 GPS Verification

Last year, the verification was extended to include the vertically integrated water vapour content (IWV) derived from the Global Positioning System (GPS). Several processing centres throughout Europe provide zenith total delay (ZTD) measurements, each primarily focussing on its home country but still providing some overlap with other European countries. The ZTD values of three centres are deemed reliable from the experience during COST-716 and are used here. The calculation of the IWV from ZTD requires the knowledge of the air density above the GPS antenna. This is calculated with the temperature and pressure measurements from a nearby SYNOP station. The processed IWV data is provided by KNMI in the framework of the COST-716 and the TOUGH project. The aLMo derives the IWV

value directly from the specific water vapour content. A future aLMo version will calculate ZTD values that can be directly compared to the ZTD values measured by any of the present (GPS) and future (Galileo, GLONASS) global navigation satellite system (GNSS).

An example of the verification of the aLMo IWV is shown in Fig. 5. The stations shown are those processed by Swisstopo. The IWV bias shows a seasonal cycle, with smaller bias in winter than in summer. This bias is largest in the mountains, so that it could be related to the height difference between the GPS antenna, the SYNOP station, and the model surface. This dependence on height differences remains to be explored in the future work.

References

Kaufmann, Pirmin, 2003: Verification of aLMo runs at SYNOP-Stations. COSMO Newsletter no 3, G. Doms and U. Schttler (Eds.), DWD, Germany (available at www.como-model.org), p. 76 - 79.

Verification of Surface Weather Parameters at DWD

Ulrich Damrath

Deutscher Wetterdienst, P.O.Box 100465, 63004 Offenbach a.M., Germany

1 Time Series of Forecast Quality During the Last Year

Figs. 1 – 4 illustrate the behaviour of forecast errors for valid times 06 and 18 UTC from January to December 2003. The most important features of the seasonal variation of scores are similar to the results presented last year.

- Cloud cover: best results for winter months, overestimation of high cloud covers during summer at 6 UTC, general overestimation of high cloud covers at 12 UTC, but pronounced during summer.
- Cloud cover in different heights: frequency biases of low cloud covers near 1, non systematic behaviour of forecast quality concerning high cloud covers (frequency biases are sometimes higher than the maximum value drawn), possible reason: high cloud covers of high and medium clouds do not occur very often, small sample size compared to low clouds.
- Temperature: general underestimation of temperature at 18 UTC due to phase error in the diurnal variation (see section on diurnal cycle).
- Dew point depression: negative bias during most months (i.e. too moist especially for 18 UTC), better results for summer at 6 UTC.
- Extreme Temperatures: Minimum: underestimation during winter, small overestimation during summer, Maximum: best biases during Spring and Autumn, underestimation especially during the hot summer 2003.
- Wind direction: worst forecast during summer.
- Wind speed: in general slow underestimation, except for summer 6 UTC.
- Gusts: overestimation of gusts except for those greater than 25 m/s, worst forecasts during summer.
- Precipitation: worst forecasts during summer, small precipitation values are overestimated.

2 Diurnal Cycle of Forecasts and Observations for the Gridpoint Frankfurt/Main Airport

During summer conditions (Fig.5 for July 2003, Fig. 6 for August 2003) the diurnal cycle of temperature is predicted relatively well. The remaining old problem is that maximum values occur too early and the decrease during the afternoon is too rapid. During wintertime (Fig. 7 for January 2004) a strong negative bias occurs for all forecast times! It is worth mentioning that the extreme temperatures during July and August 2003 were predicted relatively well,

although predictions of dew point during August were bad with a maximum bias around 18 UTC of more than 3K. Wind speed is a little bit underestimated during daytime and decrease also too fast during afternoon (as could be expected due to the behaviour of temperature).

3 Results of QPF Verification Using Stations of High Density Network

During last year nearly the same patterns of errors in precipitation forecasts appeared as during the last years. A change of these error patterns can be expected, if the prognostic equation for drifting precipitation will be introduced into operational use. Until this time we will have:

- overestimation of precipitation in the windward side of obstacles and
- underestimation of precipitation in the leeward side,
- strong overestimation of precipitation during winter at the windward side of the obstacles.

Figs. 8 – 11 illustrate these typical errors.

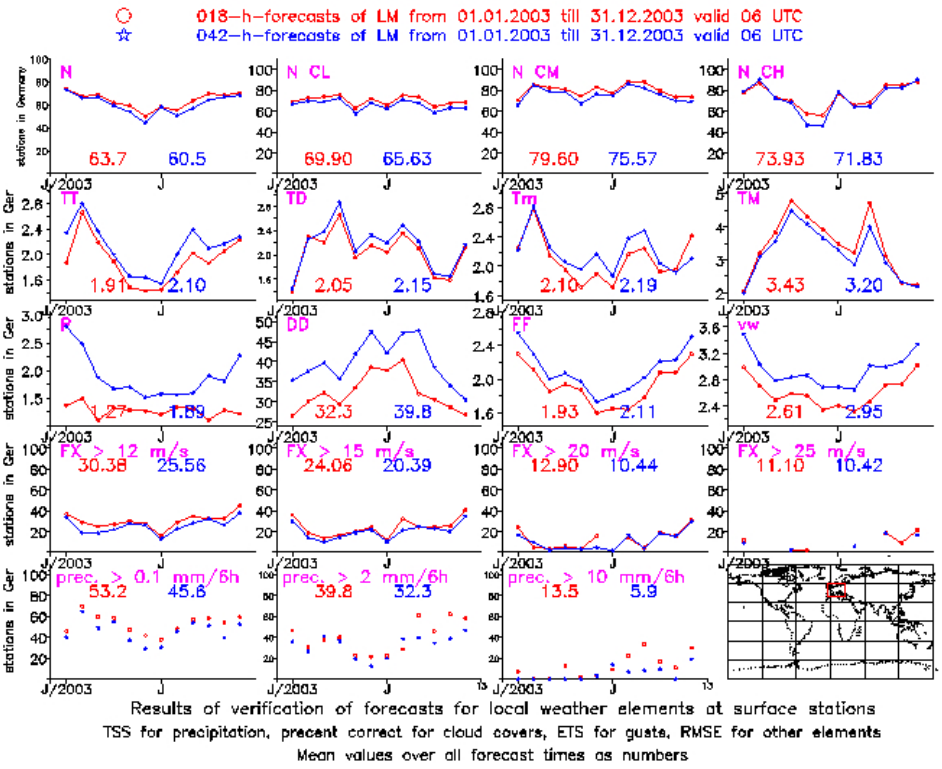

Figure 1: Results of verifcation for 18h and 42h forecasts at all Synop stations in Germany from January to December 2003. Percent correct for cloud covers, TSS for precipitation, ETS for gusts, Root mean square error for other elements (horizontal: time, vertical: score). Valid time: 06 UTC.

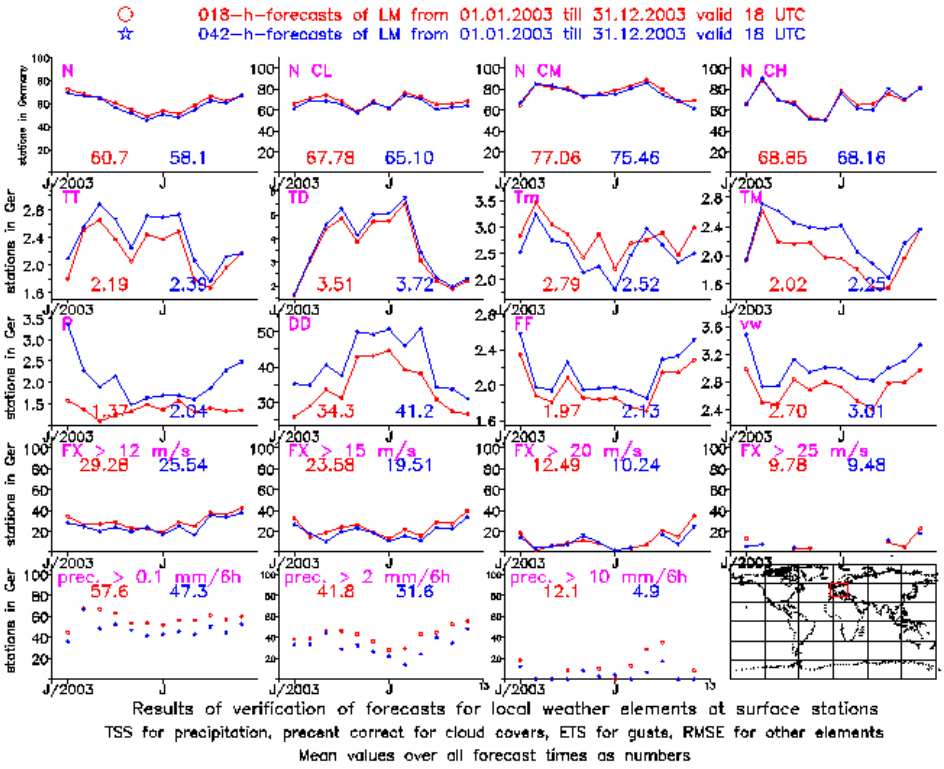

Figure 2: Results of verifcation for 18h and 42h forecasts at all Synop stations in Germany from January to December 2003. Percent correct for cloud covers, TSS for precipitation, ETS for gusts, Root mean square error for other elements (horizontal: time, vertical: score). Valid time: 18 UTC.

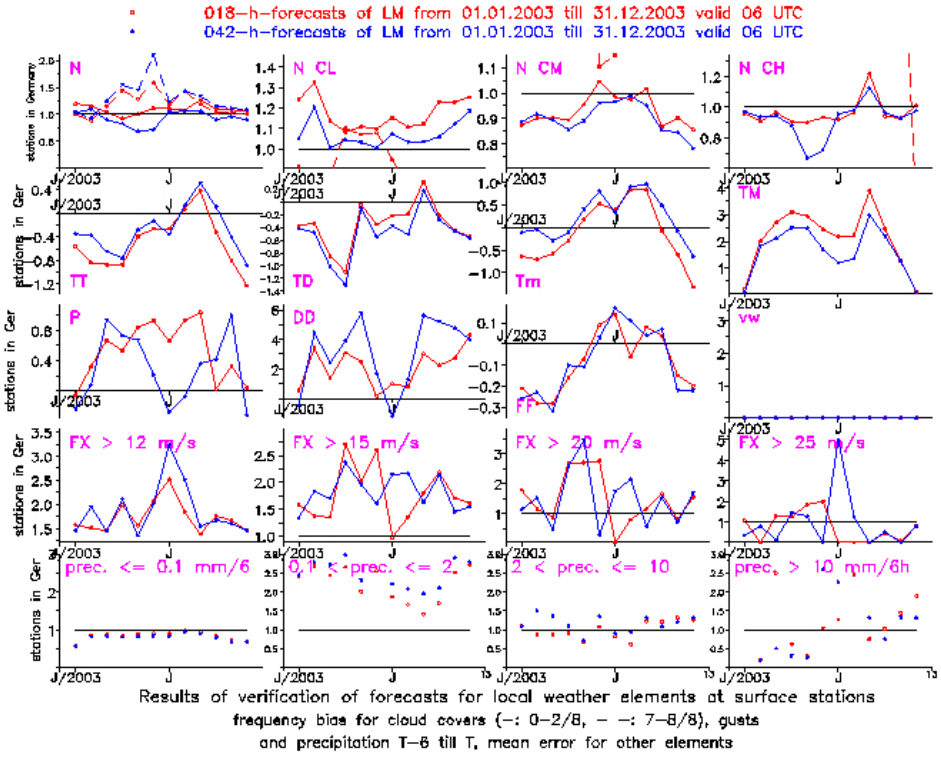

Figure 3: Results of verifcation for 18h and 42h forecasts at all Synop stations in Germany from January to December 2003. Frequency bias for cloud covers, precipitation and gusts. Bias for other elements (horizontal: time, vertical: score). Valid time: 06 UTC.

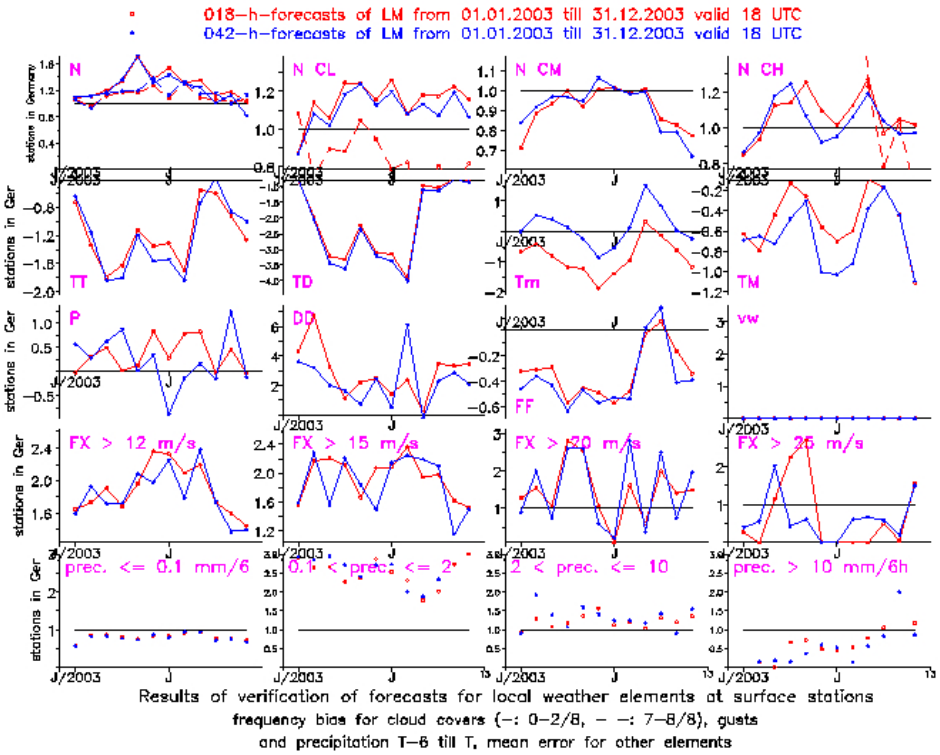

Figure 4: Results of verifcation for 18h and 42h forecasts at all Synop stations in Germany from January to December 2003. Frequency bias for cloud covers, precipitation and gusts. Bias for other elements (horizontal: time, vertical: score). Valid time: 18 UTC.

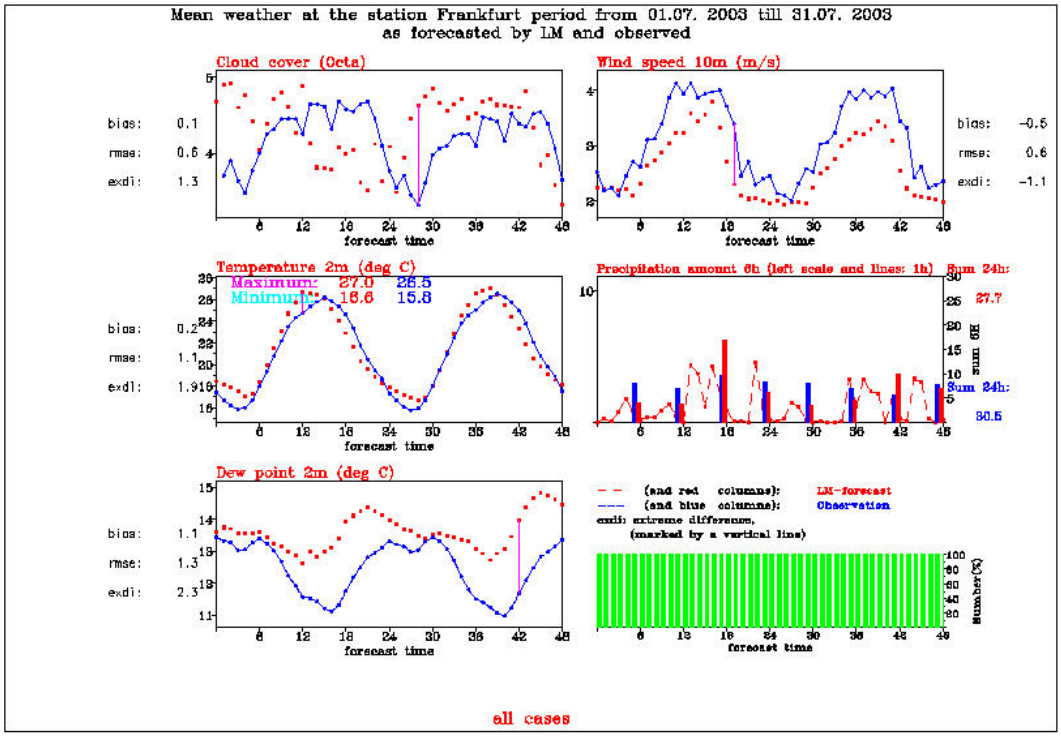

Figure 5: Diurnal cycle of different surface weather elements for the gridpoint Frankfurt/Main airport for July 2003 as forecasted and observed.

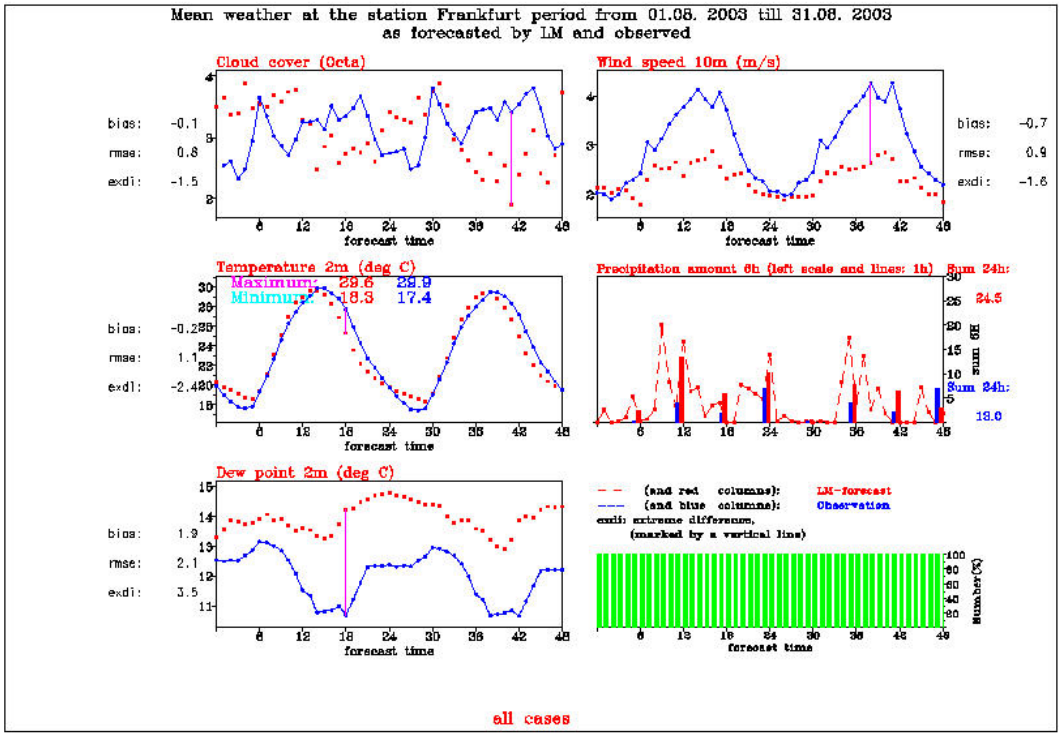

Figure 6: Diurnal cycle of different surface weather elements for the gridpoint Frankfurt/Main airport for August 2003 as forecasted and observed.

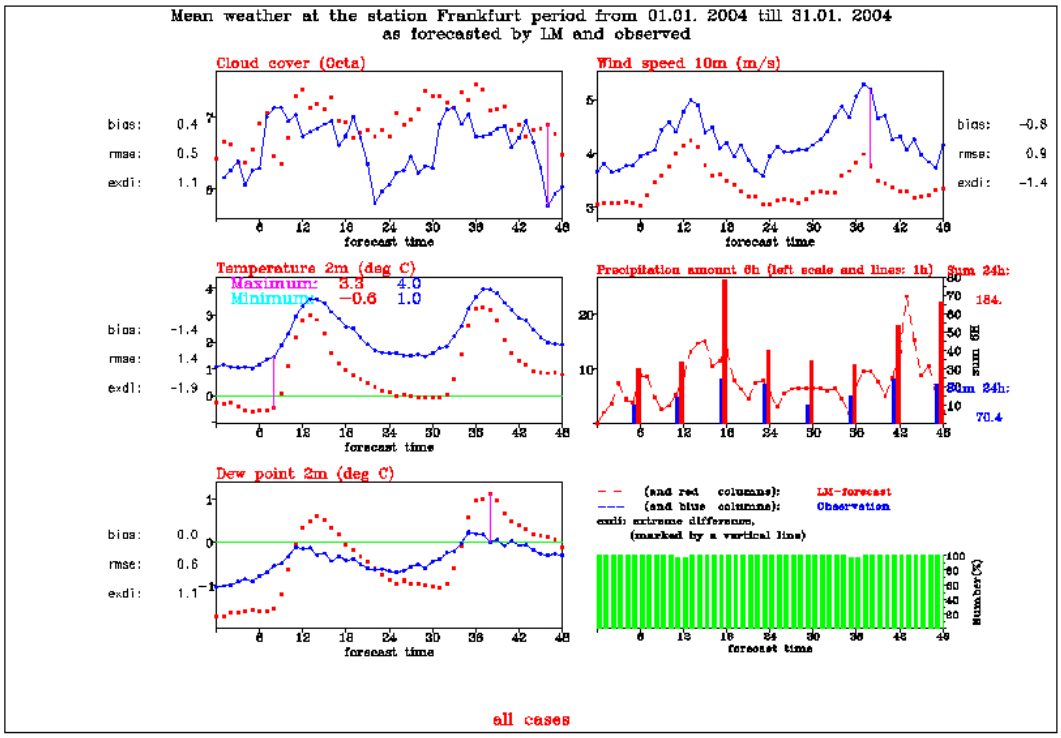

Figure 7: Diurnal cycle of different surface weather elements for the gridpoint Frankfurt/Main airport for January 2004 as forecasted and observed.

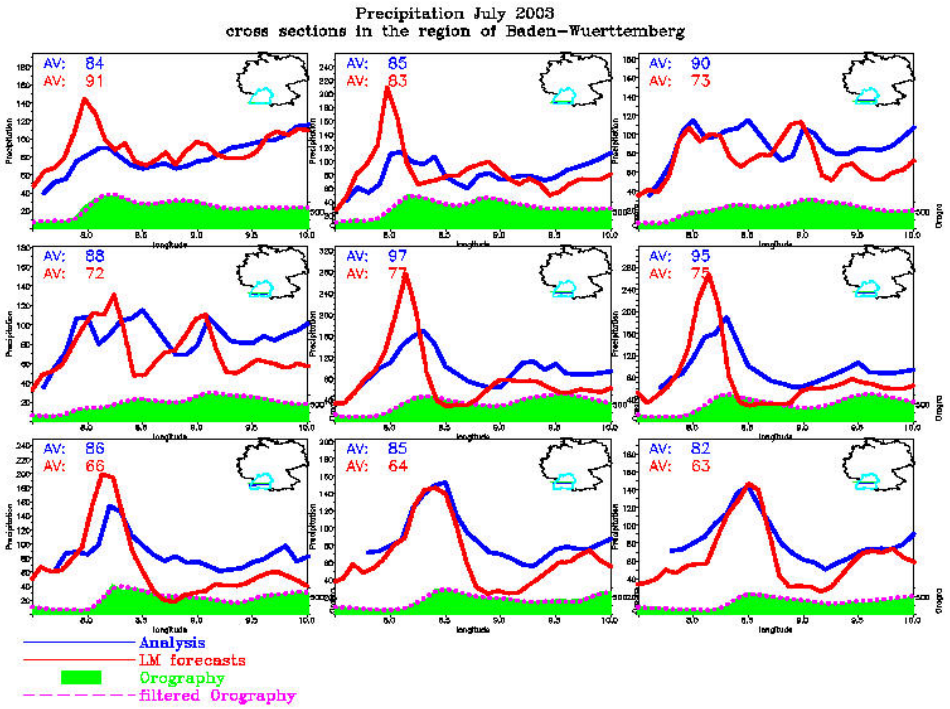

Figure 8: Various cross sections of observed and forecasted precipitation amounts for July 2003 over the southwestern part of Germany.

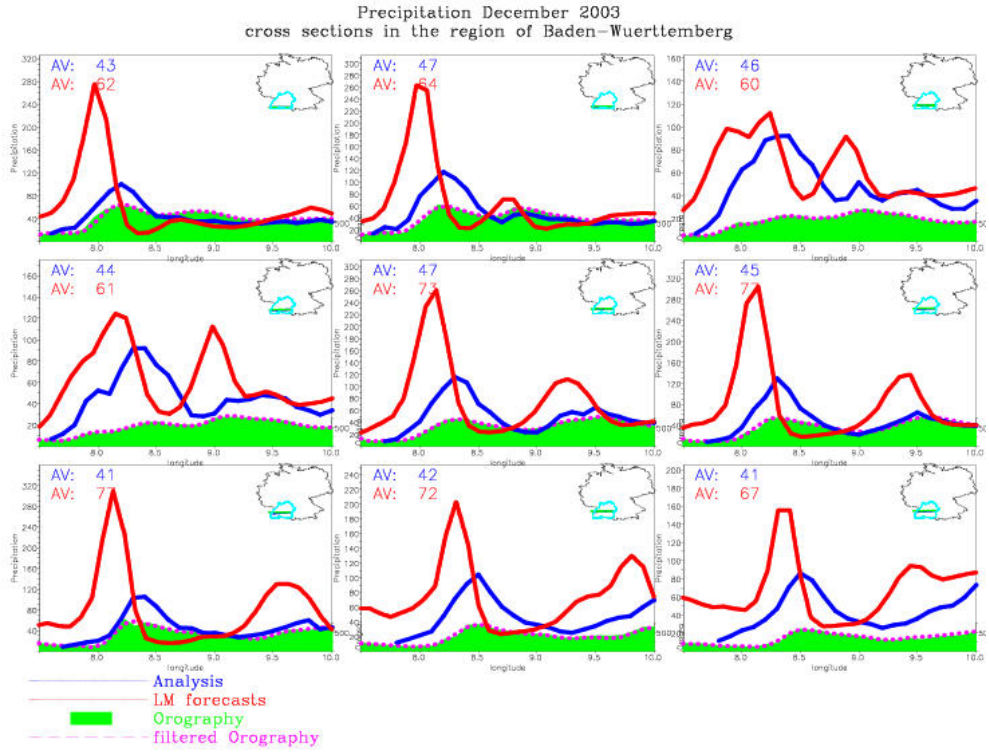

Figure 9: Various cross sections of observed and forecasted precipitation amounts for December 2003 over the southwestern part of Germany.

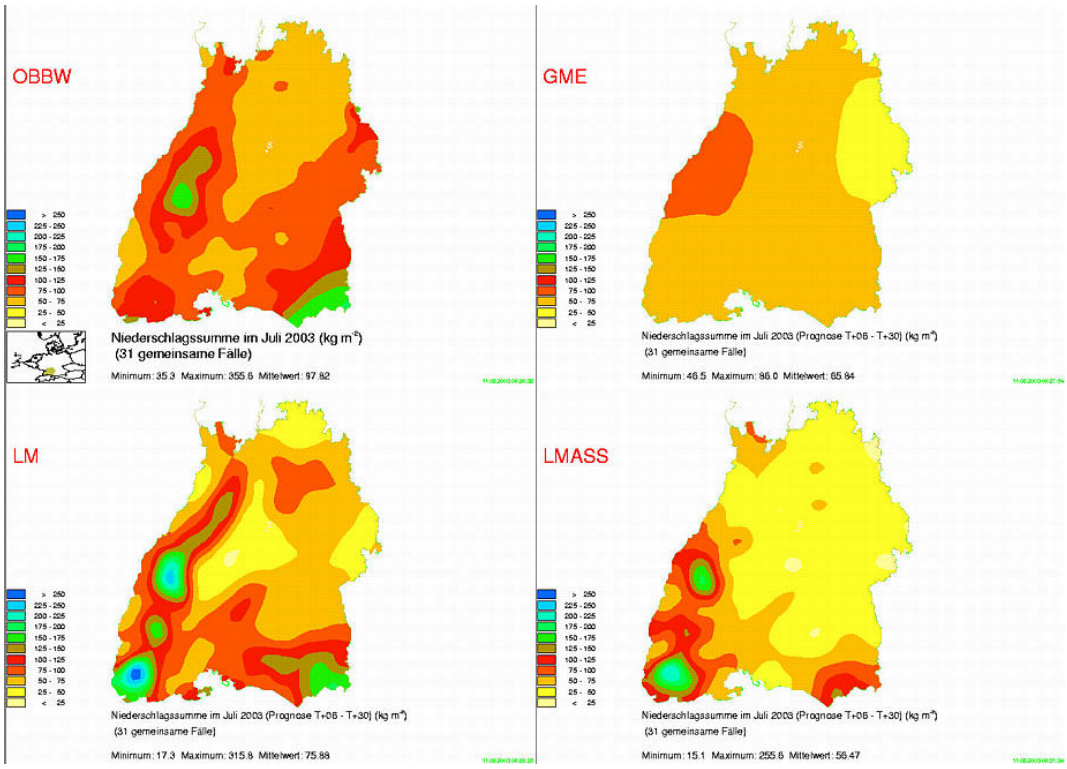

Figure 10: Horizontal distribution of observed and forecasted precipitation amounts for July 2003 over the southwestern part of Germany (OBBW: observation, GME: global model, LM: Lokal-Modell, LMASS: assimilation run of LM).

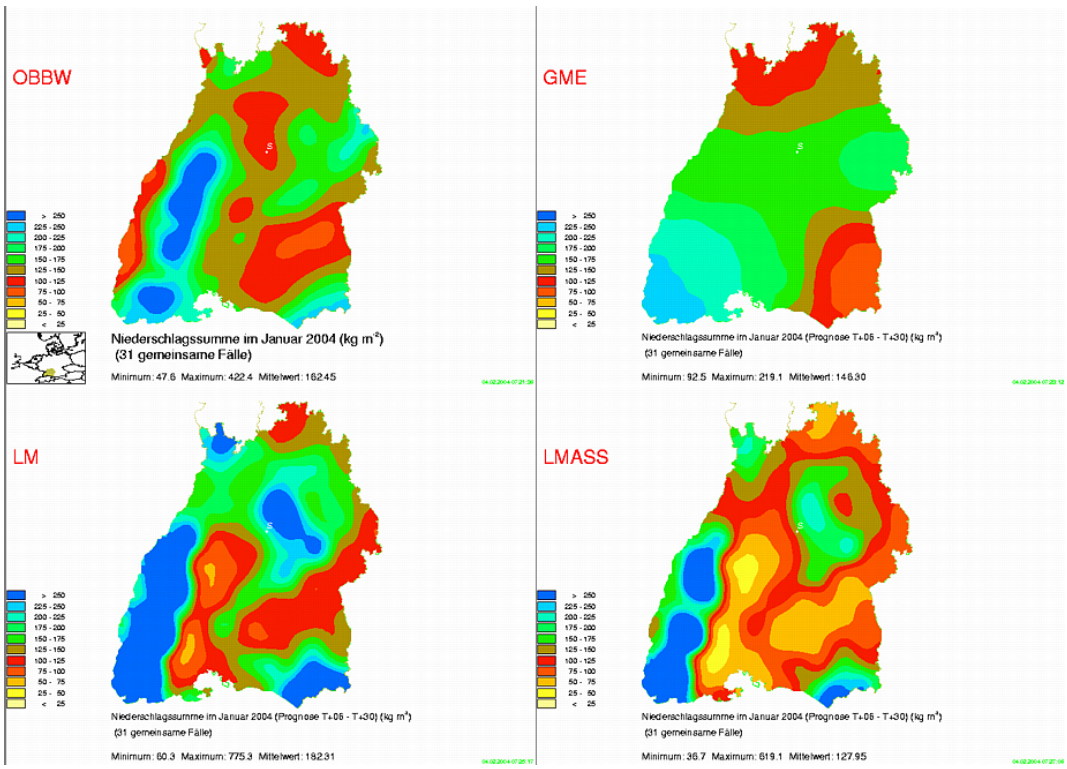

Figure 11: Horizontal distribution of observed and forecasted precipitation amounts for January 2004 over the southwestern part of Germany (OBBW: observation, GME: global model, LM: Lokal-Modell, LMASS: assimilation run of LM).

Verification of LAMI at Synop Stations

Patrizio Emiliani, M. Ferri, A. Galliani and E. Veccia

Ufficio Generale per la Meteorologia (UGM), Roma, Italy

1 Introduction

A synthesis of LAMI (the Italian version of LM) verification results for year 2003 is presented. The surface parameters analysed are 2m Temperature (2m T), 2m Dew Point Temperature (2m TD), 10m Wind Speed (10m WS), Mean sea Level Pressure (MSLP) and precipitation (PP). Rainfall verification has been considered only for the last quarter, since in October there was a change in LAMI version (from lm_f90 3.0 with initial state interpolated from GME, to lm_f90 3.5 version with initial state given by Nudging data assimilation scheme).

These five parameters are not explicit model variables but they are computed through some internal post-processing which may introduce extra errors. Nevertheless, since the internal post-processing is generally based on some diagnostic balance among the model variables, which is derived from physical constraints, it is still possible to have some important information about problems in the formulation and in the configuration of the model itself.

The observations forming the control data set were collected on 3-hourly basis from synoptic Italian network, including 91 manned stations and distributed over the Italian area; Fig. 1. shows the distribution of the stations used to compute verification. Stations were divided in three classes according to geographical location; mountain stations ($>$ 700m), valley stations or inner lowland stations and coastal stations. Station subdivision in classes has designed in order to check systematic errors related with different geographical and surface conditions. This approach can give two type of results: information about models ability in reproducing correct surface processes through a correct climatology in different geographical areas and indication of possible error source through error comparison in different areas.

In the following it will be given account of the results obtained in the verification of daily cycle for 2m T, 2m TD, 10m WS, MSLP and in categorical rainfall verification for precipitation.

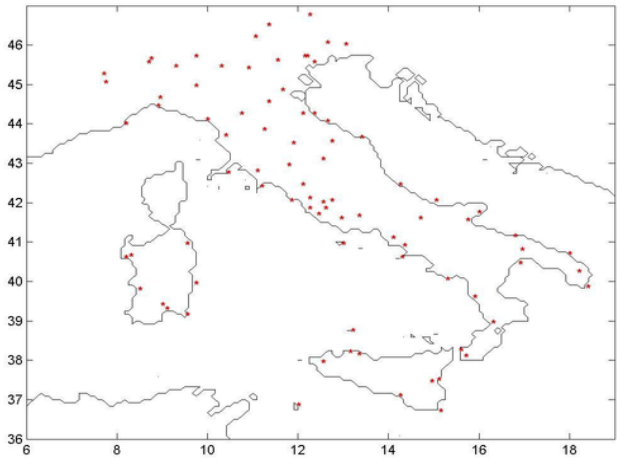

Figure 1: Synoptic Italian network.

2 Daily Cycle

In order to verify the diurnal behaviour of the model, the couples observation-forecast were stratified according to the hour of the day (3-hourly frequency), the month of the year and the forecast range (day 1 and day 2). Synchronous and co-located couples observation-forecast independently from the station position then form each sample. In such way systematic errors due to inconsistency in the surface representation of the model (inconsistency in the terrain elevation and in the percentage of the surface covered by water are the main error sources over Italy) are somewhat dumped and the signal of daily and seasonal oscillation is retained. For each of the 192 obtained samples, whose size is about 200 elements, the mean error (ME, forecast-obs) and mean absolute error (MAE) were computed.

Fig. 2a, 2b, 2c shows the behaviour of 2m-Temperature forecast error for coastal, valley and mountain stations. A clear diurnal cycle is present for all months in the mean error pattern. Coastal and valley stations ME patterns present, both for day 1 and day 2, positive peaks around sunrise hours (06 UTC in the cold months and 03 UTC in the warm months) and negative peaks near sunset. Negative peaks in ME mountain stations pattern still occur near sunset while positive peaks have a delay of 3-6 hours respect to coastal-valley stations, since occur at 09 UTC during the warm months and at 12 UTC during the cold months.

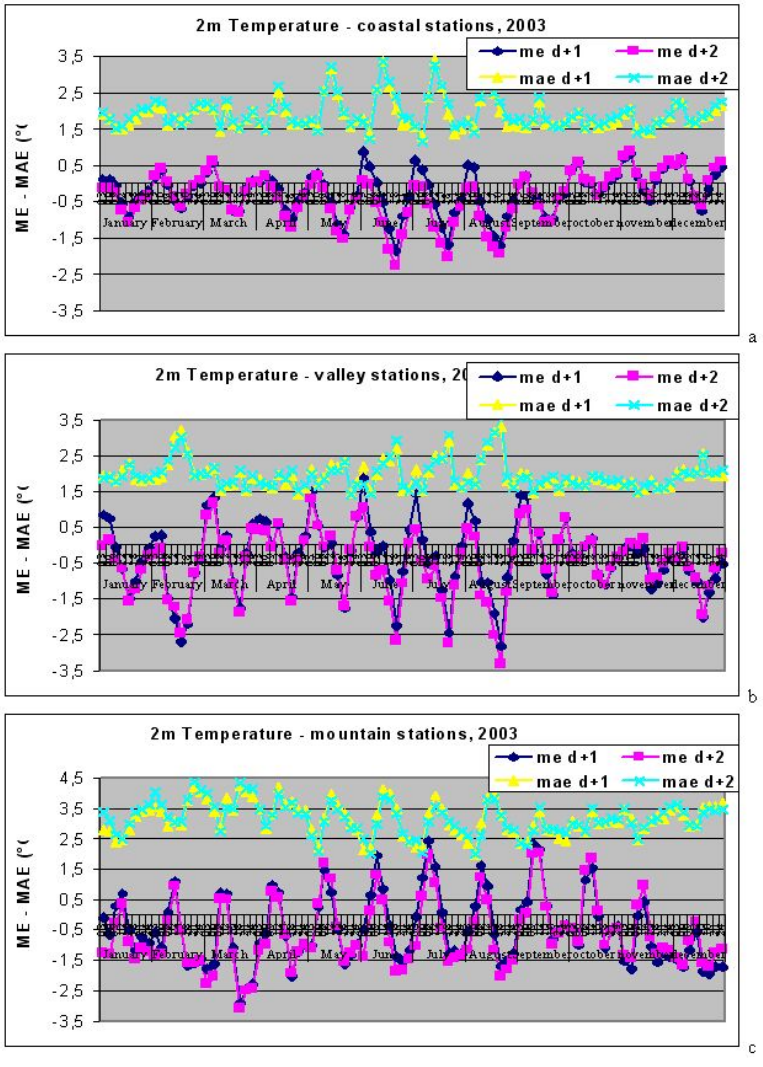

Figure 2: LAMI monthly mean error and mean absolute error of 2m Temperature for 2003.

Concerning the Mean Absolute Error a diurnal cycle is still present in the curve, even if not so clear like in ME curves. Minimum in MAE curves, corresponding to better absolute accuracy, occur in the early morning.

A diurnal cycle is also presents in ME curves of 2m Dew Point Temperature, see Fig. 3a, 3b, 3c. Beginning with coastal stations, Fig 3a, positive peaks in ME pattern occur in nocturnal hours like 2m Temperature ME. An increase in ME, with positive BIAS, occurs in the last three months of the year probably associated to nudging data assimilation scheme.

For valley stations peaks in ME curves occur in the afternoon in correspondence of low absolute accuracy (MAE peaks, 3-4.5 °C); then, a rapid decrease of ME occurs between 18 and 21 UTC. The same happens for mountain stations but with a delay of 3 hours and with high ME-MAE values. A great improvement, in MAE and ME, is associated to nudging data assimilation scheme; in fact, from October a discontinuity in the curves is well visible. For valley stations is possible to observe an amplitude reduction of ME cycle with curves oscillation centred close to zero while for mountain stations is obtained a great ME-MAE reduction but is still present a small positive BIAS.

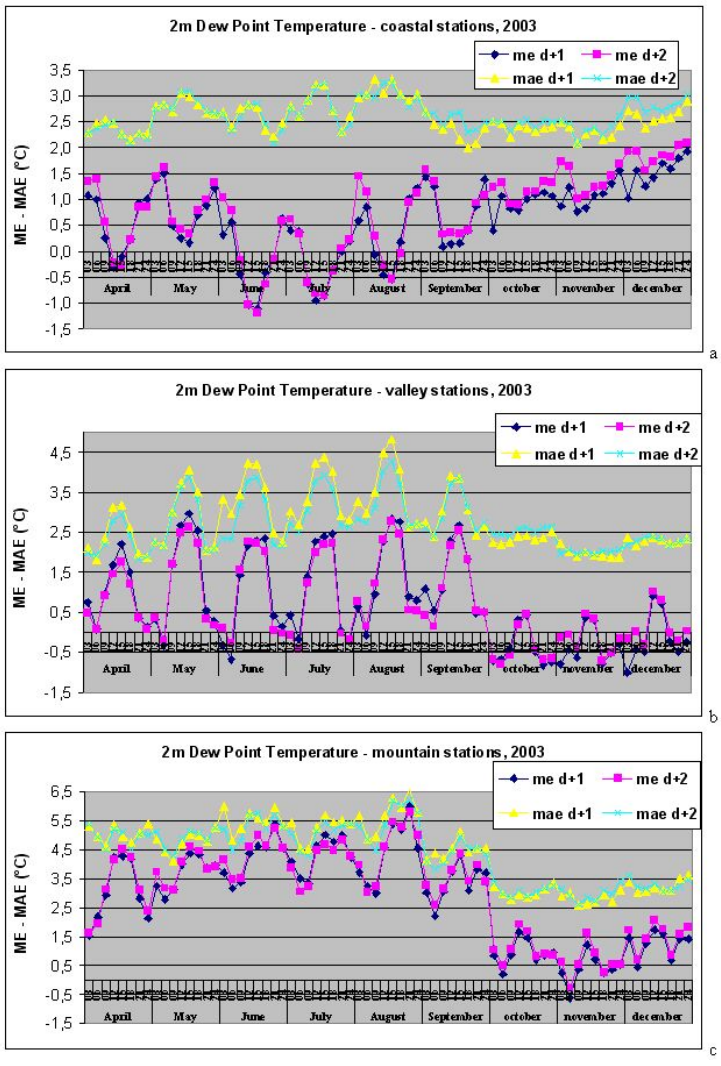

Figure 3: LAMI monthly mean error and mean absolute error of 2m Dew Point Temperature for 2003.

In Fig. 4 the curves relative to mean error and mean absolute error of 10m wind speed are showed. Even if the amplitude is small (less then 1 m/s for coastal stations, 1.5-2 m/s for valley and mountain stations) a diurnal cycle is present in ME curves. An overestimation of wind speed, positive bias, occurs during the cold months for valley and coastal stations, when dynamical circulation is dominant. Is interesting to point the attention to low ME and MEA values in summer months for coastal stations meaning a good model interpretation of local breeze circulation. Cycle peaks occur during the nocturnal hours or at sunrise for valley-coastal stations and at mid-day for mountain stations.

Fig. 5 shows MSLP mean error and mean absolute error for 2002 and 2003. A negative slope in the MAE linear tendency is present in the figure, meaning an improvement of the model performance during the last two years. Mean error curves does not show any diurnal cycle; in the warm months there is an opposite phase between ME d+1 curve and ME d+2 curve. MAE curves in Fig. 5 shows how the mean sea level pressure is less affected by local circulations or by model physics and is dominated by atmosphere dynamic; in fact, MAE increases quasi-linearly in function of forecast range (for each month, d+1 curve starts with +03 hrs and stops with +24 hrs while d+2 curve starts with +27 hrs to +48hrs forecast

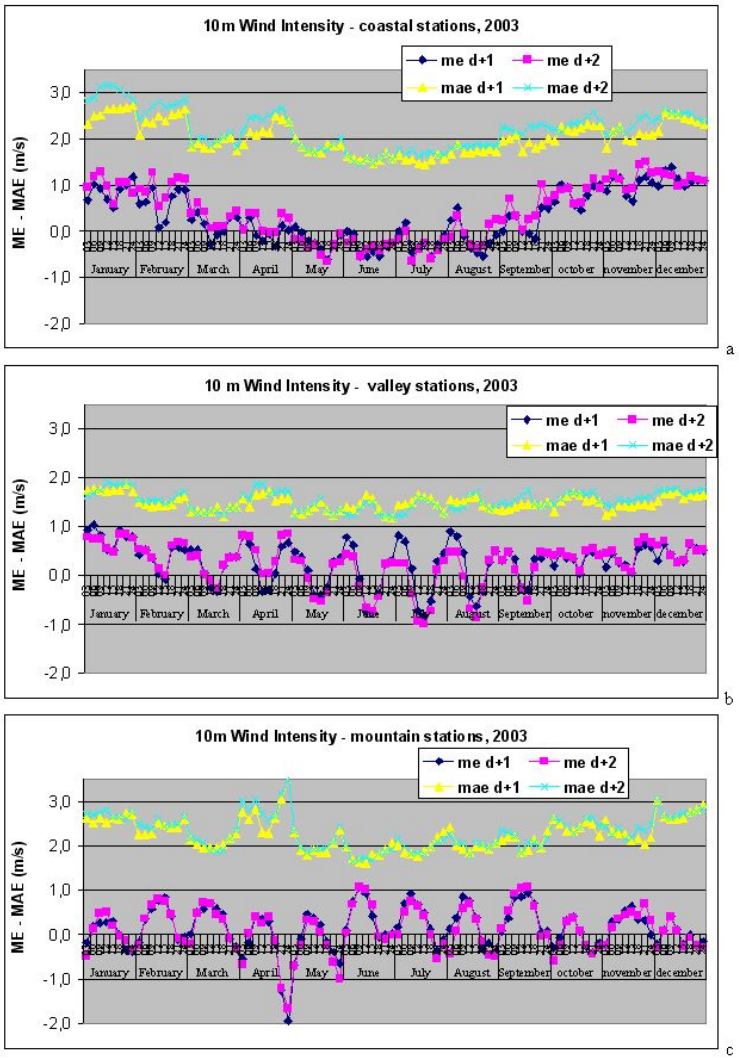

Figure 4: LAMI monthly mean error and mean absolute error of 2m Dew Point Temperature for 2003.

range) with an high degradation in MAE values during the months characterized by strong atmospheric motions.

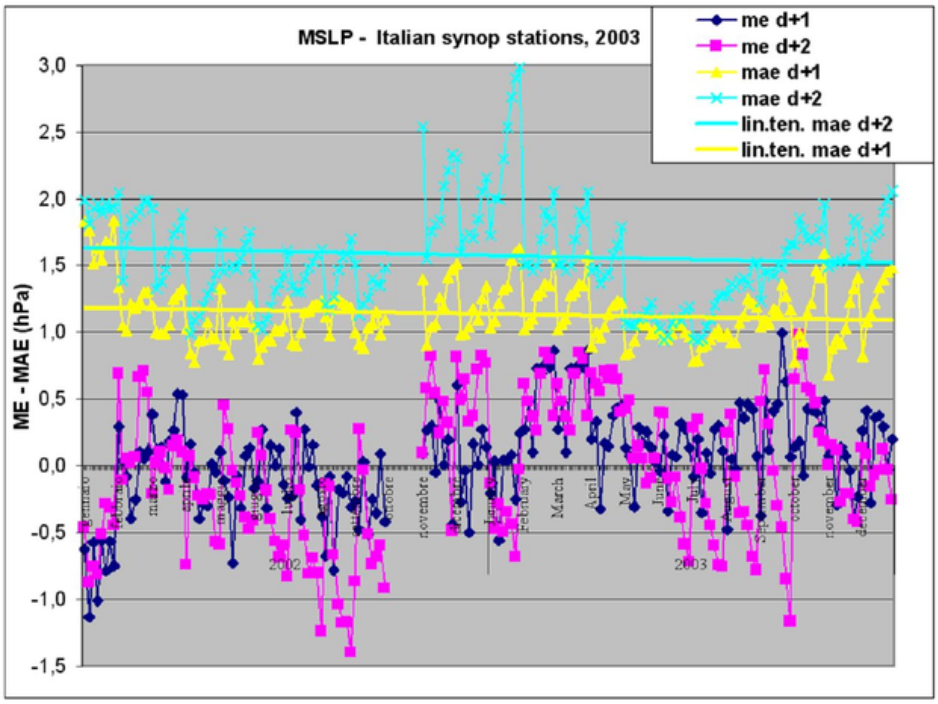

Figure 5: LAMI monthly mean error and mean absolute error of MSLP for 2003.

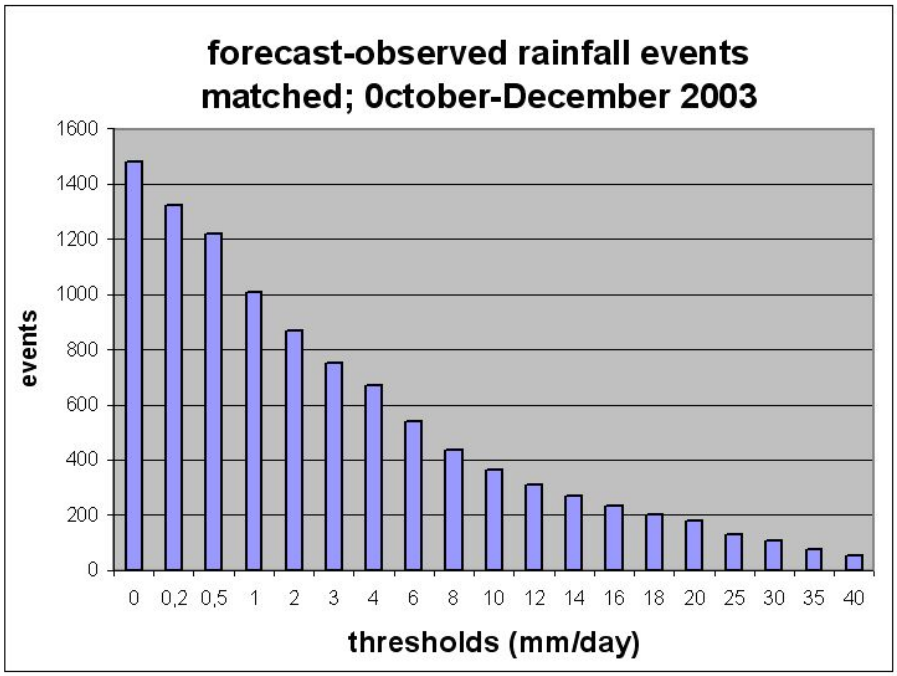

Figure 6: Number of forecast-observed rainfall events matched for verification during the last quater 2003.

3 Precipitation

The results for 2003 last quarterly precipitation are summarized in Fig. 6, 7, and 8, where FBIAS, TS, POD and FAR scores are presented for all Italian stations, without any stratifications (for details about stratified precipitation score see COSMO web site).

Fig. 7a shows a FBIAS comparison between LAMI, 00-UTC run, and ECM global model, 12-UTC run; for low threshold values, until 4mm/day, LAMI shows an overestimation of 20-30% (60% for ECM model). LAMI FBIAS increases with threshold values and a split between the forecast curves of the first and the second day occurs. The first day curve has a small FBIAS increment, showing for high threshold values an overestimation of about 50%, while the second day curve increase up to an overestimation of 100%.

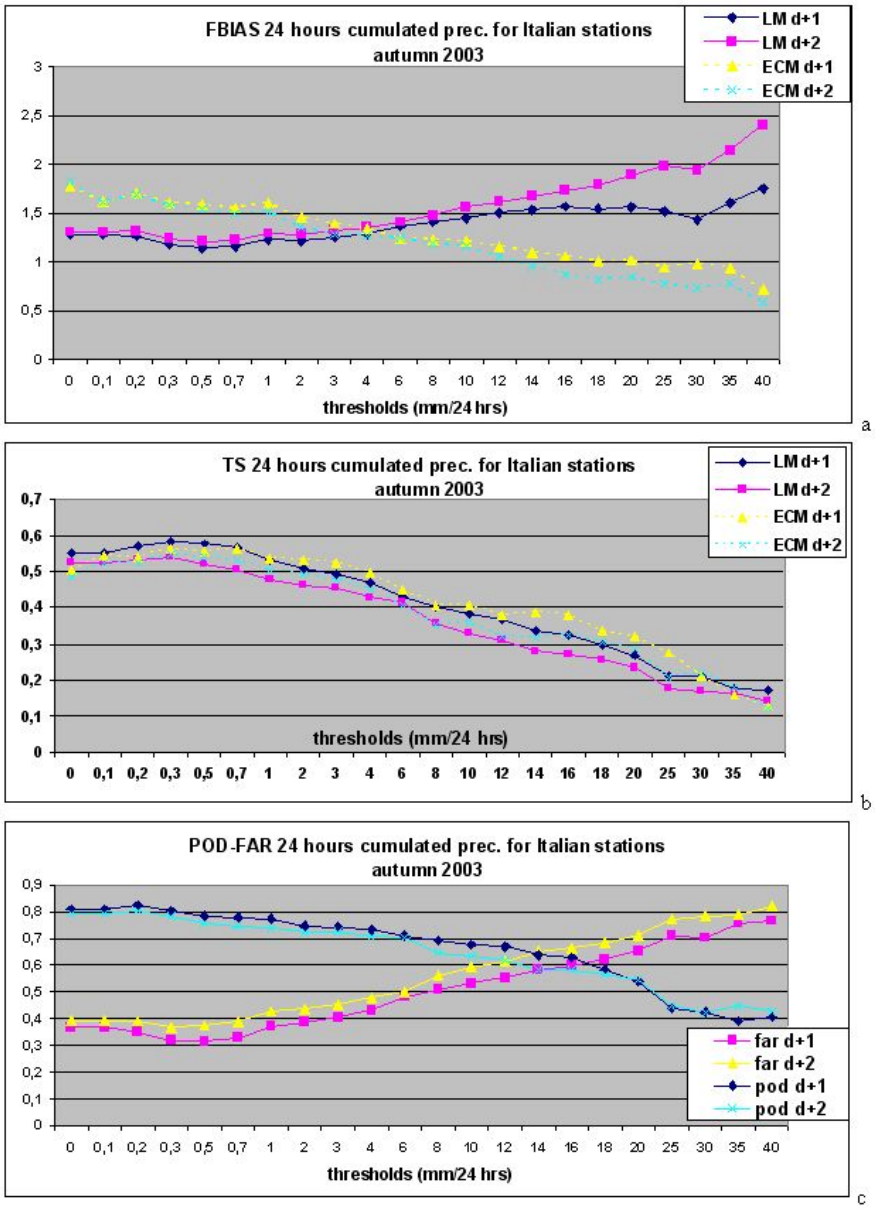

Figure 7: a: LAMI (00UTC-run) and ECM (12UTC-run) POD/FAR for 24/hours cumulated rainfall. b: FBIAS for 12/hours cumulated rainfall (both for LAMI and ECM model). c: LAMI FBIAS for 6/hours cumulated rainfall.

Threat Score for 24 hours cumulated rainfall are reported in Fig 7b. Both models show comparable TS values decreasing in function of thresholds.

LAMI Probability of detection and False Alarm Ratio plots, Fig. 7c, give useful information to understand the threshold range where forecast can be used with high benefit, that is the plot area where POD >FAR. This interpretation is more clear in Fig. 8a, where POD/FAR ratio is plotted against thresholds. In this way, model usefulness is represented by green area (POD/FAR>1) and for LAMI day-1 curve this transition threshold is around 16-18 mm/day while for day-2 curve the cross point happens at a threshold of 12mm/day. Both LAMI and ECM model seem to have the same behaviour except for intense precipitation, >30mm/day, where LAMI score results grater than ECM model score.

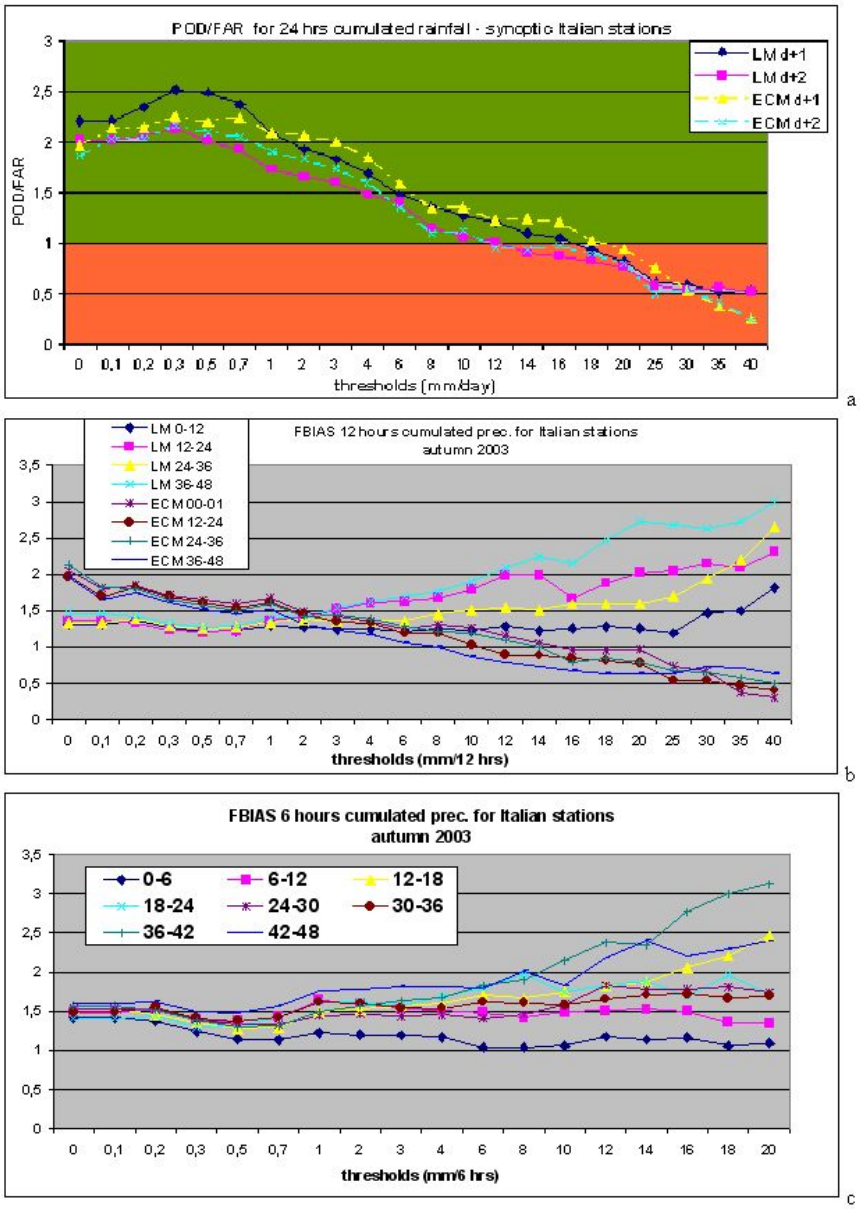

Figure 8: a: LAMI (00UTC-run) and ECM (12UTC-run) POD/FAR for 24/hours cumulated rainfall. b: FBIAS for 12/hours cumulated rainfall (both for LAMI and ECM model). c: LAMI FBIAS for 6/hours cumulated rainfall.

Examples of Verification of the LM Results Vs. Synoptic Observations and Vertical Soundings

Andrzej Mazur and Katarzyna Starosta

Institute of Meteorology and Water Management,
Centre for Development of Numerical Weather Forecasts
61 Podlesna str., PL-01673 Warsaw, Poland

Introduction

The goal of weather forecast is to reproduce all the physical processes occurring in the atmosphere together with time extrapolation of them. Numerical models, developed for many years, try to get with their results as close as possible to real meteorological situations and to elongate the period of a forecast. Direct model output (DMO) is used for many other applications (PPP - Post Processed Products), including graphical presentations, meteograms, statistical corrections (e.g. Kalman's filter) and dedicated End Products (EP) for end-users. Numerical weather forecast, obtained from COSMO-LM model is the basis for IMWM meteorologists. It is also the basis for many other forecasts like hydrological or bio-meteorological. Extremely important issue for the proper interpretation and further post-processing is the knowledge of errors of the forecast. The quality of 72-hour mesoscale forecast of DWD model for Poland was estimated through comparison of forecast results to routine meteorological observations at surface (meteorological) stations (see Fig.1) as well as to upper-air soundings, carried out at three Polish stations, located in Leba, Legionowo and Wroclaw. The location of a selected station in a particular grid square may have a big influence on a quality of forecast for this station. For example, the elevation of mountain station (calculated for the model needs) may differ and it does from a real one. In turn for station located at a seacoast influence of a neighboring sea may be also a crucial factor.

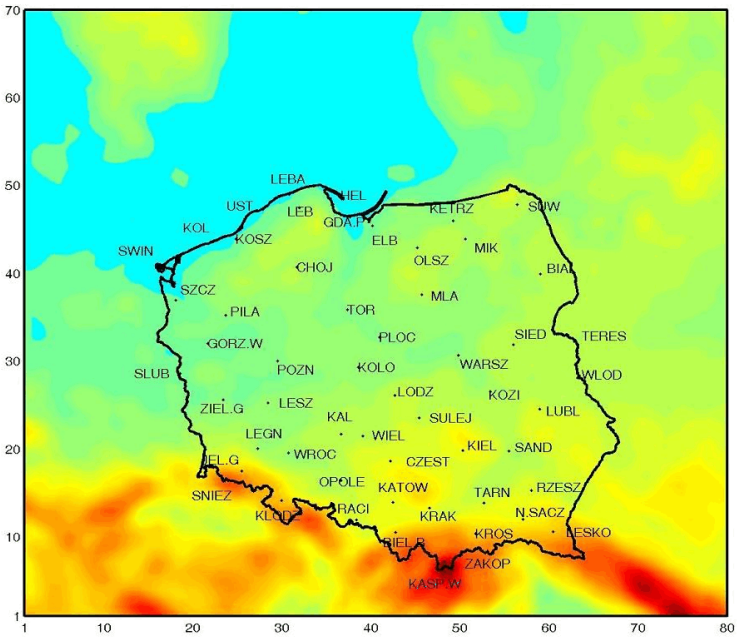

Figure 1: Locations of meteorological (surface) stations in Poland.

Figure 2: Aerological (upper-air) stations in Europe. Arrows indicate locations of Polish stations selected for comparison.

Results

The results of COSMO-LM were compared to actual values, observed at the stations. Data from regular model grid were interpolated to locations of selected meteorological stations. Following meteorological elements were concerned:

- Temperature at 2 m above ground level;
- Dew point temperature at 2 m a.g.l;
- Air pressure at sea level;
- Wind speed at 10m a.g.l.

Verification was carried out for midnight forecast for 0, 6, 12, 18, 24, 30, 36, 42, 48, 54, 60, 66 and 72 hours ahead. The following scores were calculated:

Mean Error (ME, BIAS)

$$\frac{1}{N}\sum_{i=1}^{N}(for_i - obs_i)$$

Root Mean Square Error (RMSE)

$$\sqrt{\frac{1}{N}\sum_{i=1}^{N}(for_i - obs_i)^2}$$

Mean error (average over one month) may be interpreted as a systematic forecast error and thus may be considered during further processing. Root mean square error is a pattern describing the range of deviation. Results of this verification are shown in the following pictures.

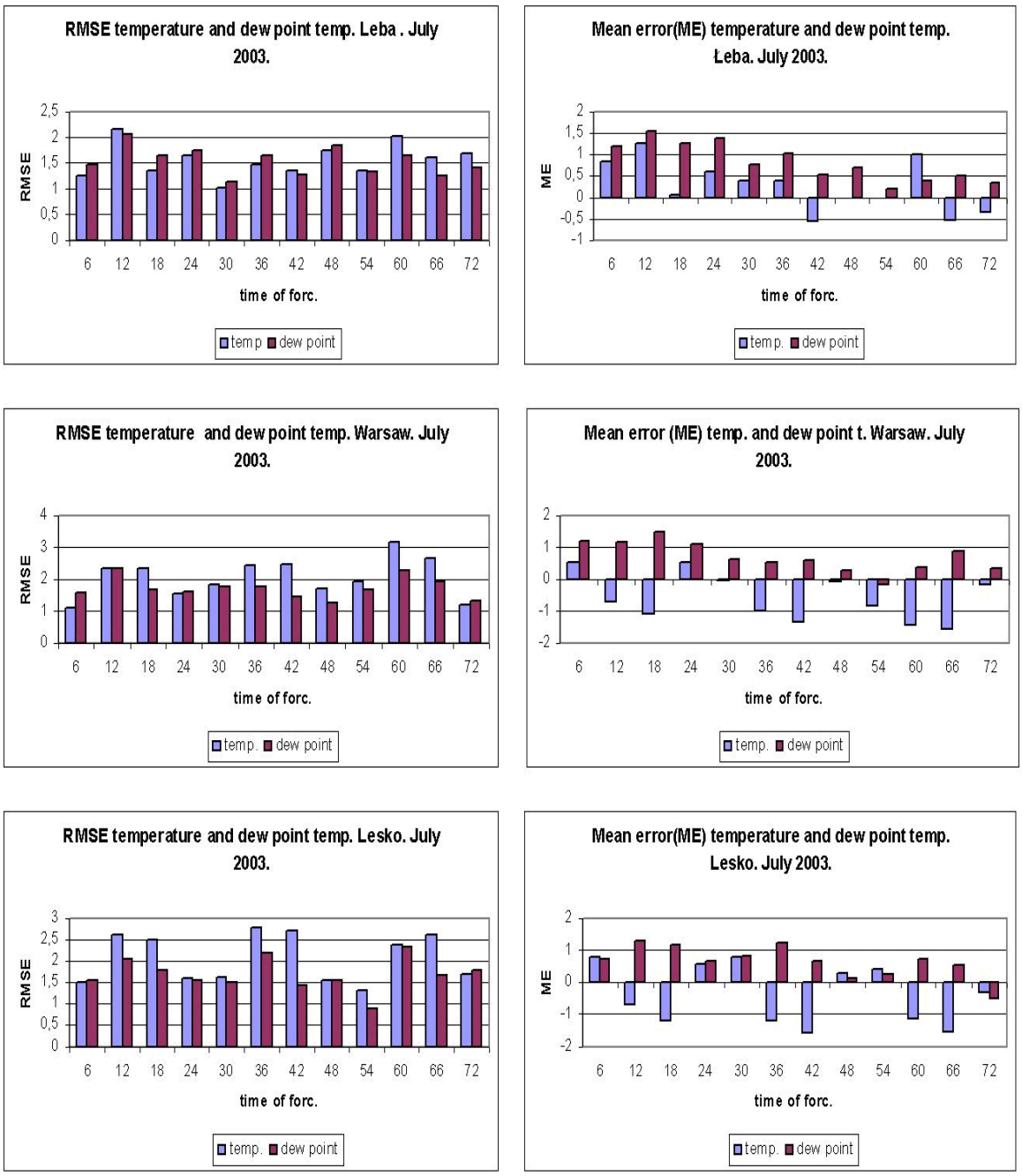

Figure 3: RMSE (left) and ME (right) of temperature and dew point temperature at 2m a.g.l for selected Polish meteorological stations.

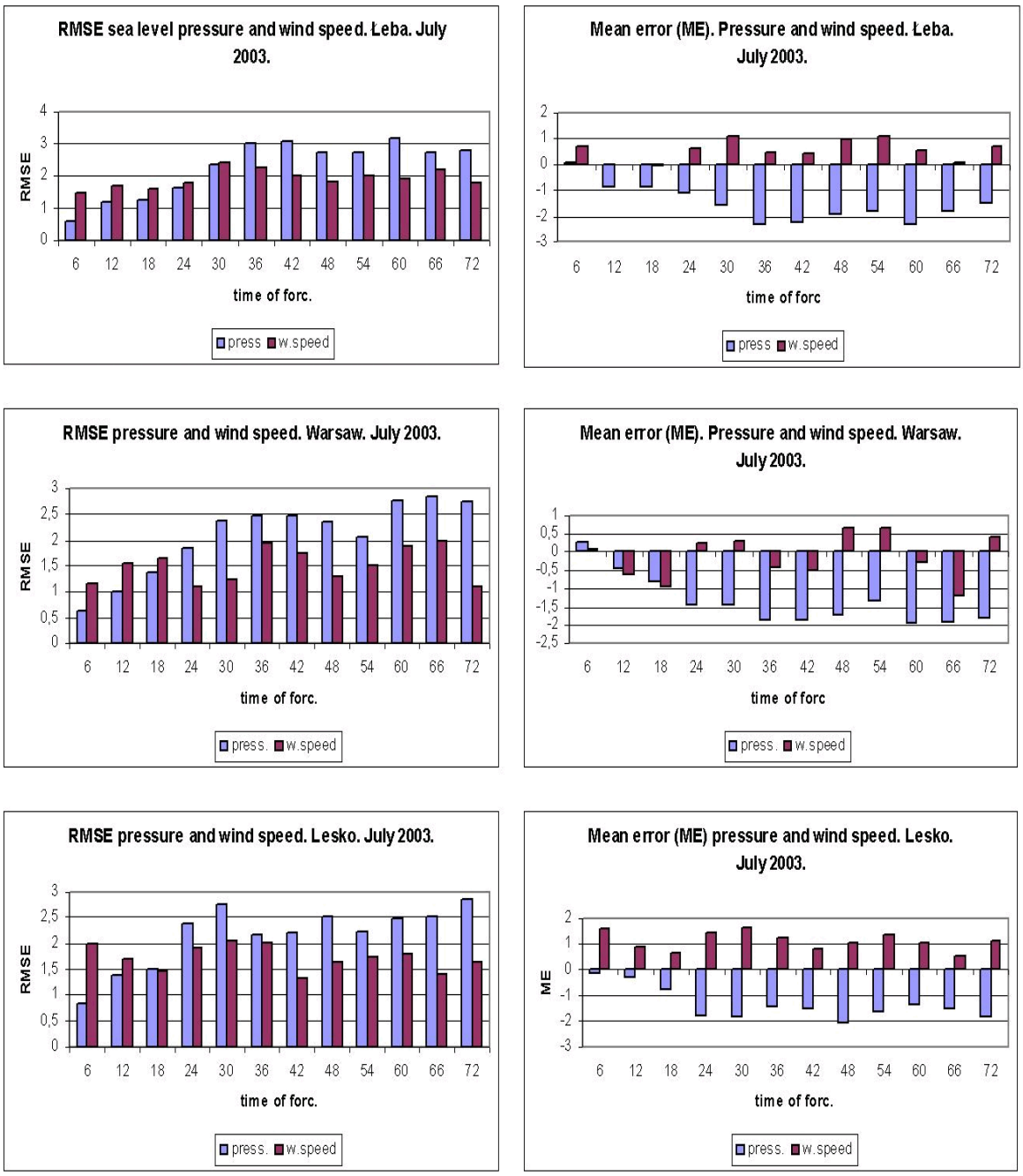

Figure 4: RMSE (left) and ME (right) of sea-level pressure and wind speed for selected Polish meteorological stations.

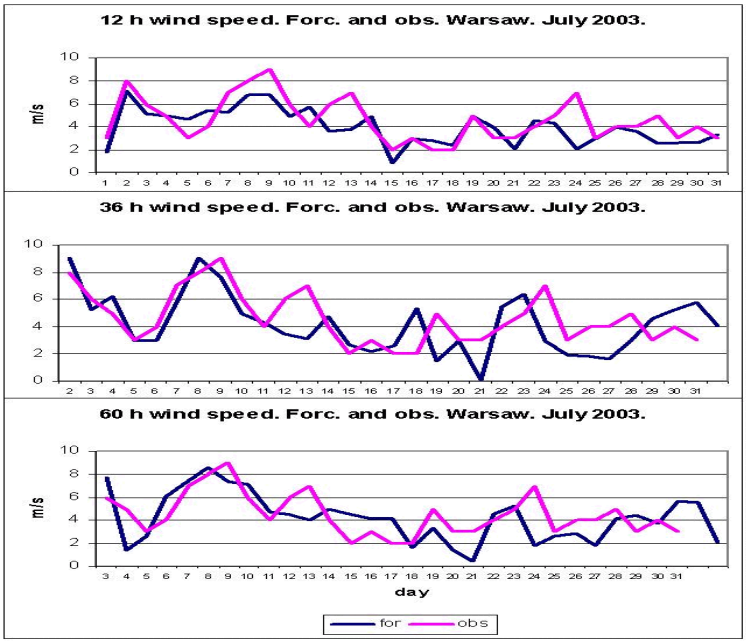

Figure 5: Wind speed - forecast and observations in Warsaw, July 2003. Upper panel - forecast for 12 hours, middle - for 36 hours and lower - for 60 hours ahead.

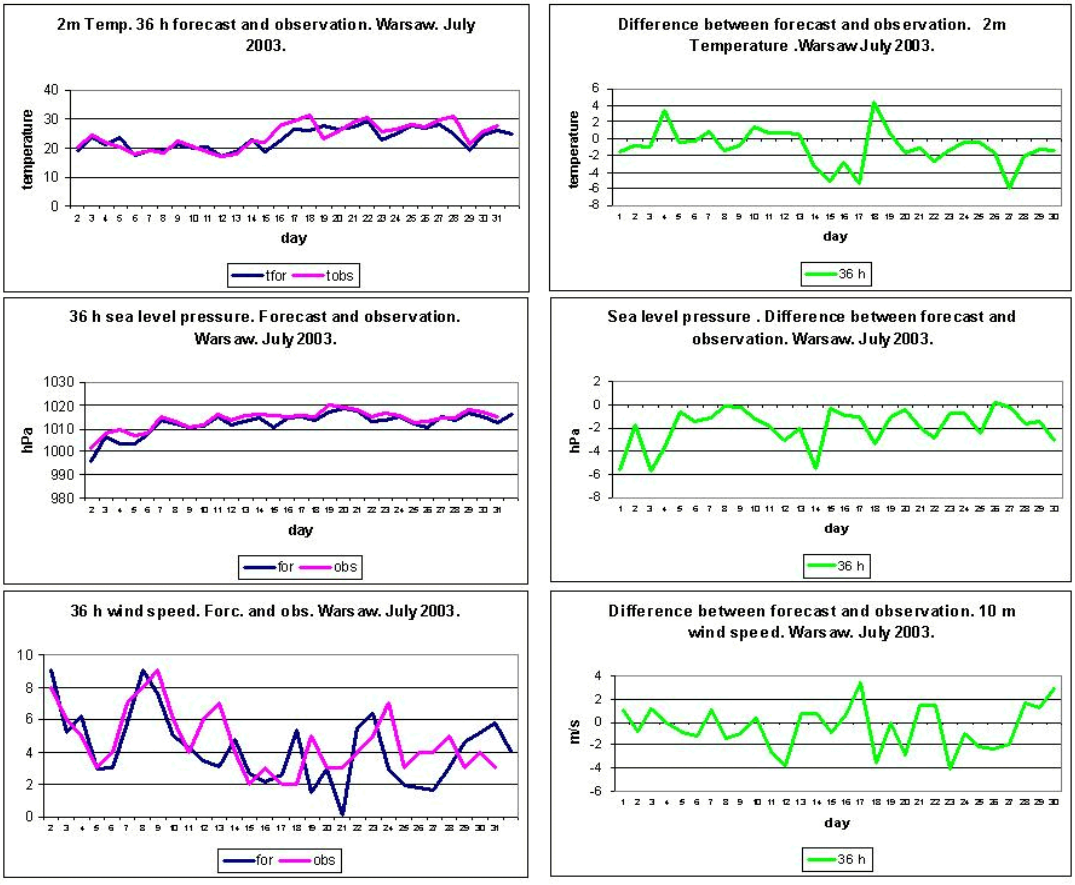

Figure 6: Air temperature, pressure and wind speed - forecast, observations and difference between them in Warsaw, July 2003. Forecast valid for 36 hours ahead.

As far as upper-air verification is concerned, it was done in 12-hour intervals, namely 12, 24, 36, 48, 60, and 72 hour of forecast with similar scores. The following meteorological elements (at standard pressure levels 1000, 850, 700, 500, 400, 300, 250 and 200hPa) were considered:

- Temperature;
- Relative humidity;
- Height of standard pressure level(s);
- Wind speed.

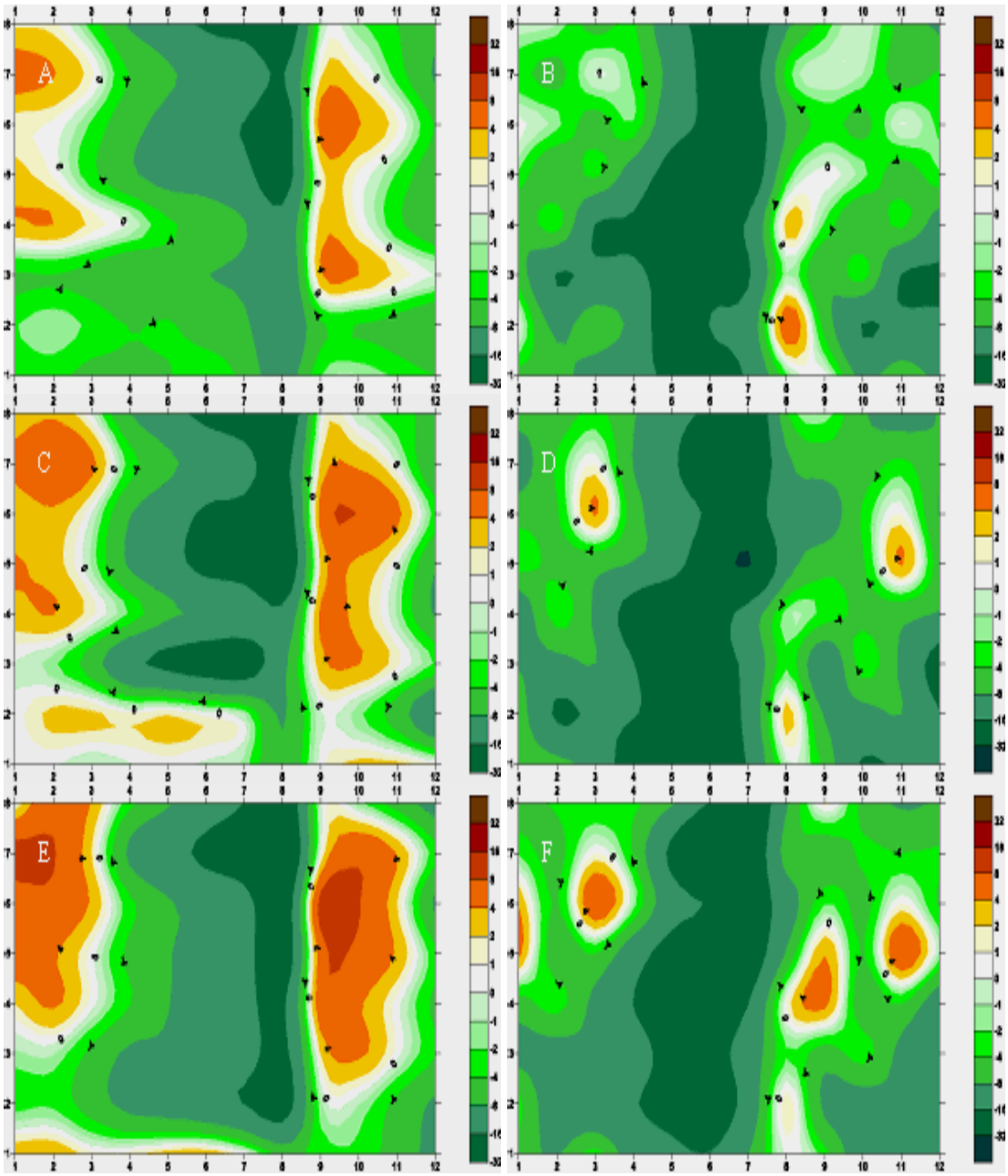

Figure 7: Monthly mean ME at standard pressure levels (1000, 850, 700, 500, 400, 300, 250 and 200 hPa). Left column - height of pressure level, right - relative humidity (forecast valid for 12 hours ahead). Comparison with upper-air soundings at: A and B - Leba station, C and D - Legionowo station, E and F - Wroclaw station. X-axis - months, Y-axis - pressure levels.

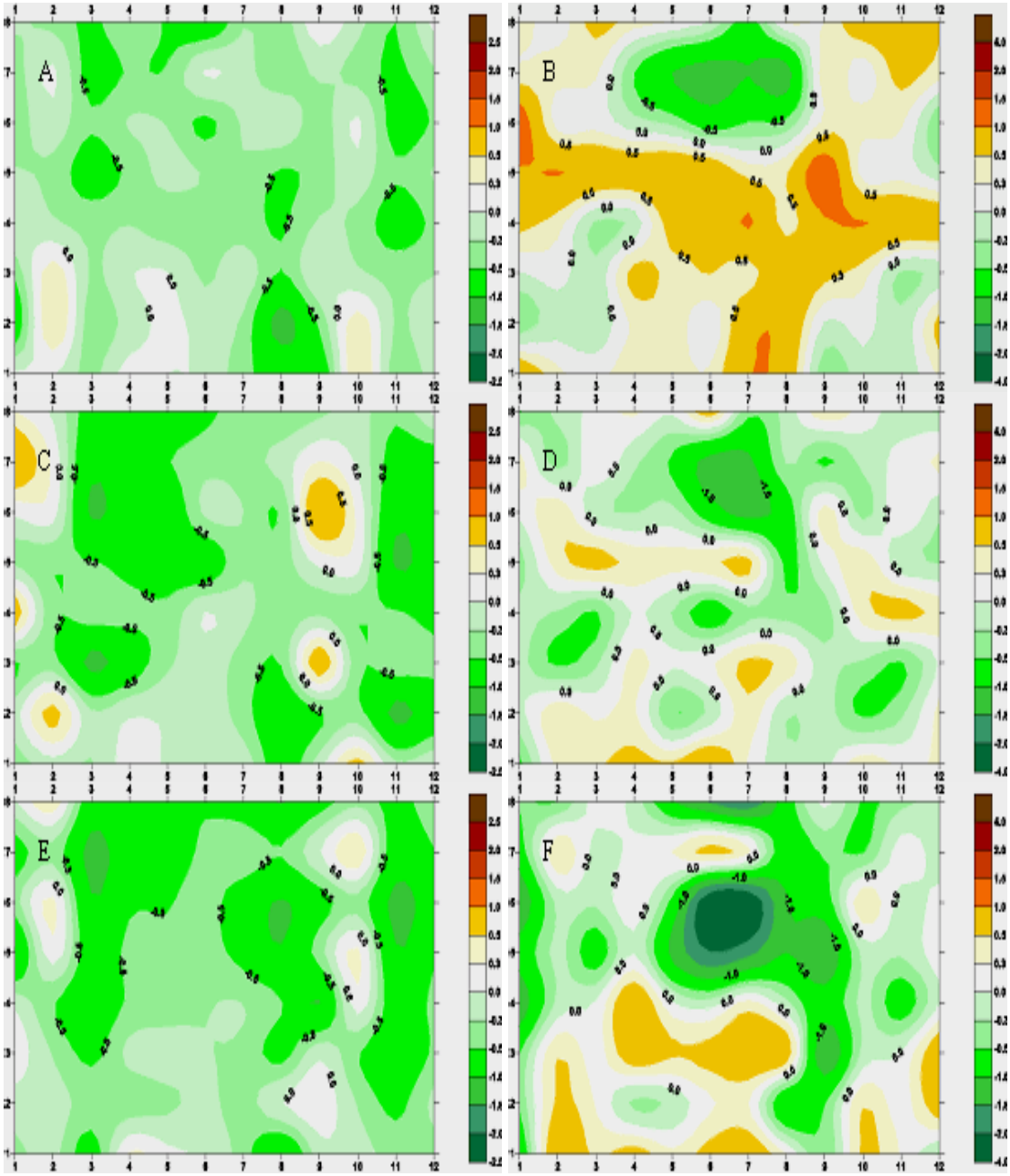

Figure 8: Monthly mean ME at standard pressure levels (1000, 850, 700, 500, 400, 300, 250 and 200 hPa). Left column - temperature, right - wind speed (forecast valid for 12 hours ahead). Comparison with upper-air soundings at: A and B - Leba station, C and D - Legionowo station, E and F - Wroclaw station. X-axis - months, Y-axis - pressure levels.

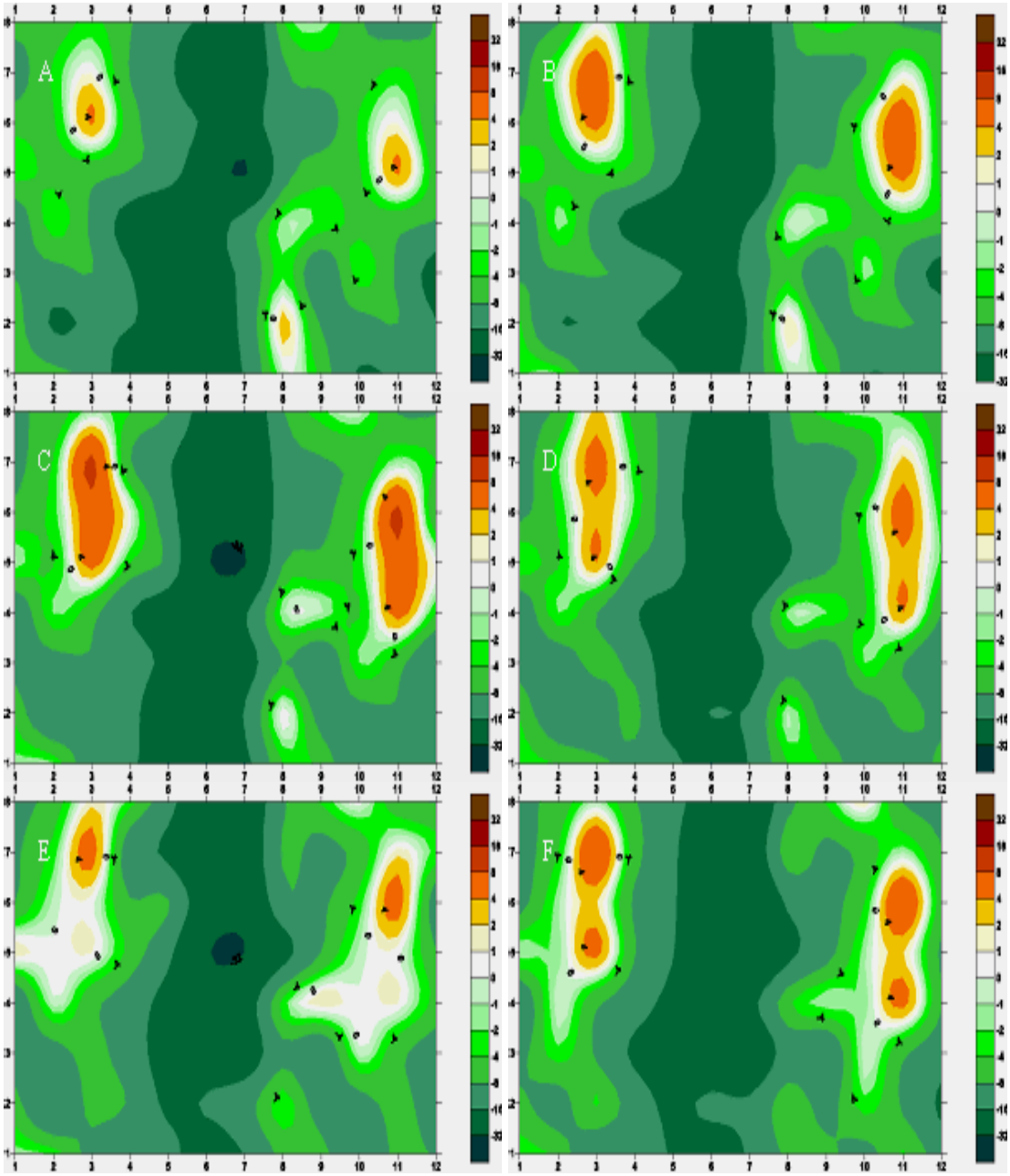

Figure 9: Monthly mean ME of relative humidity at standard pressure levels (1000, 850, 700, 500, 400, 300, 250 and 200 hPa). Comparison with upper-air soundings at: Legionowo station. Forecasts valid for: A - 12 hours, B - 24 hours, C - 36 hours, D - 48 hours, E - 60 hours, F - 72 hours ahead. X-axis - months, Y-axis - pressure levels.

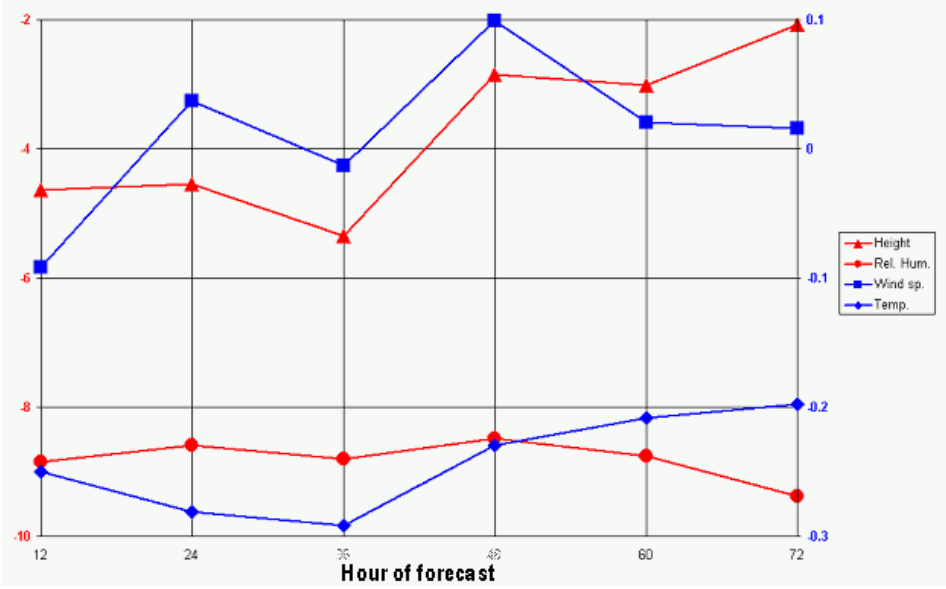

Figure 10: Annual average ME for height of pressure levels (m, left Y-axis), relative humidity (%, left Y-axis), wind speed (m/s, right Y-axis) and temperature (°C, right Y-axis) for forecast up to 72 hours ahead.

Discussion

A) Surface Parameters

RMSE for air temperature (and dew point) shows clear diurnal tendency. Large errors are observed for 12 and 18 hours (daytime) of forecast. For nighttime, error is significantly smaller (Warsaw and Lesko). Similar tendency can be seen for wind speed, and value of an error is considerably smaller for nighttime than for daytime. The tendency for air pressure is notably different. RMSE, very small in the beginning of the forecast, increases with the time of forecast.

In Warsaw, considered as typical station in middle Poland, monthly mean error is almost zero for nighttime of the forecast (0- and 6 hour) and is very small (and less than zero) for daytime (12- and 18 hour of forecast). Similar character of error can be seen at Lesko. For dew point temperature, almost all errors are positive while the opposite situation occurs for air pressure. All the errors are rather small for the beginning of the entire forecast and time courses (of forecast and observations) are very similar. The forecast of wind speed for very close to the real values, at least as July 2003 is concerned.

B) Upper-Air Soundings Conclusion that can be derived from the results gained is that the forecast is "surprisingly good" for temperature and wind speed and, moreover, that model is "too wet". Indeed, especially close to ground level, ME for both temperature and wind speed is very small, approximately ± 1 degree and $\pm$ 1m/s, respectively. The poorest (still interesting, however) situation appears in case of relative humidity, where - especially during a summer season - ME appears to be greater than 30%, which makes the value of relative error of about 50%. Furthermore, the quality of forecast of relative humidity (and only this forecast) decreases monotonously with time. For other parameters this tendency - naturally expected - is not so clearly seen.

Operational Verification of Vertical Profiles at DWD

Ulrich Pflüger

Deutscher Wetterdienst, P.O.Box 100465, 63004 Offenbach a.M., Germany

1 Introduction

The operational upper-air verification at the Deutscher Wetterdienst uses all the available radiosonde stations over the integration domain of LM to verify the vertical structure of the forecasts. The parameters considered are geopotential, relative humidity, temperature, wind direction and wind speed.

In addition, so-called multi-level aircraft reports, which are created from aircraft observations from the ascent or descent flight phase are used for verification purposes. Each of the multi-level reports comprises of a group of at least 4 original single-level aircraft reports, which must be within a 20 km radius and a 15 minute interval from the lowest report in the group. Furthermore, the vertical spacing between successive reports may not exceed 55 hPa. These multi-level aircraft reports can be regarded as piecewise vertical profiles, and are treated like radiosonde profiles but considered separately in the verification. The parameters verified are temperature, wind speed and wind direction.

Vertically the atmosphere is divided into bins of 25 hPa below the 800-hPa level and of 50 hPa between the 800-hPa and 100-hPa levels. Above 100 hPa, the bins are bounded by the pressure levels 100, 70 ,50 ,30 , 20 and 10 hPa. Complying with the height, every observation, respectively every forecast increment is allocated to one bin.

2 Annual Mean Profiles of BIAS and RMSE

Figure 1a displays the profile of the annual mean error (bias, left column) and the annual root mean square error (rmse, right column) against all radiosonde data at 00 UTC within the LM domain for different forecast times (analysis, 12h, 24h, 36h, 48h) and different parameters (geopotential, relative humidity, temperature, wind direction and wind speed from top to bottom) for 2003. On the right side of each panel, the number of observations used in each bin is shown as a bar chart.

Figure 1b shows the same illustration but for verification time 12 UTC.

Figure 1c and Figure 1d are like Figure 1a and 1b but for the year 2002.

The comparison of the corresponding figures demonstrates that generally the annual mean profiles of bias and rmse do not change very much between the year 2002 and the year 2003.

The bias of geopotential reduces somewhat for both verification times and for all forecast times, except for the 48 h forecast below 600 hPa. Especially at verification time 12 UTC there is a negative bias of about 2 m in 2003. Changes in rmse are very small too, whereas with longer forecast times a rmse reduction of about 1 m has occurred.

Above 600 hPa, there are some changes in the bias of relative humidity. At verification time 00 UTC, the slight negative bias shifts to a positive bias, and at verification time 12 UTC, the slight positive bias increases clearly. The reduction of rmse of relative humidity above

400 hPa is ascribed to the implementation of a prognostic cloud ice scheme in October 2003. Since then there is a reduction of up to 10 % in the monthly mean profiles. Note that this is partly resulting form the smaller range of humidity values because, in contrast to the old scheme the ice scheme rarely produces relative humidity values close to 100 % at that height.

Between 600 hPa and 300 hPa, there is a slight decrease in the bias of temperature, while below 800 hPa in particular at verification time 00 UTC, the negative bias increases, compared to the year 2002. Rmse of temperature remains predominantly unchanged.

In 2002, the bias of wind direction was close to zero nearly everywhere above 700 hPa but in 2003 a negative bias up to 2 degrees has appeared. The rmse profiles of wind direction remain unchanged.

The bias of wind velocity has the same structure in 2003 as in the year before, but exhibits a slight tendency for a decrease. The rmse of wind velocity has decreased predominantly in the range of tropopause.

3 Time Series of Monthly Mean Profiles of BIAS and RMSE

In order to show both the seasonal and interannual variation of the bias and rmse, time series of the vertical distribution of the monthly bias (left column) and rmse (right column) and rmse are presented in Figure 2 to Figure 9 for each parameter. For lack of space and in favour of a comparison of verification against radiosonde data and verification against aircraft observations, only the verification time 00 UTC for 3 forecast times (analysis, 24 h and 48 h, from top to bottom) is shown. Because aircraft observations are only used below the 250 hPa level, the vertical range of the time series differs from that of the annual profiles in Figure 1a to Figure 1d.

Figure 2 displays the time series of the vertical profiles of the monthly geopotential bias and rmse against radiosonde data. It shows that the relatively small bias below 600 hPa in the annual mean (especially at 48 h forecast in the year 2003, see Figure 1a) has a strong seasonal variation with values less than -10 m in summer and up to +8 m during the rest of the year. Furthermore, the negative bias in summer is coupled with a relatively small rmse.

Figure 3 shows that in 2003 compared to 2002, there is an increase of the positive bias of relative humidity in the middle atmosphere during the autumn and winter months and a slight decrease of the negative bias during summer at forecast times 24 h and 48 h. This can also be seen in the profiles of the annual means as aforementioned. In the lower troposphere below 800 hPa, a positive bias during spring and summer months is found. It was larger in the year 2003 compared to 2002 The aforementioned decrease of rmse of relative humidity above 400 hPa due to the implementation of prognostic cloud ice in October 2003 is also evident in Figure 3.

Figure 4 displays the time series of the vertical profiles of the monthly temperature bias and rmse against radiosondes. Figure 5 is analogous but verifying against multi-level aircraft observations as described before. It is evident that the behaviour of bias and rmse of temperature against radiosondes and against aircraft data in the years 2002 and 2003 is very similar, and there are also no major differences between verification against radiosonde and verification against aircraft data. Compared to both observing systems, the middle troposphere of the LM simulations is to warm in the summer and too cold in the winter, while the lower troposphere is predicted too cold except for December 2002. Also, the rmse of temperature has similar variations with both observing systems, but is about 0.2 K greater in the verification against radiosonde data.

Figure 6 and Figure 7 display the same as Figure 4 and Figure 5 but for the wind velocity. A comparison of Figure 6 left column (bias of wind velocity against radiosondes) with Figure 7 left column (bias of wind velocity against multi-level aircraft measurements) shows in the lower troposphere big systematic differences between the verification against the two observing systems. While the bias against radiosondes is negative below 950 hPa the bias against multi-level aircraft measurements is positive below 850 hPa. The monthly variation of the bias is similar in both cases but the numerical values are shifted. Above 850 hPa a negative bias exists with similar variations in both cases, with the negative bias against aircraft observations being a little bit stronger.

The reason for the difference in the bias at low levels is possibly due to the accuracy of the measurement of wind speed depending on the flight attitude of aircraft. Figure 11 (WMO No. 958, 2003) shows the combined effect of pitch and roll at an airspeed of 150kt. For definition of roll/pitch angle see Figure 10. Thus, with 5 degrees pitch angle and 10 degrees roll angle, a wind vector error of some 2kt (1m/s) can be expected regardless of the true wind vector. At 300kt airspeed, the wind error doubles to 4kt (2m/s). The observation error increases with increasing aircraft roll angle at a given pitch angle. Below 850 hPa, aircraft are turning frequently (large roll angle) and have in parallel the strongest climb and descent rates (large pitch angle). In the LM data assimilation the pitch and roll angles are not yet taken into account, so aircraft measurements with relatively great observing errors may be used and could cause perhaps this behaviour of bias. Below 500 hPa the rmse of forecasts against aircraft observations is about 0.5 m/s larger than that against radiosondes.

The bias of wind direction forecasts (Figure 8,9 left columns) against radiosondes and aircraft observations does also have different signs below 950 hPa (negative with radiosondes and positive with aircraft measurements), with the bias against aircraft observations being stronger than the bias against radiosondes.

Below 800 hPa rmse of wind direction forecasts (Figure 8,9 right columns) is about 5 degrees lower at verification against radiosondes, whereas above 800 hPa at least at 48 h forecast, rmse is lower at verification against aircraft measurements.

4 References

WMO No. 958, 2003: Aircraft Meteorological Data Relay (AMDAR) Reference Manual.

1a: 2003 00 UTC

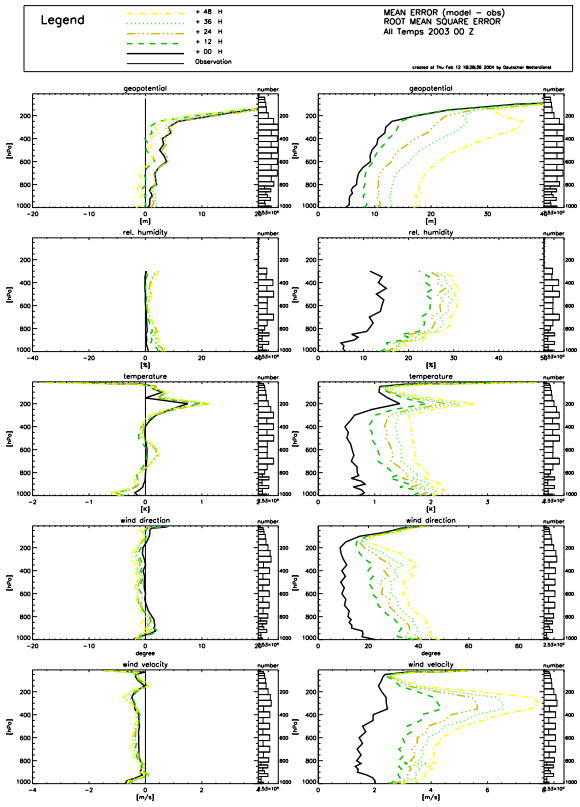

1b: 2003 12 UTC

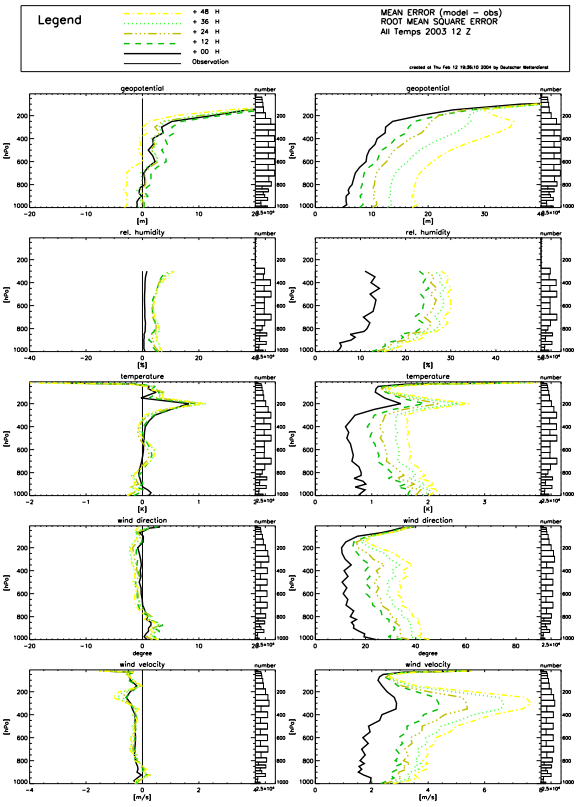

1c: 2002 00 UTC

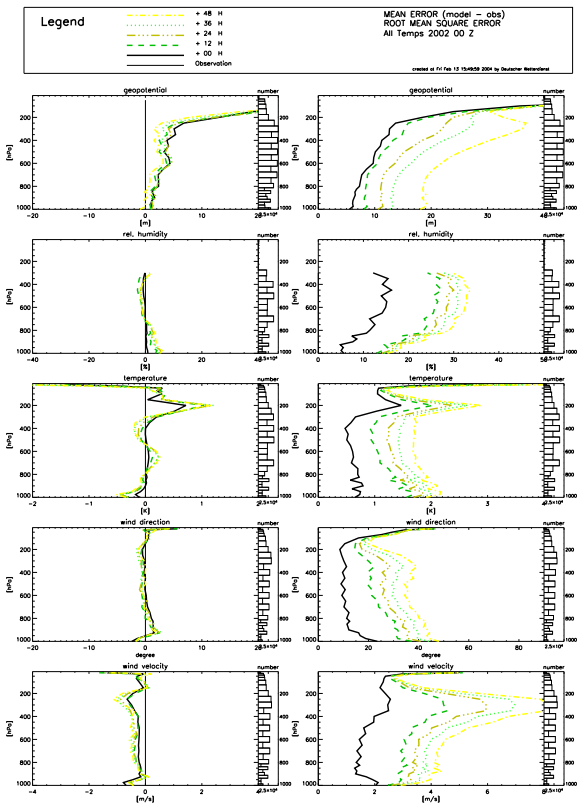

1d: 2002 12 UTC

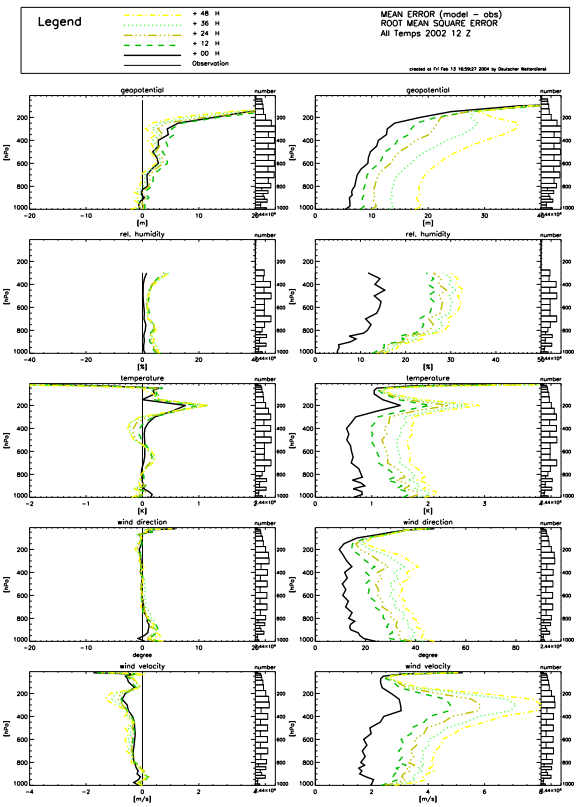

Figure 1: Vertical profiles of annual mean of bias (left column) and rmse (right column) at all radiosonde stations for different forecast times of LM runs at DWD. 1 a: 2003 00 UTC, 1 b:2003 12 UTC 1 c: 2002 00 UTC 1 d: 2002 12 UTC. From top to bottom at each column: geopotential, relative humidity, temperature, wind direction and wind velocity.

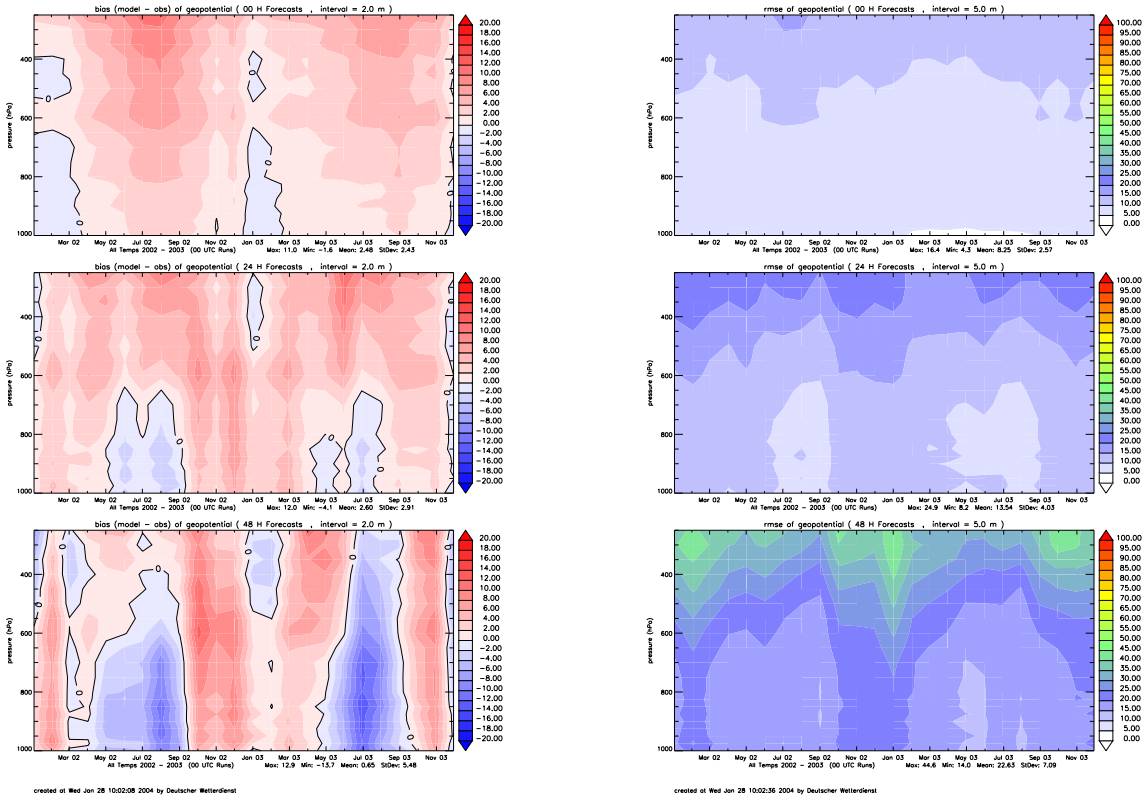

Figure 2: Time Series (January 2002 - December 2003) of gepotential bias (left column) and rmse (right column) against radiosonde data based on monthly mean profiles for 00 UTC LM runs at DWD. From top to bottom: Analysis, 24 h, and 48 h forecast.

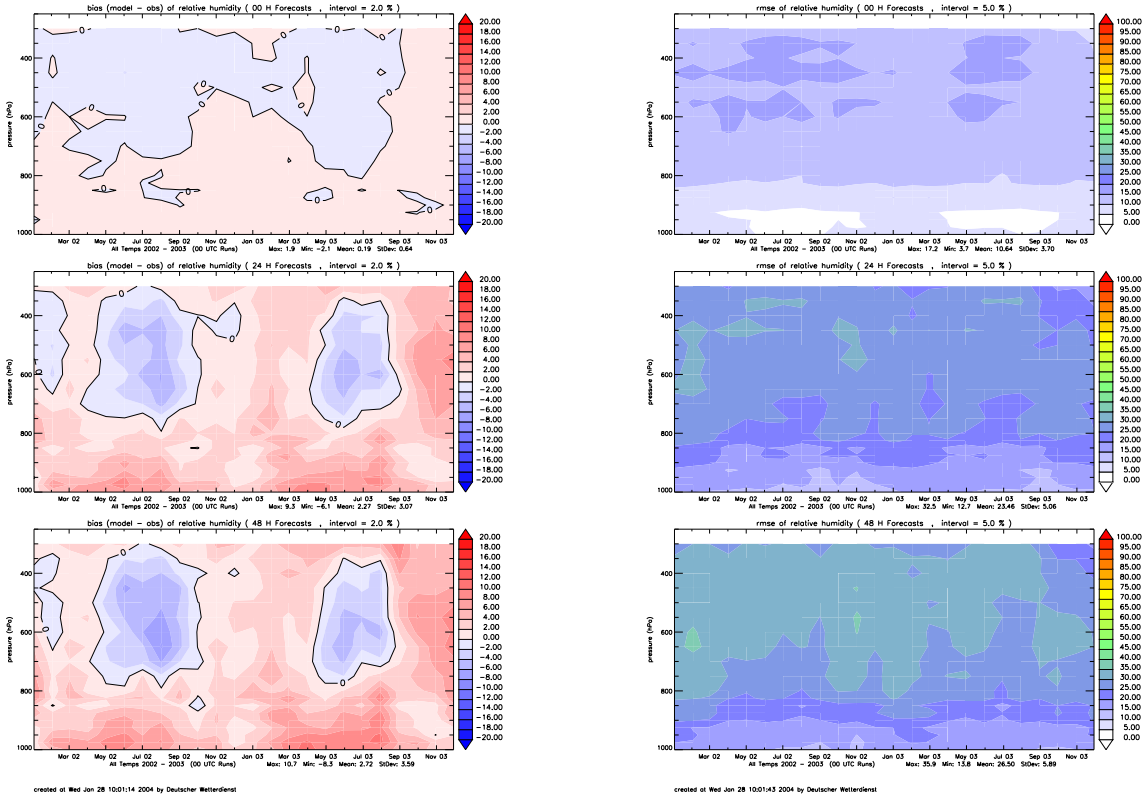

Figure 3: Time Series (January 2002 - December 2003) of relative humidity bias (left column) and rmse (right column) against radiosonde data based on monthly mean profiles for 00 UTC LM runs at DWD. From top to bottom: Analysis, 24 h, and 48 h forecast.

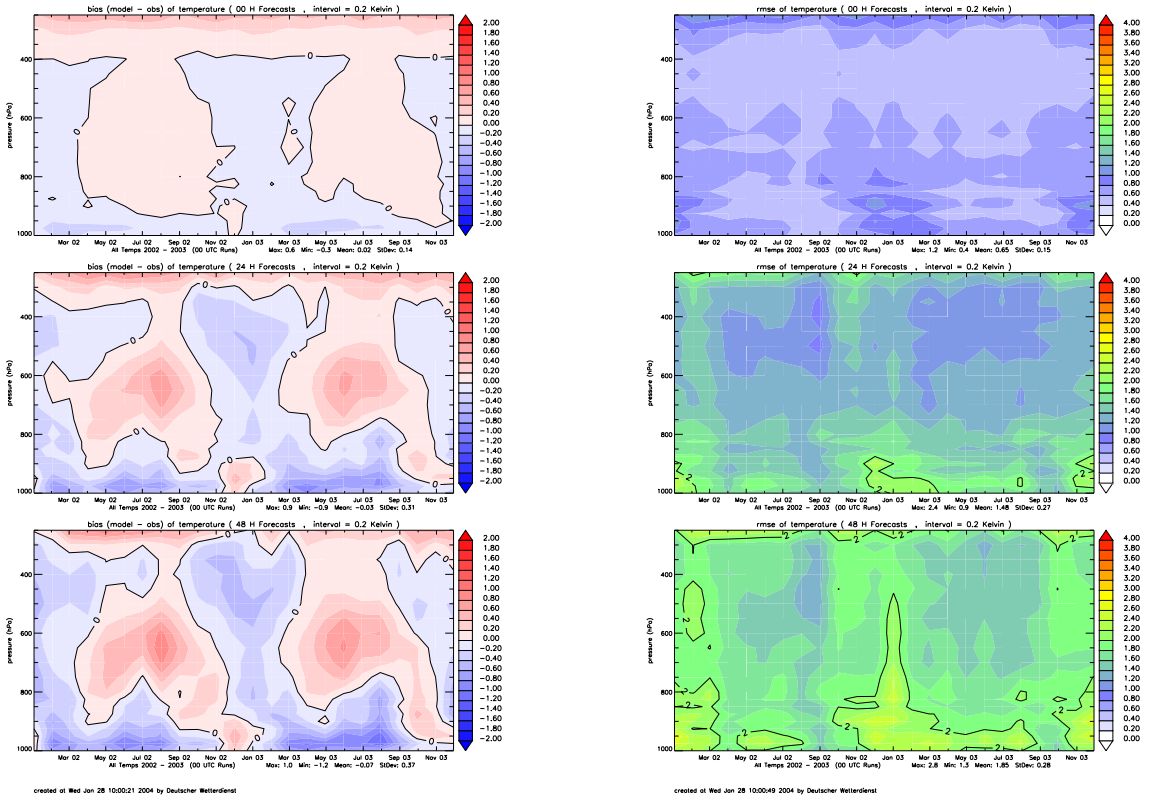

Figure 4: Time Series (January 2002 - December 2003) of temperature bias (left column) and rmse (right column) against radiosonde data based on monthly mean profiles for 00 UTC LM runs at DWD. From top to bottom: Analysis, 24 h, and 48 h forecast.

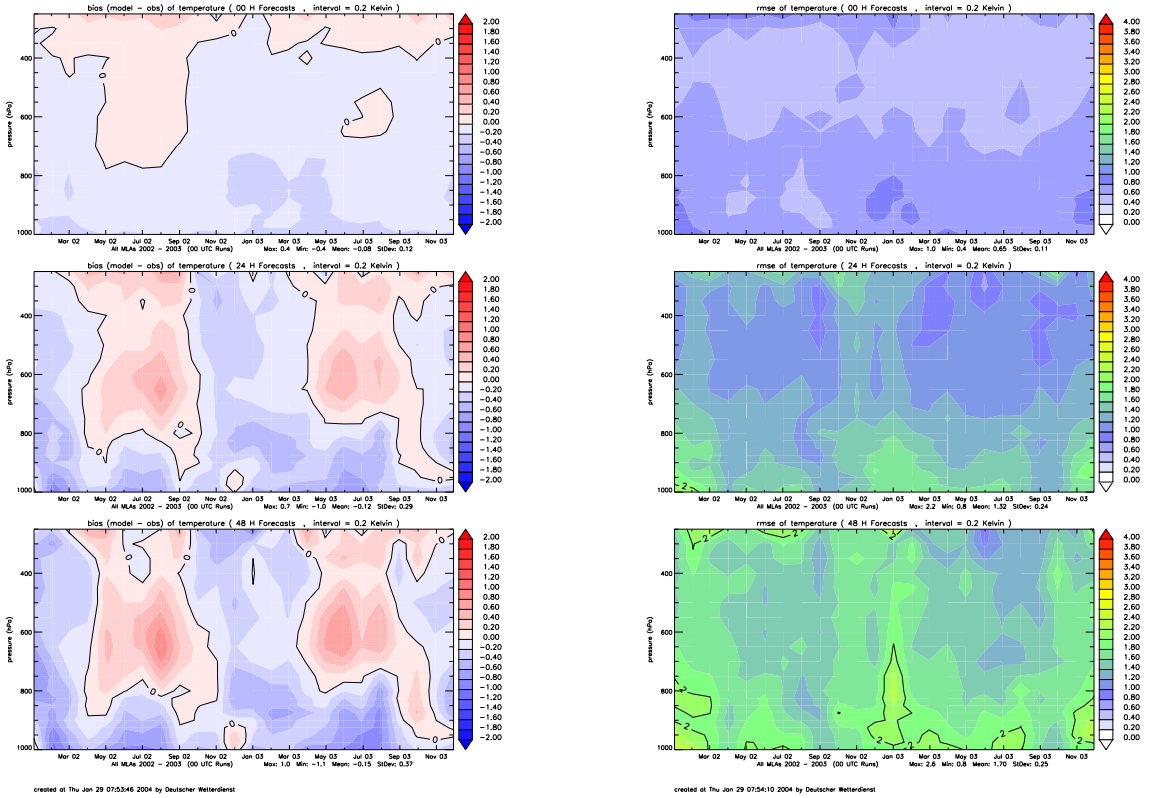

Figure 5: Time Series (January 2002 - December 2003) of temperature bias (left column) and rmse (right column) against aircraft data based on monthly mean profiles for 00 UTC LM runs at DWD. From top to bottom: Analysis, 24 h, and 48 h forecast.

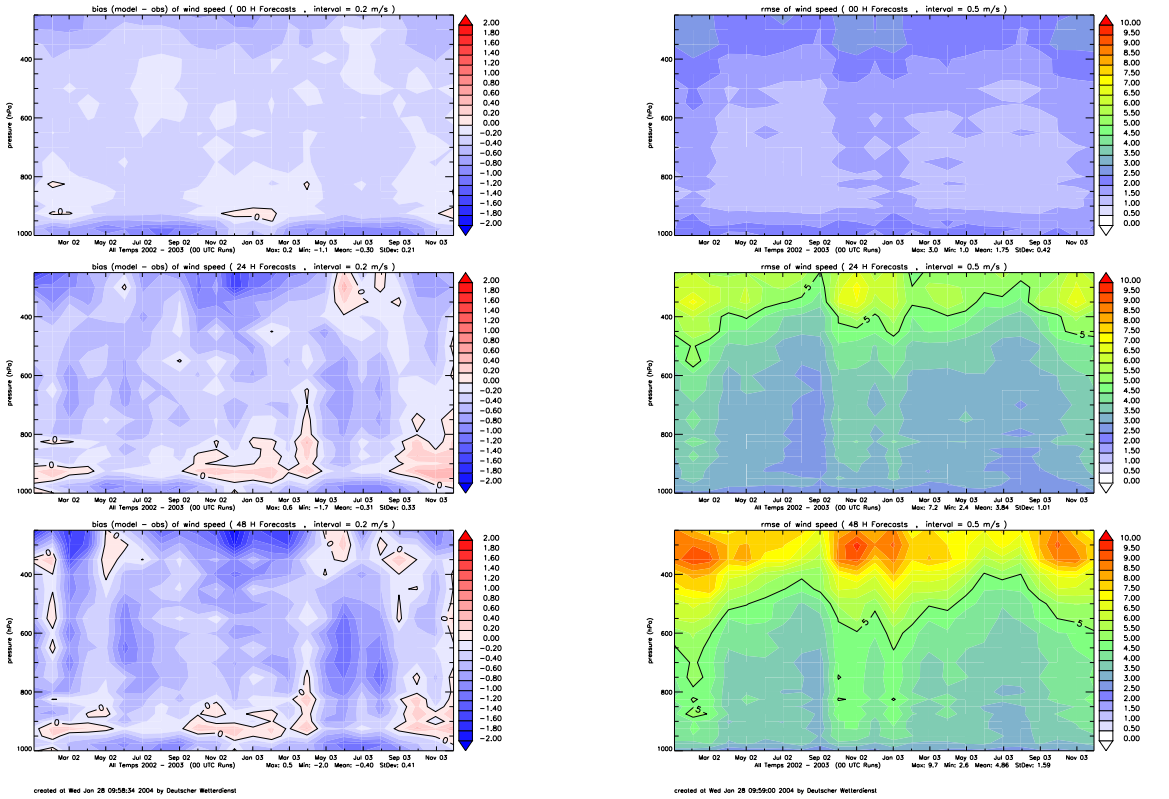

Figure 6: Time Series (January 2002 - December 2003) of wind speed bias (left column) and rmse (right column) against radiosonde data based on monthly mean profiles for 00 UTC LM runs at DWD. From top to bottom: Analysis, 24 h, and 48 h forecast.

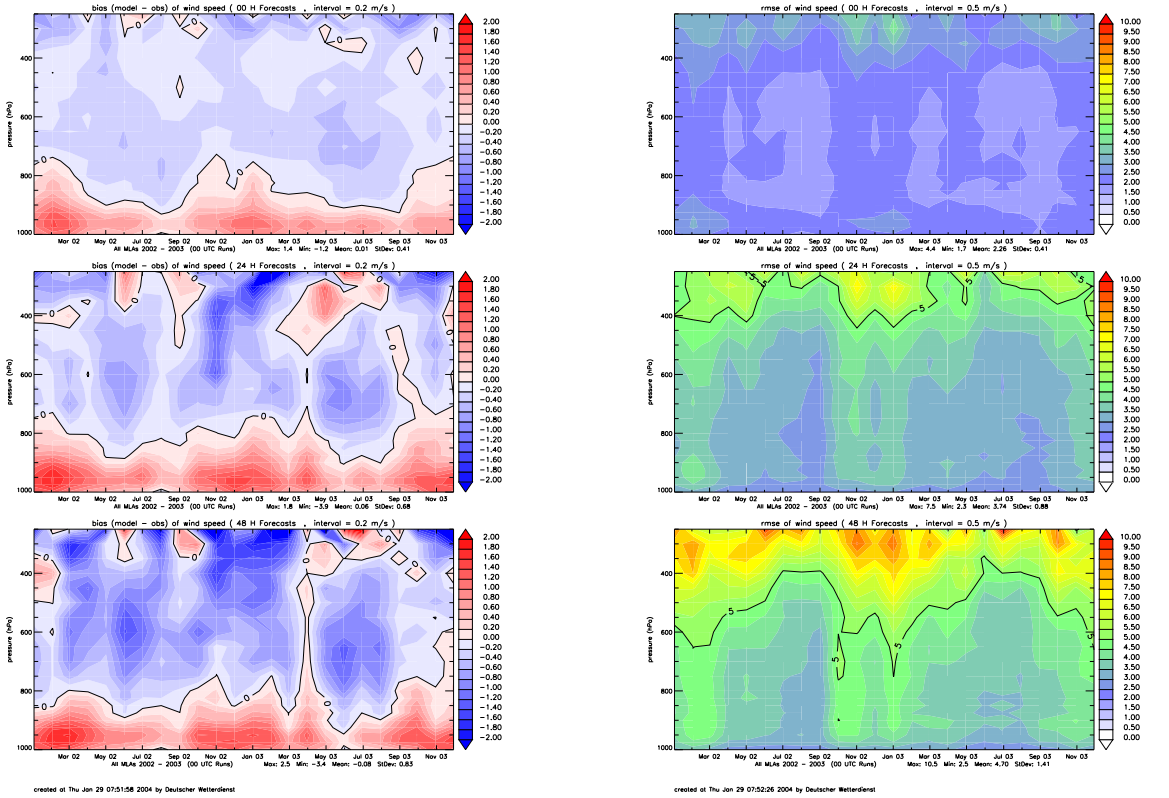

Figure 7: Time Series (January 2002 - December 2003) of wind speed bias (left column) and rmse (right column) against aircraft data based on monthly mean profiles for 00 UTC LM runs at DWD. From top to bottom: Analysis, 24 h, and 48 h forecast.

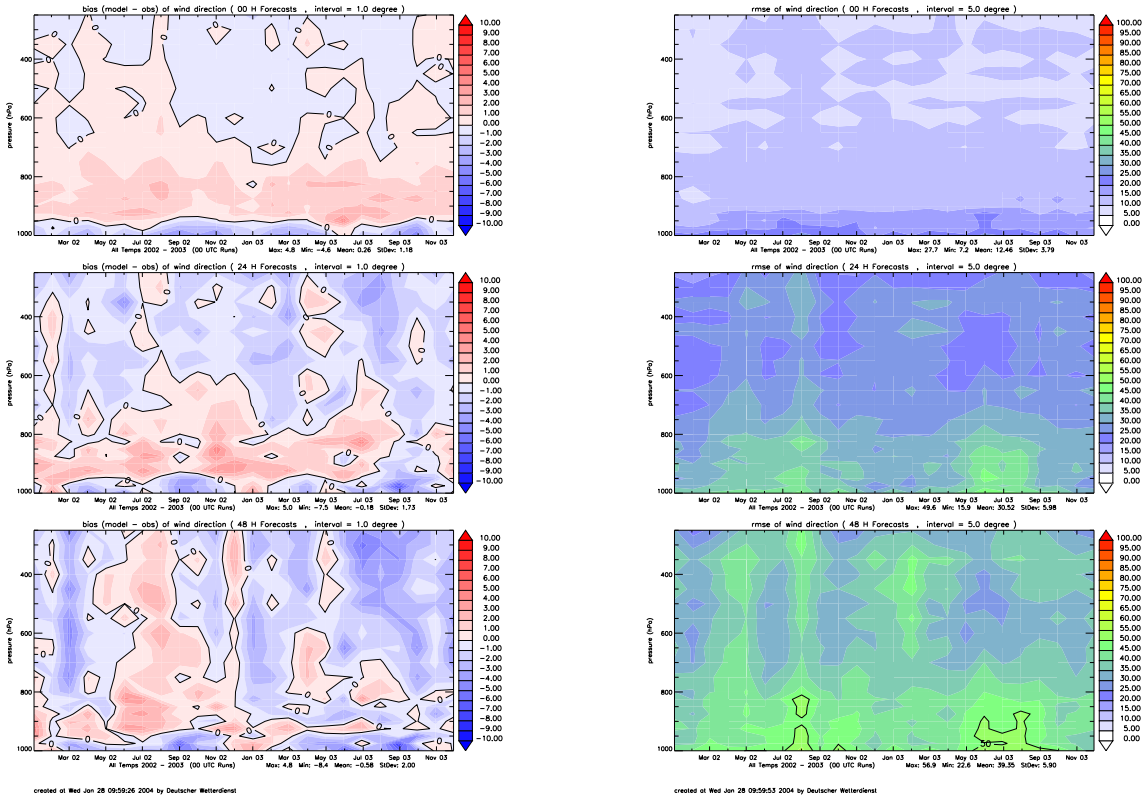

Figure 8: Time Series (January 2002 - December 2003) of wind direction bias (left column) and rmse (right column) against radiosonde data based on monthly mean profiles for 00 UTC LM runs at DWD. From top to bottom: Analysis, 24 h, and 48 h forecast.

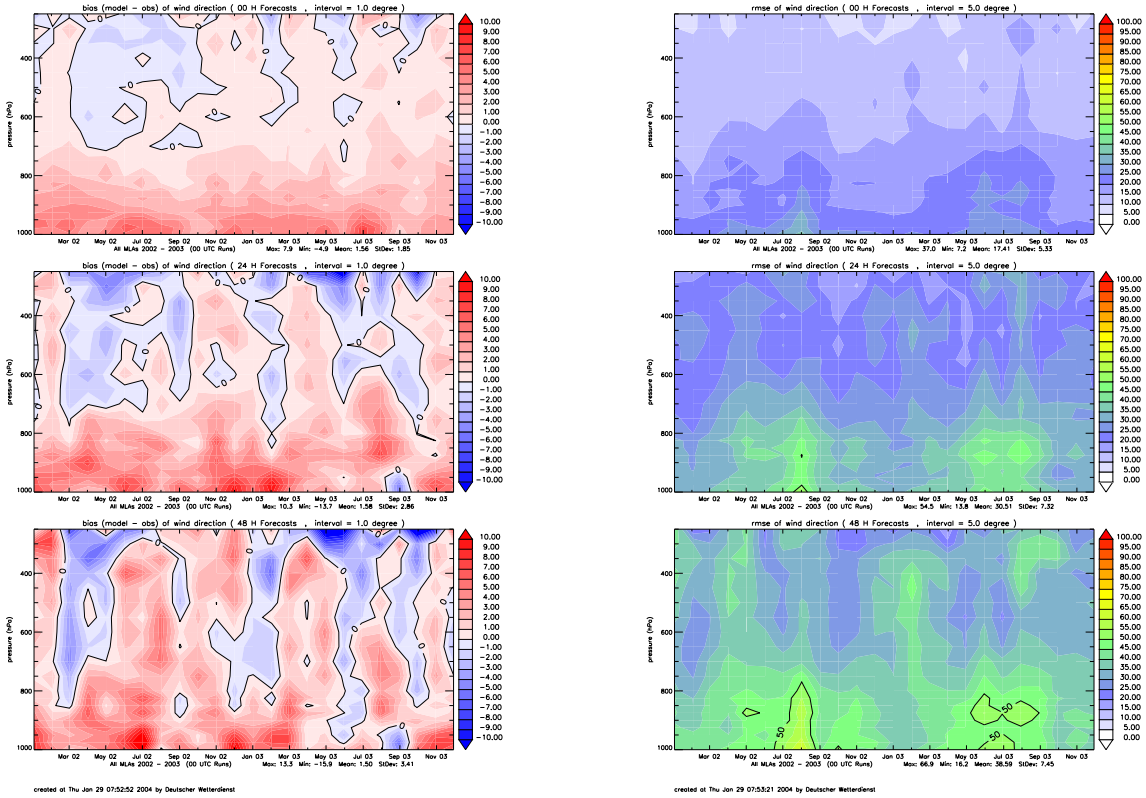

Figure 9: Time Series (January 2002 - December 2003) of wind direction bias (left column) and rmse (right column) against aircraft data based on monthly mean profiles for 00 UTC LM runs at DWD. From top to bottom: Analysis, 24 h, and 48 h forecast.

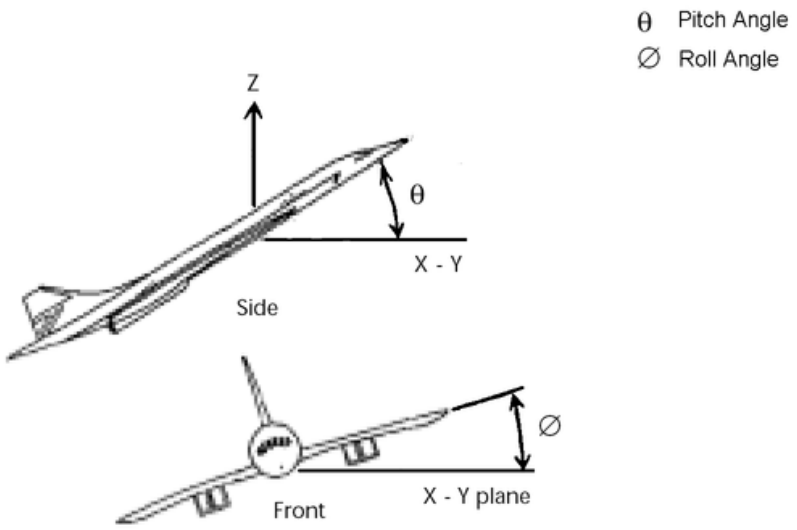

Figure 10: Aircraft reference axes and altitude angles (from WMO No. 958, 2003).

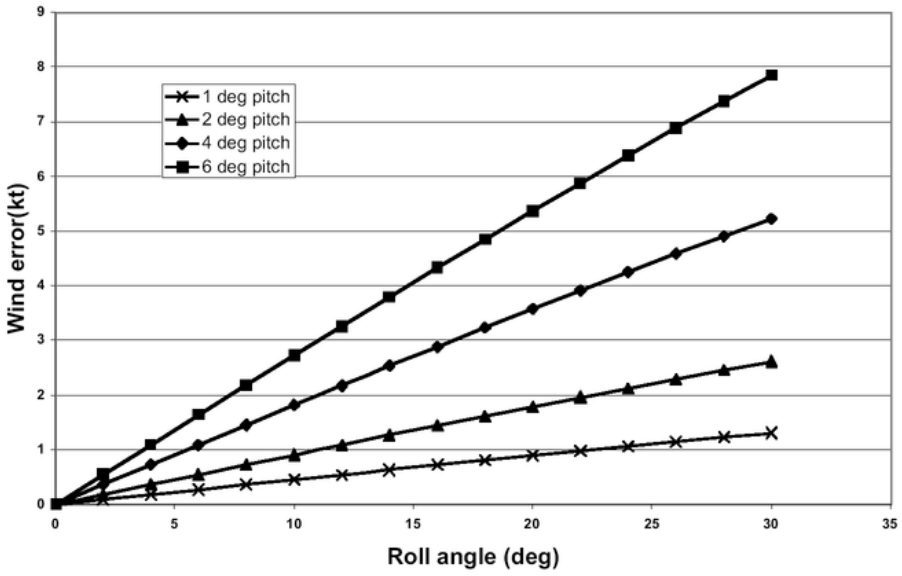

Figure 11: Effect of pitch/roll angle on wind speed at airspeed 150 Kt (from WMO No. 958, 2003).

Operational Verification of Vertical Profiles at MeteoSwiss

Marco Arpagaus

MeteoSwiss, Krähbühlstrasse 58, 8044 Zurich, Switzerland

The operational upper-air verification at MeteoSwiss uses TEMP stations all over the integration domain to verify the vertical structure of the forecasts. For the operational setup of the Alpine Model (aLMo), refer to Section 4 in this newsletter. However note that the aLMo runs with ECMWF lateral boundary conditions rather than GME lateral boundary conditions since September 16th, 2003.

In the following, we present the average vertical structure for 24 TEMP stations for the full climatic year 2003 (averaged over verification times 00 & 12 UTC; see figures 1 – 4).

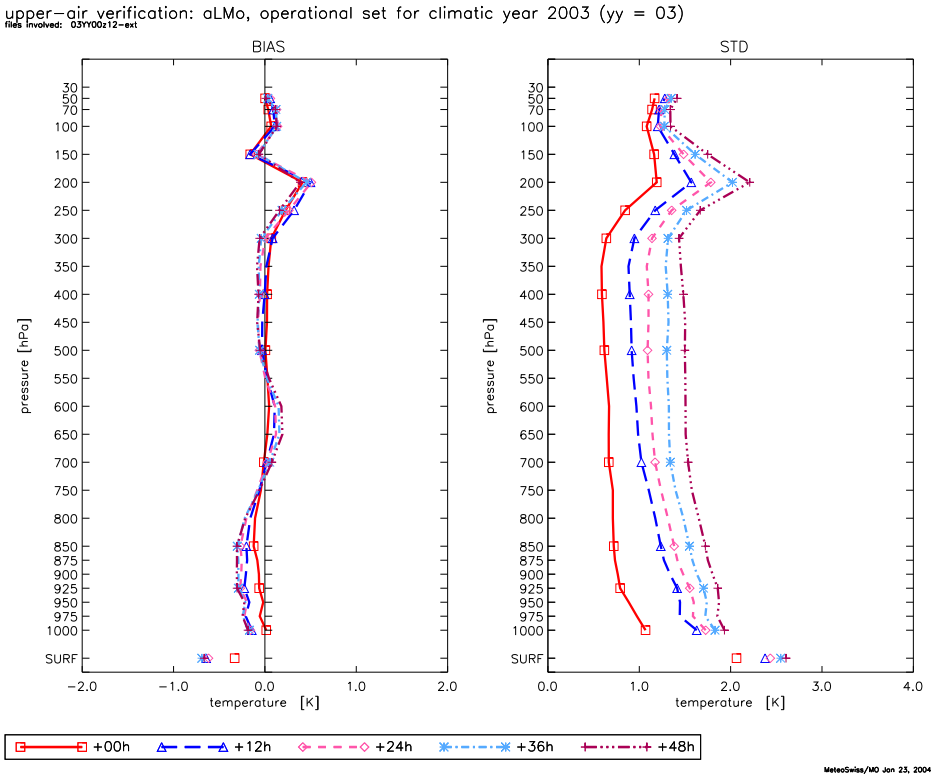

Figure 1: Mean error (BIAS) and standard deviation (STD) for temperature. Various forecast times (averaged over all stations and verification times 00 & 12 UTC) for the climatic year 2003 (1.12.2002 – 30.11.2003).

The verification plot for *temperature* (*cf.* figure 1) shows different mean errors (biases) for different regions of the atmosphere. Starting from the surface, a cold bias is observed up to 750 hPa, followed by a warm bias between 750 and 550 hPa, both of which are mainly caused by the summer season. A cold bias from the middle atmosphere up to the tropopause, mainly observed in autumn and winter, is followed by a saw-like structure in the mean error of temperature at and above the tropopause level. The fact that most temperature biases increase with increasing forecast time hints at a systematic model deficiency, which is not yet understood. Concerning the standard deviation, largest spread is seen around the tropopause level.

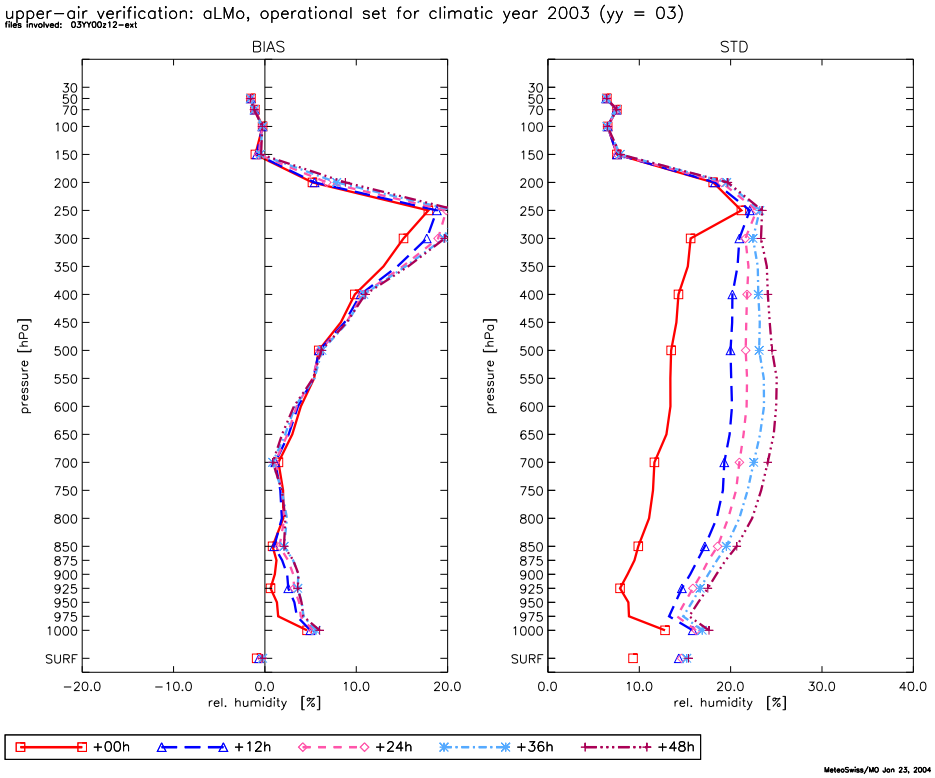

Figure 2: Mean error (BIAS) and standard deviation (STD) for relative humidity with respect to water. Various forecast times (averaged over all stations and verification times 00 & 12 UTC) for the climatic year 2003 (1.12.2002 – 30.11.2003).

Looking at the verification results for the *relative humidity* (*cf.* figure 2) the mean error is moderate up to 700 hPa, with a clear and increasing moist bias towards the surface. Above 700 hPa, relative humidity with respect to water is systematically biased towards positive values, since for the current grid-scale precipitation scheme (no cloud ice) specific humidity values need to be artificially increased at analysis time to compensate for the difference in saturation vapour pressure over water and ice at temperatures below freezing. The standard deviation is reasonably uniform throughout the troposphere, with a slight increase towards the surface.

Wind direction (*cf.* figure 3) exhibits a very small mean error, especially above the boundary layer. As expected, there is a marked increase for both mean error and standard deviation towards the surface. A deterioration of the standard deviation is also observed in the stratosphere.

The mean error of the *wind speed* (*cf.* figure 4) is small. The largest bias is observed for the boundary layer and at the tropopause height. Worth remarking is the non-negligible slow-down of the atmosphere with increasing forecast time throughout most of the troposphere, especially for the winter season (not shown), hinting at another systematic model error or a systematic bias of the driving global model. The standard deviation is largest at the tropopause, consistent with the highest winds at this level.

Finally, we note that the standard deviation increases almost linearly from forecast time +12 h to +48 h with a substantially larger difference between analysis time (*i.e.*, +00 h) and +12 h for all parameters except the (un-nudged) geopotential (not shown).

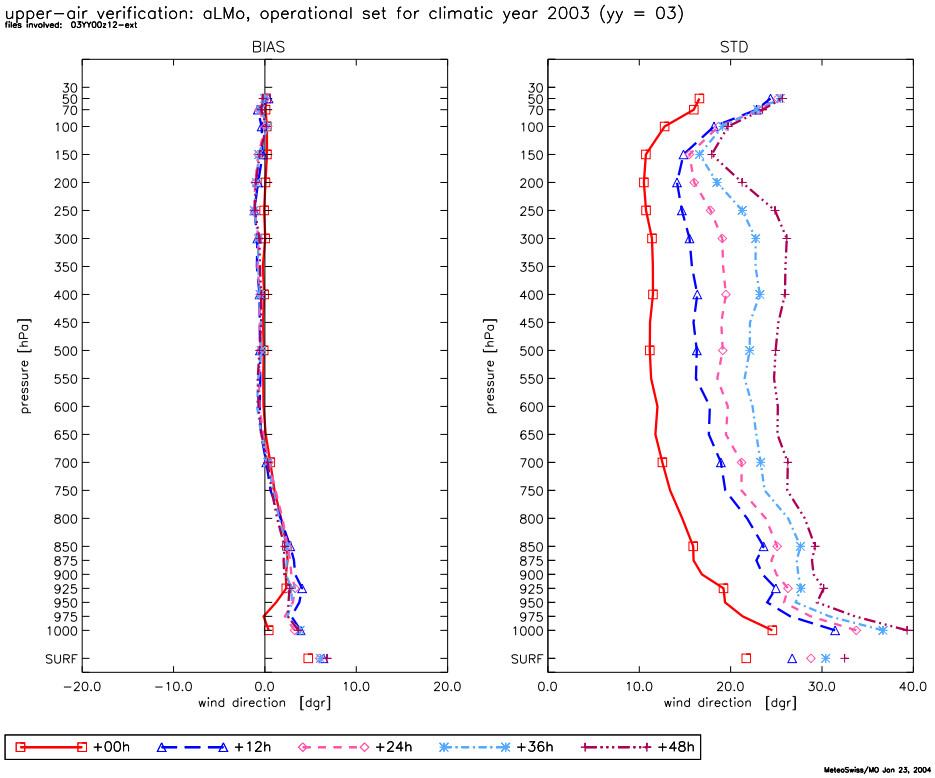

Figure 3: Mean error (BIAS) and standard deviation (STD) for wind direction. Various forecast times (averaged over all stations and verification times 00 & 12 UTC) for the climatic year 2003 (1.12.2002 – 30.11.2003).

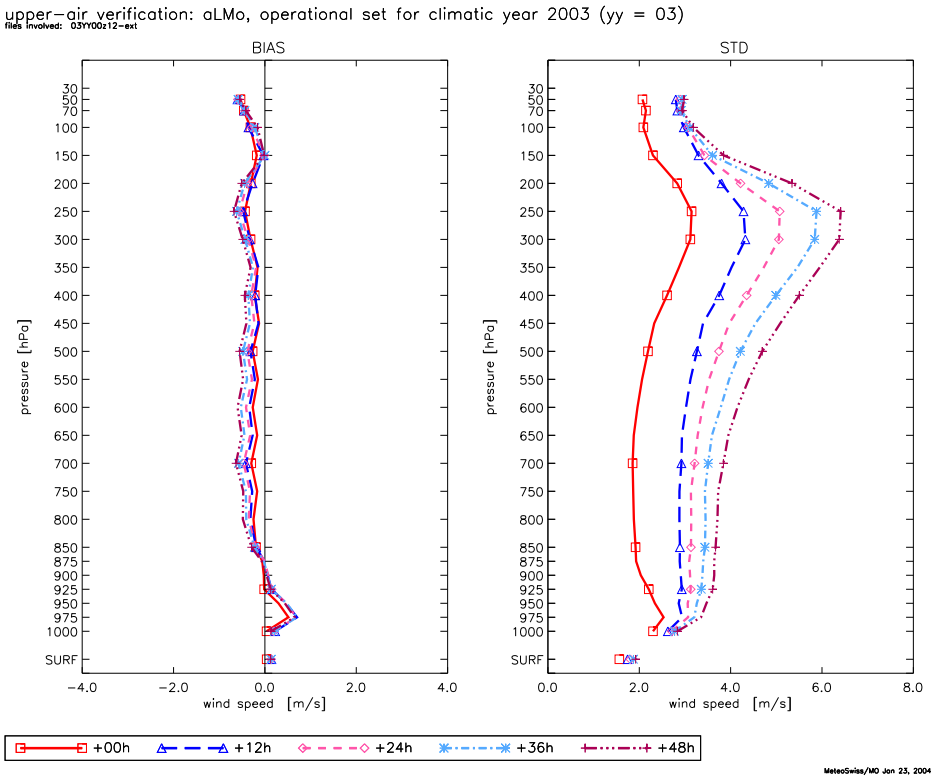

Figure 4: Mean error (BIAS) and standard deviation (STD) for wind speed. Various forecast times (averaged over all stations and verification times 00 & 12 UTC) for the climatic year 2003 (1.12.2002 – 30.11.2003).

Verification of Vertical Profiles at UGM

Patrizio Emiliani, M. Ferri, A. Galliani and E. Veccia

Ufficio Generale per la Meteorologia (UGM), Roma, Italy

The operational upper-air verification at UGM uses a set of seven TEMP stations over Italian area to verify the vertical structure of atmosphere forecasted by LAMI. The parameters analysed are the geopotential height (ZZ), Temperature (T), Dew Point Temperature (TD), wind direction (WD) and wind speed (WS) averaged for all seven stations for the period June-December 2003, except for Dew Point Temperature averaged from October to December 2003.

Geopotential height, Fig. 2, shows a general positive bias in the medium-high troposphere: generally negative bias occurs in the last forecast ranges at low levels. Careful is needed in geopotential error interpretation since radio-sonde instrumental error amplitude is comparable to typical forecasted error, Fig. 1.

Temperature vertical profiles, Fig. 3, show an error independency with forecast ranges; generally positive bias occurs, 0.3-0.7 °C, except near the ground where a negative bias of about 0.5 °C is observed. Absolute accuracy seems increase with height until 200 hPa where MAE has a rapid increment.

Dew Point Temperature, Fig. 4, presents a general positive bias, that increases with height; a discontinuity in ME with a negative bias occurs only at 200 hPa, at tropopause proximity.

Wind direction vertical profiles, Fig. 5, are characterized by high absolute accuracy especially above boundary levels (low MAE values) but decreasing in function of forecast ranges, while wind speed, fig. 6, presents a negative bias for all model output and a small increment of MAE values in function of time steps. Absolute wind error increase with height but it is consistent with the high wind speed reached at this levels.

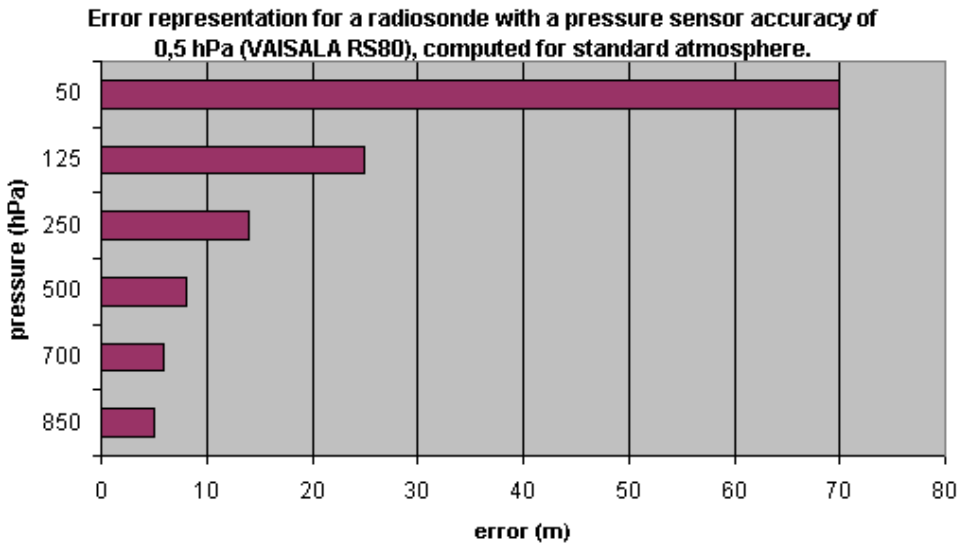

Figure 1: Error representation for a radiosonde with a pressure sensor accuracy of 0.5 hPa (VAISALA RS-80), computed for standard atmosphere.

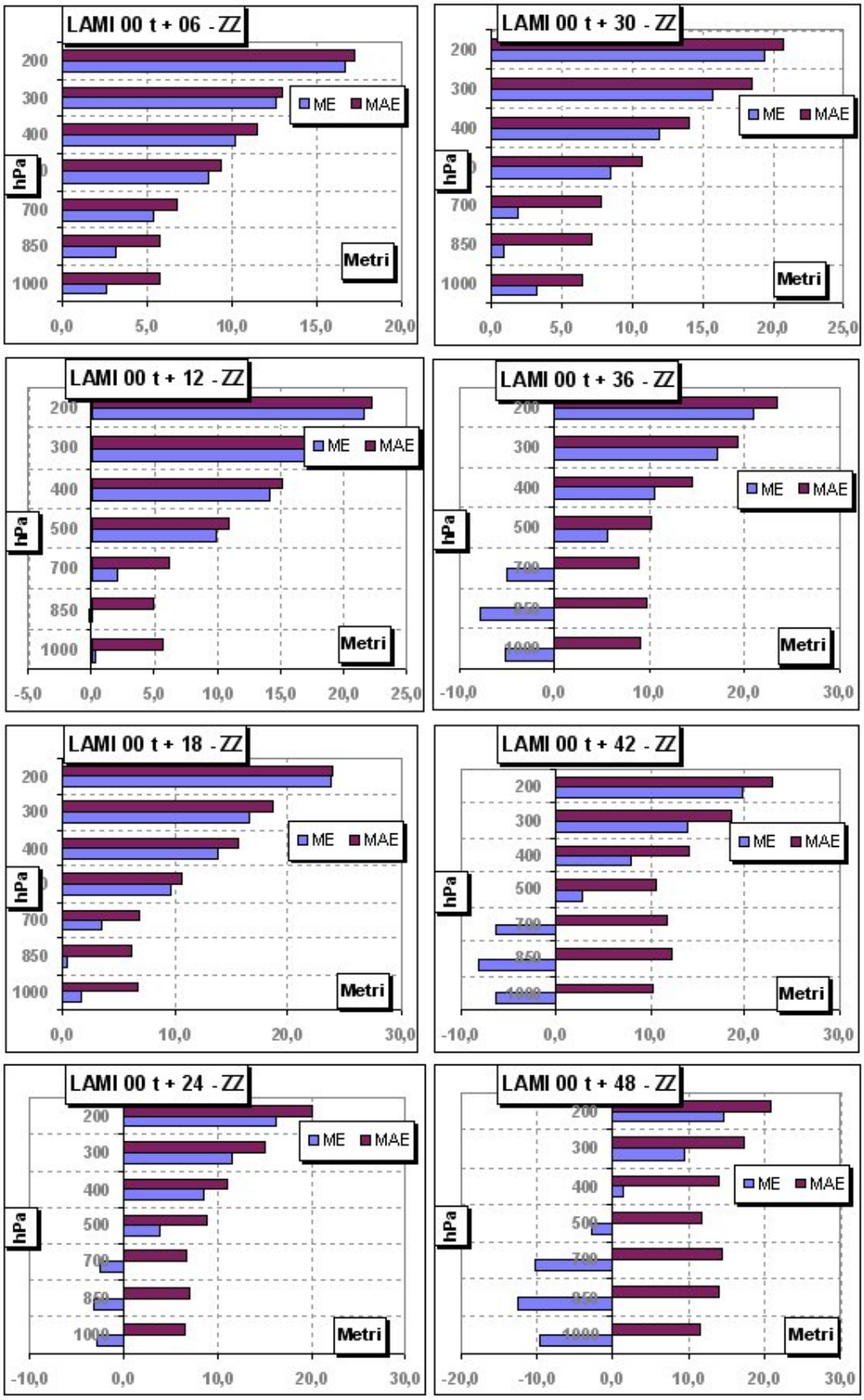

Figure 2: Median Error and Mean Absolute Error for geopotential.

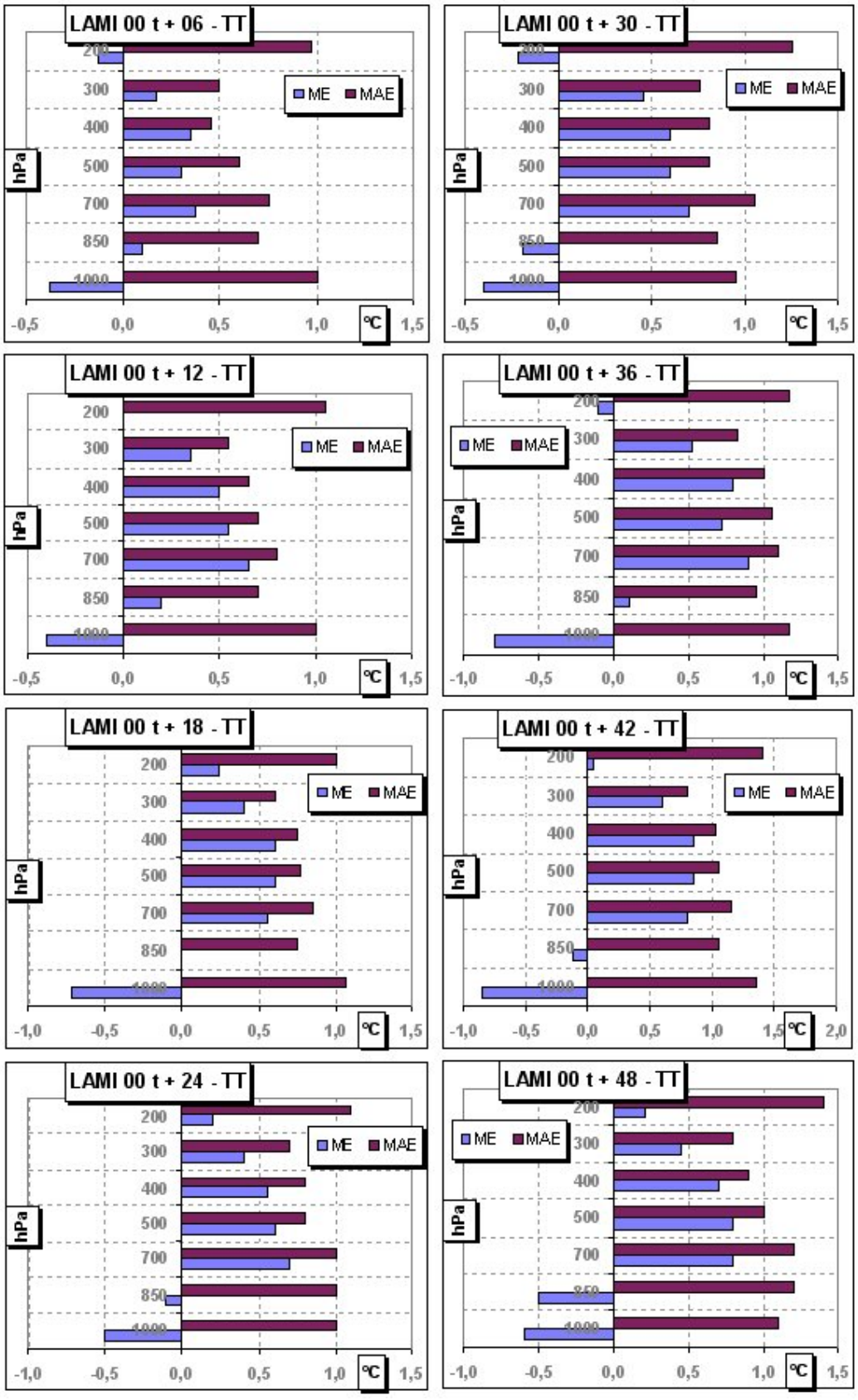

Figure 3: Median Error and Mean Absolute Error for temperature.

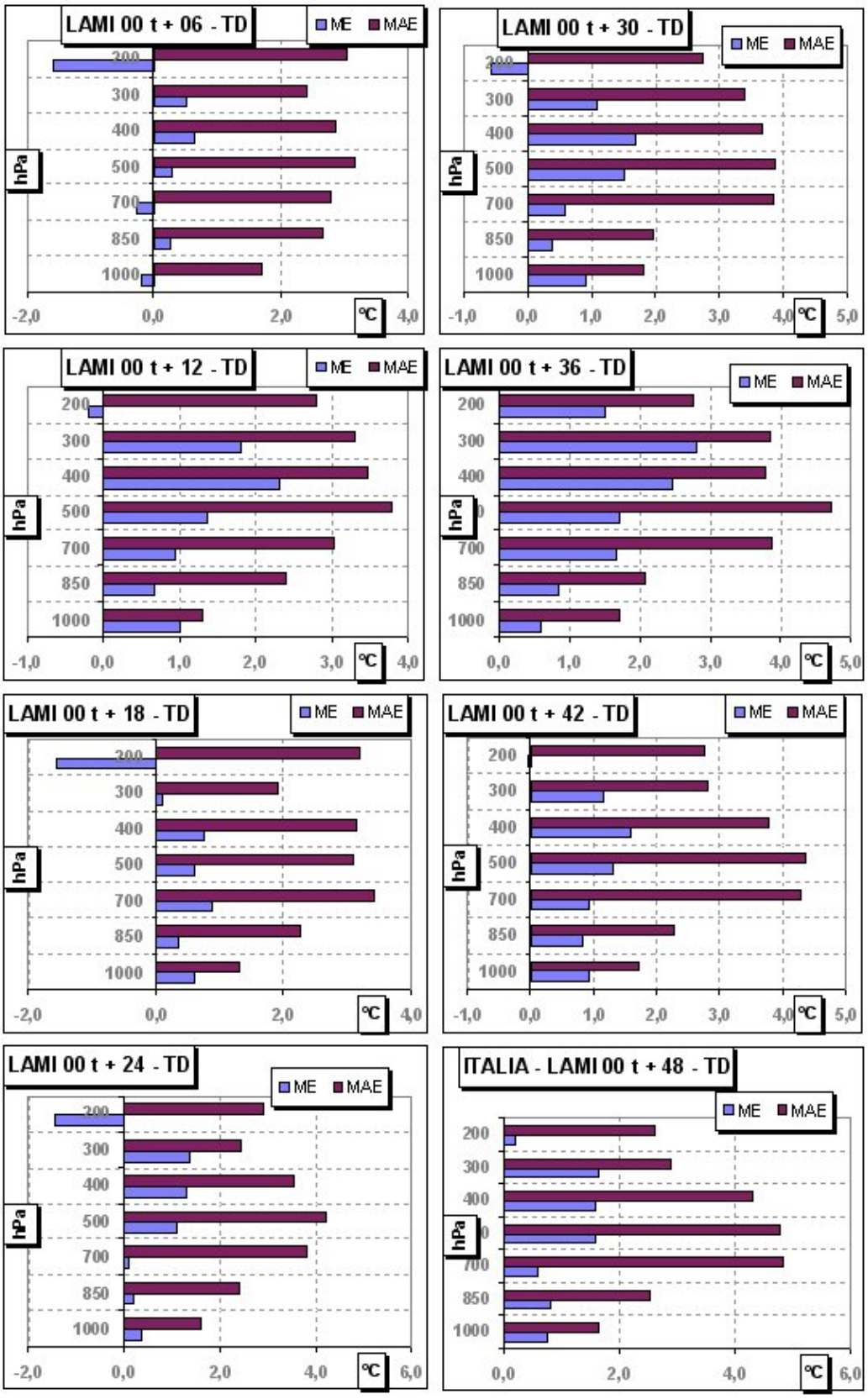

Figure 4: Median Error and Mean Absolute Error for dew point temperature.

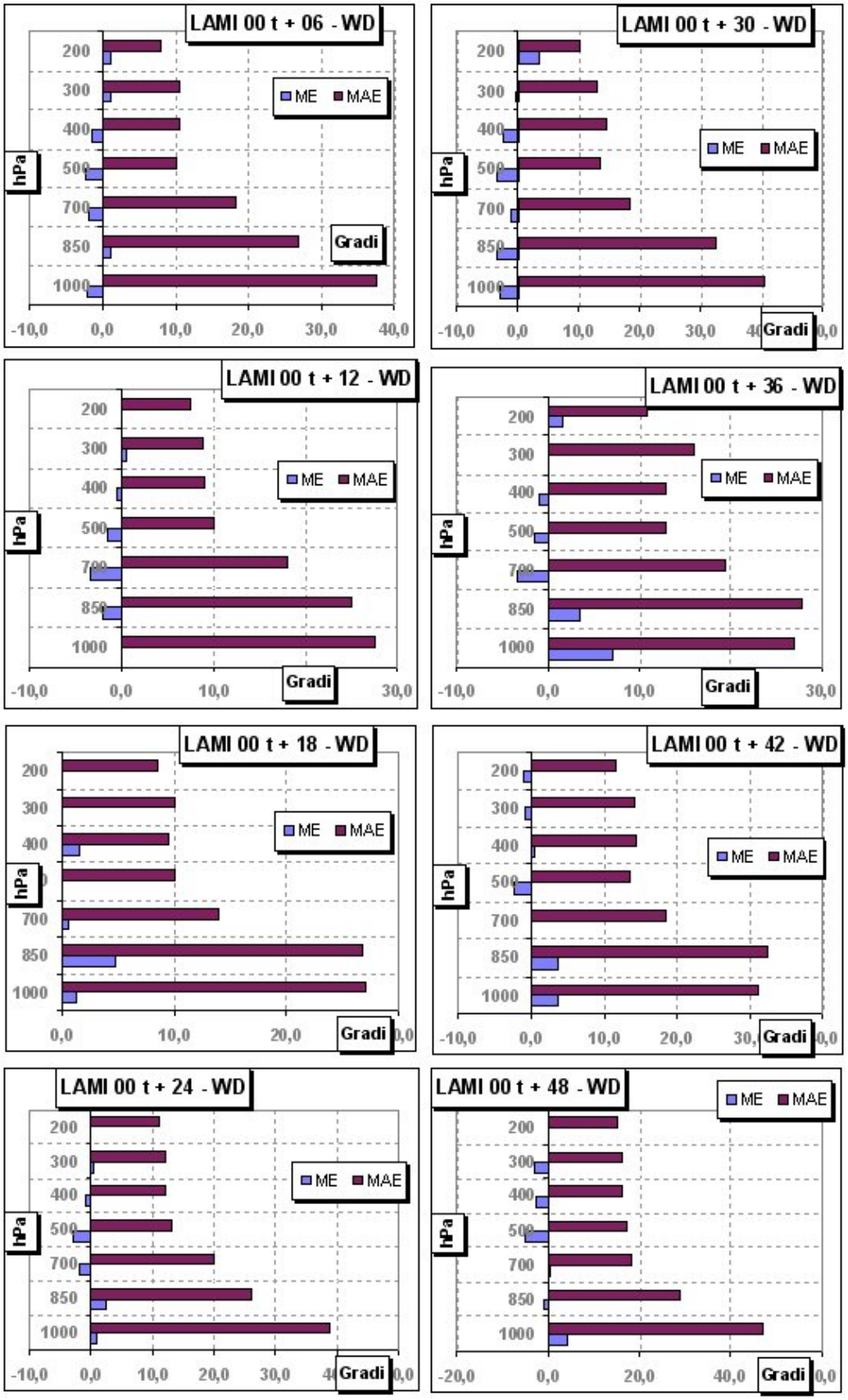

Figure 5: Median Error and Mean Absolute Error for wind direction.

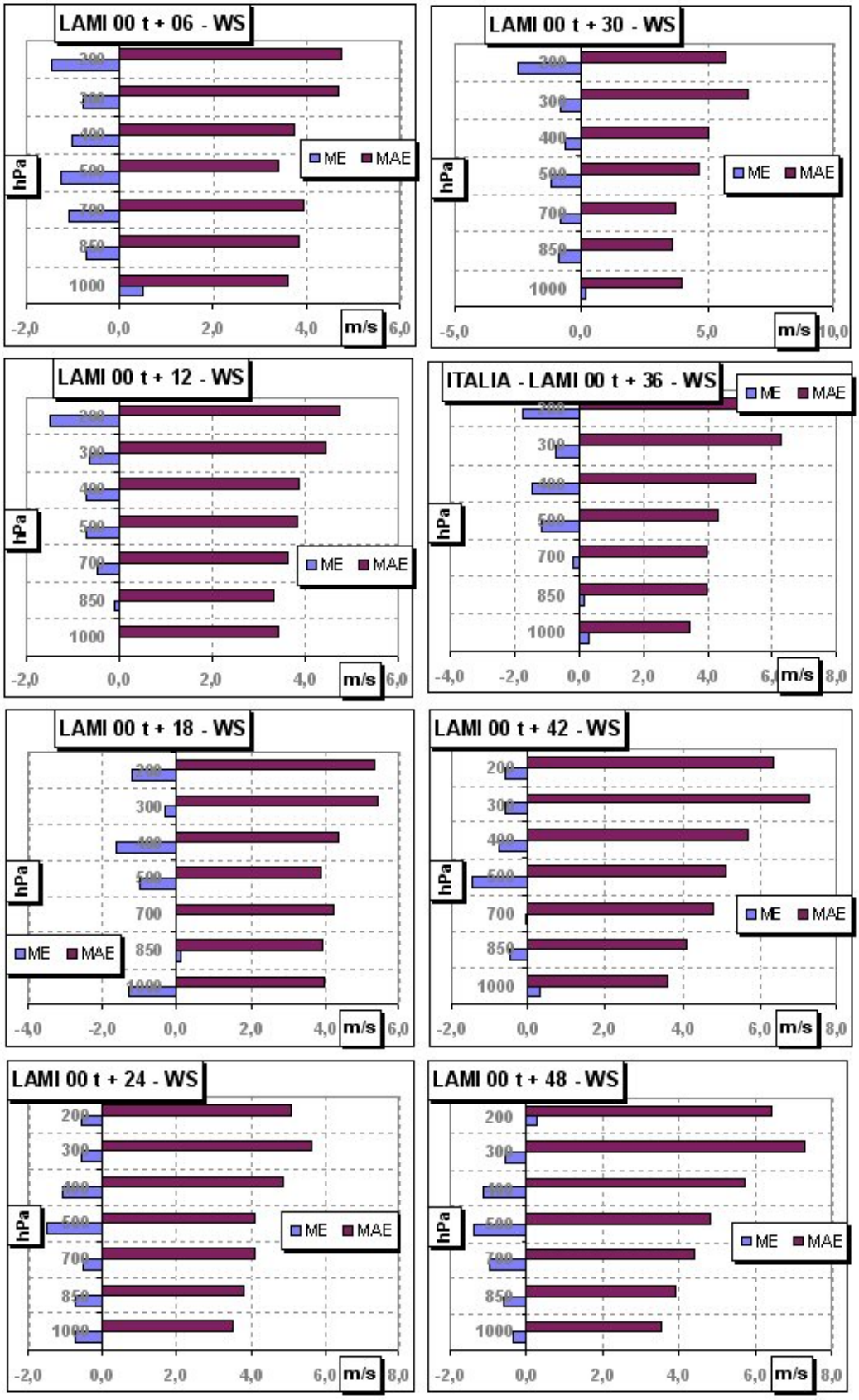

Figure 6: Median Error and Mean Absolute Error for wind speed.

Verification of Lokal-Modell Operational Suites at ARPA-SIM: Impact of the Nudging-based Assimilation Scheme.

F. Boccanera, C. Marsigli, T. Paccagnella and P. Patruno

ARPA-SIM, Bologna, Italy

Abstract

High resolution Quantitative Precipitation Forecast (QPF) obtained by non-hydrostatic model Lokal-Modell (LM) has been verified. In particular, standard version and nudging version (where temperature, wind, surface pressure and humidity are assimilated) of LM, both utilized at ARPA-SIM, have been compared. A comparison in terms of temperature and dew-point temperature has also been carried out.

1 Introduction

1.1 Lokal-Modell

The operational implementation of Lokal Modell (LM) at ARPA-SIM consists of two 72-hour integrations every day (starting at 00 UTC and 12 UTC) with an horizontal resolution of 7 km and a vertical discretization of 35 levels, over the domain reported in Fig. 1. In this work the 00 UTC suite is compared with a parallel experimental suite starting at the same time but where a mesoscale data assimilation based on a nudging scheme (horizontal wind, temperature, humidity and surface pressure are assimilated) is performed. At the time of writing (January 2004), both 00 and 12 UTC operational suites make use of the mesoscale data assimilation.

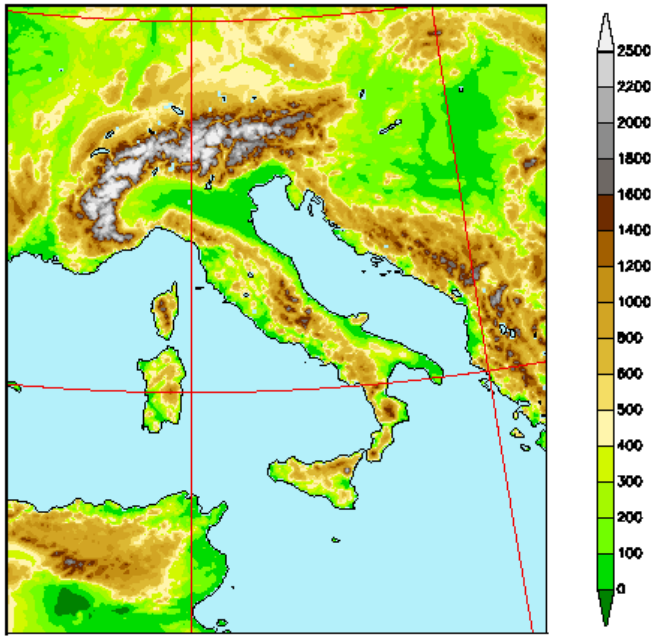

Figure 1: Operational domain of LM at ARPA-SIM.

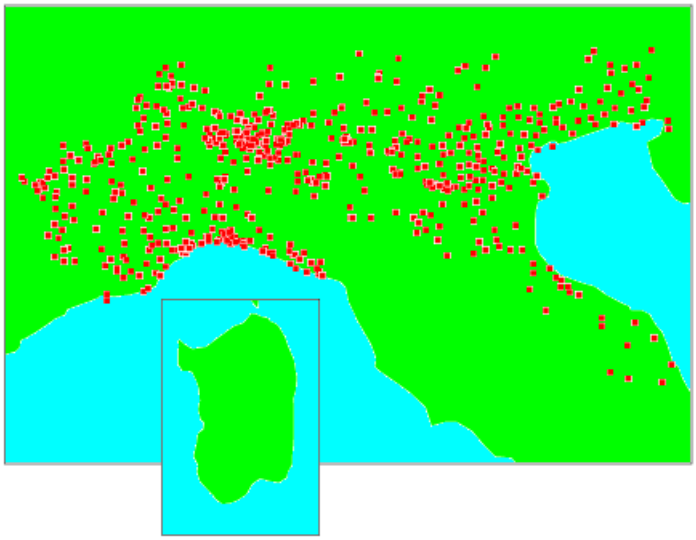

Figure 2: Operational domain of LM at ARPA-SIM.

1.2 Verification Methodology

An objective verification has been performed in order to assess the impact of the use of a mesoscale data assimilation on the operational model runs. In this report, the analysis is done in terms of three meteorological parameters: precipitation, temperature and dew-point temperature.

The precipitation (TP) verification is based on the evaluation of contingency tables for different precipitation thresholds, from which is possible to deduce some verification indices: Bias Score (BS), Threat Score (TS), False Alarm Rate (FAR) and Heidke Skill Score (HSS) have been used in this work. This verification has been carried out in terms of 6-hour cumulated precipitation, comparing the observed value at a station point against the forecast value of the nearest grid point. Observations are derived from a raingauge network covering Northern Italy, showed in Fig. 2 and the considered period is from 1 March to 30 June 2003. Two thresholds have been considered: precipitation exceeding 1mm/6h and 10mm/6h. The considered period has been characterized by very little precipitation, so the number of observations exceeding the two thresholds is not so high (about 1000 and 400, respectively).

The temperature (T) and dew-point temperature (Td) verification has been carried out using the same network but the verification period goes from 1 March to 31 May 2003 (spring). The value observed at a station point has been compared against the forecast value of the nearest grid point, without any corrections for the differences in height between station point and grid point. When this difference exceeds 500m, the point has not been considered in the computation. The indices used are the mean absolute error (MAE) and the BIAS.

The definitions of the indices used in this work are the following:

Contingency Table		observed	
		yes	no
forecasted	yes	a	b
	no	c	d

$$BS = \frac{a+b}{a+c}, \qquad TS = \frac{a}{a+b+c}, \qquad FAR = \frac{b}{a+b},$$

$$BIAS = \frac{1}{N}\sum_{i=1,N}^{N}(p_i - o_i), \qquad MAE = \frac{1}{N}\sum_{i=1,N}^{N}|p_i - o_i|.$$

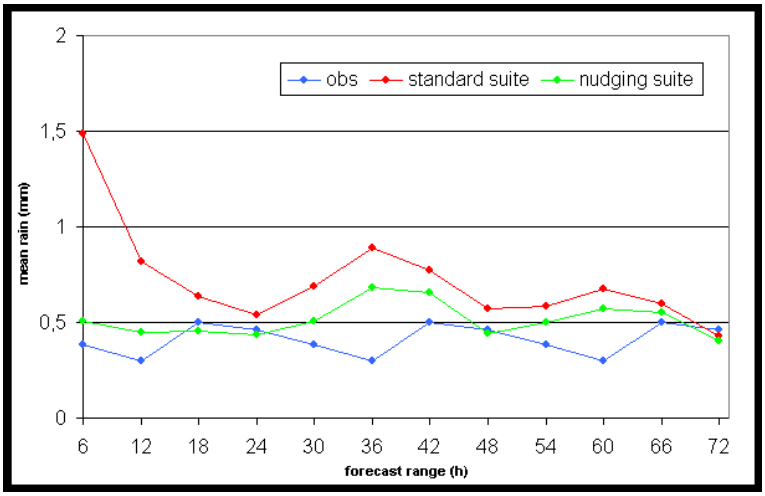

Figure 3: Trends, as a function of the forecast range, of the observed (blue line) and forecast (red line for the standard suite and green line for the nudging suite) precipitation, averaged over all station points and over the whole period.

2 Results

2.1 Precipitation

Precipitation trends averaged over the whole period and over all the station points with varying forecast range are shown in Fig. 3. Blue line is relative to the observed values, while the red and the green lines are relative to the forecast values interpolated on station points (LM standard version in red and the nudging one in green). It can be seen that the strong overestimate of the precipitation by the standard suite at the beginning of the integration ("spin-up" problem) is not present in the nudging suite. A 6-hour temporal phase shift between observed and forecast maxima is also evident.

- *Bias Score*
  The values of the Bias Score computed for the two LM suites at the different forecast range are shown in Fig. 4. A general improvement of the nudging suite with respect to the standard one is evident for both precipitation thresholds and for the whole integration period. The improvement is greater in the first 12 hours, especially for the highest threshold. Therefore the nudging scheme seems to be effective in order to eliminate the spin-up effect.

- *Threat Score*
  The values of the Threat Score computed for the two LM suites at the different forecast range are shown in Fig. 5. The performance of the nudging LM version is slightly better than the standard LM one. A convergence of the two lines at the end of the forecast period (third day of integration) is also evident.

- *False Alarm Rate*
  The values of the False Alarm Rate computed for the two LM suites at the different forecast range are shown in Fig. 6. The amount of false alarms is greatly reduced with the use of the mesoscale assimilation, for both precipitation thresholds. This is especially true in the first half of the integration period, while the two lines tend to converge after 60 hours.

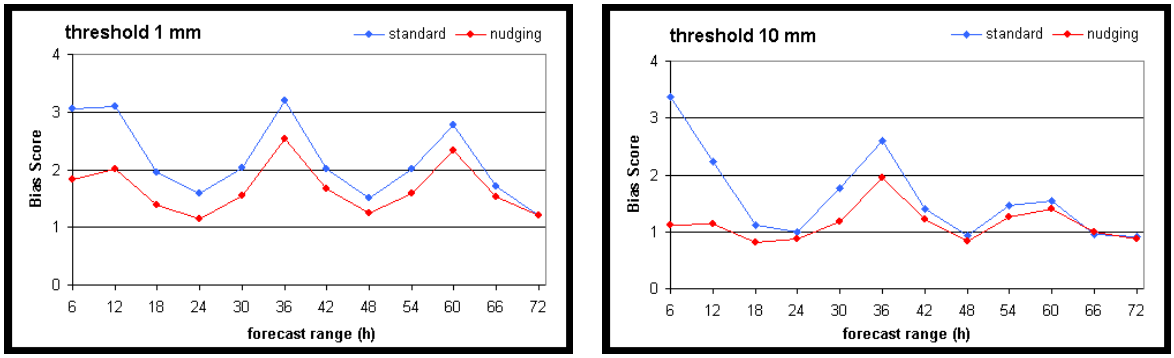

Figure 4: Bias Score as a function of the forecast range, for two precipitation thresholds (1mm/6h in the top panel and 10mm/6h in the bottom panel). Blue line is relative to the standard suite, while red line is relative to the nudging suite.

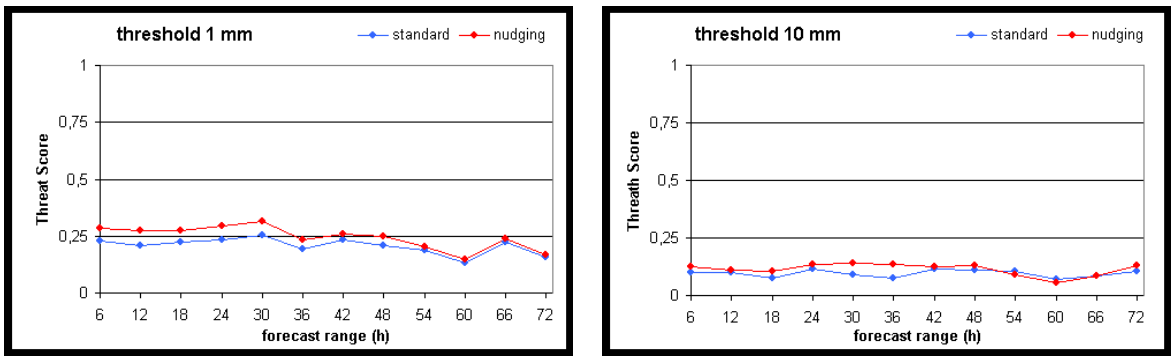

Figure 5: Threat Score as a function of the forecast range, for two precipitation thresholds (1mm/6h in the top panel and 10mm/6h in the bottom panel). Blue line is relative to the standard suite, while red line is relative to the nudging suite.

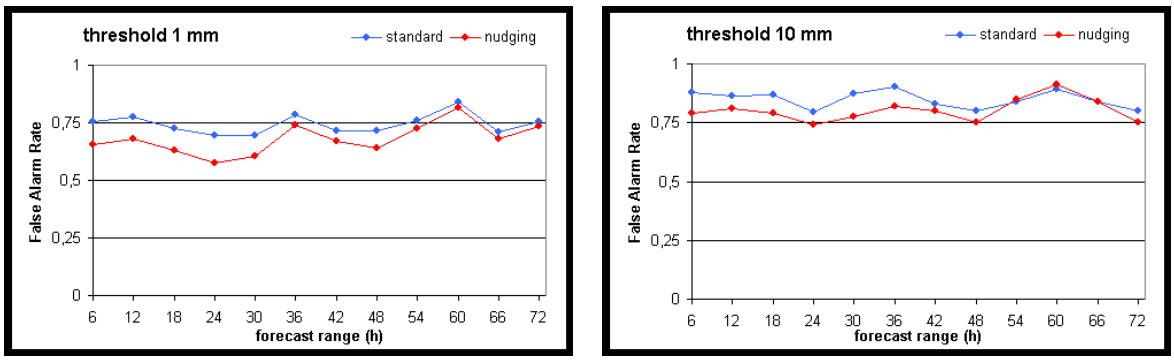

Figure 6: False Alarm Rate as a function of the forecast range, for two precipitation thresholds (1mm/6h in the top panel and 10mm/6h in the bottom panel). Blue line is relative to the standard suite, while red line is relative to the nudging suite.

2.2 Temperature

The values of the mean absolute error (MAE) and of the bias (as defined at the end of Section 1.2) computed for the two LM suites at the different forecast ranges are shown in Fig. 7. The performance of the two suites are almost identical, a negative bias being evident along the whole integration period. The bias exhibits a diurnal cycle, with a minimum in

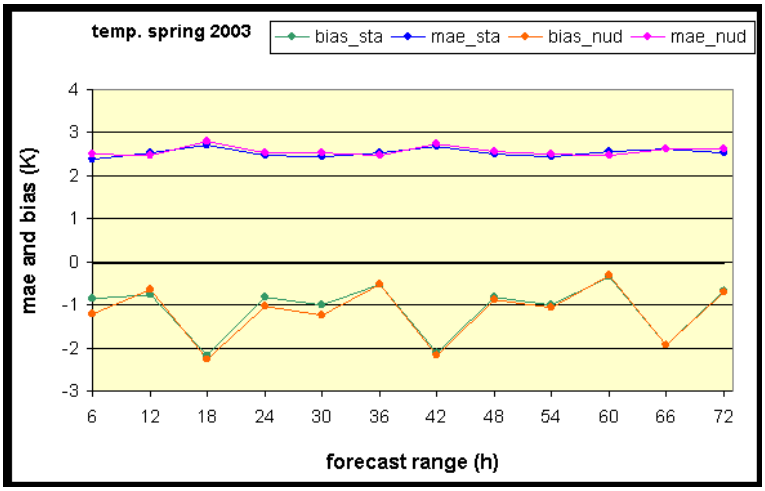

Figure 7: Mean Absolute Error and Bias of 2m-temperature as a function of the forecast range. The blue line is the MAE relative to the standard suite, while the pink line is the MAE of the nudging suite. The red line is the bias of the nudging suite while the green line is the bias of the standard suite.

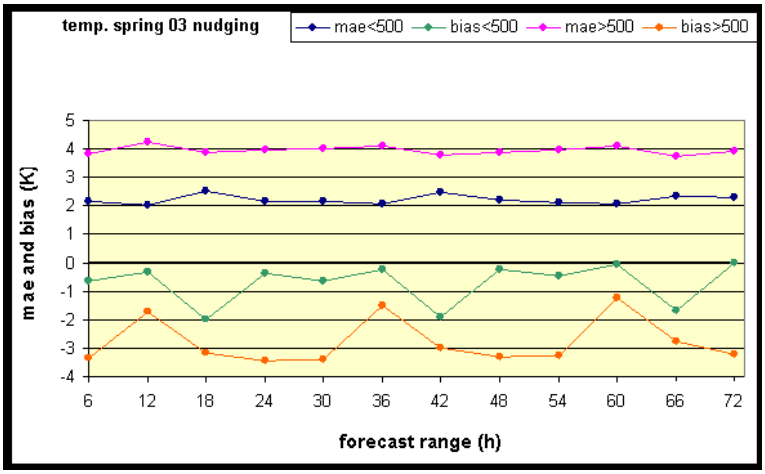

Figure 8: Mean Absolute Error and Bias of 2m-temperature as a function of the forecast range. The blue line is the MAE for the stations below 500 m, while the pink line is the MAE for the stations above 500m. The green line is the bias for the stations below 500 m, while the red line is the bias for the stations above 500 m.

the afternoon. The mean absolute error is about 2.5 degrees.

In Fig. 8, verification has been carried out by subdividing the sample according to the station height (below and above 500 m) but only for the nudging suite. The negative bias in much stronger for the mountain stations and also the mean absolute error reaches 4 degrees for these stations.

2.3 Dew-point Temperature

The values of the mean absolute error (MAE) and of the bias computed for the two LM suites at the different forecast ranges are shown in the Fig. 9. The nudging version of LM is able to reduce both the bias and the mean absolute error, especially in the first day of integration. Both measures exhibit a diurnal strong cycle, with the maximum value of the error at 12 UTC.

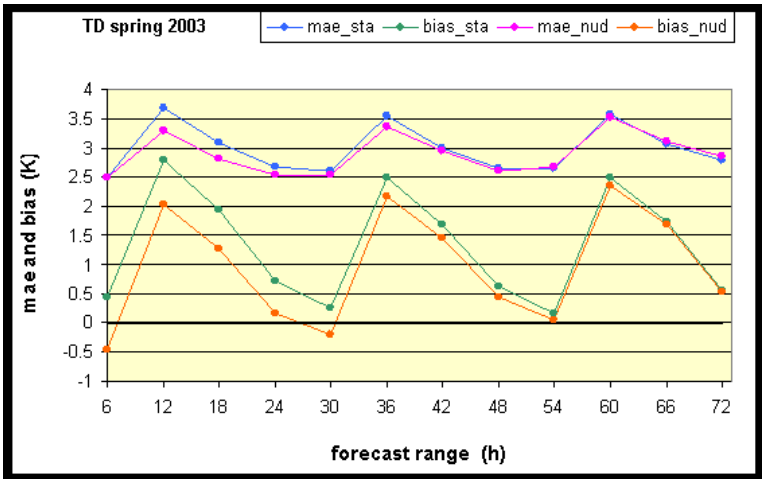

Figure 9: Mean Absolute Error and Bias of 2m-dewpoint temperature as a function of the forecast range. The blue line is the MAE for the stations below 500 m, while the pink line is the MAE for the stations above 500m. The green line is the bias for the stations below 500 m, while the red line is the bias for the stations above 500 m.

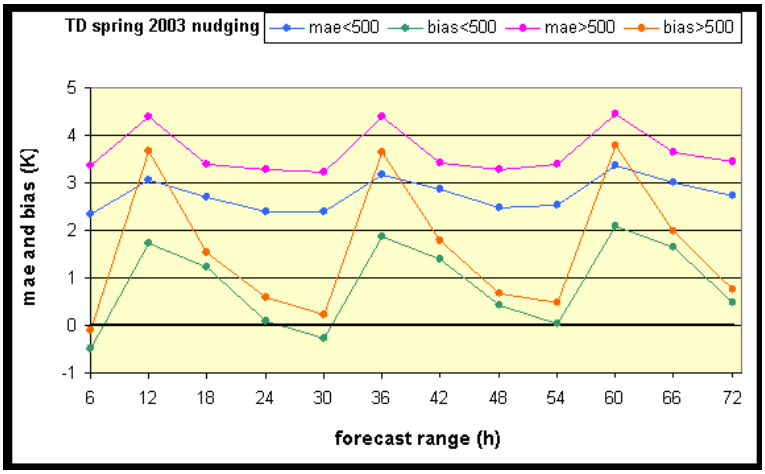

Figure 10: Mean Absolute Error and Bias of 2m-dewpoint temperture as a function of the forecast range. The blue line is the MAE for the stations below 500 m, while the pink line is the MAE for the stations above 500m. The green line is the bias for the stations below 500 m, while the red line is the bias for the stations above 500 m.

Also for this variable verification has been carried out by subdividing the sample according to the station high (below and above 500m), but only for the nudging suite. Both the bias and the MAE have higher values for the stations above 500 m.

The COSMO_LM_PL Precipitation Forecasts are Verified on Daily Rainfall Data Averaged over Selected River Basisn

Malgorzata Mierkiewicz and Jan Parfiniewicz

Institute of Meteorology and Water Management, Warsaw, Poland

The COSMO model forecasts are used in Warsaw Operational Hydrology System to run HBV hydrological model every day giving discharge forecasts for 20 river basins. These are tributaries of main Polish River – Vistula, in the lowland part of Poland. As an input to the hydrological model daily rainfall forecasts and mean daily air temperature are needed. The assumed lead-time is equal 3 days. In this study the rainfall forecast errors have been estimated over chosen 7 river basins (Fig.1) for the 8-months period starting from Jan 2003.

Results of analysis are presented in the Table 1 and Figures 2 - 4. The mean square errors (MSE) and efficiency coefficient (E) were calculated. The index E is considered as a comparison of forecast errors to the errors of "no forecast case" (for details see Mierkiewicz at al., COSMO Newsletter No 3, 2003 p.120). Thus, if the model produces errors equal or greater than inertial forecast it means that the model does not contribute any information gain. The value E *ge* 1.0 disqualifies the model, the value E between 0.8 and 1.0 presents an index of little progress produced by model, and E < 0.8 can be considered as an index of fair model performance.

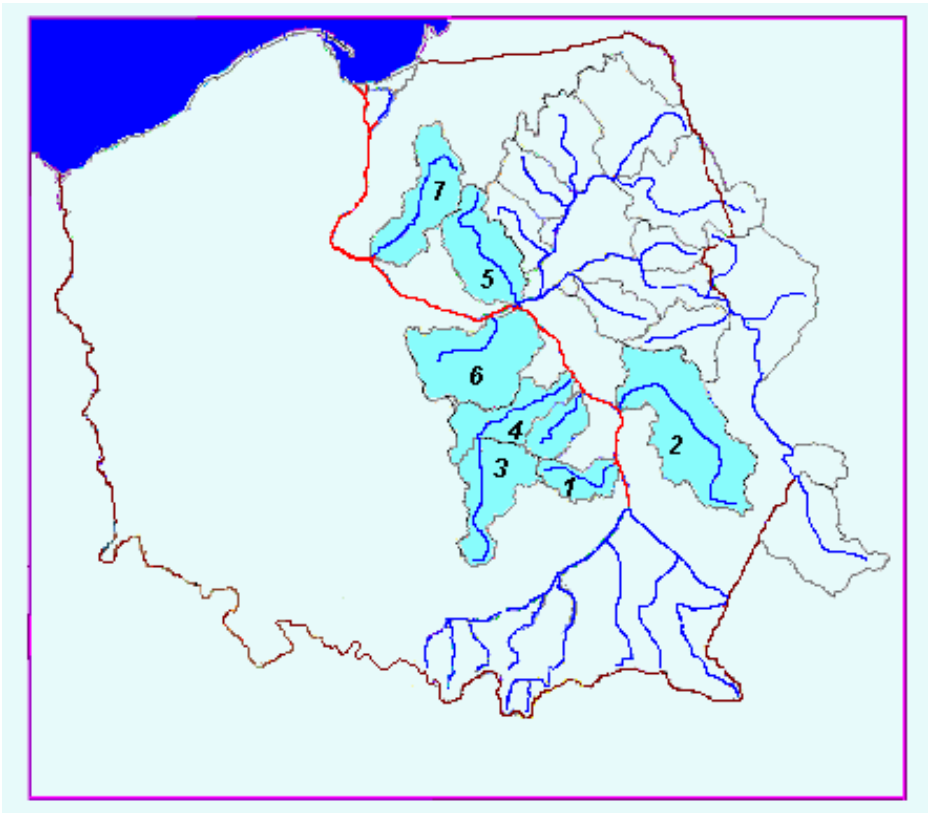

Figure 1: Tributaries of the Vistula River. The COSMO_LM model forecasts for river basins No 1-7.

Table 1: Results of operational run of the COSMO_LM model Errors of rainfall forecasts for the network of 14x14 and 7x7 km (MSE: mean square error, E: efficiency coefficient.

No	River basin	Area (km^2)	COSMO_LM model forecasts of rainfall							
			1-day ahead				2-days ahead		3-days ahead	
			LM-14km		LM-7km		LM-14km		LM-14km	
			MSE	E	MSE	E	MSE	E	MSE	E
1	Kamienna	2007.9	3.15	**0.93**	2.91	**0.71**	4.22	**0.98**	3.82	**1.02**
2	Wieprz	10415.2	3.80	**1.39**	3.29	**1.27**	2.88	**0.94**	3.12	**0.98**
3	Pilica_1	3908.6	3.86	**0.72**	4.45	**0.74**	3.62	**0.71**	4.37	**0.79**
4	Pilica_2	5364.4	2.85	**0.62**	2.65	**0.56**	4.01	**0.85**	3.46	**0.77**
5	Wkra	5322.1	3.71	**0.91**	3.86	**0.98**	3.74	**0.84**	3.84	**0.88**
6	Bzura	7787.5	3.02	**0.70**	2.77	**0.62**	3.29	**0.72**	3.36	**0.78**
7	Drweca	5343.5	3.54	**0.73**	3.62	**0.79**	3.69	**0.70**	4.96	**0.93**

Table 2: Number of observational stations vs. number of model grid nodes taken into account for calculating average daily mean.

No	River Basin	Area (km^2)	Number of observational stations	Number of grid nodes of LM 14	Number of grid nodes of LM 7
1	Kamienna	2007.9	9	9	41
2	Wieprz	10415.2	5	53	214
3	Pilica_1	3908.6	9	20	83
4	Pilica_2	5364.4	8	11	39
5	Wkra	5322.1	4	28	109
6	Bzura	7787.5	6	39	162
7	Drweca	5343.5	4	28	108

Conclusions

The analyse of table and graphs shows that:

- The probability distribution of observed precipitation is similar to the distribution of errors of forecasted precipitation (QPF) - that means, the range of QPF errors is comparable to the range of observed precipitation (especially for two and three days lead-time).
- Generally, the QPF for one day ahead contributes some information about future precipitation.
- There are not essential differences between QPF errors for 14x14 km and 7x7 km networks of the LM_DWD model.

Final Remarks

As seen from Table 1 obtained results are not quite coherent concerning the two obvious facts (expectations): 1) For such long time series the LM_07 model results should be obviously better (not worse) then LM_14 – what is violated for 3 (nearly 50%) basins: Pilica_1 No3, Wkra No5, Drweca No7, and the 2) The (un)efficiency coefficient E should increase with the lead-forecast time. This is true only for Kamienna (No 1) and Bzura (No 6). For other basins this rule is violated. The best results are for Pilica_2, the worse – quite not understandable

for Wieprz (No 2). One of possible explanations is that number of stations relevant to each of basins was not adequate enough for given simple averaging procedure. Beneath, in the Table 2 are gathered numbers that show the irregularity of station redistribution between basins.

When the same evaluation calculus be repeated on simulated hydrographs – what is presumed in near future – that will eventually clarify revealed ambiguities.

Fig. 2. The Pilica_1 River basin - rainfall forecasts from COSMO_LM model (14x14km network) Observed precipitation (Pobs) and 1-day (W1), 2-days (W2) and 3-days (W3) ahead forecast errors Period: 1.01. - 8.09.2003

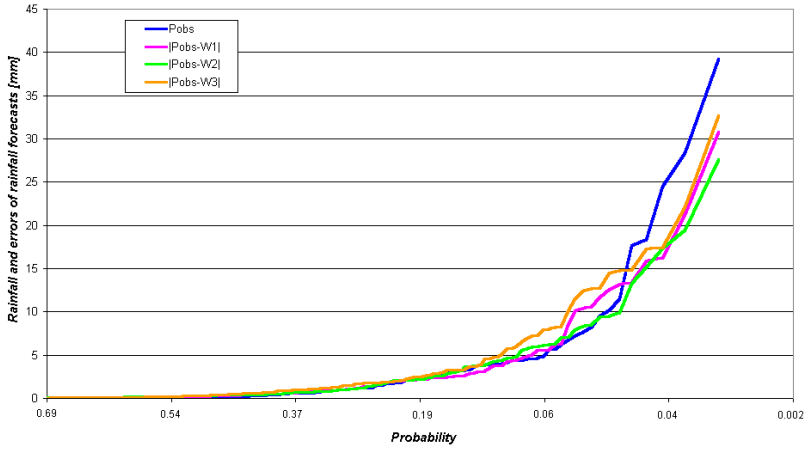

Fig. 3. The Pilica_1 River basin - rainfall forecasts from COSMO_LM model (7x7 km network) Observed precipitation (Pobs) and 1-day (W1) ahead forecast errors Period: 1.01. - 8.09.2003

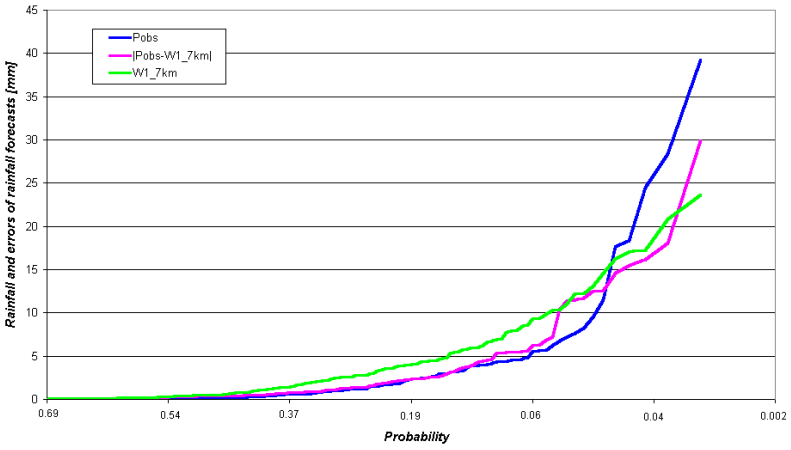

Fig. 4. The Wieprz River basin - rainfall forecasts from COSMO_LM model (14x14km network) Observed precipitation (Pobs) and 1-day (W1), 2-days (W2) and 3-days (W3) ahead forecast errors Period: 1.01. - 8.09.2003

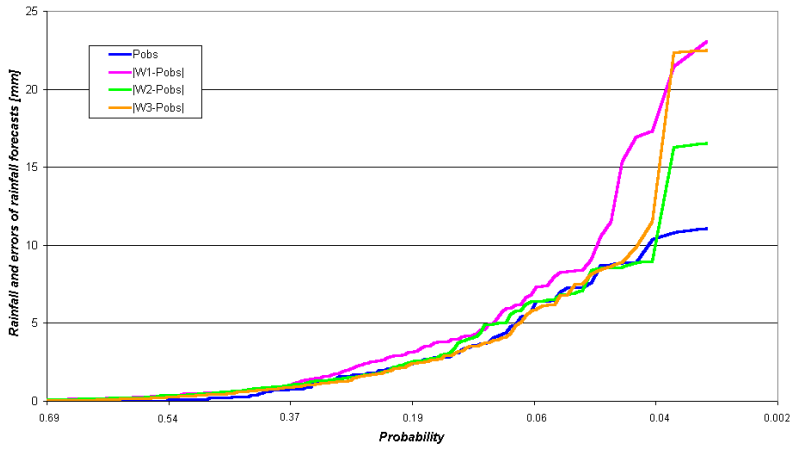

Quasi Real-Time Verification of aLMo Radiation Budget Forecast with Payerne Measurements

Marjorie Perroud and Dominique Ruffieux

MeteoSwiss, Aerological Station of Payerne, Switzerland

1 Surface Energy Budget Estimate and Measurement

In order to validate the weather prediction model used by MeteoSwiss (aLMo), analyses were performed with measured components of the energy budget at Payerne. The aerological station of Payerne is located in the Swiss Mittelland at 491 m asl (46.813°N, 6.943°E). The region is characterized by rollings hills surrounded to the N-NW by the Jura mountains (1000-1500 m asl) and to the S-SE by the Alps (1000-3000 m asl).

For this analysis, the parameters taken into account are the energy budget components:

– radiation budget components:

$$Q^* = (K\downarrow - K\uparrow) + (L\downarrow - L\uparrow) \tag{1}$$

– surface energy balance:

$$Q^* = Q_h + Q_e + Q_g \tag{2}$$

By merging (1) and (2), we obtain:

$$(K\downarrow - K\uparrow) + (L\downarrow - L\uparrow) = Q_h + Q_e + Q_g \tag{3}$$

Among those components, the model calculates the short-wave (K^*) and the long-wave (L^*) balance, the sensible heat (Q_h) and the latent heat (Q_e). The ground flux (Q_g) is estimated by considering the residual of Eq.(3). The different radiation fluxes going down and up are deduced from the following equations :

$$K^* = K\downarrow - K\uparrow \tag{4}$$
$$K^* = K\downarrow (1-\alpha) \tag{5}$$
$$L^* = L\downarrow - L\uparrow \tag{6}$$
$$L^* = L\downarrow - \varepsilon\sigma T_g^4 \tag{7}$$

where α is the albedo, ε is the emissivity, σ is the Stefan-Boltzmann constant and T_g is the surface ground temperature.

To judge the ability of the model to forecast these components, aLMo data are compared with the measurements of the Basic Surface Radiation Network (BSRN) station of Payerne (Switzerland) and of a sonic anemometer for the sensible heat. The value of the ground flux is obtained from (Stull, 1998):

$$\frac{\partial T}{\partial t} = -\frac{1}{C_g}\frac{\partial Q_g}{\partial z}\,. \tag{8}$$

By a reformulation of this equation, the ground flux is calculated by adding the measured flux at a depth, z, to the energy stored in the layer above the heat flux plates (Campbell, 1999).

The stored energy (S) is given by

$$S = C_g(\Delta T/\Delta t)\Delta z\,, \tag{9}$$

and the soil heat flux (Q_g) by

$$Q_g = Q_{gz} + S\,, \tag{10}$$

where Q_{gz} is the flux measured at 8 cm, C_g the soil heat capacity, 2.6 $\mathrm{Jm^{-}3K^{-}1}$ in Payerne (Mühlemann, 1996), T, the temperatures, Δt, the time interval and z, the depth.

To measure Q_g, sensors giving the flux at 8 cm below surface and the temperature at 2 cm and 6 cm below surface have been installed. The temperature was determined by averaging the 2 measured temperatures and the Δz corresponds to the depth of the soil heat flux plate. Finally, the latent heat being not measured in Payerne, its value will be equal to the residual of the equation.

2 Quasi Real-Time Comparisons and Statistics

An operational validation of the surface energy budget was set within MeteoSwiss. Every day, all forecasted and measured components of eq (3) are automatically extracted and the various time series displayed on a MeteoSwiss intranet web page. Furthermore, statistics are made available at the end of each month and of each season. The mean seasonal diurnal cycle of the differences of surface energy budget components are shown in Figure 1 (model minus measurements). One can notice an overall good estimate of the calculated parameters while both residuals (latent heat for measurements and ground flux for the model) show a significant temporal shift illustrated by a sinus shape curve of the differences. The maximal differences occurred in summer when the incoming solar intensity is the highest.

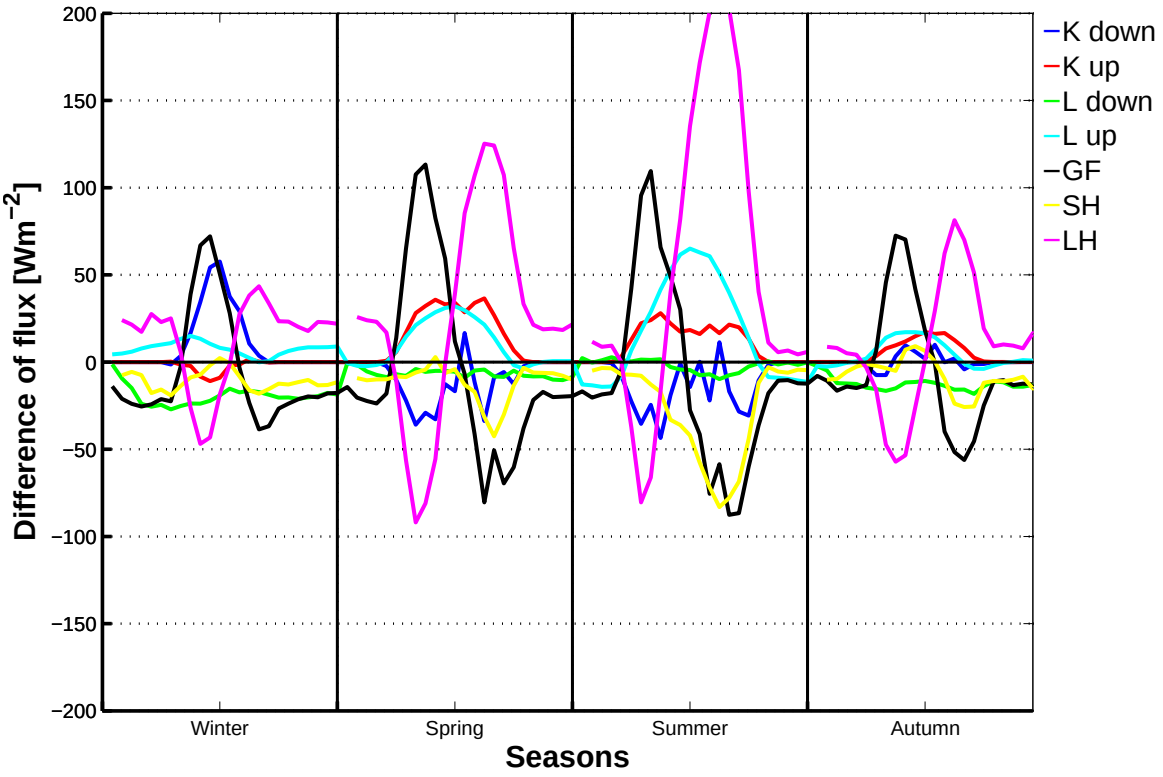

Figure 1: Differences of mean seasonal diurnal cycle of the surface energy budget between aLMo and measurements at Payerne for the year 2003.

3 Summary

A summary of conclusions taken from the analysis of a limited number of months is presented below. The quality of the $K\downarrow$ can be greatly influenced by the meteorological situation, with anticyclonic situations going together with good simulations. The $K\downarrow$ radiation is better predicted in summer than in winter because the low stratus are difficult to model. If the $K\uparrow$ is not so badly modeled in June compared to January, it has nevertheless a strong tendency to be underestimated by the model. The problem is certainly due to a too low value of the modeled albedo.

Concerning the $L\downarrow$, it seems that stable situation corresponds to a good prediction whereas an unstable situation to predictions of lower quality. In a great number of cases, the modeled $L\downarrow$ are underestimated, probably due to a wrong estimate of the clouds (their presence, their height). The difference between the modeled and measured $L\uparrow$ radiation being in general insignificant, the meteorological situations do not seem to have any influence on the quality of $L\uparrow$ simulations.

For the cases when the sensible heat is badly predicted, the model is either overestimating either underestimating. Nevertheless, in January, there are not only intensity shifts but also temporal shifts. The meteorological situation does not influence that much the value of the sensible heat. If the sensible heat for perturbed days is badly modeled in June, it can be in some cases extremely well modeled in January. That can be explained by the weak solar energy income which softens the shift of some of the components.

4 References

Campbell Scientific Inc., (1999):
www.atd.ucar.edu/rtf/facilities/isff/sensors/micromet/hft.pdf

Mühlemann, P., *Vergleich von Parametrisierungen des Bodenwärmeflusses sowie des sensiblen und latenten Wärmeflusses in Bodennähe mit Einbezug der Energiebilanz*, Geographisches Institut der Universität Bern, 1996.

R.B. Stull, *An Introduction to Boundary Layer Meteorology*, Kluwer Academy Publisher, Dordrecht, 680 pp, 1988.

COSMO–LEPS Verification: First Results.

C. Marsigli, F. Boccanera, A. Montani, F. Nerozzi, T. Paccagnella

ARPA-SIM, Bologna, Italy

Abstract

An objective probabilistic verification of the Limited–area ensemble system COSMO–LEPS is being carried out at ARPA–SIM. In particular, results for the 24–cumulated precipitation is considered in this work. Forecast values are compared against observations covering Northern Italy, but results for a bigger part of the COSMO–LEPS domain (covering also Germany and Switzerland) are presented. COSMO–LEPS is compared with ECMWF ensembles and different verification techniques are used. Finally, an analysis of the performances of the system at different spatial scales is shown.

1 Introduction

COSMO–LEPS is a probabilistic system for weather forecasts which combines the probabilistic information coming form the ECWMF global ensemble system with the mesoscale information introduced by Lokal Modell. Therefore the two main features of the system are the probabilistic approach and the capability of forecasting surface parameters with a greater detail with respect to global ensemble systems, leading to a better representation of mesoscale–related processes. The verification package of COSMO–LEPS is designed keeping in mind these characteristics, in order to retain and to evaluate the information coming from both of them. As regards the necessity of understanding the behaviour of a probabilistic forecast, probabilistic verification tools have been developed. Among them, the computation of Relative Operating Characteristic (ROC Curves), Brier Score and Brier Skill Score, Cost–Loss Analysis and Percentage of Outliers has been implemented in the COSMO–LEPS verification package. Though the computation of these scores is rather simple, their interpretation is not straightforward, different indices describing different features of the forecast system. In addition to this, the relationship between these scores is not a linear one. Therefore, a global evaluation of the forecast system should rely on a set of indices. In this report, for brevity reasons, only results in terms of the Brier Skill Score, ROC area and Percentage of Outliers will be presented. A description of these indices is reported in Appendix. Bearing in mind the other characteristic of COSMO–LEPS, which is the use of a mesoscale resolving model, the probabilistic evaluation is performed only in terms of surface variables, using a high–resolution dataset. In this report the focus is on the ability of the system of forecasting intense precipitation events. A verification of the 2–meters temperature is also being carried on. Different ways of comparing forecast and observed values are followed, in order to have a clean comparison and aming at the understanding of the spatial–scale properties of the forecast fields. After a brief description of the system (Section 2), verification results are presented (Section 3), organised as follows: a comparison with the ECMWF ensemble in terms of forecast precipitation over Northern Italy is shown in Section 3.1, while an evaluation over a bigger part of the COSMO area is presented in Section 3.2. Results obtained by comparing aggregated forecast and observed values over boxes of different sizes are reported in Section 3.3. Finally, the used evaluation idices are described in Section 4.

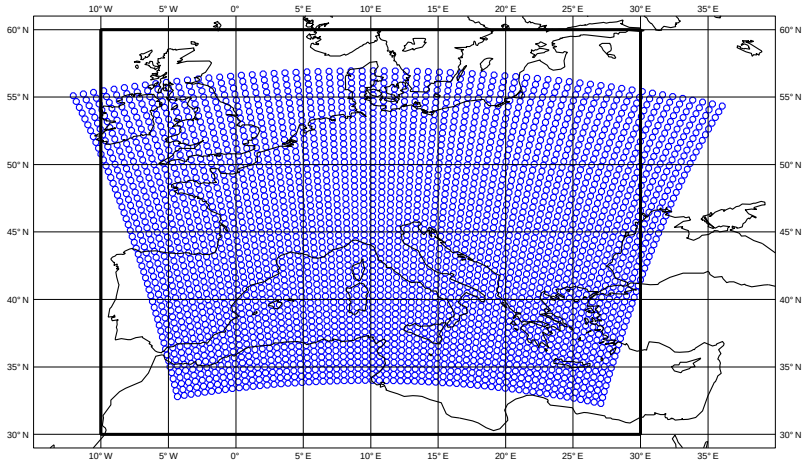

Figure 1: COSMO–LEPS operational domain (small circles) and clustering area (big rectangle).

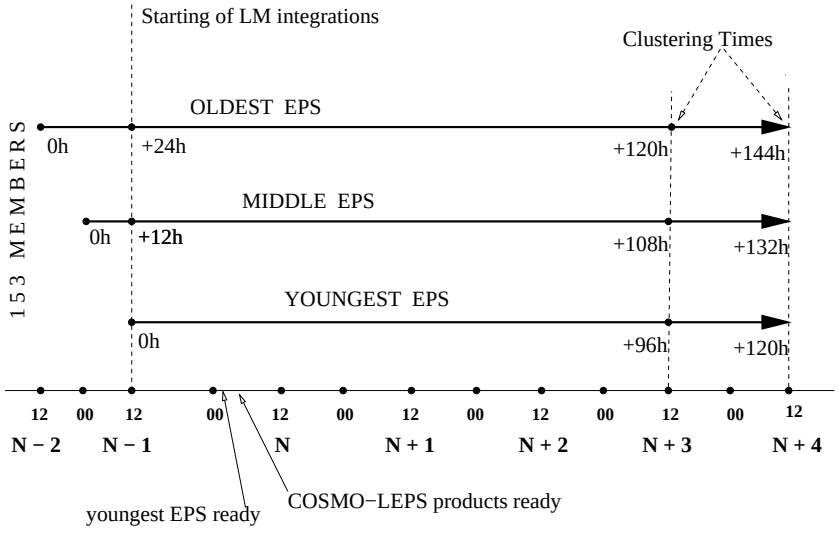

Figure 2: Details of the COSMO–LEPS suite.

2 The COSMO–LEPS operational system

The limited–area ensemble prediction system COSMO–LEPS has been running operationally at ECMWF since November 2002. The suite is run and maintained remotely by ARPA–SIM, with support given by ECMWF, and the necessary Billing Units are made avilable by the ECMWF COSMO countries. Five runs of the non–hydrostatic limited–area model Lokal Modell (LM) are available every day, nested on five selected members (the so–called Representative Members, or RMs) of three consecutive 12–hour lagged ECMWF global ensembles. The five selected members are representative of five clusters, built by grouping all the global ensemble members on the basis of their similarity in terms of upper–air fields (see Fig.2; for details on the suite implementation, the reader is referred to Montani et al., 2003b). The limited–area ensemble forecasts range up to 120 hours and are integrated over a domain covering all the countries involved in COSMO (Fig. 1). The model version is 3.3, the horizontal resolution is about 10 km and 33 vertical levels are used. LM–based probabilistic products covering a "short to medium–range" (48–120 hours) are disseminated to the weather services involved in COSMO.

Objective verification of the system has been carried out in order to quantify abilities and shortcomings of the system.

3 Verification results

The objective verification is mainly made in terms of probabilities of occurrence of selected weather events. In principle, each of the 5 COSMO–LEPS member contributes to the forecast probability of occurrence of the event by 20%. Nevertheless, due to the way the RMs driving the 5 LM integrations are selected form the super–ensemble, a weight can be assigned to each LM run, computed as the percentage of members from the super–ensemble that falls in its own RM's cluster. Scores computed by assigning this weight to each LM forecast are referred to "weighted". This "weighting procedure" is applied to the COSMO–LEPS members when probability maps are computed. Nevertheless, first verification results show that the "not–weghited" COSMO–LEPS performs slightly better than the "weighted" one or, at least, that difference between the two are not significant. In this report, results from the comparison between the two configurations are shown in Section 3.2.

Verification has been performed in two ways: by interpolating the gridded forecast values on station points where observations are available or by individuating a couple of representative observed and forecast values on boxes of fixed size. The interpolation of forecast values on station points has been performed in either of this two ways: by taking for each station the value on the nearest grid point or by averaging the values on the 4 nearest grid points. On the other hand, the unique value per each box is obtained either by computing the average value in the box or by choosing the maximum value in the box.

3.1 Comparison against ECMWF ensembles

A comparison between the COSMO–LEPS ensemble and the ECMWF available ensemble systems has been carried out over the network of stations covering Northern Italy, collected for the purpose of verifying LM. The period considered ranges from November 2002 to January 2003. Verification has been performed in terms of 24–hour cumulated precipitation.

3.1.1 Interpolation on station points

The first verification results compare COSMO–LEPS performance with that of the ECMWF ensembles. The indices have been computed for the entire super–ensemble, made up of three consecutive EPS ("epsse" model) as well as for the most recent EPS used in the construction of the super–ensemble ("eps51" model) and for the ensemble made up of the 5 ECMWF RMs chosen from the super–ensemble ("epsrm" model). Results are presented in terms of Brier Skill Score, a higher value corresponding to a better results and the zero level indicating the limit of usefulness of the forecasting system.

An interesting result is that the performance of the super–ensemble is comparable with that of the most recent EPS alone (Fig.3, black and blue lines, respectively). The 5–RM ensemble (green line) is almost always less skillful than COSMO–LEPS (red line), which benefits from the gain due to the nesting of the limited–area model. COSMO–LEPS performance is slighlty worse than that of the super–ensemble at the lower threshold (top left panel) and comparable to it at the intermediate thresholds (top right and bottom left panels). When heavy precipitation is considered (over 50mm/24h, bottom right panel), COSMO–LEPS has some skill at the 4–5 days forecast range, where the ECMWF ensembles show no skill. In order to better understand the results, it is important to remind that a bigger ensemble is favoured in terms of the Brier Skill Score (Talagrand et al., 1999). The reason of the good performance of the super–ensemble can be understood also looking at the percentage

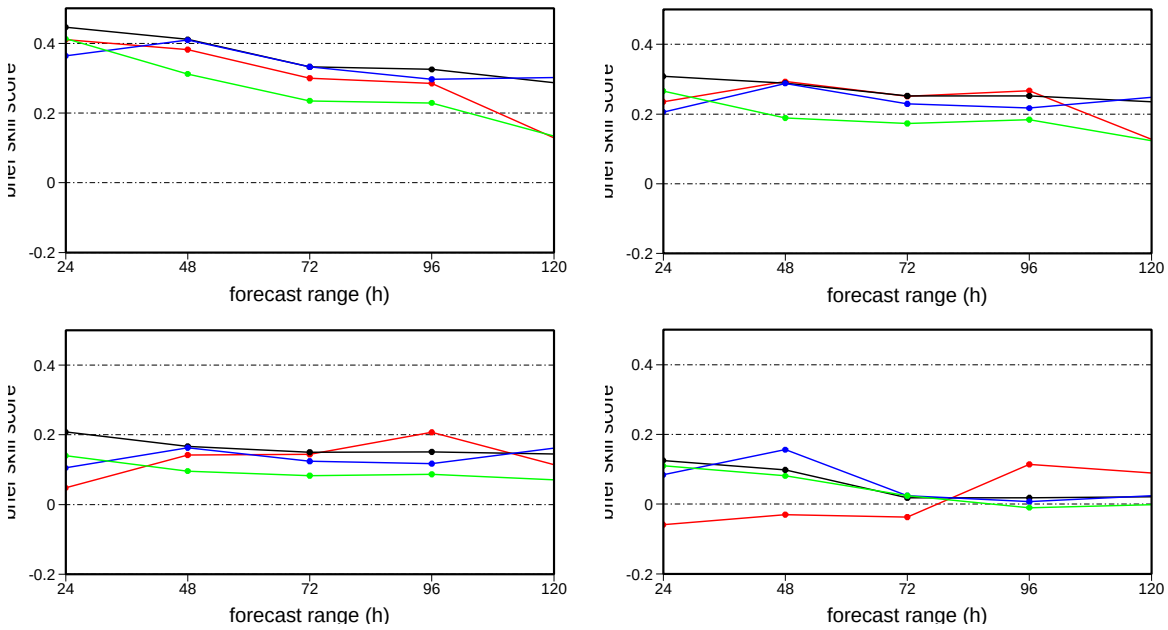

Figure 3: Brier Skill Score (the higher the better) as a function of the forecast range (in hours) relative to the 24–hour cumulated precipitation forecasts by COSMO–LEPS (cleps, red line), by the ECMWF super–ensemble (epsse, black line), by the most recent of the three EPS (eps51, blue line) and by the 5 ECWMF RMs ensemble (epsrm, green line) for different precipitation thresholds: over 10 (top left), 20 (top right), 30 (bottom left) and 50 mm/24h (bottom right). Forecast values are bilinearly interpolated over station points.

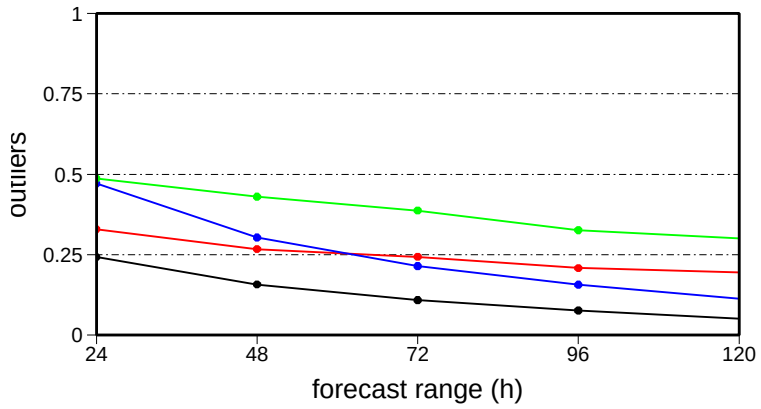

Figure 4: Percentage of outliers as a function of the forecast range (in hours) relative to the 24–hour cumulated precipitation forecasts by COSMO–LEPS (cleps, red line), by the ECMWF super–ensemble (epsse, black line), by the most recent of the three EPS (eps51, blue line) and by the 5 ECWMF RMs ensemble (epsrm, green line).

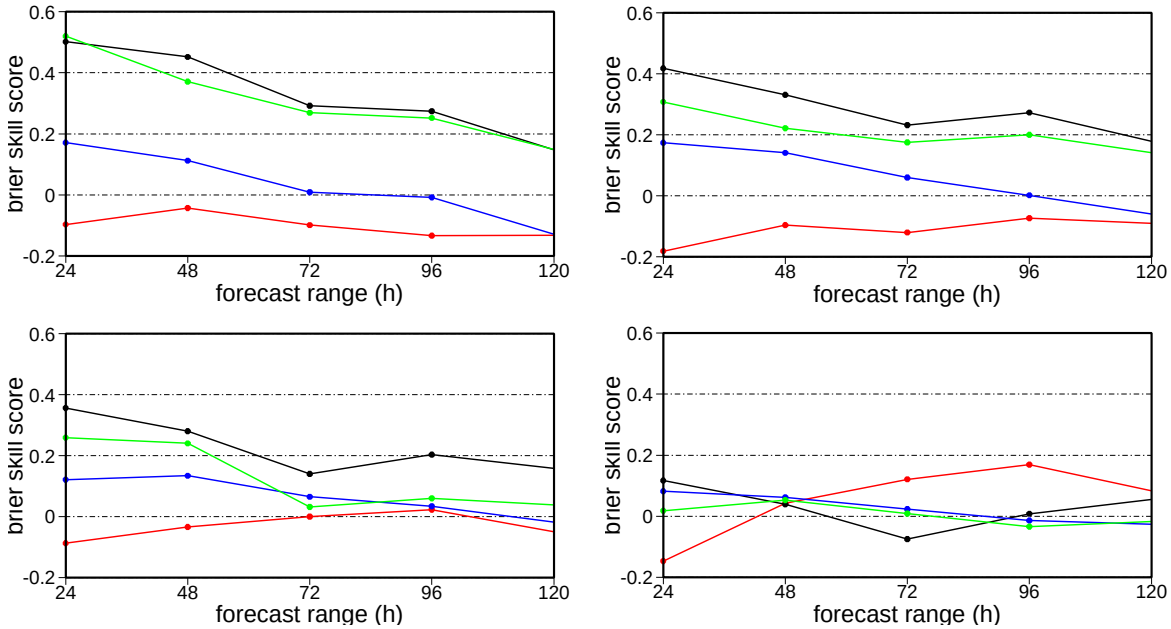

Figure 5: Brier Skill Score (the higher the better) as a function of the forecast range (in hours) relative to the 24–hour cumulated precipitation forecasts by COSMO–LEPS (red and black lines) and by the ensemble made up with the 5 RMs of ECMWF (blue and green lines) for different precipitation thresholds: over 10 (top left), 20 (top right), 30 (bottom left) and 50 mm/24h (bottom right). Black and green lines are relative to the scores computed for the average values over boxes 1.5 x 1.5, while red and blue lines are obtained by comparing the maximum values over the same boxes.

of outliers, which is the percentage of cases in which the observed value lies out of the range of the forecast values. As shown in Fig. 4, the use of the 153–member ensemble permits to have enough spread to reduce to its mimumum value the percentage of outliers for every forecast range.

3.1.2 Average and maximum values in boxes

The aggregation of both forecast and observed values over boxes seems to be very important in order to properly compare the two. This is particularly true when comparing models with different spatial resolution. In this case, COSMO–LEPS has an horizontal resolution of about 10 km, while ECWMF EPS runs have a resolution of about 80 km. In this work, boxes are built in a way that permits a partial overlapping between them, in order to avoid sharp and somewhat artificial boundaries between one box and the other. Average observed and forecast values over partially overlapping boxes with size 1.5 x 1.5 degrees are compared in this section. Due to the fact that averaging tends to smooth the precipitation field and to reduce the maximum values and having COSMO–LEPS be designed for the forecast of intense precipitation, a comparison of maximum forecast and observed values in each box has also been carried out. This analysis has been performed for COSMO–LEPS and for the 5–RM ECMWF ensemble ("epsrm") only, the verification of the super–ensemble over a great amount of boxes being highly computationally demanding.

Results are shown in Fig. 5. Black and green lines are relative to the scores computed by comparing the average observed and forecast values over boxes 1.5 x 1.5 degrees, for COSMO–LEPS and epsrm respectively. Red and blue lines are obtained by comparing the maximum observed and forecast values over the same boxes, for COSMO–LEPS and epsrm respectively. It is evident that the average values are more skillful than the maxima for moderate rainfall thresholds (10 and 20 mm/24h) and that COSMO–LEPS mean values over

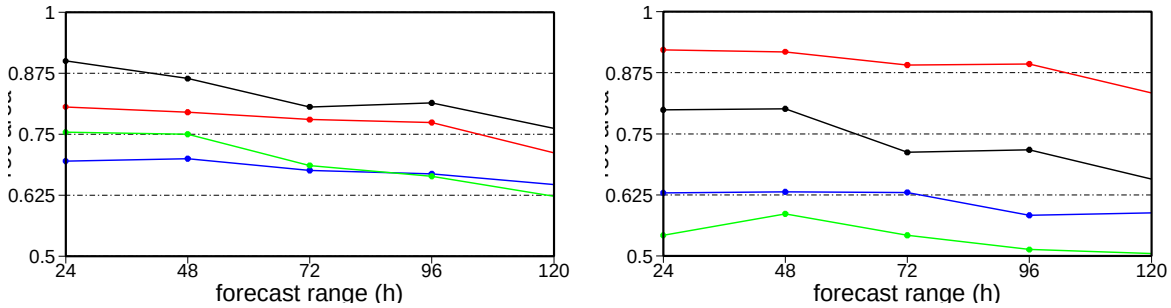

Figure 6: The same as in Fig. 5 but in terms of ROC area.

the boxes are more skillful than epsrm ones, especially for the 20 and 30 mm/24 thresholds. At the higher precipitation threshold (50mm/24h, bottom right panel), only COSMO–LEPS maxima have some skill, especially from +72 hours onward. In Fig. 6 results on terms of ROC area are also reported for the highest precipitation thresholds: 30 (left panel) and 50 mm/24h (right panel). According to this measure the better performance of COSMO–LEPS for intense precipitation is more evident, especially in terms of maximum values for the 50mm/24 threshold. The difference between the two indices can be understood referring to the Brier Score decomposition presented in Section 4.2. When an event is correctly forecast with low probability, the Brier Score increases, that is it worsens, while the ROC area increases.

3.2 Verification over Germany, Switzerland and Italy

The observational database used for COSMO–LEPS verification has recently enlarged, thanks to the efforts of the COSMO community. An agreement has been established and 24–hour cumulated precipitation data (06–06 UTC) from Germany, Switzerland and Italy are collected, put in a common format and redistributed by Ulrich Damrath. The available network is shown in Fig. 7.

This great amount of station (over 4000) has been used to verify COSMO–LEPS over a larger domain. Verification has been carried out by comparing the observed value with the forecast value on the nearest grid point. Computations is being repeated by averaging the values over boxes of different sizes and will be presented in the next future. The results obtained so far are quite unexpected: the Brier Skill Score values decrease substantially (that is, they worsen) when computed over the bigger network with respect to the values obtained by repeating verification over Northern Italy only.

This is shown in Fig. 8, where the two areas are compared: the black and the red lines are relative to the verification over Northern Italy (weighted and not–weighted, respectively), while the green and the blue line are relative to the verification made by using all the stations (weighted and not–weighted, respectively). For precipitation exceeding 10mm/24h (left panel), a decrease of the score when the whole network is used is evident, though its values are still positive. At the highest threshold (50mm/24h, right panel), the skill showed by COSMO–LEPS for the longer time ranges is missing when computations are made over the whole network. The reason for this discrepancy cannot be ascribed to the different altitude of the stations, the German stations (which constitutes the greatest part of the network) being located mainly in the plain. An analysis has been performed by subdividing the sample according to the stations' altitude (not shown) and no differences able to explain this discrepancy have been found. The different size of the two dataset can certainly play a role and a clean comparison between the two different samples is not possible. Nevertheless,

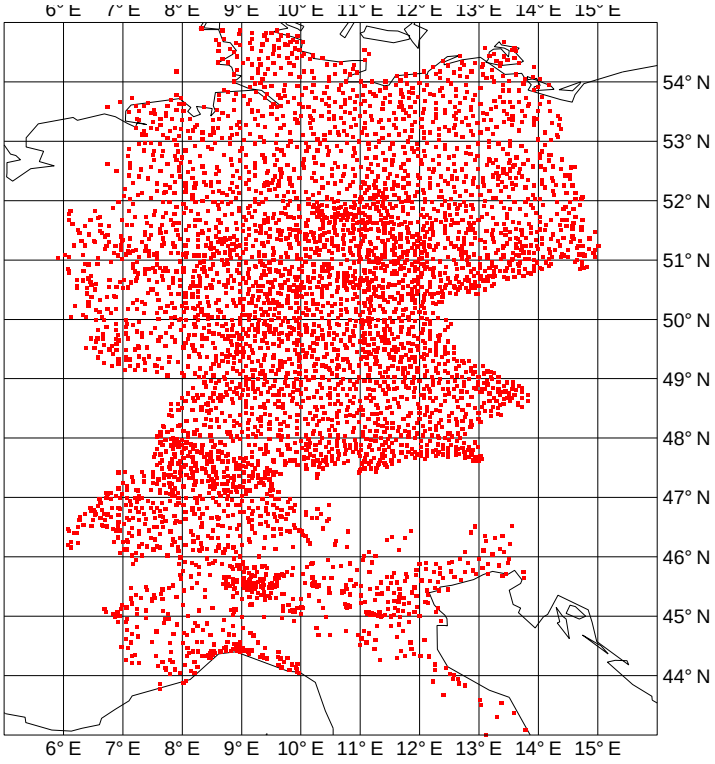

Figure 7: COSMO network of stations were observed precipitation is available. Precipitation data are cumulated over 24 hours from 06 to 06 UTC.

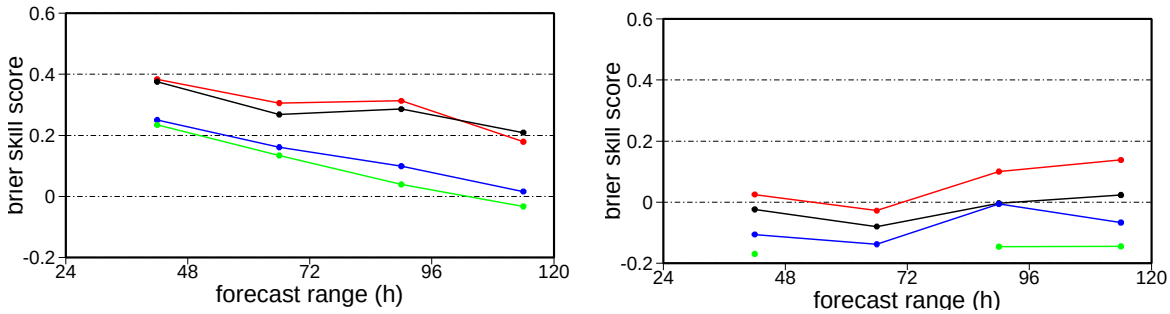

Figure 8: Brier Skill Score (the higher the better) as a function of the forecast range (in hours) relative to the 24–hour cumulated precipitation forecasts by COSMO–LEPS for precipitation thresholds 10 (left panel) and 50 mm/24h (right panel). Black and red lines are relative to the scores computed only over the italian stations (black line for the weighted configuration and red line for the not–weighted one), while green and blue lines are obtained by computing the scores over all the stations (green line for the weighted configuration and blue line for the not–weighted one).

it is possible to suggest that COSMO–LEPS, at least in Autumn, performs better over Italy than over Germany. This can be understood thinking at the mountainous terrain of the Northern Ialy, with alternating mountains and plains in a narrow region, where mountains act as a major forcing for the precipitation field, increasing the predictability associated to this parameter, especially in case of intense events. In Switzerland the situation is different with respect to Italy: the terrain is also mountainous, but we are mainly considering Autumn cases, that is cases associated with flow form the south over the Alps. The tendency of LM to underestimate the precipitation downwind could explain the rather poor performance over this area (not shown). Of course, this analysis is a very preliminar one and further investigations are needed.

As the difference between weighted and not–weighted ensemble is concerned, it is possible to notice from Fig. 8 that the weighting procedure does not imply an improvement of the scores. This is an example of a more general results: comparing the two configuration in different ways, either the not–weighted one is more skillful or no difference between the two has been found.

3.3 Comparison of different box sizes

The idea underlying the use of aggregated observed and forecast values in boxes is that the very detailed information provided by Lokal Modell contains a non–negligible stochastic component that has to be removed. This has already been expressed by Theis et al. (COSMO Newsletter No. 2). The size of the boxes, which is related to the spatial scale badly resolved by the model, is still an open problem. Every box has to be large enough to contain a number of points that permits a robust statistics, both for observations and forecasts, but the box size has to be also related to the characteristics of the model we are using, if we accept the idea that aggregating Lokal forecasts on a certain scale will lead to more robust and reliable estimate of surface parameters.

As the behaviour of the system for different spatial scales is concerned, the verification indices have been computed by comparing average and maximum values over boxes of different sizes. Forecast and observed values can have different densities in the boxes, COSMO–LEPS forecast density being about 100 points in a box of 1 x 1 degrees. In order to reduce the impact of this difference, a constraint has been imposed: only boxes where at least 10 observations are available are considered. Computation has been performed for November 2002 only, using the Northern Italy network. Precipitation has been cumulated over 24 hours, between 06 and 06 UTC.

Results (Fig. 9) indicate that the skill of the average forecast value for the moderate rainfall threshold (20mm/24h threshold, top left), is maximum when box size is 1 x 1 or 1.5 x 1.5 degrees (blue and green lines). The scores drop when the 50mm/24h threshold is considered (bottom left panel), with every box size. At this high threshold, only the maximum values are still skillful (bottom right panel), especially for bigger boxes (1 x 1 or 1.5 x 1.5 degrees, blue and green lines). At the moderate threshold, the maximum value is more skillful when little boxes are considered (top right panel). In every panel the scores obtained by comparing the observed value with the value forecast in the nearest grid point has been showed as a reference (red line).

4 Description of the probabilistic indices

The forecast produced by a probabilistic prediction system of M members can be regarded as subdivided in M+1 probability classes. The probability associated to each class is k/M, $k \in \{0, 1, \ldots, M\}$. For each probability class k and for each event, a contingency table is

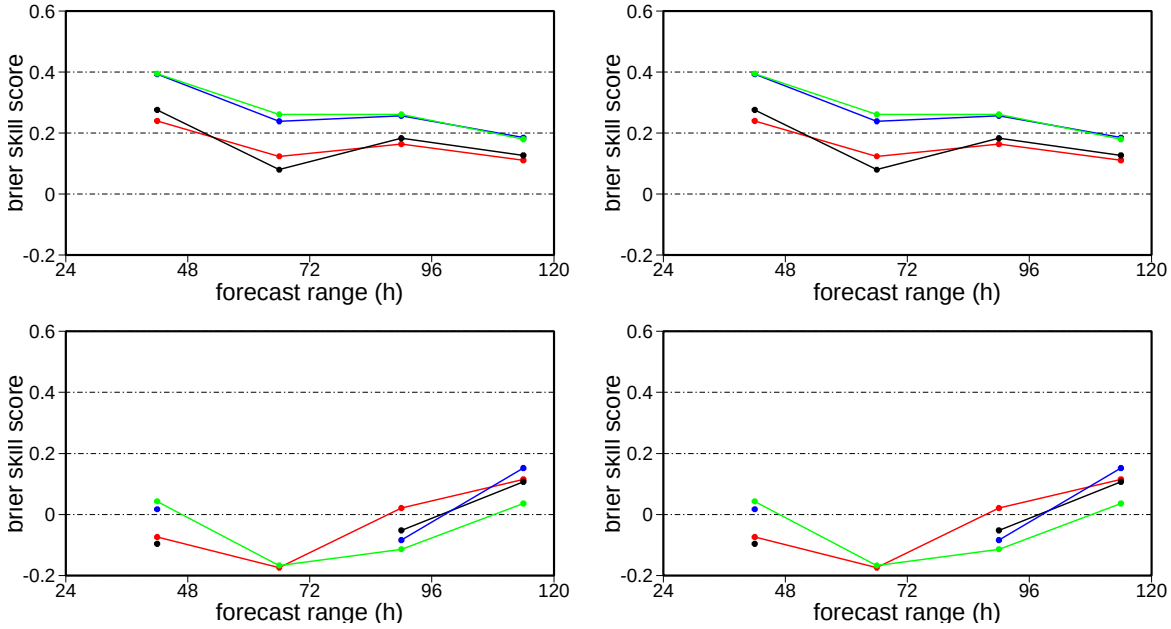

Figure 9: Brier Skill Score (the higher the better) as a function of the forecast range (in hours) relative to the 24–hour cumulated precipitation forecasts by COSMO–LEPS. Scores are relative to the average values in the left panels and maximum values in the right panels. Two precipitation thresholds have been considered: 20 mm/24h in the top panels and 50 mm/24h in the bottom panels. The red line is for the nearest point, black line for boxes of 0.5 x 0.5 degrees, blue lines for 1 x 1 degrees and green lines for 1.5 x 1.5 degrees.

built.

Contingency Table		observed	
		yes	no
forecast	yes	a_k	b_k
	no	c_k	d_k

The following relations hold: $a_k + b_k + c_k + d_k = N$, $a_k + c_k = N\bar{o}$, $b_k + d_k = N(1-\bar{o})$, $a_k + b_k = N_k$, $a_k = N_k\bar{o}_k$ and $b_k = N_k(1-\bar{o}_k)$. N is the dimension of the verification domain, while $\bar{o}$ is the observed frequency of the event. For each probability class, N_k is the dimension of the subspace where the event is predicted with probability k/M and $\bar{o}_k$ is the observed frequency of the event when it is predicted with probability k/M.

4.1 ROC area

The accuracy of probabilistic forecasts can be evaluated using the Relative Operating Characteristic (ROC) curves (Mason and Graham, 1999). According to the Contingency Table, the Hit Rate (H) and the False Alarm Rate (F) for each probability class are defined as:

$$H_k = \frac{a_k}{a_k + c_k} = \frac{N_k\bar{o}_k}{N\bar{o}},$$

$$F_k = \frac{b_k}{b_k + d_k} = \frac{N_k(1-\bar{o}_k)}{N(1-\bar{o})}.$$

The two scores indicate, respectively, the proportion of events which were predicted by k members and actually happened, and the proportion of events forecast by k members and did not occur. If several warning thresholds are used for the event, corresponding to a set of forecast probabilities, a set of cumulative hit and false alarm rates can be determined for

the same threshold. The accumulation is made for the probability classes form the k–th to the M–th. The set of cumulative H, plotted against the set of the corresponding cumulative F, generates the ROC curve. The area under the curve is commonly used as a probabilistic score, its maximum value being 1, and a value of 0.5 indicating a no–skill forecast system (Mason and Graham, 1999).

4.2 Brier Score and Brier Skill Score

The Brier Score (BS) is the mean–square error of the probability forecasts (Brier, 1950). The BS averages the squared differences between pairs of forecast probabilities and the corresponding binary observations, representing the occurrence (or non–occurrence) of the event. It is defined as follows:

$$BS = \frac{1}{N}\sum_{i=1}^{N}(p_i - o_i)^2,$$

where the observation is $o_i = 1$ ($o_i = 0$) if the event occurs (does not occur), while p_i is the fraction of ensemble members which forecast the event and the index i denotes a numbering over the whole domain. BS can take on values in the range [0,1], the perfect forecast having $BS = 0$ (Stanski et al., 1989; Wilks, 1995). The Brier Score can be also expressed as a function of Hit Rate and False Alarm Rate. The relation, expressed in a different form by Talagrand et al. (1999), is:

$$BS = \bar{o}\sum_{k=0}^{M} H_k\left(1 - \frac{k}{M}\right)^2 + (1-\bar{o})\sum_{k=0}^{M} F_k\left(\frac{k}{M}\right)^2.$$

When an event is correctly forecast (high value of H_k) with a low probability (high value of $(1 - \frac{k}{M})^2$), the Brier Score increases, that is it worsens.

The Brier Skill Score (BSS) is defined as the BS percentage improvement of the forecast system with respect to climatology and it is computed as

$$BSS = \frac{BS_{cli} - BS}{BS_{cli}} = 1 - \frac{BS}{\bar{o}(1-\bar{o})}.$$

A positive BSS indicates that a system has predictive power; the perfect deterministic forecast has BSS = 1 (Stanski et al., 1989).

4.3 Percentage of Outliers

The Percentage of Outliers of a probabilistic forecast system is defined as the probability of the analysis lying outside the forecast range (Buizza, 1997). Here, it is computed as the fraction of points of the domain where the observed value lies outside the range of forecast values. The M values predicted at each grid–point by a probabilistic forecast system can be put in increasing order, thus determining M+1 intervals: v ¡ f_1, f_1 ¡ v ¡ f_2, ..., v ¿ f_M. In this way, it is possible to compute the percentage of times the observed value lies in each interval. If a sufficiently large number of cases is considered, the expected probability of the analysis being inside each of the M+1 intervals is 1/M+1 (Buizza, 1997). The percentage of times the observation lies in the first or in the last interval provides the percentage of outliers. The percentage of times the observed value is smaller than the lowest forecast value is called outliers below the minimum (first interval) and the percentage of times the observed value is greater than the highest forecast value is called outliers above the maximum (last interval).

References

Brier, G. W, 1950. Verification of forecasts expressed in terms of probability. *Mon. Wea. Rev.*, **78**, 1–3.

Buizza, R., 1997. Potential forecast skill of ensemble prediction and spread and skill distributions of the ECMWF ensemble prediction system. *Mon. Wea. Rev.*, **125**, 99–119.

Marsigli, C., Montani, A., Nerozzi, F., Paccagnella, T., Tibaldi, S., Molteni, F., Buizza, R., A strategy for High–Resolution Ensemble Prediction. Part II: Limited–area experiments in four Alpine flood events, 2001. *Quart. J. Roy. Meteor. Soc.*, **127**, 2095–2115.

Marsigli, C., Montani, A., Nerozzi, F., Paccagnella, T., Probabilistic high-resolution forecast of heavy precipitation over Central Europe, 2003. *Natural Hazards and Earth System Sciences*, in press.

Mason, S. J. and Graham, N. E., 1999. Conditional probabilities, relative operating characteristics and relative operating levels. *Wea. and Forecasting*, **14**, 713–725.

Molteni, F., Buizza, R., Marsigli, C., Montani, A., Nerozzi, F. and Paccagnella, T., 2001. A strategy for High–Resolution Ensemble Prediction. Part I: Definition of Representative Members and Global Model Experiments. *Quart. J. Roy. Meteor. Soc.*, **127**, pp. 2069–2094.

Montani, A., Marsigli, C., Nerozzi, F., Paccagnella, T. and Buizza, R., 2001. Performance of ARPA–SMR Limited–area Ensemble Prediction System: two flood cases. *Nonlinear Processes in Geophysics*, **8**, 387–399.

Montani, A., Marsigli, C., Nerozzi, F., Paccagnella, T., Tibaldi, S. and Buizza R., 2003a. The Soverato flood in Southern Italy: performance of global and limited–area ensmeble forecasts *Nonlinear Processes in Geophysics*, **10**, 261–274.

Montani, A., Capaldo, M., Cesari, D., Marsigli, C., Modigliani, U., Nerozzi, F., Paccagnella, T., Patruno, P. and Tibaldi, S., Operational limited–area ensmeble forecasts based on the Lokal Modell, 2003b. *ECMWF Newsletter Summer 2003*, **98**, 2–7.

Stanski, H. R., Wilson, L. J. and Burrows, W. R., 1989. Survey of common verification methods in meteorology. WMO World Weather Watch Tech. Rep., **8**, pp. 144.

Talagrand, O., Vautard, R. and Strauss, B, 1999. Evaluation of probabilistic prediction systems. Proceedings of the ECMWF workshop on predictability, 20–22 October 1997, Reading, UK, pp. 372.

Wilks, D. S., 1995. Statistical methods in the atmospheric sciences. Academic Press, New York, 467 pp.

9 Model Development and Application

This section includes several reports on various research topics and model applications as well as progress and status reports of the COSMO Working Groups. Within this section, we omit a subdivision by themes and the numbering of equations and figures refers to each paper. The contributions are ordered such that follow the topics of WG1 – WG4 and WG6. Papers related to model verification have been included in the preceding section.

Most of the papers included in this section are write-ups from the COSMO annual meeting 2003 in Langen (Germany). Many thanks to all who provided contributions for the present issue of the Newsletter.

We have not included longer reports that have been or are going to be published in the COSMO Technical Report (TR) series. The TRs are intended for a documentation of research activities, to present and discuss results from model applications and from verification and interpretation, and to document technical changes and new components of the LM package. The purpose of these reports is to communicate results, changes and progress related to the LM model system relatively fast within the COSMO consortium. Technical Reports No. 1 - 5 are available at www.cosmo-model.org, unfortunately no new report could be published in 2003.

The following issues are planned so far for 2004. Of course, any additional paper is welcome, and we would like to encourage all of you to submit a contribution.

No. 6, Matthias Raschendorfer:
A New TKE-Based Scheme for Vertical Diffusion and Surface-Layer Transfer.

No. 7, Günther Doms:
The LM Cloud Ice Scheme.

No. 8, Andrea Montani et al.:
COSMO-LEPS: Description of the Methodology, Configuration of the system, Products and User Guide

No. 9, Jochen Förstner and Günther Doms:
RK3-TVD time integration with high order spatial discretization.

No. 10, Michael Baldauf, Thorsten Reinhardt an Günther Doms:
Prognostic precipitation for 2- and 3 timelevel integration schemes.

Impact of a Bias Correction Scheme for Vaisala RS80 Radiosonde Relative Humidity Observations

Christoph Schraff

Deutscher Wetterdienst, P.O.Box 100465, 63004 Offenbach a.M., German y

Introduction and Outline of the Bias Correction Scheme

For most types of radiosondes, observed humidity is known to have a dry bias near saturation in general. Hence in the current operational version of the observation processing in the LM, saturation is assumed for observed relative humidity values greater than 96 % irrespective of temperature. The assumption for saturation, however, is not made for data which have already been comprehensively bias-corrected before being written to the AOF, as is the case for the Lindenberg radiosonde data. (For model runs without prognostic cloud ice, the observed humidity below freezing is additionally enhanced in a later step by the fraction of saturation vapour pressure over water e_{sat}^{water} and saturation vapour pressure over ice e_{sat}^{ice}, irrespective of the bias correction applied. This ice-to-water adjustment renders the observational data model compatible in the sense that it accounts for neglecting cloud ice.)

The current study evaluates a new type of bias correction. It is applied to the observed relative humidity $U_{ob\,V80}$ from the Vaisala RS80 A-Humicap sondes (except for the Lindenberg sonde) in two steps as derived from parallel ascents with Vaisala RS90 H-Humicap sondes (see Nagel et al., 2001). The first step, the so-called weather screen ground check correction,

$$U_{ob}^{corr,1} \;=\; U_{ob\,V80} \;+\; 0.056 \cdot U_{ob\,V80} \tag{1}$$

is applied at any temperature. The temperature-dependent second step

$$U_{ob}^{corr,2} \;=\; U_{ob}^{corr,1} \;+\; \frac{U_{ob}^{corr,1} \;\cdot\; (0.005 \cdot (T\text{–}T_0)^2 \;+\; 0.112 \cdot (T\text{–}T_0) \;+\; 0.404)}{100 \cdot e_{sat}^{ice}/e_{sat}^{water} \;-\; (0.005 \cdot (T\text{–}T_0)^2 + 0.112 \cdot (T\text{–}T_0) + 0.404)} \tag{2}$$

is applied only if temperature $T < T_0 - 12[\mathrm{K}]$ (where $T_0 = 273.15\,\mathrm{K}$).

Note that this correction is derived statistically purely from the observations themselves. It does not attempt to render the observational data explicitly model-compatible by making use of the model's relative humidity – cloud fraction relationship, as is done e.g. in Sharpe and Macpherson (2002).

Trial 1: A Case of Thick Cirrus

Since the bias correction is greatest at a very low temperature and near saturation (i.e. up to 15 %, or even more than 20 % relative humidity after the ice-to-water adjustment), the largest impact is expected on the simulation of high-level cloudiness. In a first experiment with a parallel assimilation cycle and 2 daily forecasts, it was applied for the period of 28 March to 1 April 2002 and compared to the operational version as a reference. This period included the event of a thick cirrus cloud band extending from the Mediterranean to Northern France and moving northeastward across Germany. The operational LM forecasts did not capture well the cloudiness and hence severly overestimated the daytime surface-level temperature in the western half of Germany on 30 March (Easter Saturday). Note that below 500 hPa, the air was very dry over Germany and its near environs at that day.

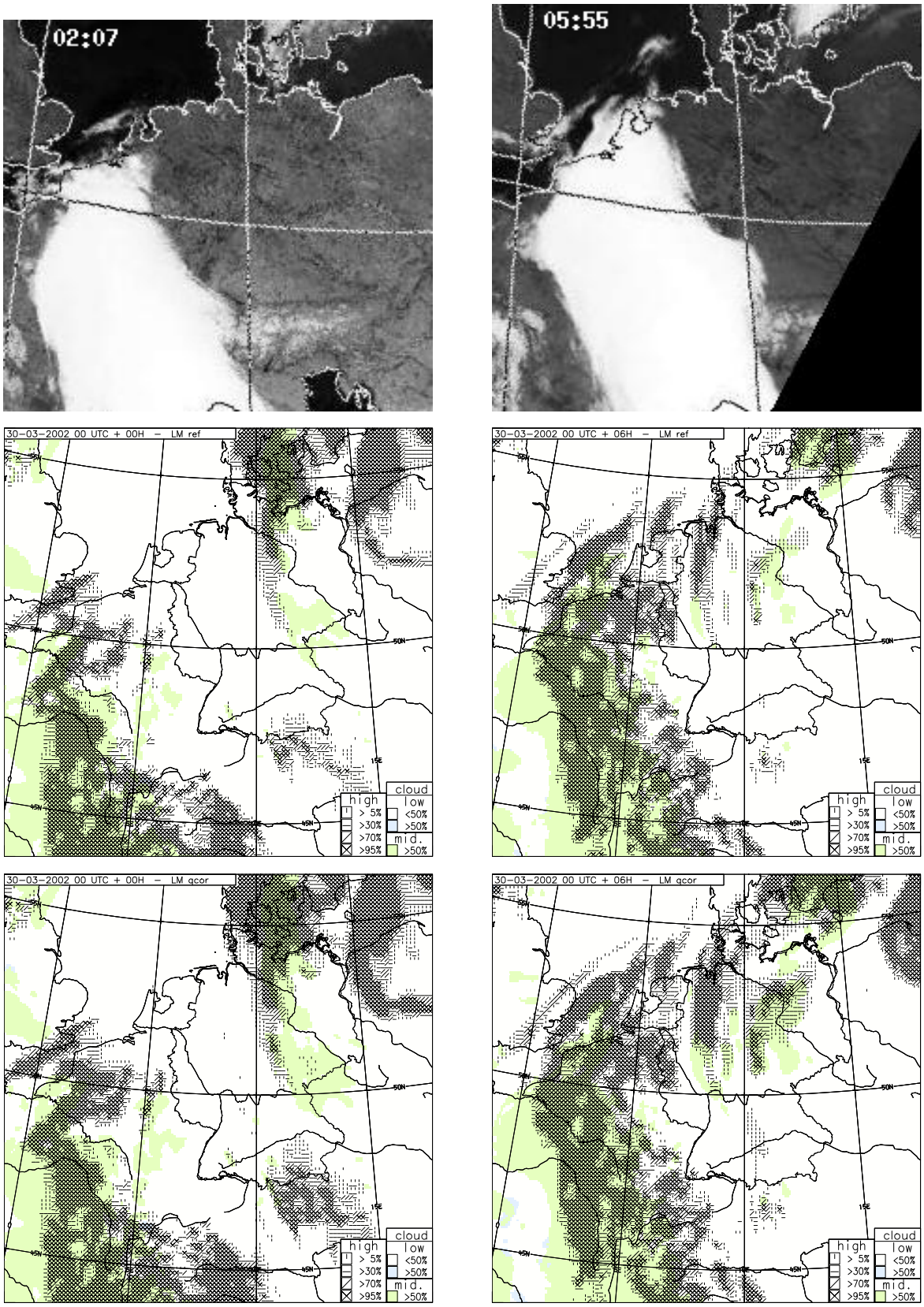

Figure 1: Top row: NOAA IR satellite images; middle row: *high* cloud cover (patterns), mid-level cloud cover (green shading), and low cloud cover (grey shading) of reference LM forecasts without new bias correction; bottom row: as middle row, but for LM forecasts with new bias correction. Left column (a): IR image at 02:07 UTC and LM analyses valid for 00 UTC on 30 March 2002; right column (b): IR image and 6-hour LM forecasts valid for 06 UTC on 30 March 2002.

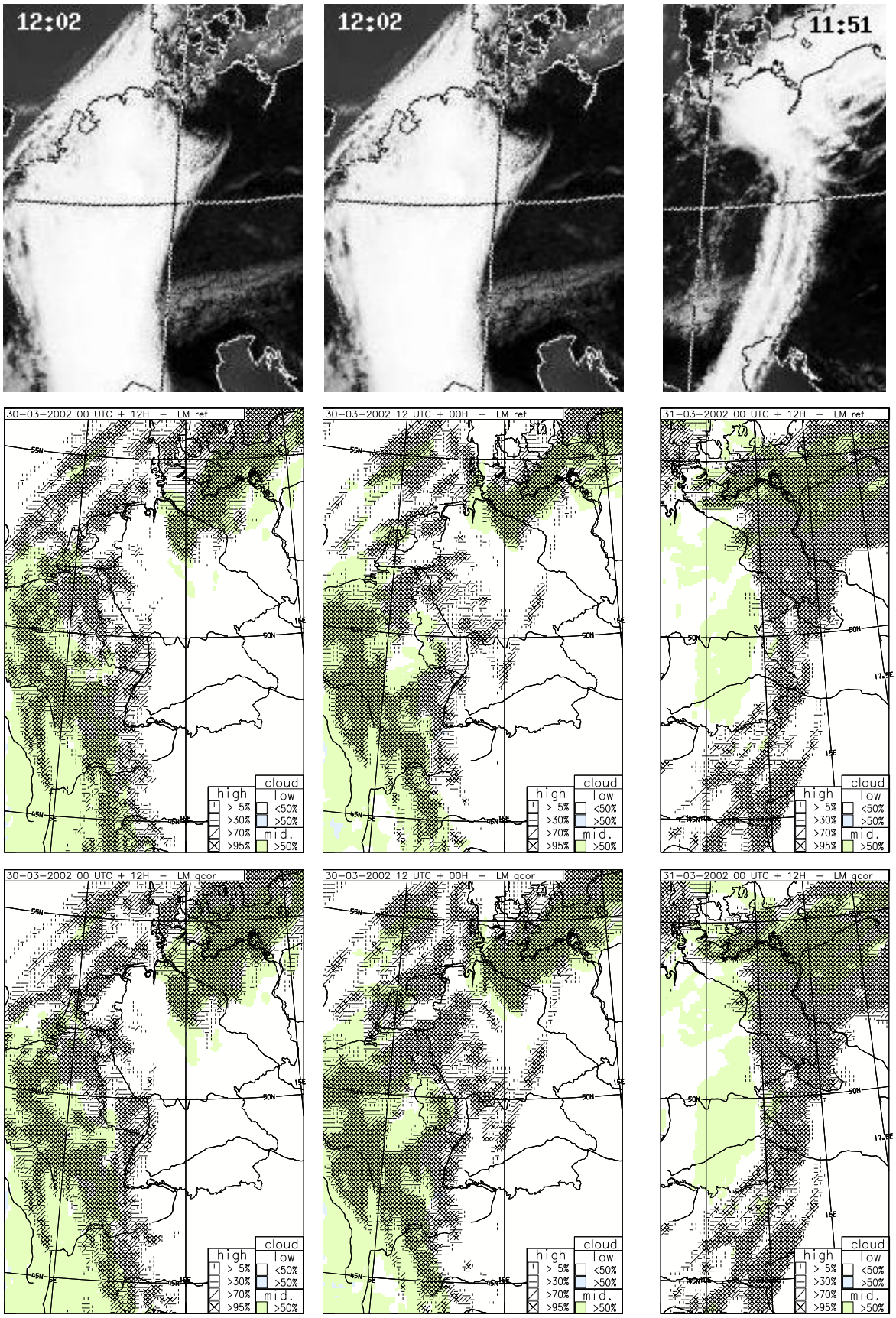

Figure 2: Set-up as in Figure 1. Left column (a): IR image and 12-hour LM forecasts valid for 12 UTC on 30 March 2002; middle column (b): IR image and LM analyses valid for the same time; right column (c): IR image and 12-hour LM forecasts valid for 12 UTC on 31 March.

In the forecasts starting at 29 March 12 UTC or before, the enhancement of the cloud band at 12 UTC on 30 March is very limited in the experiment. In the analysis of 30 March 00 UTC (Figure 1a), the cloud band is moderately enhanced e.g. over northeastern Italy and northern France. A more pronounced increase in high and partly even mid-level cloudiness, however, is found over Austria, the eastern half of Germany, and Poland, i.e. areas, where the 02 UTC (and subsequent) IR satellite images do not appear to indicate any cloudiness. (Thin cirrus extends from Czechia to Denmark on 29 March, 16 UTC.) In the subsequent 6-hour and 12-hour forecasts (Figures 1b, 2a), the differences decrease gradually, yet tend to remain to be largest in the cloud-free areas in northern Germany. In contrast, the enhancement in cloudiness in the 12-UTC analysis (Figure 2b) is largest in the area of the observed cloud band (i.e. between western Germany and the North Sea). The same is true in subsequent forecasts, but the enhancement is small. The 12-hour forecast for 31 March 12 UTC (Figure 2c) is another example for such a (limited) positive impact and also for the fact, that the bias correction does not decrease phase errors (the cloud band propagates eastward too slowly).

In the upper-air verification against radiosonde data for this period (Figure 3), the impact of the bias correction on humidity is moderately negative up to $+24\,\mathrm{h}$, if the model fields are verified against those observation values that have been used in the respective model versions. If, however, the new bias correction is assumed to correct for the true observation bias and hence the bias-corrected radiosonde data are taken as reference observations used to verify both model runs, then the impact is neutral. The relative humidity bias between the two model versions decreases from $2-3\,\%$ ($4-5\,\%$ above $400\,\mathrm{hPa}$) at the analyses to $1\,\%$ at the 24-hour forecasts. This decrease may be due to the lateral boundary conditions provided by GME to which the bias correction is never applied. The impact on temperature tends to be negative but is negligibly small.

Trial 2: A Low Stratus Period

In a second parallel assimilation and forecast experiment, the bias correction is tested for the period of 7 to 13 February 2003, which was characterized by the alternation of low stratus and clear sky over Germany and its environs. In such situations, the operational model forecasts typically underestimate the low cloudiness, and increasing the humidity due to the bias correction has a potential to improve these forecasts. This is shown in Figure 4a to apply to Bavaria and around Denmark in the 14-hour forecast for 11 February 02 UTC. However, erroneous cloudiness can also be enhanced, as is the case e.g. over northeastern France in the 10-hour forecast for 10 UTC on the same day (Figure 4b). Note also that the examples shown here belong to the cases with maximum impact, and the impact on most other cases is smaller. The results in the upper-air verification (not shown) are very similar to those of the first period.

Summary

A new bias correction for Vaisala RS80 humidity data has been tested on two periods with thick cirrus and low stratus respectively. It tends to generally increase the cloudiness very moderately, however it does so both when cloudiness is underestimated and when it is already overestimated. As the main problem in the cases examined is an underestimation rather than overestimation of cloudiness in the forecasts, the overall impact tends to be slightly positive. It is noted that the bias correction does not change the cloud patterns significantly or decrease phase errors. A negligible impact is found on upper-air wind, temperature, and also humidity provided that merely the bias-corrected radiosonde data are used for the verification. However, the errors of the operational reference humidity forecasts are slightly smaller if the latter are verified against the uncorrected radiosonde humidity data.

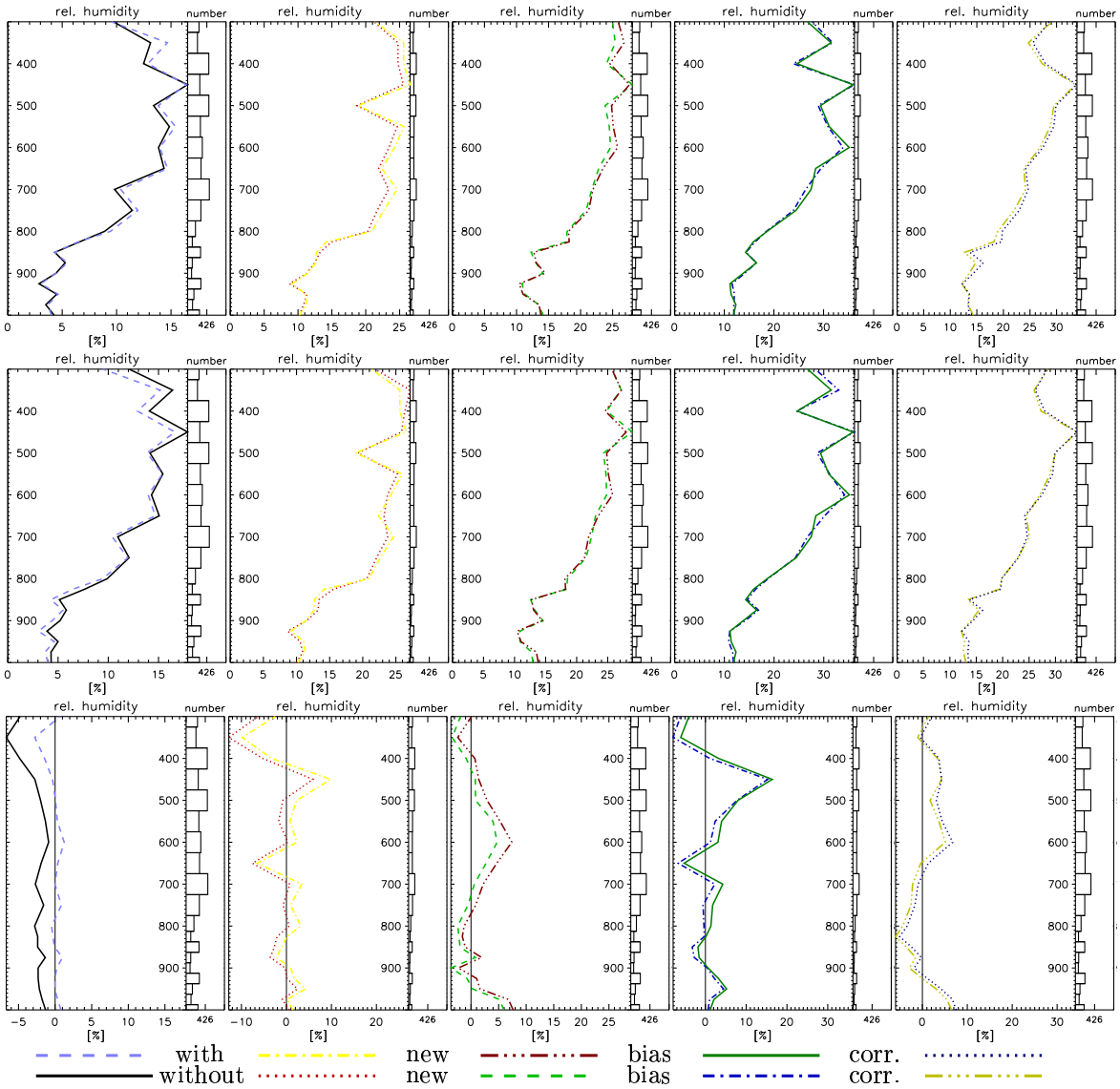

Figure 3: Upper-air verification of relative humidity against all radiosonde data (except those within 60 grid points from lateral boundaries of the LM domain) for the period of 30 March, 6 UTC, to 2 April 2002, 0 UTC. Top row: rms errors against the observation values that have been used in the respective assimilation cycles (i.e. uncorrected data for the operational forecasts, bias-corrected data for the experimental forecasts); middle row: rms errors against bias-corrected observation values; bottom row: bias against bias-corrected observation values. Columns from left to right: analyses, 6-h, 12-h, 18-h, resp. 24-h forecasts. Each panel consists of vertical profiles of errors between 1000 hPa and 300 hPa for the two model versions with line style and color as given below the bottom row, and a histogram for the numbers of observations entering the vertical bins.

With respect to forecast quality, there is no strong argument in favour or against introducing the bias correction operationally. Believing in the correction to reflect the true bias and to render the observation values more realistic would promote to introduce it. Note that the correction should become obsolete as soon as the A-Humicap sensors of the Vaisala RS80 sondes currently used operationally by about 90 % of the radiosonde stations within the LM domain are replaced by H-Humicap sensors of the Vaisala RS90 sondes.

References

Nagel, D., U. Leiterer, H. Dier, A. Kats, J. Reichardt, A. Behrendt, 2001: High accuracy humidity measurements using the standardized frequency method with a research upper-air sounding system. *Meteorol. Zeitschrift*, **10**, No. 5, 395–405 .

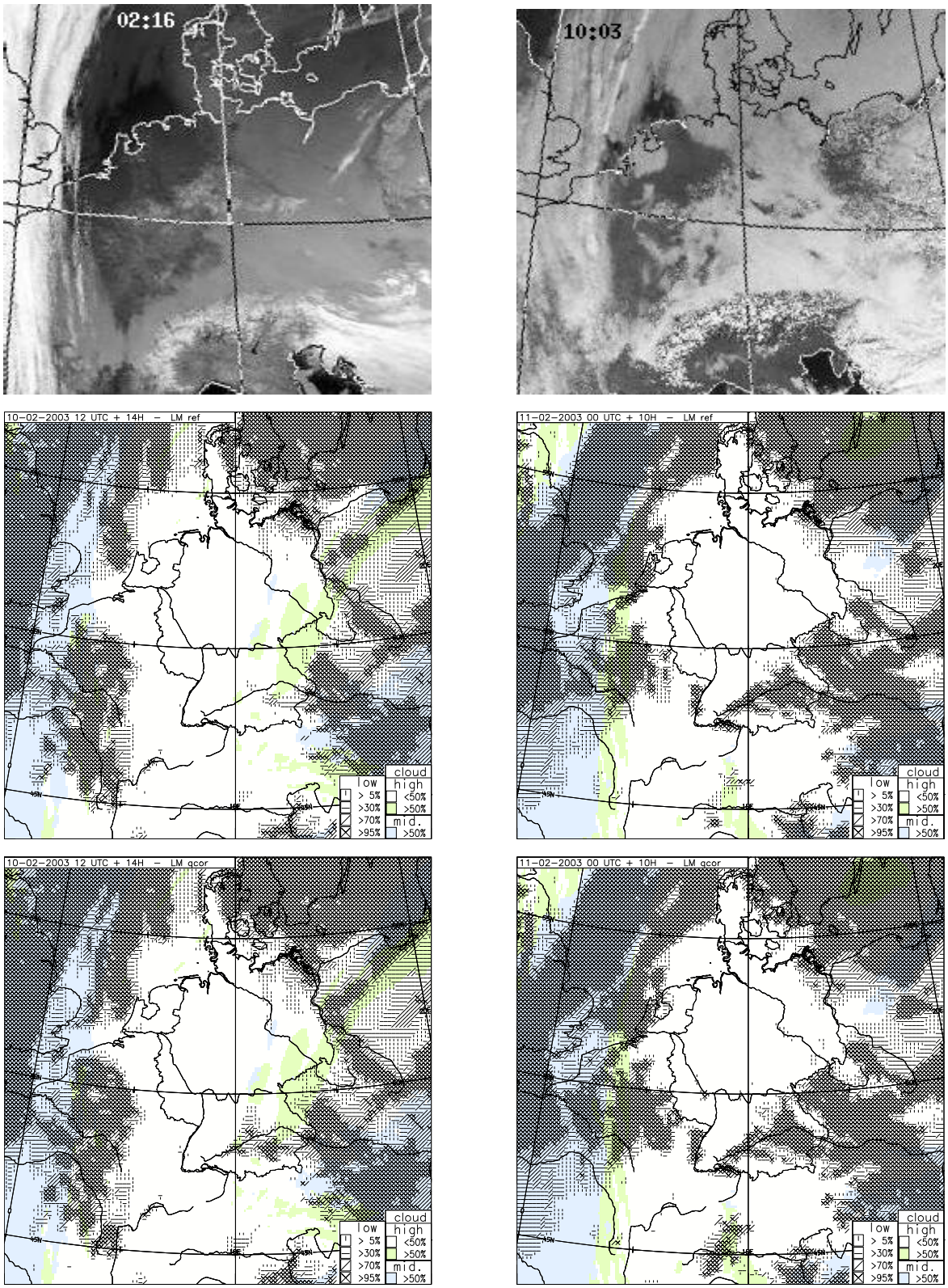

Figure 4: Top row: NOAA satellite images; middle row: *low* cloud cover (patterns), mid-level cloud cover (green shading), and high cloud cover (grey shading) of reference LM forecasts without new bias correction; bottom row: as middle row, but for LM forecasts with new bias correction. Left column (a): IR image and 14-hour LM forecasts valid for 02 UTC on 11 February 2003; right column (b): VIS image and 10-hour LM forecasts valid for 10 UTC on 11 February.

Sharpe, M., and B. Macpherson, 2003: Developments in the correction of radiosonde relative humidity biases. *Forecasting Research Technical Report No. 389, UK Met Office.*

Assimilation of Radar Data in the LM at DWD

Stefan Klink and Klaus Stephan

Deutscher Wetterdienst, P.O.Box 100465, 63004 Offenbach a.M., Germany

1 Introduction

In the matter of mesoscale modelling at DWD a very high resolution model for short term numerical weather prediction based on the existing non-hydrostatic limited area model Lokal-Modell (LM) is under development. It is intended to run this LMK (LM Kürzestfrist) every 3 hours with a forecasting range of 18 hours. One reason for this design of the NWP model cycle is to provide input data with a high update rate for the hydrological models of flood forecasting systems with . Especially to improve the quantitative precipitation forecasting (QPF) work has to be done in the area of data analysis. In addition to the assimilation of conventional data, like surface and radiosonde measurements, high-resolution observations derived from radar networks are introduced in the nudging-type analysis of the LM. Using the Latent Heat Nudging (LHN) technique (Leuenberger and Rossa, 2003a) the thermodynamic quantities of the atmospheric model are adjusted in that way, that the modeled precipitation rates resemble the observed precipitation rates.

In the framework of the project RADVOR-OP funded by a working group of the hydrological authorities of the German federal states the use of radar data in the assimilation scheme of the LM will be made operational. Some real case studies concerning flooding events in different river catchments have been carried out. The results from these experiments show the precipitation patterns introduced due to the analysis in good agreement with those observed by radar, both in position and amplitude. The influence of the assimilation of radar derived precipitation rates lasts for several hours.

Results of a real case study and sensitivity of model predictions to model setup and settings of the assimilation scheme will be shown.

2 Theory and Implementation

Contemplating an utilization of radar reflectivities in the LM, it has to be stated, that a direct assimilation of both radar reflectivities and precipitation rates is not possible, because both quantities are no prognostic variables of the LM. Even a future prognostic treatment of precipitation in the LM would not allow a reasonable direct assimilation of precipitation rates, because there is only a small feedback from the precipitation rate to model dynamics and physics. But these two components of the model are essential for the development of precipitation. Attempts have to be done in order to assimilate radar information into the model by the use of any other variables (e.g. temperature, specific humidity or components of the wind vector). Thus a relation between precipitation rate and prognostic model variables is wanted. Concepts basing on processes, normally present in the context of precipitation, are desired. One special process connected with the formation of precipitation is the condensation of water vapour. It is directly linked to the release of latent heat. Originally, most condensation processes must be considered as the formation of cloud droplets, but this is only a preliminary stage of the precipitation forming. Nevertheless it is possible to influence

the model dynamics and consequently the formation of precipitation by adjusting the model-generated latent heat release. The diabatic heating rates, which are related to phase changes of water, are tuned in that way, that the model simulates the observed precipitation rates. This is realized by adding LHN temperature increments to the 3D temperature field. This method is called "Latent Heat Nudging" (e.g. Wang and Warner, 1988). An introduction to LHN, further references to literature about this method and some aspects of the special implementation of the LHN algorithm in the LM source code can be found in Leuenberger and Rossa (2003a).

Besides the tuning of the temperature profile at a certain gridpoint, the vertical profile of specific humidity at this gridpoint can be adjusted during the LHN as well. Depending on the sign of the temperature increment, specific humidity q is increased in order to reach a value of 100% of relative humidity (positive temperature increment) or specific humidity is decreased in order to retain relative humidity (negative temperature increment).

3 Preparation of Radar Data

Input data for the assimilation is the 2D-field of the observed precipitation rate RRobs. Starting point for the provision of the LHN scheme with radar derived precipitation rates is the international composite (PI), available at DWD. The measurements of radar reflectivities gained at each individual radar site of the German radar network and at several locations in the neighbouring countries are incorporated in this product. The local reflectivity product PL of the German radar network is derived from the volume scan. The data actually used are the echos next to the ground, coded in 7 reflectivity classes. The spatial resolution of the PI, which is originally delivered in polar-stereographic projection, is $4\,km$ x $4\,km$. The product is available every 15 minutes. After a conversion of the reflectivity data into a precipitation rate by a simple Z-R-relation, an interpolation of the pixel values to the desired LM grid is performed.

Investigations of the LHN-algorithm by means of idealized experiments have shown, that a high update rate of radar data would lead to more realistic nudging-analyses and subsequent forecasts (Leuenberger and Rossa, 2003b). Thus and because of some other reasons, which will be mentioned below, a new radar composite basing on the DX product of DWD (spatial mesh: $1\,km$ x 1°, time resolution 5 min) will be used as proxy data for the LHN scheme. This product will be provided by the project RADOLAN as a preliminary product of the gauge adjustment procedure, the project is dedicated to. An advantage of this product, which is derived from the precipitation scan, is the additional correction of orographic attenuation and the use of a variable Z-R-relation for the calculation of precipitation rates from echo intensities.

4 Case Study

For a selected event LM-runs on the operational domain (mesh size $7\,km$, 325 x 325 gridpoints, 35 vertical levels) and runs on an experimental domain (mesh size $2.8\,km$, 361 x 441 gridpoints, 40 vertical levels) have been carried out. Results of horizontal fields are presented on a limited evaluation domain (see fig. 1). In general the convective parameterization scheme has been switched off, in order to give the model the chance to directly simulate convection. The provisioning of the LM with boundary data is done by the GME. After 6 hours of data assimilation (nudging and latent heat nudging, including humidity adjustment during the LHN) from 6-12 UTC a free forecast lasting from 12-18 UTC has been carried out.

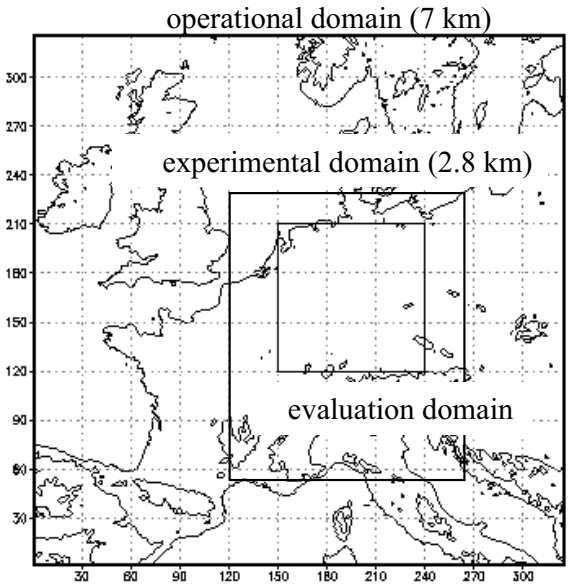

Figure 1: Domains of interest

4.1 Overview of the Meteorological Situation

At the 28th of August 2002 Germany was influenced by only small synoptic-scale pressure gradients. In the warm, moist and unstable air mass a development of showers and thunderstorms took place in the afternoon in the area of a quasi-stationary front, which lay over Germany (see fig. 2). It was reported that heavy precipitation occured locally (e.g. 70 mm between 15.15 and 16.30 UTC in Herborn, Hesse and 85.5 mm within 4 hours in Wissen, NRW).

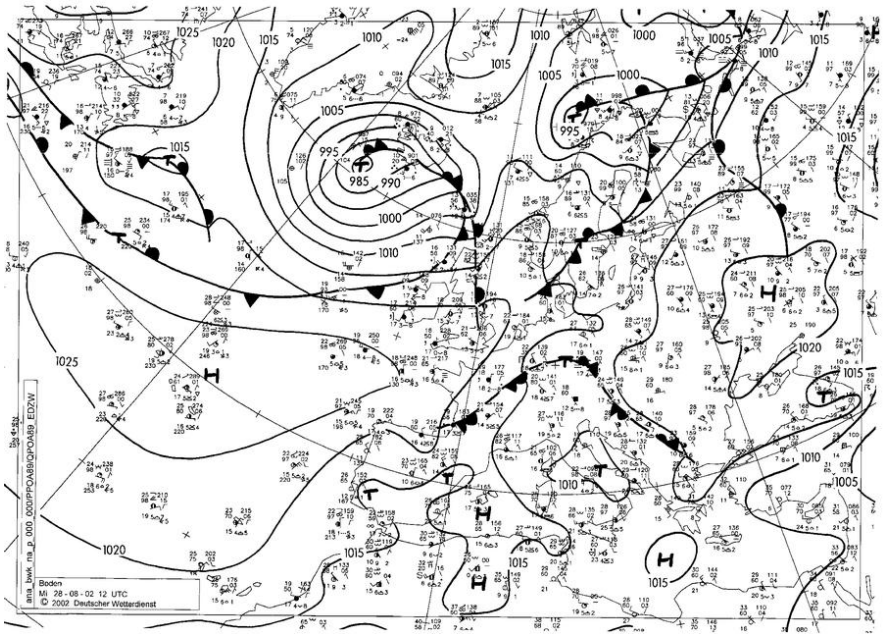

Figure 2: Meteorological situation at the 28th of August 2002

4.2 Influence of the LHN on the nudging-analysis depending on the mesh size of the LM

In this paragraph three nudging-analyses, one without LHN and two with different mesh sizes (7 km, 35 vertical levels and 2.8 km, 40 vertical levels respectively) are compared with radar derived precipitation rates. The 2.8 km run was started at 21 UTC one day before by interpolating the analysis of the 7 km run to the finer mesh. Afterwards 9 hours of conventional nudging were carried out in both suites independently. This is the reason for the distinct differences between the 7 km and 2.8 km run in the first hour (6-7 UTC) of nudging and LHN (see fig. 4a). The simulation on the finer grid contains in this case not so much erroneous precipitation as the corresponding run on the 7 km grid. Thus the LHN algorithm has not to remove much misplaced precipitation from the run but mainly has to insert observed precipitation at points where the model does not simulate precipitation so far. In the first hour of LHN this works much better on the finer grid than on the operational one. Throughout the next two hours the assimilation of observed precipitation rates turns out well in both LHN runs. In contrast with these LHN suites the control run shows a more extended area of precipitation, which is shifted moreover to the southeast. After that the convection weakens over a wide range (except Bavarian forest, compare with Radar 10-11 UTC). But the convergence line remains in the Radar as well as in the LHN assimilation runs. During the last hour of assimilation from 11 to 12 UTC a revival of the convection can be observed in the Radar and in the LHN runs respectively but not in the control run. The assimilation of small convection cells e.g. in the Thuringian forest naturally works better in the 2.8 km run than in the 7 km run. All in all, the LHN experiments show precipitation patterns which fit much better to the corresponding radar derived observations than the control experiments without LHN (see fig. 4e). The hit rate for hourly precipitation sums (threshold 0.1 mm) reaches at the end of the assimilation period values, which are on an average 30 % higher than those of the control experiments (see fig. 3).

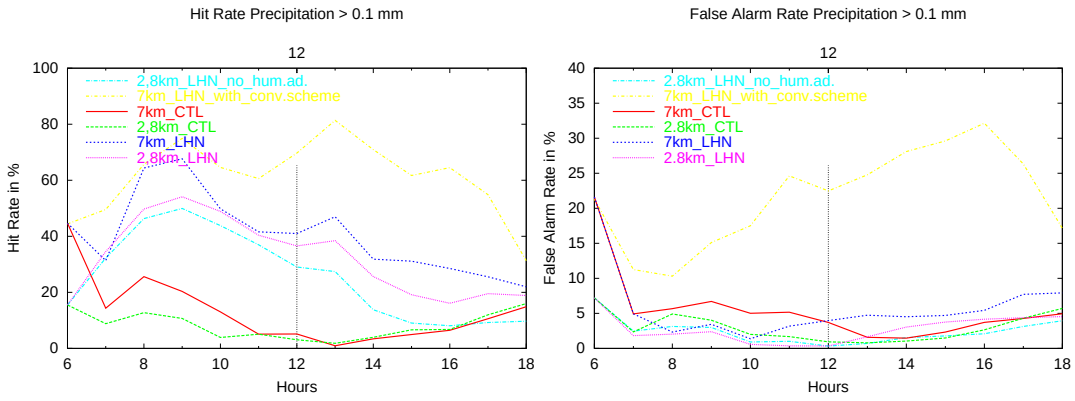

Figure 3: Hit rate (left) and false alarm rate (right) in hourly precipitation sums for different runs

At the beginning of the free forecast the convective cells are strongly intensifying in both LHN runs. The simulated intensities of precipitation reach maxima, which are clearly above the corresponding observations (see fig. 5a, 12-13 UTC). At the same time the convective cells remain strongly limited in their horizontal extension. The control run shows at this stage a further weakening of precipitaton in contrast with the radar measurements. Throughout the third hour of free forecast the LM runs basing on LHN-assimilations still have more forecast skill than the control run. This is especially true for the total amount of precipitation in the evaluation domain. But inaccuracies already occur in the correct position and intensity of single convection cells. An interesting aspect is the occurence of small convective cells over the mountain ranges of Swabian and Franconian Alb between 16 and 18 UTC. Besides

the radar only the 2.8 km run shows these structures. Altogether the precipitation patterns of all three LM simulations resemble to each other more than to the radar observation in the sixth hour (17-18 UTC) of free forecast (see fig. 5e). This is also caused by the fact, that within this hour the convergence line, which has been introduced in the LHN-runs some hours earlier, is been developed even in the control experiment.

4.3 Sensitivity of LHN concerning humidity adjustment

Two LM runs have been carried out on the experimental domain (mesh size 2.8 km), one run with humidity adjustment during the LHN, the other one without. After three hours of nudging and simultaneous LHN both runs already show a good correspondence between their precipitation patterns and the distribution given by the radar observations (see fig. 6a). While the position of the precipitation maxima is assimilated quite well, there are problems in areas with low precipitation rates. Especially the assimilation run without humidity adjustment still depicts wide areas with weak precipitation between 8 and 9 UTC, which already have been misplaced in the analysis at 6 UTC (compare to fig. 4a) and could not be dried up completely throughout the following three hours. After another three hours of assimilation, i.e. within the last hour of nudging and LHN, the position of the convergence line over western Germany is reproduced well by both assimilation runs (see fig. 6b). At a first glance the two assimilation runs do not seem to differ much. But when zooming in the area of Thuringian forest and in the mountains of "Erz- and Fichtelgebirge" (see fig. 6c), it can be seen, that the assimilation of the newly developing thunderstorms works better in the case of additional humidity adjustment. After three hours of free forecast, again the run with humidity adjustment during the LHN shows more realistic precipitation patterns than the corresponding run without humidity adjustment (see fig. 6d). This is especially true when concerning the intensity but lesser in case of the position of the maxima of the predicted precipitation fields. Both simulations have in common, that the horizontal extension of precipitation patterns is much smaller than in the corresponding radar observations. The total amount of precipitation (integrated over the evaluation domain) is too small in the forecasts compared to the radar observation.

5 Summary and Outlook

Incorporating the LHN-algorithm in the nudging-type analysis scheme of the LM makes it possible to assimilate the radar-derived precipitation rates during the assimilation runs very well. Experiments have shown that the explicit simulation of convection leads to more realistic results than model runs with parameterized convection. Using a finer grid within the simulation shows a potential for further improvements of the quantitativ precipitation forecast. An additional humidity adjustment during the LHN results in a more exact analysis of the atmospheric state and in more realistic free forecasts.

References

Leuenberger, D. and A.M. Rossa, 2003a: Assimilation of Radar Information in aLMo. COSMO Newsletter, No. 3, 164-172 (available at www.cosmo-model.org).

Leuenberger, D. and A.M. Rossa, 2003b: Assimilation of Radar Information in aLMo. Oral presentation, 5th General COSMO-Meeting, Sep. 2003, Langen (Germany)

Wang W. and T.T. Warner, 1988: Use of Four-Dimensional Data Assimilation by Newtonian Relaxation and Latent-Heat Forcing to Improve a Mesoscale-Model Pricipitation Forecast: A Case Study. *Monthly Weather Review*, **116**, 2593-2613.

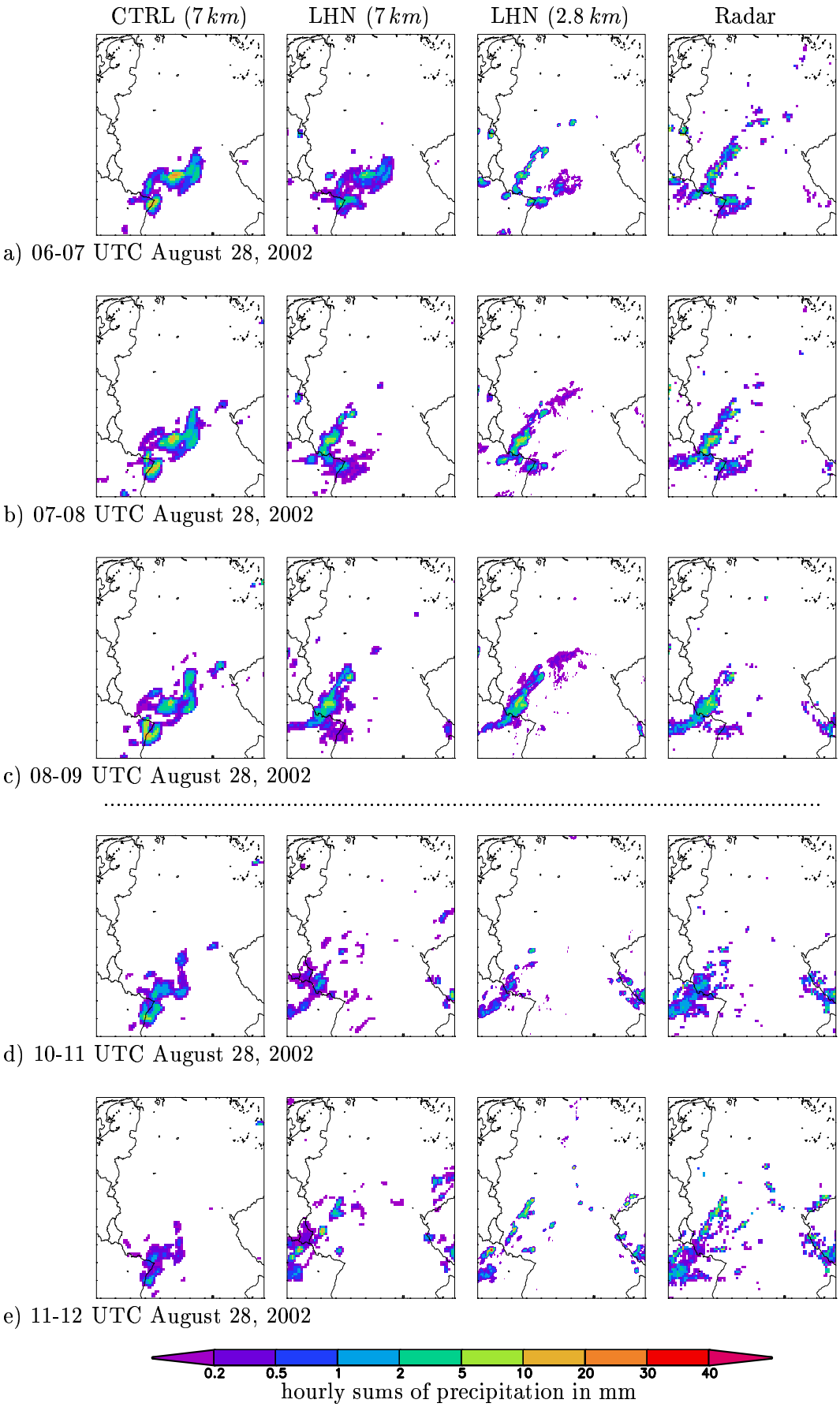

Figure 4: Influence of the LHN on the nudging-analysis depending on the mesh size of the LM, assimilation (1st column: CTRL (7 km), 2nd column: LHN (7 km), 3rd column: LHN (2.8 km), 4th column: Radar)

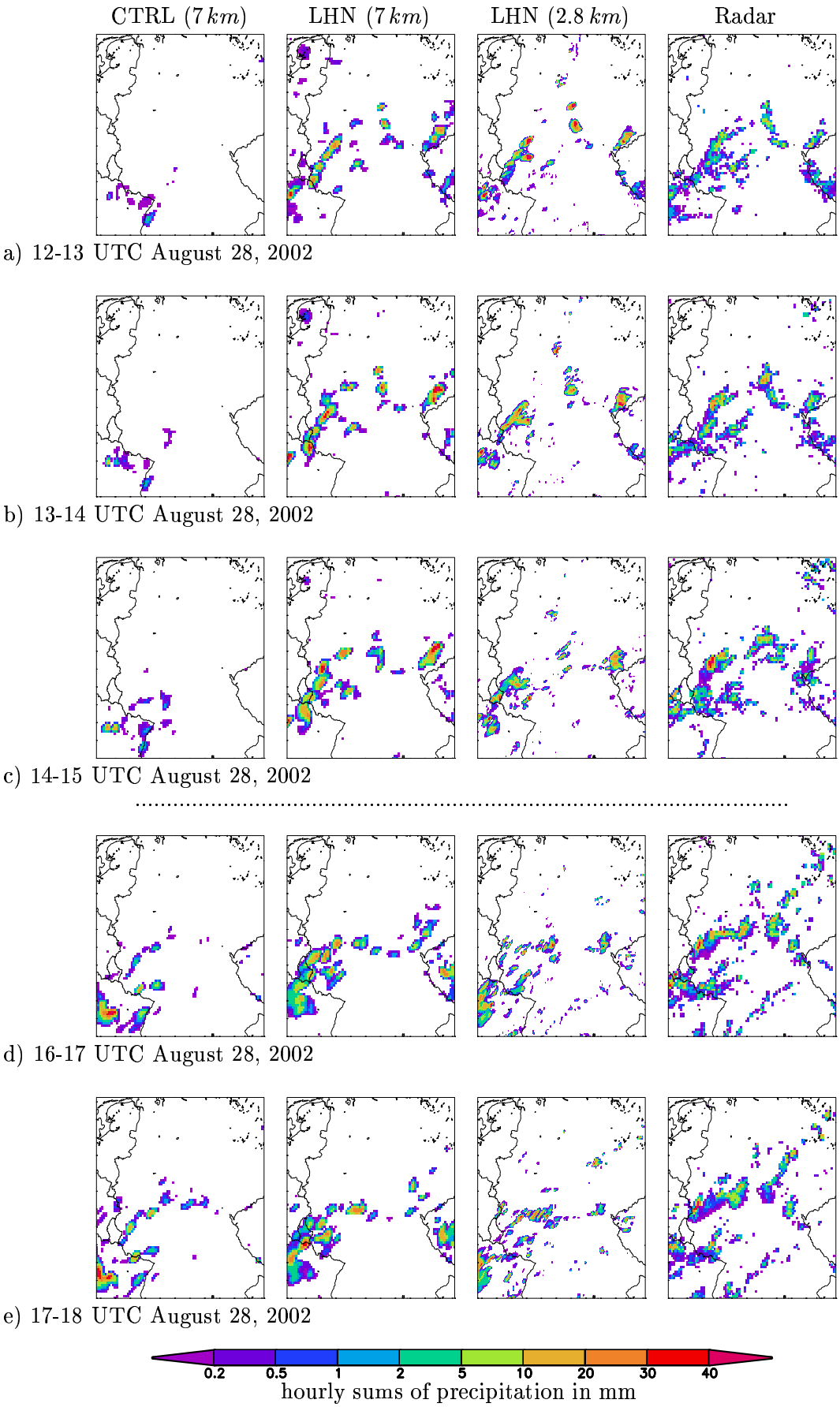

Figure 5: Influence of the LHN on the nudging-analysis depending on the mesh size of the LM, free forecast (1st column: CTRL (7 km), 2nd column: LHN (7 km), 3rd column: LHN (2.8 km), 4th column: Radar)

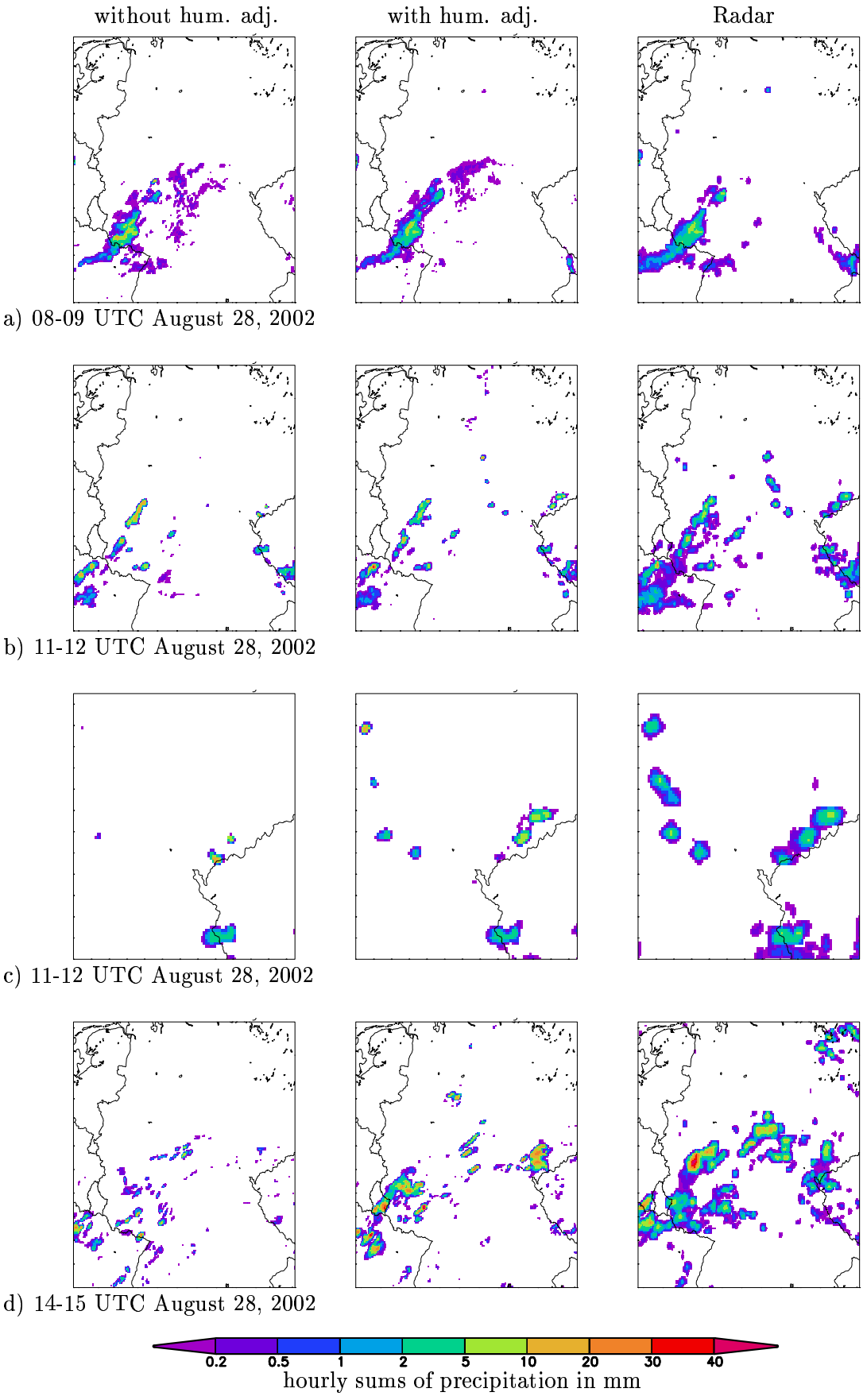

Figure 6: Sensitivity of LHN concerning humidity adjustment, (1st column: without humidity adjustment, 2nd column: with humidity adjustment, 3rd column: Radar)

The Z-coordinate LM

J. Steppeler, S. Janjic[1)], H.-W. Bitzer[2)], P. Prohl and U. Schättler

Deutscher Wetterdienst, Offenbach am Main, Germany
[1)] NCEP, Washington, USA; [2)] AWGeophys, Traben-Trarbach, Germany

The Z-coordinate LM is available in two versions, the Eulerian and semi Lagrangian approach. The current presentation concentrates on the Eulerian approach. For the state of the semi Lagrangian version it is referred to the COSMO meeting in Offenbach 2003 and the COSMO work plan.

Z-Coordinate numerical models of the atmosphere have the advantage of representing the atmosphere at rest properly and therefore justify the expectation of improved forecasts of orographically induced winds. An example for such a Z-coordinate model is the eta-model, which is based on the step orography. The step approach does not allow for a proper representation of the meso-scale flow over smooth and well resolved mountains. This problem was pointed out by Gallus and Klemp (2000). Steppeler et al. (2003) showed that the problem can be solved by formulating lower boundaries using a representation of the mountains by linear splines rather than the step approach. On this basis a Z-coordiante version of the model LM (see Steppeler et al. (2002)) was developed and tested extensively in idealised situations using bell shaped mountains and the orography of Scandinavia.

A physical parameterisation package was created by using the parameterization package for the terrain following model LM and developing an interface between the z-levels and the terrain following levels. The tendencies of the physics routine in the terrain following grid are interpolated by cubic splines to the z-representation.

A number of idealised tests were done. A bell shaped mountain of height 2000 m was used with an atmosphere being initially at rest. Different circulations developed at night and day, corresponding to mountain and valley winds. In comparison, the model version using terrain following coordinates produced a mountain wind even without radiation being switched on. When a homogeneous velocity field of 10 m/sec is used with the same mountain, a warming or cooling is produced in the wake of the mountain, leading to a rotational motion perpendicular to the axis of the main motion. With radiation switched off the temperature in the wake of the mountain is unchanged.

Fig. 1 shows a test where the step type z-coordinates had a disadvantage as compared to terrain coordinate models. A shallow mountain of 400 m height is used with a homogeneous velocity field of 10 m/sec. The cloud water field in a vertical cross section through the centre of the mountain and the precipitation field is shown. Due to the proper treatment of the gravitational wave, these results come out in the expected way.

In Fig. 2 a run with the orography of Scandinavia and realistic initial and boundary values is shown. The combination of realistic initial values and realistic orography revealed a number of errors in the formulation of the lower boundary conditions at the orography, which had not been apparent in the test made before. The result shown was obtained after these errors had been corrected. The corresponding run including physics is shown in Fig. 3. Fig. 4 shows the precipitation field. The precipitation field of the control run has a very similar structure, but considerable stronger amplitude for the precipitation in the upwind area of south Norway. Fig. 5 gives a cross section of the water vapour field.

References

Gallus, W. and J. Klemp, 2000: Behaviour of flow over steep orography. *Mon. Wea. Rev.*, 128, 1153-1164.

Steppeler, J., G. Doms, U. Schättler, H.-W. Bitzer, A. Gassmann, U. Damrath and G. Gregoric, 2003: Meso-gamma scale forecasts using the non-hydrostatic model LM. *Meteorol. Atmos. Phys.*, 82, 75-96.

Steppeler, J., H.-W. Bitzer, M. Minotte and L. Bonaventura, 2002: Nonhydrostatic atmospheric modelling using a z-coordinate representation, *Mon. Wea.Rev. 130*, 2143-2149.

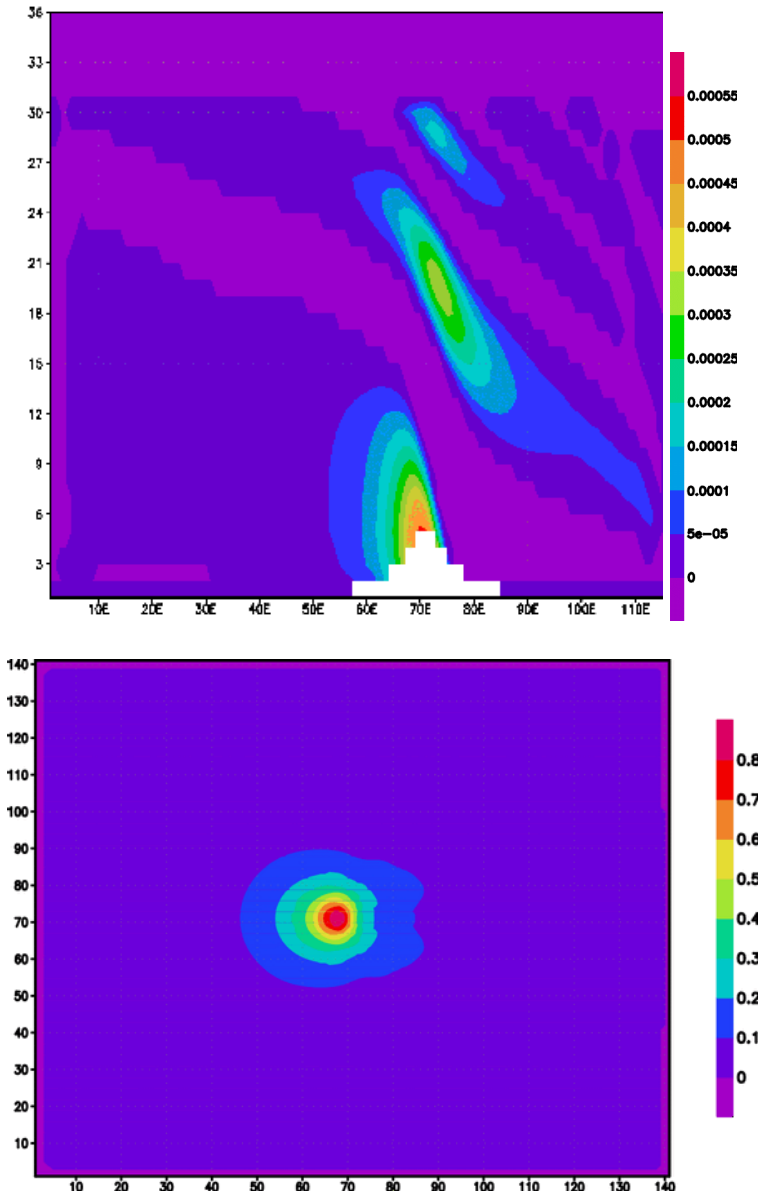

Figure 1: Top: Cloud water (kg/kg) on a cross section through the centre of the mountain. Bottom: Precipitation (mm) for the bell shaped mountain of height 400 m in a homogeneous velocity field.

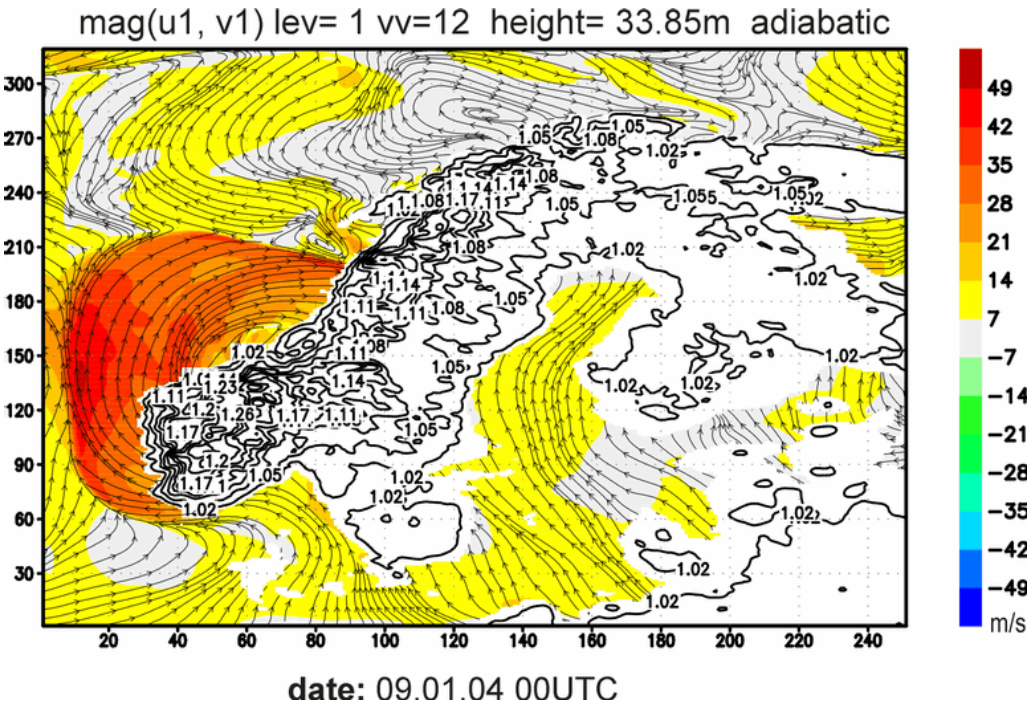

Figure 2: A Z-coordinate run of LM using the orography of Scandinavia and no physics.

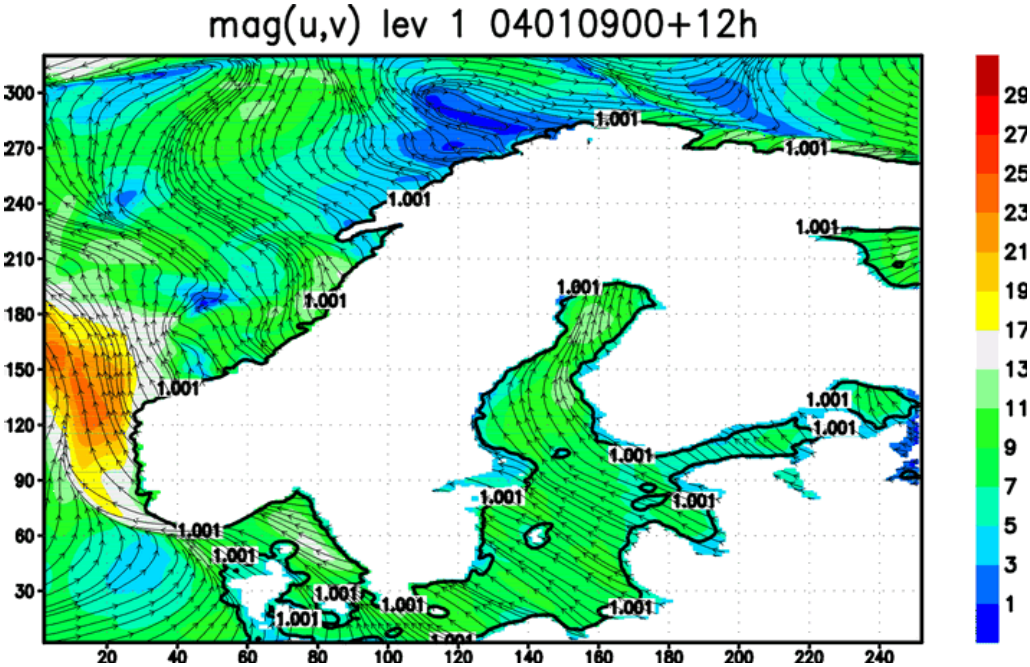

Figure 3: As Fig. 2, for the run including physical parameterisation. Please note the different color coding.

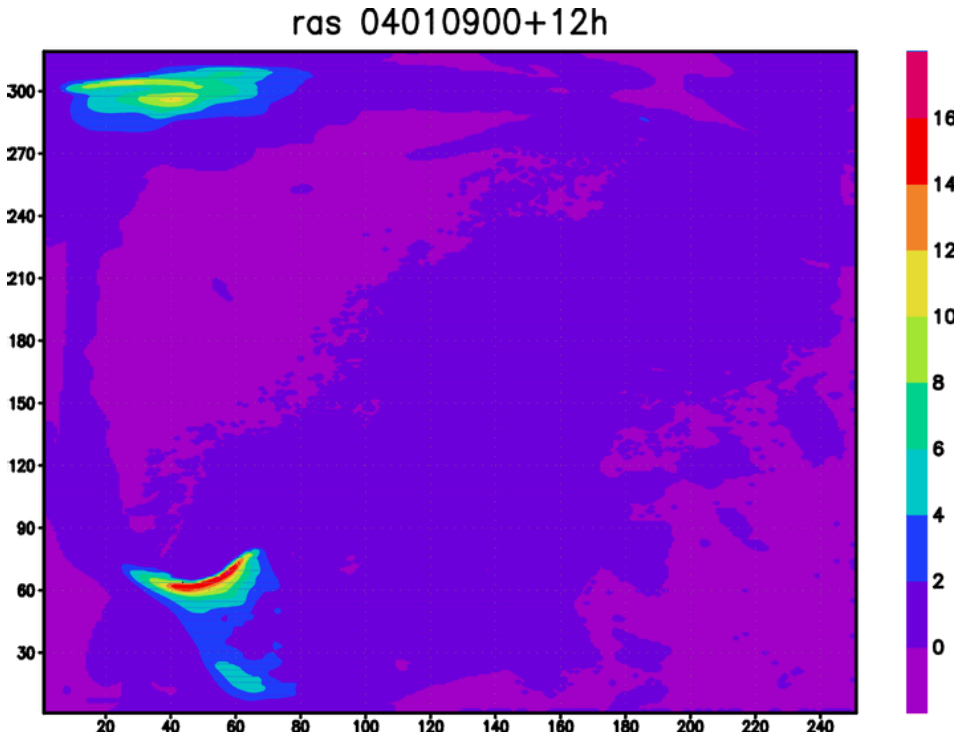

Figure 4: The precipitation field corresponding to the run shown in Fig. 3.

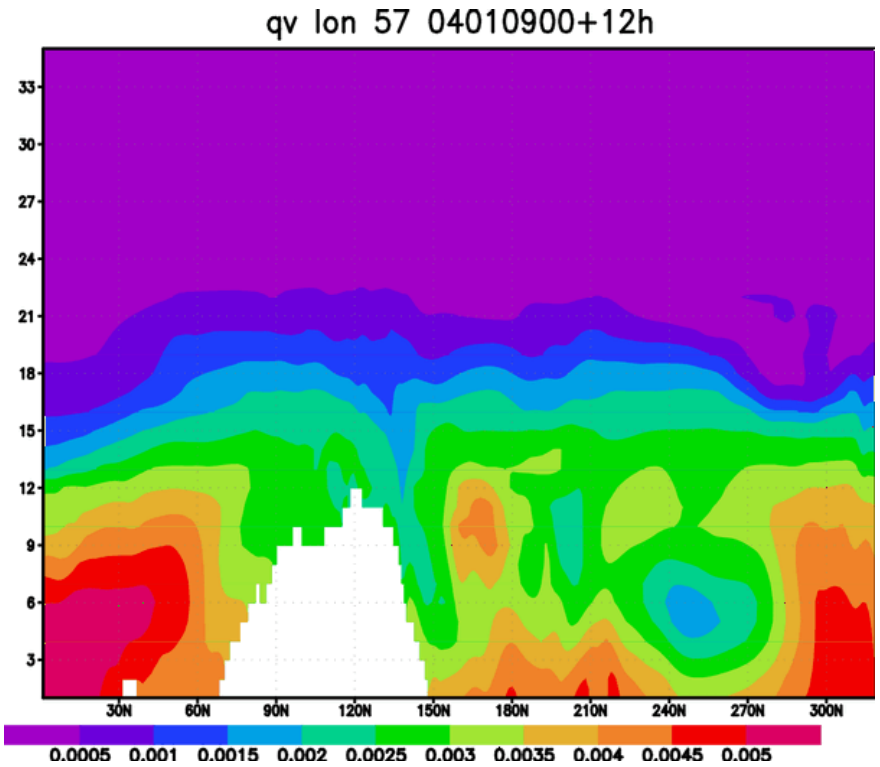

Figure 5: Cross section of the water vapour field in north south direction for grid point 57 on the x-axis.

Formulation of the LM's Dynamical Lower Boundary Condition

Almut Gassmann

Meteorologisches Institut der Universität Bonn, Auf dem Hügel 20, 53121 Bonn, Germany

1 Motivation

What do you expect, if you perform idealized 2D LM-experiments with the following parameters and initial conditions?

- No physics parameterization (pure dynamic core)
- High gaussian mountain (1500m)
- Resting atmosphere (no winds, no horizontal gradients)
- Stable stratification (constant N)
- No Coriolis force
- $\Delta x = 7km, \Delta t = 40s$, 40 predefined unequally spaced vertical levels
- Standard horizontal diffusion

Physically, no change should happen in any of your prognostic variables !
But actually, you will find disastrous errors, $2\Delta z$-structures and large absolute values of the vertical wind (cf. Figure 2). In this study, the reason for that behaviour is investigated and a way to cure the problem is outlined.

2 First small time step error

The LM employs a Klemp-Wilhelmson time splitting method. While stepping through the small time steps and computing the fast-waves contributions large time step advective tendencies are kept constant. In the presented experiment, the first small time step yields only contributions from the fast-waves for advection tendencies vanish. The following equation is integrated for the horizontal wind component

$$\frac{\partial u}{\partial t} = -\frac{1}{\rho a \cos\varphi}\left(\frac{\partial p'}{\partial \lambda} - \frac{1}{\sqrt{\gamma}}\frac{\partial p_0}{\partial \lambda}\frac{\partial p'}{\partial \zeta}\right). \tag{1}$$

The metrical terms (second term in parantheses) become important near steep slopes. Prognostic variables are staggered on a C-grid. Generally, all differentials are approximated by centered finite differences. Vertical differences are one-sided at the lower boundary and no free slip boundary condition is considered at this stage explicitely.

Using the discontinous level distribution indicated by the blue dots in in Figure 1(a), the horizontal wind at the left slope of the mountain is obtained as shown in Figure 1(b) (light blue line) for the first small time step. Expected to be exactly zero, the deviations of u from zero signify the numerical error.

(a) (b)

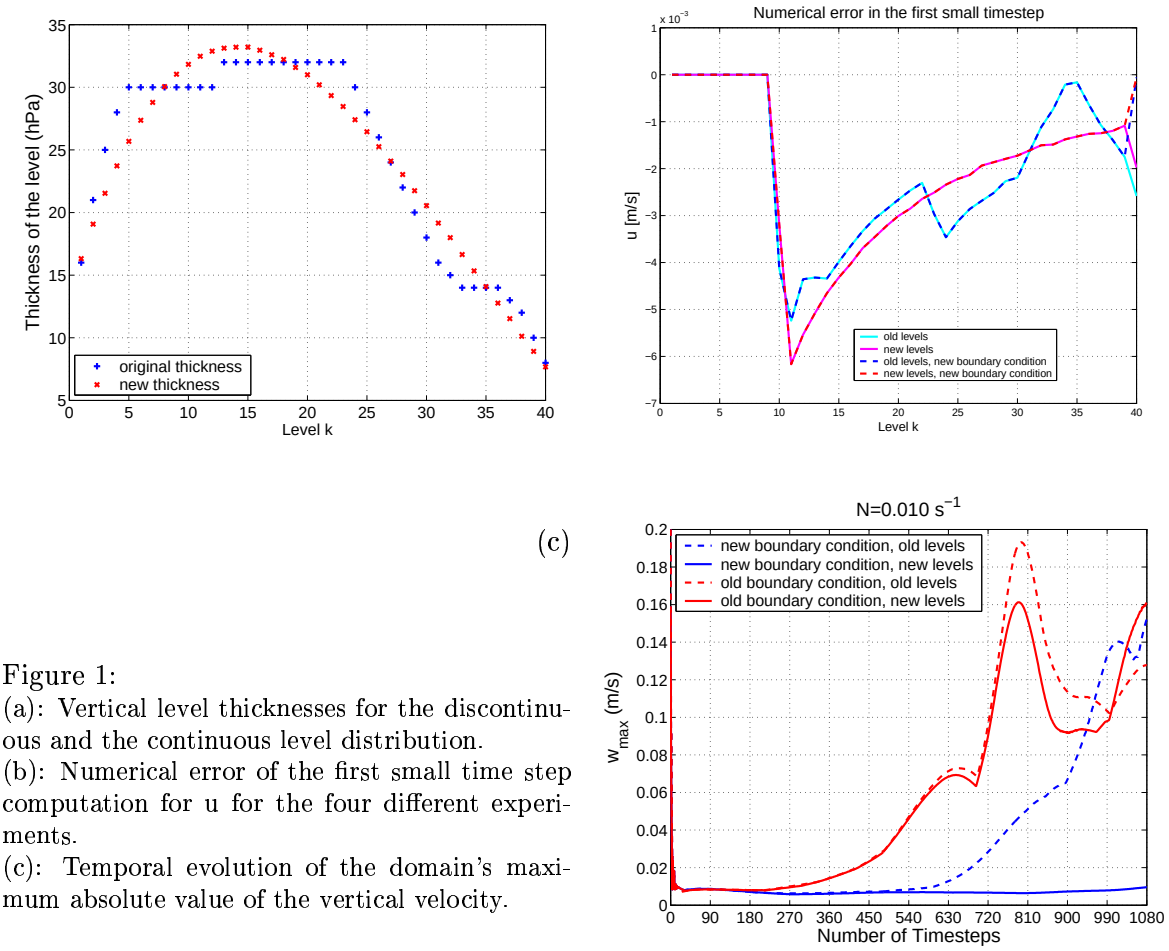

Figure 1:
(a): Vertical level thicknesses for the discontinuous and the continuous level distribution.
(b): Numerical error of the first small time step computation for u for the four different experiments.
(c): Temporal evolution of the domain's maximum absolute value of the vertical velocity.

The numerical error turns out to be quite large at the lowest model level (k=40). But also the numerical error in other levels is very erratic. The upper flat levels are free of errors per definition. In further time steps, $2\Delta z$ noise is induced by the erratic vertical gradients. These occur not only at the lower boundary, but also at higher levels. A deeper inspection reveals that the discontinuous distribution of the level thickness is responsible for a large part of the error-growing.

Using a continuous level distribution, indicated by the red dots in Figure 1(a), reduces the first-step numerical error discontinuities significantly (pink line in Figure 1(b)).

3 Lower boundary condition

The physical definition of the lower boundary is the free slip condition. In the LM, this condition is given by the satisfaction of the requirement

$$\dot{\zeta} = -\frac{1}{\sqrt{\gamma}} \left(\frac{u}{a \cos\varphi} \frac{\partial p_0}{\partial \lambda} + \frac{v}{a} \frac{\partial p_0}{\partial \varphi} + g \rho_0 w \right) = 0.$$

But as already mentioned, this condition is not considered when computing the vertical gradient of p' in equation (1), in fact, one-sided finite differences are used. Accordingly, we deal with an overspecified boundary condition. Omitting this overspecification is expected

to improve the lower boundary problem and to prevent growing $2\Delta z$ noise. Thus, use the prognostic equation for the vertical velocity

$$\frac{\partial w}{\partial t} = \frac{g}{\sqrt{\gamma}} \frac{\rho_0}{\rho} \frac{\partial p'}{\partial \zeta} + g \frac{\rho_0}{\rho} \left(\frac{T - T_0}{T} - \frac{T_0 p'}{T p_0} \right)$$

together with $\partial \dot{\zeta} / \partial t = 0$ to obtain the requested $\partial p' / \partial \zeta$ at the lower boundary and determine the horizontal wind. The first step error shrinks with this new condition, as indicated by the dashed lines in Figure 1(b).

The temporal evolution of the maximum absolute value of the vertical velocity in the domain over 12 hours is shown in Figure 1(c) for the four investigated cases that are different combinations of the lower boundary condition type and level distribution type.

Using the continuous level distribution and the new lower boundary implementation prevents the development of noise effectively. If the old boundary condition is applied, level distribution is of minor importance. But the new lower boundary conditioon should be used only together with the continous distribution.

Further experiments suggest that the error growth is the smaller the stronger the stability (Brunt-Vaisala-frequency N) is. The error growth is more or less independent of the ratio of grid spacing to time step and errors grow certainly at some time to a significant value. Thus, error growing might be suppressed but not circumvented by this method.

The vertical wind fields at different times are compared in Figures 2. Here, the continuous level distribution is used to compare the influence of the lower boundary condition alone. The errors with the new condition stay propotionally small, at least for the forecast time investigated. Very erroneous results with strong $2\Delta z$ structures occur for the old boundary formulation. An interesting feature is the negative vertical velocity that occurs exactly over the top of the mountain. It is assumed that it is caused by the divergence introduced by different algebraic signs of the numerical error for u at the two slopes.

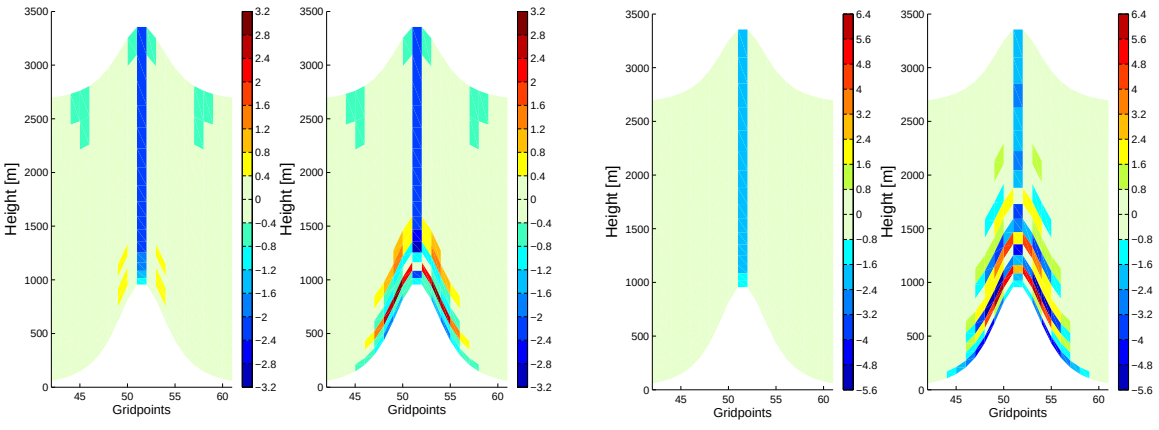

Figure 2: Vertical wind field at 6 hours forecast (left two panels) and 12 hours forecast (right two panels). Results with the new condition are given at the left hand side and the reference result is shown at the right hand side, color scales are chosen to be comparable.

4 Relevance

A realistic experiment reveals no or very little influence of the lower boundary formulation. Physical processes and a non-vanishing wind field help to dissolve the gradients responsible for the error growth in the idealized experiments.

Nevertheless, a physically consistent boundary condition is numerically tidier. The same is true for the choice of the vertical levels, whose vertical distribution should be a continuous function. The experiments elucidate the importance of a consistent formulation of the model dynamics. In this connection it is worth to pursue these investigations as well as enforce the development of the z-coordinate (Steppeler) and inspect the question of grid-staggering (Herzog).

Development of a Kilometer-Scale NWP-System: LMK

Günther Doms and Jochen Förstner

Deutscher Wetterdienst, P.O.Box 100465, 63004 Offenbach a.M., Germany

1 Overview

For very detailed short range forecasts, the Deutscher Wetterdienst (DWD) has started the development of a meso-γ version of the operational nonhydrostatic regional model LM. This new version, called LMK, will utilize a grid-spacing of 2-3 km with about 50 vertical layers and an integration domain of about 1300 x 1300 km^2 (see Fig. 1). LMK is aiming at the explicit prediction of deep convection and will provide 18-h forecasts for Germany eight times per day based on all observations available, including satellite and radar data. The development work is organized by an internal 3-years project from end 2003 to end 2006, with the operational implementation of the LMK system scheduled for late 2006. This project is embedded in a DWD programme (Aktionsprogramm 2003) aiming at an improvement of global and regional forecast systems and products.

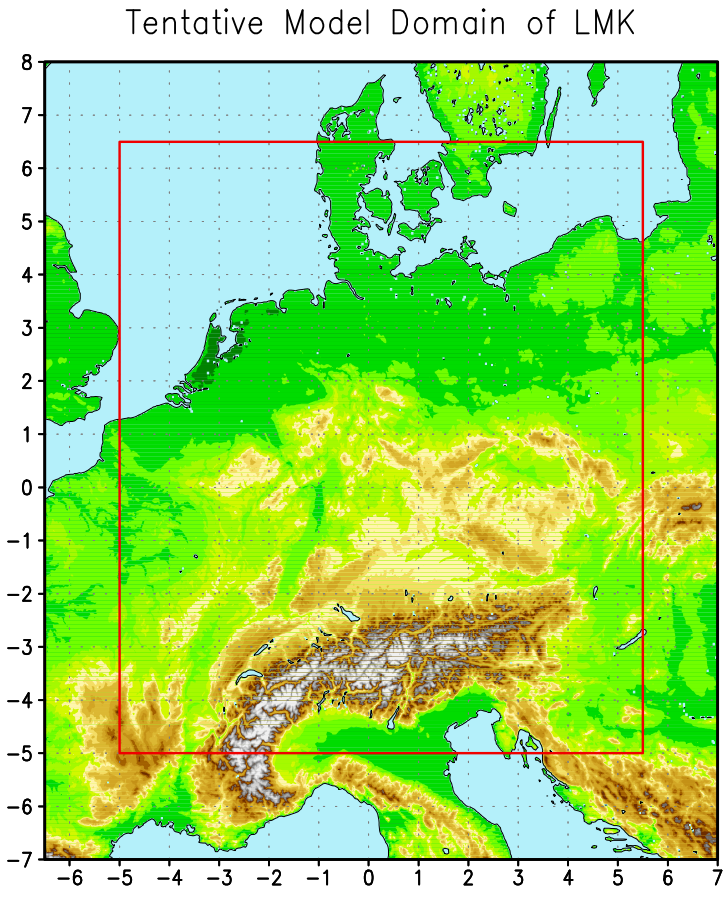

Figure 1: Tentative integration domain for LMK (red frame) with respect to a rotated lat-lon coordinate system (North pole at 40° N and 170° W). Using a grid-spacing of 2.8 km results in 421×461 grid points.

2 Background

With the new system, it is intended to fill the gap between traditional nowcasting methods for severe weather events (up to 3-6 hrs) and current short-range NWP with grid spacings of about 10 km and forecast ranges up to 48-72 hrs. In the time range of 18 hrs severe weather often forms in context with deep moist convection (such as super- and multi-cell thunderstorms, squall-lines, mesoscale convective complexes and mesocyclones) or due to interactions with fine-scale topography (such as fog, severe downslope winds, Föhn-storms, flash-floodings, etc.). As these events cannot be resolved with the resolution of present models, their prediction is in general very poor. However, there is a strong public demand for improved weather forecasts at finer scales and shorter ranges. An accurate prediction of extreme rainfall events or severe wind gusts in both time and space is especially required for hydrological, civil protection and environmental agencies to issue adequate warnings.

We expect a number of potential benefits of running a forecasts model routinely with a grid spacing better than 3 km on a quite large domain (to keep some internal predictability), since many more mesoscale weather systems and their scale interactions including local topographical effects can be properly resolved. Such a resolution will allow to simulate deep convective clouds directly and many deficiencies introduced by parameterized convection are removed. This means that the life-cycle of individual clouds can be represented in detail together with dynamic interactions and organization, resulting in features like supercell and squall-line formation or storm-cell initiation by gust fronts. It is expected that this will allow for much more realistic and hopefully more accurate forecasts of severe weather events.

3 Project Structure

Deriving the convective-scale LMK from the LM requires not only an adjustment of the existing schemes but also a development of new components within data assimilation, dynamics and numerics, physical parameterization, verification and validation. The project structure is organized along these points into four basic work packages (see below). Five new staff members are in employment on the project and additional support comes from collaboration within COSMO. Also, a more close collaboration is planned with NWP groups working on similar systems (ALADIN, UK-MetOffice, HIRLAM and WRF).

Work Package:	**Main Issues**
Radar Data	– Correction methods and quality control of 5-min DX-scans, – Generation of a 5-min DX composite using European radar sites, – Use of radar wind in the LMK assimilation cycle.
Latent Heat Nudging:	– Investigation of the latent heat nudging algorithm of LM, – Improvement and modification of the scheme to achieve a "long-lasting" impact of radar information.
Model Development	– Numerical Methods and basic model dynamics – Physical parameterization schemes – Lateral boundary conditions – Test Cases, sensitivity studies, model intercomparisons – Installation and evaluation of a LMK test suite
Verification	– Provision of model-derived remote sensing data (radar simulation model, pseudo satellite radiances) – Application of new verification methods (pattern recognition) – Standard surface and upper-air verification

4 Current Work and Plans

With respect to numerics, current work focuses on the implementation of a TVD-variant of the 3rd-order in time Runge-Kutta time integration. The scheme can easily be combined with the standard time-split forward-backward methods to integrate fast compression waves and furthermore allows for flexible use of high-order spatial advection operators. From the latter, we expect noticeable benefits for simulating processes such as deep convective cloud evolution which is at or close to the grid-scale. Using a 5th-order advection scheme, the new scheme allows for a time step almost twice as large as with the standard Leapfrog/2nd-order centered differencing scheme of LM. This advantage is somewhat reduced since the advection operator has to be calculated three times. The main reason for applying the new time scheme, however, is not to save CPU-time but to achieve a more accurate and thus much better converged numerical solution at neutral computational costs. For first results from the RK3 time integration see the paper by Förstner and Doms in this volume.

The equations for the hydrological cycle have also to be reconsidered for very high spatial resolution, since advective transport of precipitation particles (like rain and snow) may no longer be neglected as it is done in current schemes. Hence, the present diagnostic treatment of precipitation has to be replaced by an algorithm based on the full 3-d budget equations for rain and snow. For LMK and LM, a numerical algorithm to solve these prognostic equations has been constructed by combining a 3-d semi-Lagrangian advection scheme with an implicit treatment of precipitation fallout (see paper by Baldauf and Schulz, this volume) using a Marchuk time splitting technique. Tests of the scheme indicate that the horizontal transport of snow is essential for correcting an erroneous spatial distribution of precipitation of orographically forced rainfall in case of stable stratification. In case of high-resolution applications, the vertical advective transport of precipitation will be of crucial importance for describing the life-cycle of deep convective storms correctly.

Considering physical processes on the meso-γ scale, parameterization issues related to deep convection and gravity waved drag will disappear due to a direct simulation of these processes. Shallow convection, however, will still remain sub-grid scale and can play a significant role for initiating deep convection. At present, it is not clear if standard global-scale convection schemes based on steady-state plume cloud models with a moisture- or moist static energy convergence closure can cope with shallow convection at very high resolution. We plan to develop a shallow-convection scheme based on a dynamic cloud model, which allows for an explicit calculation of entrainment and detrainment, and a closure based on PBL turbulent kinetic energy.

Remaining parameterized physical processes are turbulent mixing, microphysics, radiation and surface fluxes. For the latter two, we initially rely on the standard parameterization used in LM. Turbulent transport becomes essentially 3-d at very high resolution, e.g. lateral exchange across cloud boundaries will be important for the evolution and organization of deep convection. A new 3-d turbulence scheme based on turbulent kinetic energy using a non-isotropic closure for fluxes has been developed (Herzog et al., 2003) and is currently implemented. A more comprehensive treatment of the ice-phase is also important when simulating deep clouds directly. In this aspect, we will upgrade the present microphysics scheme to include graupel (and later on hail) as an additional precipitation category.

It is planned to run the LMK every 3 hours from a continuous data assimilation stream based on the LM observational nudging technique (Fig. 2). Such a rapid update cycle will require a short data cut-off (less than 30 min) and the successful use of available non-synoptic remote sensing data. In this respect, the assimilation of radar reflectivities using the latent heat nudging (LHN) technique is under evaluation (see the paper by Klink and Stephan,

this volume) and satellite data will be assimilated by using profiles obtained with 1-D var retrievals. The LHN will be based on 5-min reflectivities, which requires the development of corresponding data correction algorithms and data quality control methods as well as the development of a European composite.

Verification and validation of high-resolution model forecasts is very difficult as representativity errors, spatial and temporal variability, and lack of suitable data become important - resulting in a less meaningful applicability of traditional quantitative scores. In the LMK project, we will focus on the use of a radar simulation model (to compare directly with radar measurements) and pseudo satellite images in various channels, combined with new verification tools such as pattern recognition methods. These activities go along with the development of appropriate diagnostic tools and derivation of necessary products for customers.

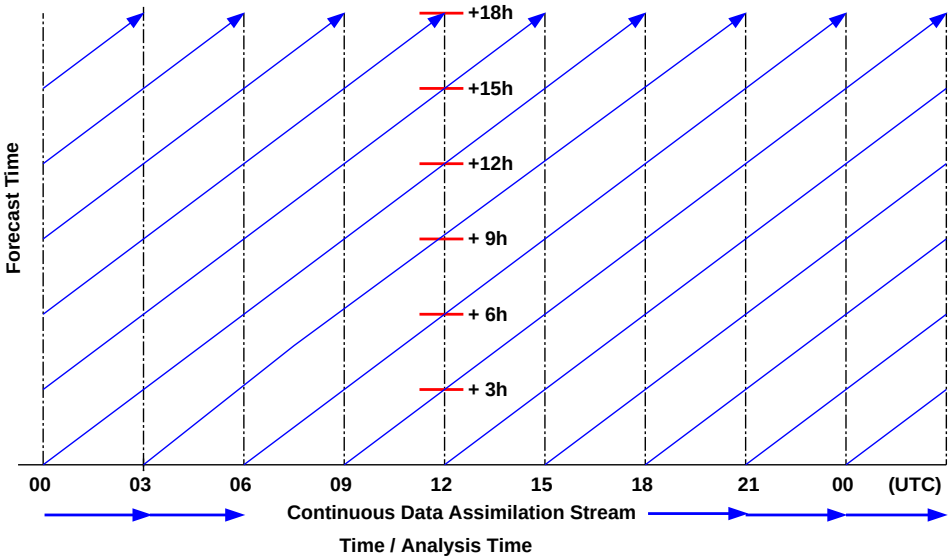

Figure 2: Planned update/forecast cycle with forecasts every 3 hours (right). At a given time, 6 forecasts are available, allowing to generate some lagged averaging ensemble products.

5 A First LMK Test Suite

In order to investigate the general behaviour of the LM at the meso-γ scale, a first test suite has been installed at DWD. Some preliminary case studies on a number of convective situations have shown a certain skill of the model to predict severe weather conditions as e.g. squall-line formation at the presence of large scale forcing (Doms et al., 2002). The behaviour of the model for 'normal' non-convective situations, however, is not yet known and a number of deficiencies and problems may be present. The LMK test suite aims at the detection of such problems at an early stage of the project.

The set-up of the test suite is quite simple: We start from interpolated initial and boundary conditions from the operational LM using the interpolation program LM2LM, i.e. there is no data assimilation for LMK yet. The dynamics and physics is the same as in LM at DWD, except that the convection scheme is switched off. LMK is integrated for the domain shown in Fig. 1 using a 2.8 km grid spacing and 50 vertical layers, where the hybrid Gal-Chen coordinate is used as vertical coordinate. The time-step is set to 16 sec for the Leapfrog time-integration. The test suite started at 18 December 2003 and was run until 29 February 2004, performing two 18-h forecasts a day stating at 00 and 12 UTC.

The overall impression from the test runs (an automatic generation of plot products with posting on the DWD Intranet has been established) is quite encouraging: The model runs stable (no blow-ups) and no grid-point storm like effects have been observed; also, the severe winter storms during January were robustly integrated. The spin-up time for the dynamical adaptation to the new high-resolution topography is in general less than one hour, but amplitudes can be quite high over the Alps. Another spin-up effect comes from the time needed to build up convective cells explicitly, which can also be noticed along the lateral inflow boundaries for unstable weather situations. This type of lateral boundary spin-up will not be removed by future continuous data assimilation.

Two main deficiencies have been detected during the experiment: One is related to the pressure field at the lateral boundaries, and the other with a missing shallow convection scheme. To illustrate these problems we consider two cases from the test suite. The first is related to the winterstorm on 13 January 2004, the second to a thermal unstable situation on 28 February 2004.

For the first case, Fig. 3 displays the vertically integrated water vapour and the vertically integrated cloud condensate (cloud water and cloud ice) for the LMK run and the corresponding operational LM run at 12 UTC. High values of the latter indicate deep clouds and can be associated with resolved stratiform or convective clouds – depending on the spatial cloud scale. The frontal cloud structures over the northern and eastern parts of Germany look quite similar in both simulations, except that some convective scale cloud structures are embedded within the front. In the cold air in the rear of the front (over the North Sea, the Netherlands and Belgium), explicit convective cells are simulated in the LMK run - which are not visible in the LM run since these are represented only as subgrid-scale clouds in parameterized form. There is also some type of organization into cloud-bands both along

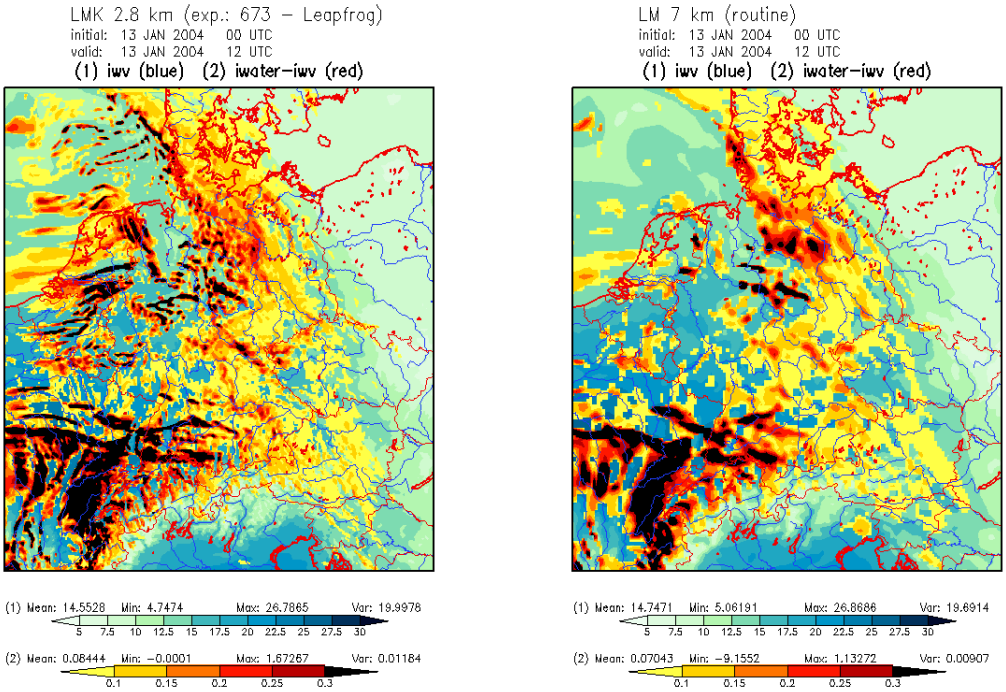

Figure 3: Vertically integrated water vapour (green-blue colors) and vertically integrated cloud water and ice (yellow-red colors) for 13 January 2004 00 UTC + 12 h. Left: LMK (total domain). Right: Operational LM with 7km grid spacing on the corresponding subdomain.

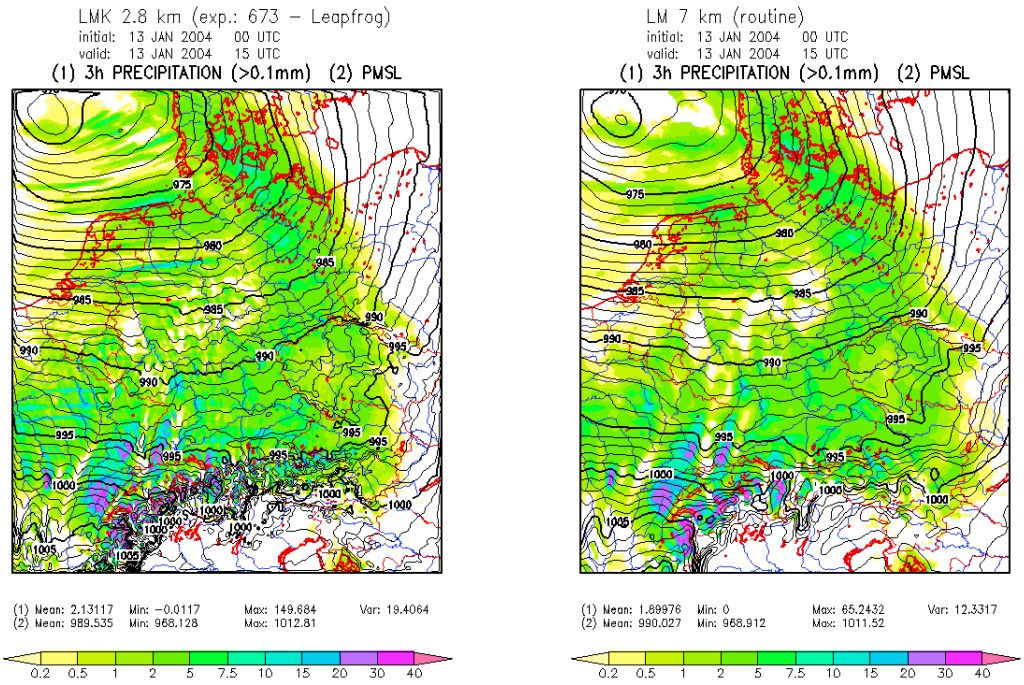

Figure 4: 3-h precipitation amount from 12 UTC to 15 UTC for forecasts starting on 13 January 2004 00 UTC. The contour lines indicate the mean sea level pressure at a 1 hPa interval. Left: LMK (total domain). Right: Operational LM with 7km grid spacing on the corresponding subdomain.

and cross to the mean wind direction. A comparison with satellite images, however, has not yet been done. In the southwestern part of the integration domain we see deep orographic grid-scale cloudiness, which is quite similar in both runs, except that the cloud structures are more sharp and more detailed in the LMK run.

The corresponding precipitation amount from 12 to 15 UTC is displayed in Fig. 4. There is not much difference in the precipitation patterns from both runs, the LMK gives a somewhat higher area mean precipitation amount and obviously much too high peak values related to orographic rain in the Alps. The latter effect is expected from the steeper orography and will probably be removed when using the prognostic precipitation scheme later on. In the northwest of the integration domain some tracks of precipitation from explicit convective cells are visible, which is consistent with the cloud structure shown in Fig. 3.

The pressure problem along the lateral boundaries mentioned above is clearly visible in Fig. 4. There is a drop in pmsl – and in the pressure perturbation on model levels – of about 0.5 to 1.0 hPa from the boundary value to the inner domain within the relaxation zone. This results in a correspondingly lower level of surface pressure in the whole inner LMK domain when compared to the driving LM. The pressure difference forms within the first hour of simulation time and then stays at about the same level for the rest of the integration. Moreover, this effect is not case dependent, i.e. it is noticeable in every simulation performed in the test suite. The cause for this behaviour is not yet clear. First experiments have shown that the distribution of vertical levels is quite sensitive to the formation of the pressure drop (indicating a substantial impact of the method used for vertical interpolation), but also the Rayleigh damping layer has a noticeable impact. Another reason might come from errors introduced from a too narrow set-up of the lateral relaxation zone (Herzog et al., 2002). A further possible source for this behaviour from the interpolation of nonhydrostatic pressure

in LM2LM instead of using an equilibrium condition (hydrostatic pressure) as in GME2LM can be excluded, since a similar error shows up when the GME2LM is applied to provide initial and boundary conditions for LMK form the global model GME. Clearly, a detailed investigation of this problem is on the work plan of the project for the next months.

Another deficiency – but case dependent – was detected for meteorological situations with a moist-convective unstable boundary layer. As an example, Fig. 5 shows the low-level cloud cover for 28 February 2004 at 18 UTC from LM and LMK forecasts starting at 00 UTC. The operational LM predicts low-level cloudiness in the southeastern part of the domain, but an almost cloud-free sky for northern and western regions – except for a meso-cyclone which formed over Belgium and the Netherlands during the day and moved eastwards in the evening (with heavy snowfall during the night). In contrast, the LMK predicts an almost closed low level cloud cover in the northern and western part of the domain.

On this day, a convectively unstable situation prevailed with some snow showers from shallow convective clouds during the afternoon. Shallow convection, however, cannot be resolved correctly with 2.8 km gridspacing. As it is not parameterized so far, moisture can be accumulated within the boundary layer during the day resulting in high relative humidity and correspondingly high subgrid-scale cloud cover (which is interpreted from relative humidity) on the lower model levels. Also, the relative humidity on the 850 hPa level is smaller in LMK than in LM (not shown), indicating that an efficient exchange mechanism between the boundary layer and the free atmosphere is missing in the LMK simulation for this case.

In order to test the sensitivity of the simulation to shallow convection, we rerun this case with a simple parameterization scheme for shallow convection. This was realized in an ad-hoc approach by just switching on the Tiedtke scheme but storing back the convective tendencies only when the resulting convective cloud depths are less than 2000 m. Fig. 6 compares the

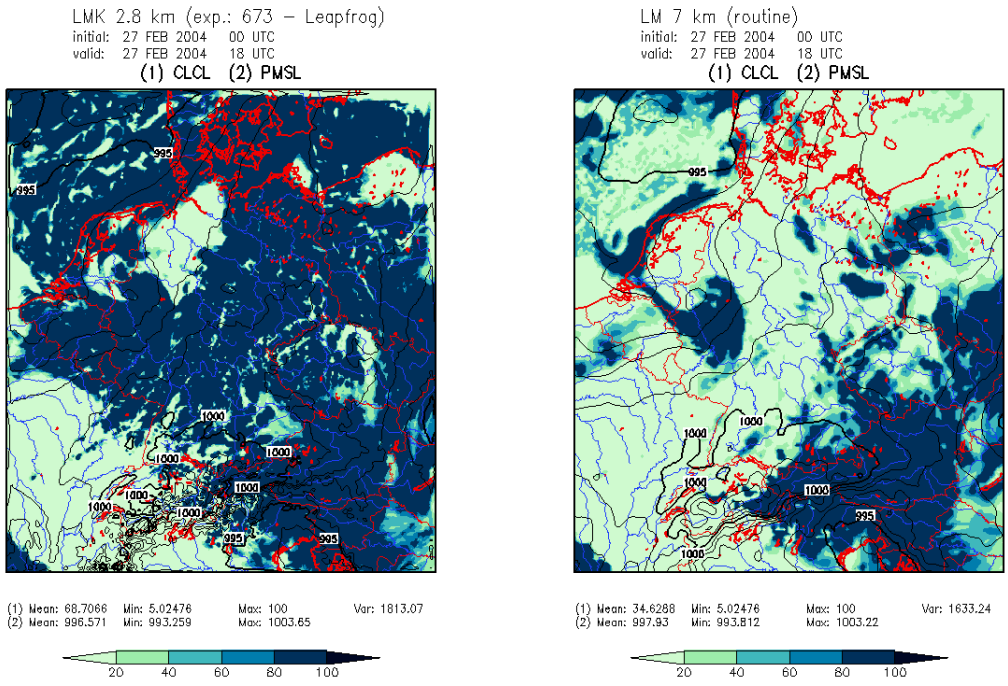

Figure 5: Low-level cloud cover valid for 27 February 2004 00 UTC + 18 h. Left: LMK (total domain). Right: Operational LM with 7km grid spacing on the corresponding subdomain.

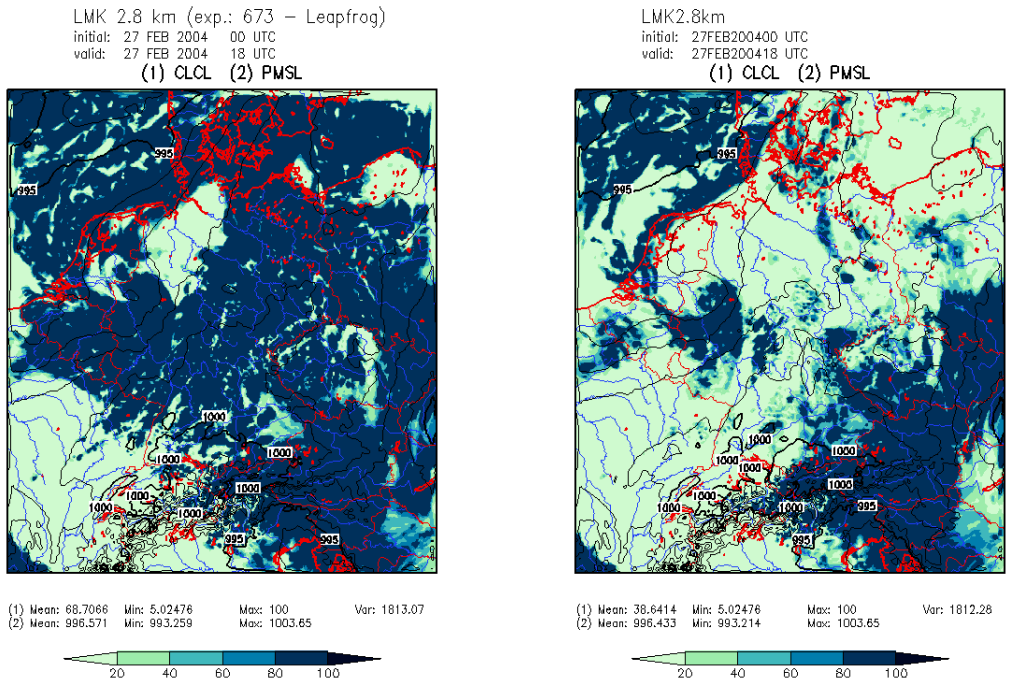

Figure 6: Low-level cloud cover valid for 27 February 2004 00 UTC + 18 h. Left: LMK (total domain). Right: LMK with a simple shallow convection scheme.

low-level cloud cover from this test run against the standard LMK simulation. As can be noticed, shallow convection has a profound impact on the low-level humidity structure: Almost all low-level cloudiness over northern Germany and the Baltic Sea has vanished, and now the meso-cyclone appears as a distinguished feature. When compared to the operational LM 7 km run shown in Fig. 5, a somewhat higher low-level cloudiness remains over the North Sea. This is related to explicit deep convection simulated by the LMK in this region and is consistent with the LM 7km run, where parameterized convections indicates cloud depths of about 8000 m.

This test experiment demonstrates that a parameterization for shallow convection is of crucial importance to properly represent non-local vertical exchange processes between the boundary layer and the free atmosphere. The current ad-hoc approach of applying a large-scale scheme is of course not suitable: First, the method is computational expensive and second, the closure condition which relates cloud-base mass flux to sub-cloud moisture convergence is certainly not scale-adequate. We plan to develop a new scheme based on a more sophisticated cloud model which will allow to determine entrainment and detrainment as diagnostic quantities in terms of convective available buoyant energy.

6 Outlook

As a next step, we plan to rerun the testsuite for January 2004 with the new TVD-RK3 integration scheme and 5th-order discretization of horizontal advective transport, combined with the prognostic precipitation scheme. Later on the testsuite will be gradually upgraded according to new developments in the dynamics/numerics and physical parameterizations.

For the more long-term planning, the following milestones have been defined.

- Summer 2004:
  A prototype version of the LMK-System (new time integration including 3-d turbulence, graupel microphysics and shallow convection) with data assimilation but without latent heat nudging is running in a test environment.

- Summer 2005:
  The prototype version of the LMK-System with latent heat nudging is running in a quasi-operational mode. Further testing, evaluation and development of new numerical schemes and physical parameterizations.

- Early 2006:
  Start of a pre-operational test-phase and begin of fine-tuning and final evaluation of all components of the system.

- End 2006:
  Start of the operational application.

7 References

Baldauf, M. and J.-P. Schulz, 2004: Prognostic Precipitation in the Lokal Modell (LM) of the German Weather Service. COSMO Newsletter No. 4.

G. Doms, A. Gassmann, E. Heise, M. Raschendorfer, C. Schraff and R. Schrodin, 2002: Parameterization Issues in the Non-Hydrostatic NWP-Model LM. ECMWF Seminar Proceedings: Key Issues in the Parameterization of Subgrid Physical Processes, 3-7 September 2001. Shinfield Park, Reading, UK.

J. Förstner and G. Doms, 2004: RK Time Integration and High Order Spatial Discretization – A New Dynamical Core for the LMK. COSMO Newsletter No. 4.

Herzog, H.-J., U. Schubert, G. Vogel, A. Fiedler and R. Kirchner, 2002: LLM - the High-Resolving Nonhydrostatic Simulation Model in the DWD - Project LITFASS. Part I: Modelling Technique and Simulation Method. COSMO Technical Report, No.4, 66 pp.

Herzog, H.-J., G. Vogel and U. Schubert, 2003: Incorporating a 3D Subgrid Scale Turbulence Scheme into the 2.8km-Version of the LM. COSMO Newsletter, No.3, 195-197.

Klink, S. and K. Stephan, 2004: Assimilation of Radar Data in the LM at DWD. COSMO Newsletter No. 4.

Runge-Kutta Time Integration and High-Order Spatial Discretization of Advection – A New Dynamical Core for the LMK

Jochen Förstner and Günther Doms

Deutscher Wetterdienst, P.O.Box 100465, 63004 Offenbach a.M., Germany

1 New Dynamical Core

LMK is the name for a new development branch of the *LM* aiming at the meso-gamma scale (horizontal resolution of 2-3 km) and shortest range ("*K*ürzestfrist") forecasts periods (3-18 h). The new dynamical core for the LMK is based on different variants of 2-timelevel Runge-Kutta schemes, which are combined with a forward-backward scheme for integrating the high-frequency modes of the elastic equations. The first one is the normal 3rd-order Runge-Kutta scheme used by Wicker and Skamarock (2002) whereas the second one is a total variation diminishing (TVD) variant of 3rd-order (Liu, Osher and Chan 1994).
For horizontal advection upwind or centered-differences schemes of 3rd- to 6th-order can be used – the operators are formulated in advection form. The vertical advection is normally treated in an implicit way using a Crank-Nicolson scheme and centered-differences in space. Most slow tendencies such as vertical diffusion, thermal/solar heating, parameterized convection and coriolis force are computed only once using values of the prognostic variables at time step n. These tendencies are fixed during the individual Runge-Kutta steps and contribute to the total slow-mode tendencies which are integrated in several small time steps together with the fast-mode tendencies in a time-splitting sense. In contradiction to this, the whole 3D-advection is computed in each Runge-Kutta step.
In the following the procedures for the two Runge-Kutta schemes are described mathematically in a simplified form – the treatment of the physical forcing terms is omitted and the only operators listed are the ones for advection.

Problem to Solve:

$$\frac{\partial \phi}{\partial t} = L^{slow}(\phi) + L^{fast}(\phi)$$

Computation of the Slow Tendency:

Normal 3rd-order Runge-Kutta:

$$\begin{aligned}\phi^{*}_{i,k} &= \phi^{n}_{i,k} - \frac{1}{3}\Delta t\, L^{h}_{i}(\phi^{n}) - \frac{1}{3}\Delta t\Big(\beta^{+}L^{v}_{k}(\phi^{*}) + \beta^{-}L^{v}_{k}(\phi^{n})\Big)\\ &= \phi^{0}_{i,k} + \frac{1}{3}\Delta t\, L^{slow}_{i,k}\Big|^{*}_{0}\end{aligned}$$

$$\begin{aligned}\phi^{**}_{i,k} &= \phi^{n}_{i,k} - \frac{1}{2}\Delta t\, L^{h}_{i}(\phi^{*}) - \frac{1}{2}\Delta t\Big(\beta^{+}L^{v}_{k}(\phi^{**}) + \beta^{-}L^{v}_{k}(\phi^{*})\Big)\\ &= \phi^{0}_{i,k} + \frac{1}{2}\Delta t\, L^{slow}_{i,k}\Big|^{**}_{0}\end{aligned}$$

$$\begin{aligned}\phi^{n+1}_{i,k} &= \phi^{n}_{i,k} - \Delta t\, L^{h}_{i}(\phi^{**}) - \Delta t\Big(\beta^{+}L^{v}_{k}(\phi^{n+1}) + \beta^{-}L^{v}_{k}(\phi^{**})\Big)\\ &= \phi^{0}_{i,k} + \Delta t\, L^{slow}_{i,k}\Big|^{n+1}_{0}\end{aligned}$$

TVD-variant of 3rd-order Runge-Kutta:

$$\begin{aligned}
\phi^{*}_{i,k} &= \phi^{n}_{i,k} - \Delta t\; L^{h}_{i}(\phi^{n}) - \Delta t\Big(\beta^{+} L^{v}_{k}(\phi^{*}) + \beta^{-} L^{v}_{k}(\phi^{n})\Big) \\
&= \phi^{0}_{i,k} + \Delta t\; L^{slow}_{i,k}\Big|^{*}_{0} \\
\phi^{**}_{i,k} &= \frac{3}{4}\phi^{n}_{i,k} + \frac{1}{4}\phi^{*}_{i,k} - \frac{1}{4}\Delta t\; L^{h}_{i}(\phi^{*}) - \frac{1}{4}\Delta t\Big(\beta^{+} L^{v}_{k}(\phi^{**}) + \beta^{-} L^{v}_{k}(\phi^{*})\Big) \\
&= \phi^{0}_{i,k} + \frac{1}{4}\Delta t\; L^{slow}_{i,k}\Big|^{**}_{0} \\
\phi^{n+1}_{i,k} &= \frac{1}{3}\phi^{n}_{i,k} + \frac{2}{3}\phi^{**}_{i,k} - \frac{2}{3}\Delta t\; L^{h}_{i}(\phi^{**}) - \frac{2}{3}\Delta t\Big(\beta^{+} L^{v}_{k}(\phi^{n+1}) + \beta^{-} L^{v}_{k}(\phi^{**})\Big) \\
&= \phi^{0}_{i,k} + \frac{2}{3}\Delta t\; L^{slow}_{i,k}\Big|^{n+1}_{0}
\end{aligned}$$

Time-Splitting Method:

After each Runge-Kutta step the fast modes are integrated forward to the desired point in time using several small time steps $\Delta\tau$ – the slow tendency is fixed. The starting point of the integration $\phi^{0}_{i,k}$ depends on the chosen variant of the Runge-Kutta scheme – for the first variant it is always equal to $\phi^{n}_{i,k}$:

1. step:

$$\phi^{0+\Delta\tau}_{i,k} = \phi^{0}_{i,k} + \Delta\tau\; L^{fast}_{i,k}(\phi^{0}) + \Delta\tau\; L^{slow}_{i,k}\Big|^{\times}_{0}$$

remaining steps:

$$\phi^{\tau+\Delta\tau}_{i,k} = \phi^{\tau}_{i,k} + \Delta\tau\; L^{fast}_{i,k}(\phi^{\tau}) + \Delta\tau\; L^{slow}_{i,k}\Big|^{\times}_{0}$$

with $\times = *,\ **$ and $n+1$ in the individual Runge-Kutta steps.

Horizontal and Vertical Operators:

$$L^{h}_{i}(\phi)^{\,(4\text{th})} = \frac{u_i}{12\Delta x}\Big[\phi_{i-2} - 8\big(\phi_{i-1} - \phi_{i+1}\big) - \phi_{i+2}\Big]$$

$$L^{h}_{i}(\phi)^{\,(3\text{rd})} = L^{h}_{i}(\phi)^{\,(4\text{th})} + \frac{|u_i|}{12\Delta x}\Big[\phi_{i-2} - 4\big(\phi_{i-1} + \phi_{i+1}\big) + 6\phi_i + \phi_{i+2}\Big]$$

$$L^{h}_{i}(\phi)^{\,(6\text{th})} = \frac{u_i}{60\Delta x}\Big[-\phi_{i-3} + 9\big(\phi_{i-2} - \phi_{i+2}\big) - 45\big(\phi_{i-1} - \phi_{i+1}\big) + \phi_{i+3}\Big]$$

$$L^{h}_{i}(\phi)^{\,(5\text{th})} = L^{h}_{i}(\phi)^{\,(6\text{th})} + \frac{|u_i|}{60\Delta x}\Big[-\phi_{i-3} + 6\big(\phi_{i-2} + \phi_{i+2}\big) - 15\big(\phi_{i-1} + \phi_{i+1}\big) + 20\phi_i - \phi_{i+3}\Big]$$

$$L^{v}_{k}(\phi)^{\,(2\text{nd})} = \frac{w_k}{2\Delta z}\big(\phi_{k+1} - \phi_{k-1}\big)$$

2 Idealized Advection Test

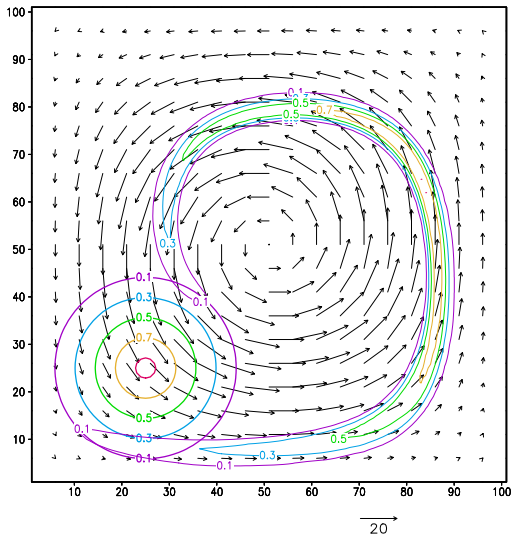

Figure 1: *Advection of a tracer in a non-divergent deformational flow (LeVeque 1996). Thick contours: initial field; thin contours: field after first half of the deformation cycle.*

An test problem of a tracer in a deformational flow field (LeVeque 1996) was used to evaluate the different time integration schemes in combination with varying high-order spatial discretization schemes for advection. The initialized field was a cone with a maximum of 1.0 and a radius of 15 grid spacings. In the first half of the simulation the tracer field is deformed vortex-like (Figure 1). The flow is reversed in the second half of the simulation cycle and the analytical solution at the end would be exactly equal to the initialized field.
The results of the simulations are given in Figure 2. The number of time steps used for the stable integration of one deformation cycle is given in the caption for each scheme. Especially in the combination with centered-differences the TVD-variant shows its benefits. Unfortunately when actually implemented in LM one still has to use a certain amount of numerical smoothing in form of artificial horizontal diffusion to control the small scale oscillations. In this regard the implicit diffusion of the upwind schemes stabilizes the overall integration and even bigger time steps are usable.

3 Test Case: Winter Storm "Lothar"

To test the robustness of the scheme, the winter storm case "Lothar" (26 December 1999) was simulated with the LM. Results are shown in Figure 3. The maximum horizontal velocity during the simulation reaches 108 m/s. For this case the new scheme in the combination TVD-RK-3rd/UP-5th allows a time step of 72 s at a resolution of 7 km compared to a time step of 40 s of the operational Leapfrog/CD-2nd scheme.
This case was also used in simulations to evaluate a new "symmetric" formulation of the thermodynamic equations (described in further detail below). The main change in this formulation lies in the use of a prognostic equation for T^* – the temperature perturbation – instead of the whole temperature T. It was necessary to use a smoother formulation of the relaxation at the lateral boundaries to control numerical problems. In addition the result for a simulation with a higher resolution of 2.8 km is shown.

4 Metric Coefficients and "Symmetric" Thermodynamic Equations

The new the dynamic core uses a different formulation of the metrics. Instead of the former pressure based one a formulation based on the geometrical height is applied:

$$\sqrt{\gamma} \equiv \frac{\partial p_0}{\partial \zeta} \quad \Longrightarrow \quad \sqrt{G} \equiv -\frac{\partial z}{\partial \zeta} = \frac{1}{g\rho_0}\sqrt{\gamma}.$$

In addition, the averaging to the half level positions is now done by a simple arithmetic mean and not a weighted mean any more.

To come to a consistent treatment of the gravity wave modes in the fast waves solver a "symmetric" formulation of the thermodynamic equations was implemented. Therefore we

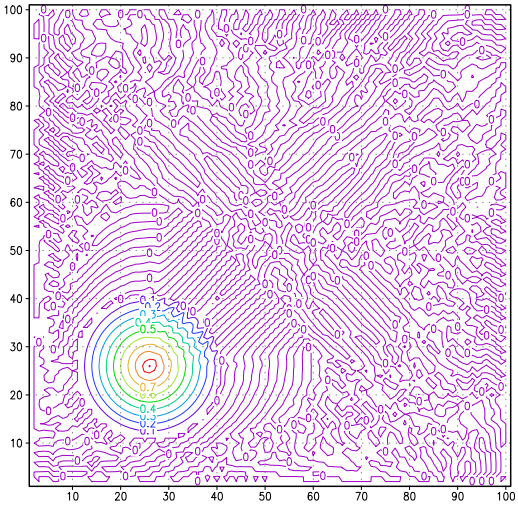

(a) RK-3rd / CD-4th – 670 time steps.

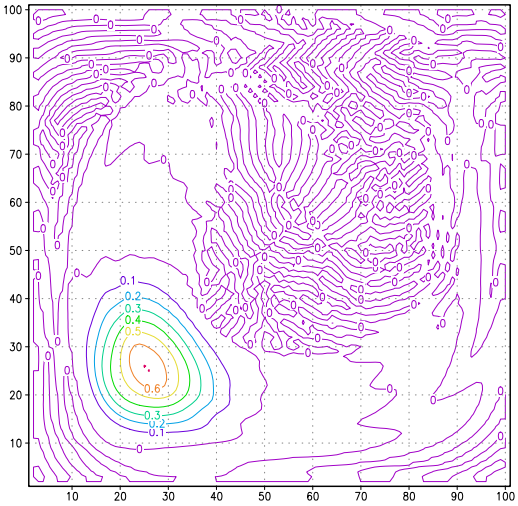

(b) RK-3rd / CD-4th with 4th-order artificial horizontal diffusion – 550 time steps.

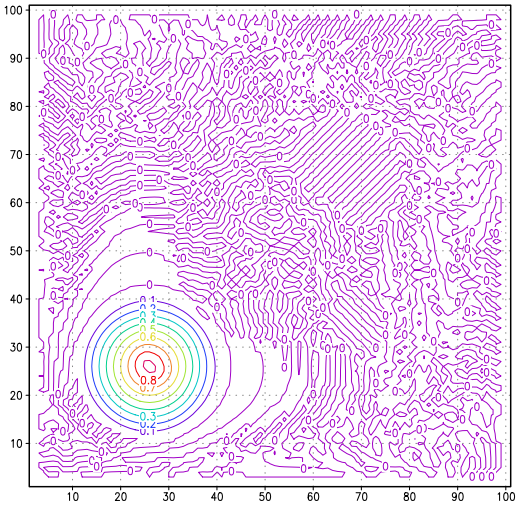

(c) TVD-RK-3rd / CD-4th – 450 time steps.

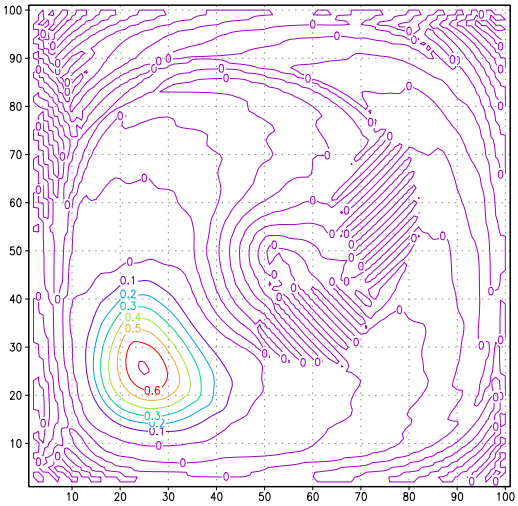

(d) RK-3rd / UP-5th – 380 time steps.

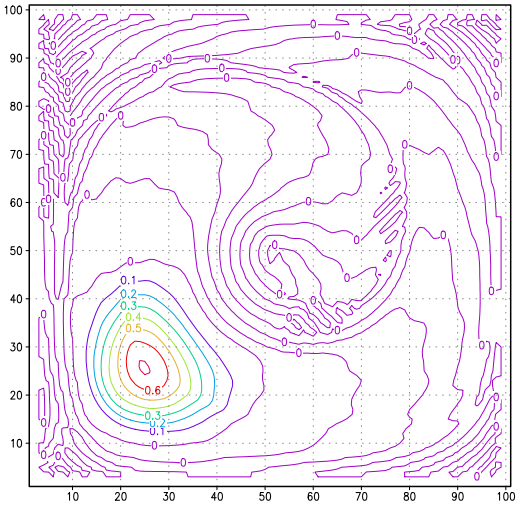

(e) TVD-RK-3rd / UP-5th – 380 time steps.

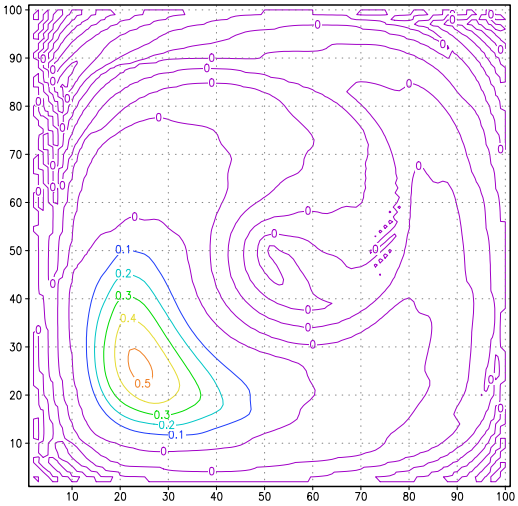

(f) TVD-RK-3rd / UP-3rd – 310 time steps.

Figure 2: *Advection of a tracer in a non-divergent deformational flow (LeVeque 1996). Results after 5 s simulation (one deformation cycle).*

change to a prognostic equation for the temperature perturbation T^*:

$$T \quad \Longrightarrow \quad T^* = T - T_0(z).$$

The resulting term of the advection of the reference temperature T_0

$$\vec{v} \cdot \vec{\nabla} T_0 = -\frac{\mathrm{d}T_0}{\mathrm{d}\ln p_0} \frac{g\rho_0}{p_0} w = \frac{\mathrm{d}T_0}{\mathrm{d}z} w$$

is treated in the fast modes part of the model.

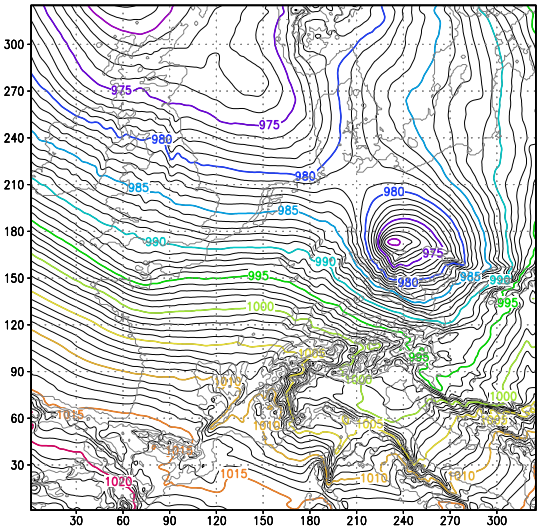

(a) TVD-RK-3rd / UP-5th – $\Delta x, \Delta y = 7$ km; $\Delta t = 72$ s. Prognostic equation for T (standard).

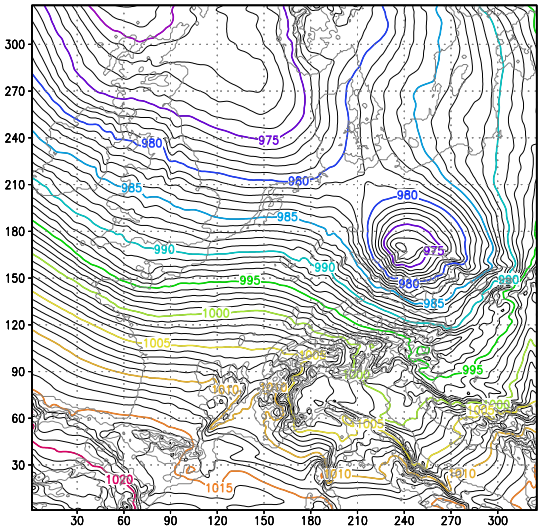

(b) Leapfrog / CD-2nd – $\Delta x, \Delta y = 7$ km; $\Delta t = 40$ s. Prognostic equation for T (standard).

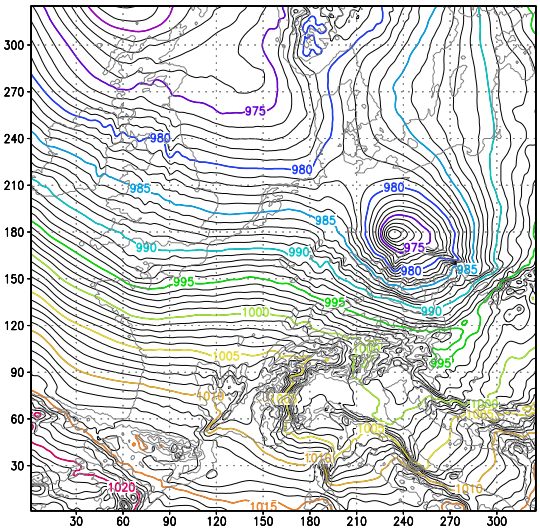

(c) TVD-RK-3rd / UP-5th – $\Delta x, \Delta y = 7$ km; $\Delta t = 72$ s. Prognostic equation for T^*; smoother relaxation LBC.

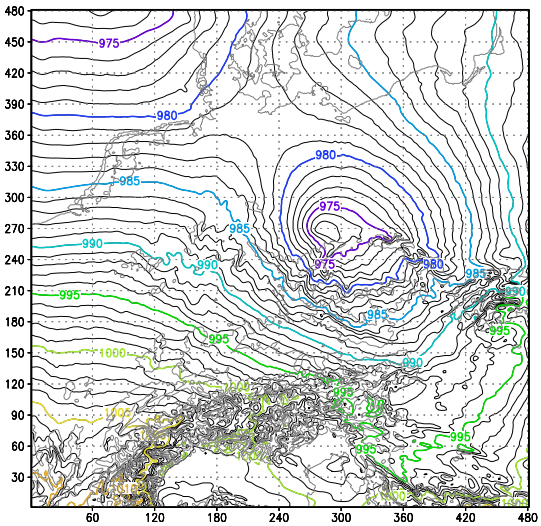

(d) TVD-RK-3rd / UP-5th – $\Delta x, \Delta y = 2.8$ km; $\Delta t = 30$ s. Prognostic equation for T^*; smoother relaxation LBC.

Figure 3: *Winter storm "Lothar": mean sea level pressure in hPa – 26 December 1999, 16 UTC.*

Now the equations for the pressure and temperature perturbation are formulated

$$p^{*(\nu+1)} = \ldots + \Delta\tau g\rho_0 \left(\beta^+ \overline{w}^{\zeta\,(\nu+1)} + \beta^- \overline{w}^{\zeta\,(\nu)} \right)$$

$$T^{*(\nu+1)} = \ldots - \Delta\tau \frac{\mathrm{d}T_0}{\mathrm{d}z} \left(\beta^+ \overline{w}^{\zeta\,(\nu+1)} + \beta^- \overline{w}^{\zeta\,(\nu)} \right)$$

and semi-implicitly coupled with the prognostic equation of the vertical velocity

$$w^{(\nu+1)} = \ldots - \Delta\tau g \frac{\overline{\rho_0}^{\zeta}}{\overline{\rho^n}^{\zeta}} \left[\overline{\left(\frac{T_0\beta^+}{T^n p_0} \right) p^{*(\nu+1)}}^{\zeta} \overline{\left(\frac{T_0\beta^-}{T^n p_0} \right) p^{*(\nu)}}^{\zeta} \right]$$

$$+ \Delta\tau g \frac{\overline{\rho_0}^{\zeta}}{\overline{\rho^n}^{\zeta}} \left[\overline{\left(\frac{\beta^+}{T^n} \right) T^{*(\nu+1)}}^{\zeta} + \overline{\left(\frac{\beta^-}{T^n} \right) T^{*(\nu)}}^{\zeta} \right]$$

in a "symmetric" way.

The "symmetric" treatment of the temperature equation is still under development. While several tests look quite promising, others reveal big differences between this and the former treatment. For example tests cases of convective storm development (Weisman and Klemp 1982) – which are not shown here – clearly show the great sensitivity of the model results with respect to the treatment of the buoyancy term. And we do not know yet, which is the correct one – at least in a numerical sense.

5 Mountain Flow: Analytic and Numeric Solutions

As a further test of the different 2-timelevel Runge-Kutta cores 2D-simulations of the flow over a bell shaped mountain were performed and compared to an analytic solution (as well as the old 3-timelevel Leapfrog core). The results are given in Figure 4. For this case the best match with the analytic solution is accomplished with the Runge-Kutta scheme using T^* as prognostic variable. This looks promising for the new "symmetric" treatment, but one has to keep in mind, that the vertical advection of T_0 is equal to zero in this case of an isotherm atmosphere. Therefore the buoyancy-related sensitivity of the model mentioned before has minor influence here.

6 Numerical Experiment: "Testsuite 2"

In addition to the first test suite (see paper by Doms and Förstner, this volume) in another numerical experiment the model with the new dynamical core was run in an operational forecast setup for the period 1 December to 31 December 2003. The Experiment was called "Testsuite 2". Besides the dynamical core the only other change we had to make was to use the old turbulent diffusion and transfer schemes. This was due to numeric instabilities in the new turbulence scheme, which uses a prognostic equation for the TKE to compute the diffusion coefficients.
As an example Figure 5 shows a comparison of the Runge-Kutta and the operational version of the 00 UTC run for 20 December 18 UTC. We see, that the pressure field looks good and corresponds well to the operational version. For precipitation the new core generates systematically smaller amounts in the mean. In this context it is noticeably, when we look at the integrated cloud condensate, that we have less clouds particularly over the sea. Further verification and comparison with precipitation measurements (of high quality) have to show, if that is desirable. The only bigger problem so far – revealed by a quick verification of the first eight days – is a bad forecast of the 2m-temperature. But that is rather an effect of the old turbulence scheme than the new dynamical core.

7 Outlook

In the meantime Matthias Raschendorfer has solved the problems leading to the numeric instabilities and the changes will probably be integrated in the operational source code of LM commencing with version 3.9. The next step is "Testsuite 3" – using the 2.8 km LMK setup, a time step of 30 s, prognostic precipitation, prognostic TKE and certainly the new TVD-Runge-Kutta core combined with 5th-order upwind for horizontal advection.

The ongoing development of LMK aims at the implementation of a 3D-turbulence scheme (Herzog et al. 2003) and further investigation of the "symmetric" formulation of the thermodynamic equations with a set of idealized test cases proposed at the last SRNWP-workshop (Bad Orb, 2003).

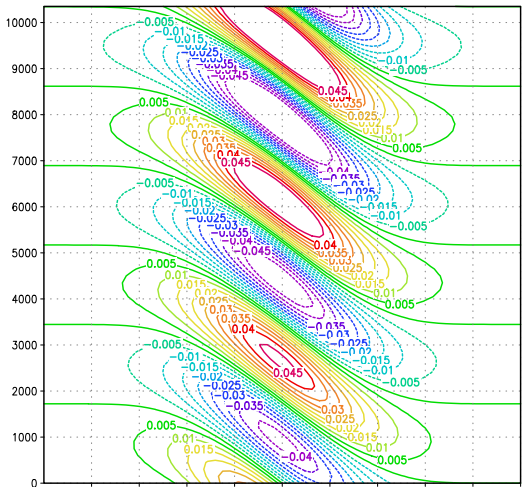

(a) Analytic solution.

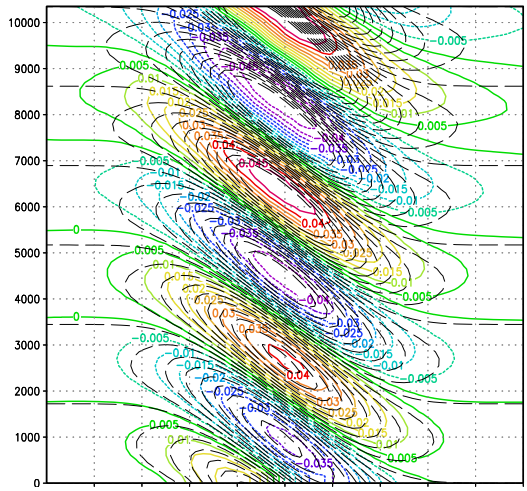

(b) Leapfrog / CD-2nd – $\Delta t = 40$ s. Prognostic equation for T (standard).

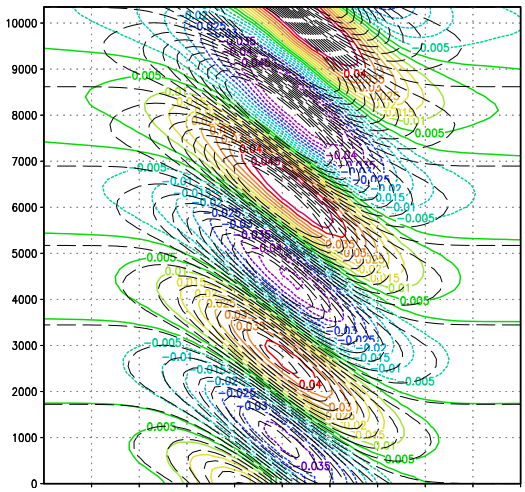

(c) TVD-RK-3rd / UP-5th – $\Delta t = 72$ s. Prognostic equation for T (standard).

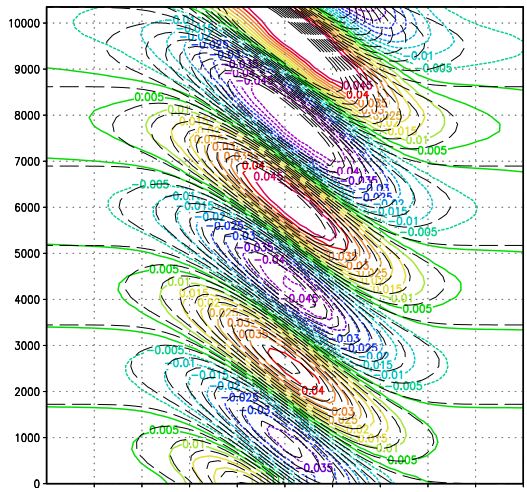

(d) TVD-RK-3rd / UP-5th – $\Delta t = 72$ s. Prognostic equation for T^*; smoother relaxation LBC.

Figure 4: *Vertical cross section of 2D flow over a mountain of 100 m height and a half width of 4 grid spacings. Shown is the vertical wind velocity w. Incoming flow: $U = 10$ m/s; stratification: isotherm – $T_0 = 285.15$ K.*
Fig. (b)-(d): Results of LM simulations after a simulation time of 30 h – $\Delta x, \Delta y = 7$ km. The analytic solution is given in thin dashed contours.

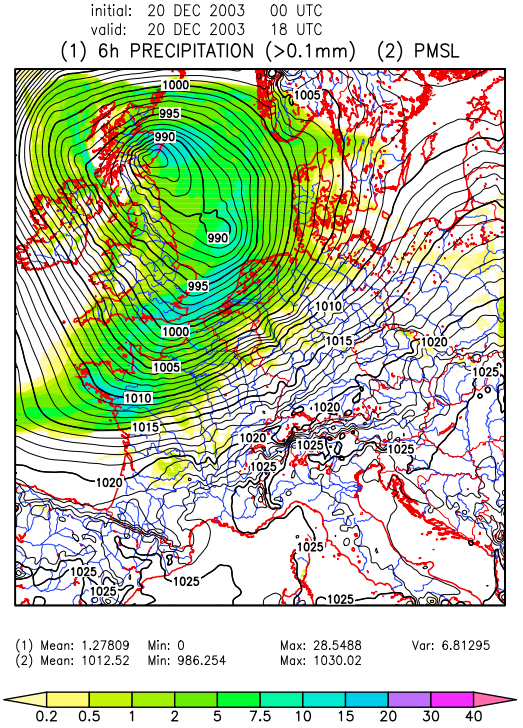

(a) **LM-RK**: Precipitation – 12-18 UTC.

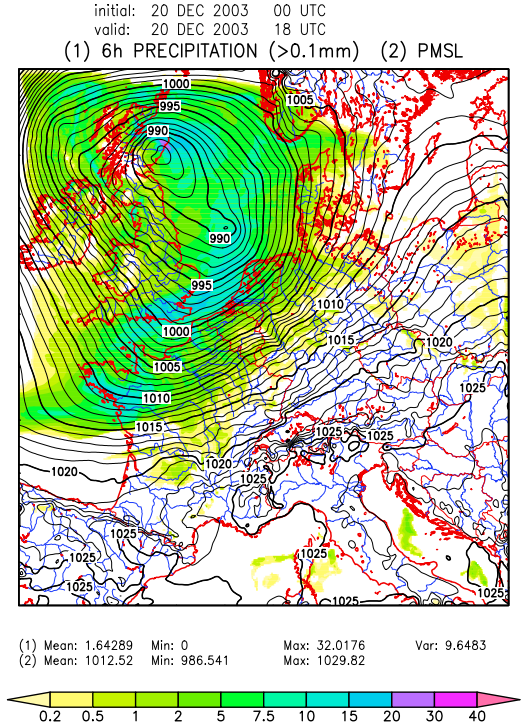

(b) **LM**: Precipitation – 12-18 UTC.

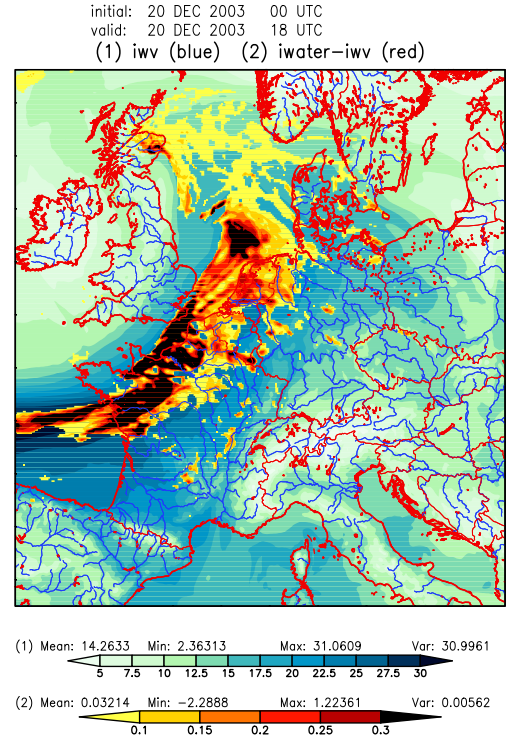

(c) **LM-RK**: Integrated water vapor (green-blue) and cloud water and ice (yellow-red) – 18 UTC.

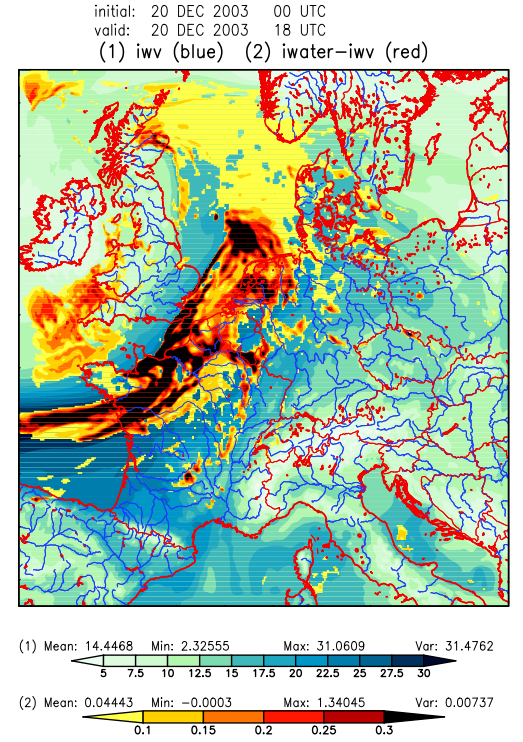

(d) **LM**: Integrated water vapor (green-blue) and cloud water and ice (yellow-red) – 18 UTC.

Figure 5: *Numerical experiment "Testsuite 2" to evaluate the new dynamical core – $\Delta x, \Delta y$ = 7 km; initial time of the simulation: 20 December 2003 - 00 UTC.*
***LM-RK**: New dynamical core – TVD-RK-3rd / UP-5th – Δt = 72 s. Old (diagnostic) TKE scheme (`itype_turb=1`, `itype_tran=1`).*
***LM**: Routine version – Leapfrog / CD-2nd – Δt = 40 s. Prognostic TKE scheme (`itype_turb=3`, `itype_tran=2`).*

8 References

Doms, G. and J. Förstner (2004). Development of a kilometer-scale NWP-system: LMK. In *COSMO Newsletter*, Number 4. Offenbach a. M., Germany: Deutscher Wetterdienst.

Herzog, H.-J., G. Vogel, and U. Schubert (2003). Incorporating a 3D subgrid scale turbulence scheme into the 2.8km-version of the LM. In *COSMO Newsletter*, Number 3, pp. 195–197. Offenbach a. M., Germany: Deutscher Wetterdienst.

LeVeque, R. J. (1996). High-resolution conservative algorithms for advection in incompressible flow. *SIAM J. Numer. Anal. 33*, 627–665.

Liu, X.-D., S. Osher and T. Chan (1994). Weighted essentially non-oscillatory schemes. *J. Comput. Phys. 115*, 200–212.

Weisman, M. L. and J. B. Klemp (1982). The dependence of numerically simulated convective storms on vertical wind shear and buoyancy. *Mon. Wea. Rev. 110*, 504–520.

Wicker, L. J. and W. C. Skamarock (2002). Time-splitting methods for elastic models using forward time schemes. *Mon. Wea. Rev. 130*, 2088–2097.

Prognostic Precipitation in the Lokal Modell (LM) of DWD

M. Baldauf and J.-P. Schulz

Deutscher Wetterdienst, Kaiserleistr. 42, D-63067 Offenbach am Main, Germany

1 Introduction

Many atmospheric limited area models have difficulties in realistically representing the distribution of precipitation in mountainous terrain. A common feature is an overestimation of precipitation amounts on the upwind side and an underestimation on the lee side. This has been known already for the former Europa Modell of the German Weather Service, which is a hydrostatic model, and it is still found in the currently operational Lokal Modell (LM, Doms and Schättler, 2002) which is non-hydrostatic.

In the currently operational LM version the conservation equations for rain and snow

$$\rho\frac{\partial q^x}{\partial t} + \rho\mathbf{v}\cdot\nabla q^x = -\nabla\cdot\mathbf{P}^x - \nabla\cdot\mathbf{F}^x + S^x \tag{1}$$

($x = r, s$ for rain, snow, q = mixing ratio, $\mathbf{P}$ = sedimentation flux, $\mathbf{F}$ = turbulent flux, S = source terms from cloud microphysics) are approximated stationary and without advection. This column equilibrium approach means that precipitation particles, arising from cloud microphysical processes, immediately fall down to the bottom of the column in the same time step.

In reality, rain drops with a mean fall velocity of about 5 m/s which develop for example at a height of 3 km, need a falling time of 10 minutes. If a horizontal wind speed of 10 m/s is assumed, the rain drops are drifted by 6 km. For snow with a mean fall velocity of about 1 m/s (and usually generated higher up) the horizontal drifting is even more efficient. Therefore, for the LM with a grid length of currently 7 km (in the next version (LMK) a grid length of about 2.8 km is aspired) and a time step of 40 s the column equilibrium approach is no longer valid. This was tested by case studies especially dedicated to the formation of precipitation in mountains: in many cases there is too much precipitation on the upwind side, and too little in the lee. In particular for hydrologists the solution of this problem is of high relevance: precipitation falls in the false catchment and is therefore not added to the correct river.

2 Semi-Lagrange-Advection

There are in principal two possibilities to handle the sedimentation term $-\partial P_z/\partial z$: either this term is discretized directly (for example implicitly), or one writes the sedimentation flux as a product of an effective fall velocity and the density $P_z = v_{\mathrm{eff}}\rho q$ and treats it in the advection scheme. In the latter case one has to consider, that in LM the layers near to the ground are so thin (about 60 m), that with the currently used time step of 40 s, particles can fall through up to three layers within one time step. Therefore, one needs an advection scheme which remains stable up to vertical Courant numbers of about 3. Apart from this, the prognostic precipitation shall be implemented in the version LMK, in which horizontal Courant numbers up to 1.8 are aspired, for which most Eulerian advection schemes are

no longer stable. For the advection of precipitation we therefore decided to use a three-dimensional Semi-Lagrange (SL) scheme (e. g. Staniforth and Côté, 1991) whose stability does not depend on the Courant number.

The application of the standard SL schemes consists of two steps: 1. calculation of the backtrajectory and 2. interpolation of the fields q^r and q^s at the starting point. The implicit equation of the backtrajectory (Robert, 1981) is solved by iteration. After one iteration step one gets a truncation error of order $O(\Delta t)$, after two steps of order $O(\Delta t^2)$. Simple tests show, that an error of only $O(\Delta t)$ delivers especially nonsatisfying conservation properties. This is in agreement with Staniforth and Côté (1991), who also recommend an order $O(\Delta t^2)$. Therefore, a second iteration step is needed which requires an interpolation of the three velocity components. This interpolation is a time consuming step in the staggered Arakawa-C-grid; currently it needs more then 80% of the computation time of the whole SL-scheme.

In the second interpolation step for the fields often a cubic polynomial is recommended, which shows the best relation between computational effort and accuracy; especially the cubic spline interpolation is even ideally conserving. In contrast, for the time being we use the simpler and computing time saving trilinear (i. e. linear in all three space dimensions) interpolation. It is well known that it has bad form properties (high diffusion) and only moderate conservation properties. However, the latter is probably not significant for rain and snow which remain only a few time steps in the model area. A test with a Gaussian rain particle distribution, which is advected with a given velocity ($u = 10$ m/s and $w = -5$ m/s), yielded a mass loss of 0.05% per time step. After 15 time steps (according to the example above) the mass loss is less than 1%. Similar tests with a velocity field over mountains even yielded a small gain of mass. But this could be explained by a non divergence free velocity field; in this case the advection itself does not conserve mass.

Some diffusion of the linear interpolation is even desired and could cure the problem of an unrealistic strong small scale structure of the precipitation in irregular terrain. Another advantage of the trilinear interpolation in contrast to higher order interpolation is its positive definiteness, an essential condition for the coupling to the cloud microphysics.

3 Coupling with cloud microphysics and real test cases

The dynamic core of the current operational LM consists of a 3-timelevel-scheme with time splitting by Klemp und Wilhelmson (1978). In the frame of this dynamic core the coupling between advection and cloud physics is done with a Marchuk-splitting, this means that in one time step the SL-advection from timelevel t^{n-1} to t^{n+1} (with velocities at t^n) is calculated and then using the updated values the cloud physics scheme is carried out. The latter is formulated implicitly, as mentioned above, but can be solved quasi-explicitly, because the sedimentation velocity is always directed downwards and therefore the system of equations has bidiagonal form.

As a real test case the precipitation distribution over Southwest Germany on 20 February 2002 is presented here. In order to illustrate the importance of the transport by drifting the trajectories of (idealized) snow particles which are injected into the simulated LM wind field at different heights over Strasbourg are given in Tab. 1. It is assumed that the snow particles fall with a constant speed of 2 m/s down to the melting zone at about 850 hPa. The table shows that, for instance, a snow particle starting at 500 hPa will drift 71.4 km within 40 minutes. This is equivalent to about 10 grid cells. A particle starting at 750 hPa will drift 13.1 km, which is still almost 2 grid cells. These results show that drifting of hydrometeors is an important transport process, in particular for snow, but also for rain, especially at higher

resolutions.

Start level [hPa]	Distance [km]	Duration of drift [min]
500	71.4	40
550	59.5	35
600	47.6	29
650	40.5	25
700	32.1	21
750	13.1	9

Table 1: Calculation of trajectories for LM for estimating the drifting of snow (provided by B. Fay, pers. comm., 2003).

Figure 1 shows the total precipitation (rain + snow) during a 24-h period on 20 February 2002, 0 UTC + 6h-30 h over Southwest Germany. The left figure shows a simulation with the operational LM, the right the same situation with the new prognostic precipitation scheme. The spatial precipitation distribution with the new scheme is in much better agreement with the observations (middle figure) than the current LM: the maxima are reduced (the operational LM overestimated them by up to 150%, the new version only by 20%), the maxima are shifted to the lee side and therefore the unrealistic dry regions in the lee do not appear. The observed precipitation distribution has a mean value of about 16 kg/m^2, the operational LM version yields 30% too much, the new version only about 10% too much. The computational effort for the new version is about 20% higher than for the operational one, which seems acceptable for two new prognostic variables (q_r and q_s).

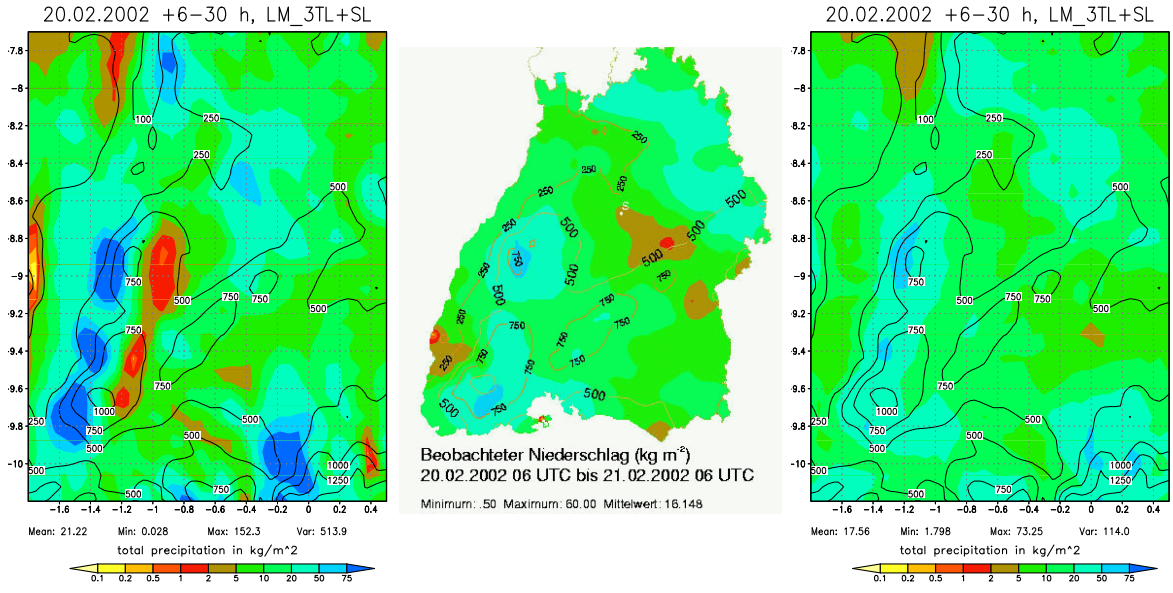

Figure 1: Precipitation forecast for 20 February 2002, 0 UTC + 6h-30 h over Southwest Germany with the currently operational LM without (left) and with (right) prognostic precipitation. Observations are shown in the middle. The isolines indicate the model orography.

References

Staniforth, A. and Côté, J. (1991): Semi-Lagrangian integration schemes for atmospheric models - A review, Mon. Wea. Rev., 119, 2206-2223.

Robert, A. (1981): A stable numerical integration scheme for the primitive meteorological equations, Atmos. Ocean, 19, 35-46.

Klemp, J. B. and Wilhelmson, R. B. (1978): The simulation of three-dimensional convective storm dynamics, J. Atmos. Sci., 35, 1070-1096

Doms, G. and Schättler, U. (2002): A description of the nonhydrostatic regional model LM, http://cosmo-model.cscs.ch/cosmoPublic/

Recent Changes to the Cloud-Ice Scheme

Günther Doms, Detlev Majewski, Aurelia Müller and Bodo Ritter

Deutscher Wetterdienst, P.O.Box 100465, 63004 Offenbach a.M., Germany

1 Introduction

Ice-phase processes play a significant role in mid-latitude frontal cloud systems and their impact should be taken into account by parameterization schemes. Since liquid water and ice cannot coexist in thermodynamic equilibrium below the freezing point, three cloud states can be realized in this temperature range, depending on the local supersaturation with respect to ice (see Fig. 1):

– supercooled water clouds, existing at (or very close to) water saturation;
– mixed phase clouds, also existing at water saturation;
– ice clouds, existing at water subsaturation but ice supersaturation.

Mixed phase clouds at subfreezing temperatures allow for precipitation enhancement, where two mechanisms are of particular importance: the Bergeron-Findeisen process and the Seeder-Feeder mechanism, which both are based on the presence of supercooled liquid water. Nucleation of ice in a water saturated environment will cause a rapid growth of the ice crystals by deposition (because of the ice supersaturation) and riming (because of the presence of supercooled cloud droplets); the ice particle growth is at the expense of liquid water, but if the cloud is kept at water saturation by thermodynamic forcings, high precipitation rates may result (Bergeron-Findeisen process). The Seeder-Feeder mechanism describes precipitation enhancement due to ice particles falling from a higher (Seeder) cloud into a lower (Feeder) cloud containing supercooled droplets; in this case, the droplets within the Feeder cloud will be also converted into precipitating ice by riming in addition to the collision-coalescence

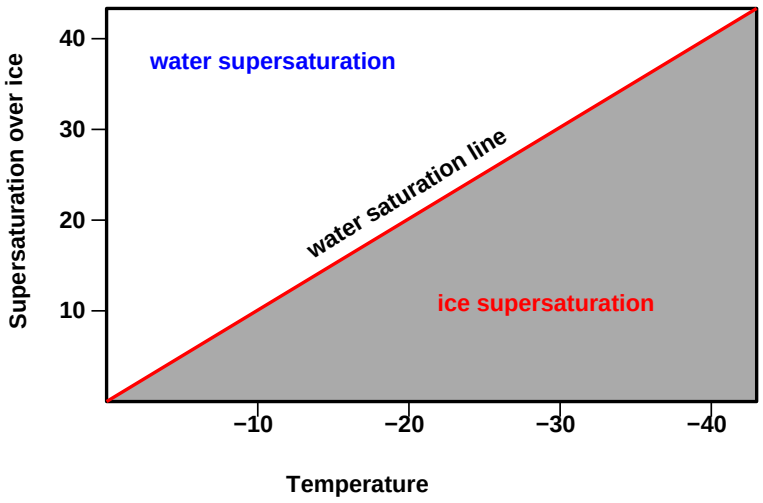

Figure 1: Supersaturation with respect to ice for a water-saturated state (red line) as function of subfreezing temperature. Both supercooled water clouds and mixed phase clouds exist at water saturation due to the presence of cloud droplets in equilibrium with water vapour. For specific humidities above or at ice saturation, but below water saturation, only ice clouds can be present (shaded area).

based warm rain precipitation formation. This results in a more efficient removal of cloud water and correspondingly higher precipitation rates than from both the Seeder and Feeder clouds alone.

The default (and former operational) parameterization scheme for grid-scale clouds and precipitation (HYDOR) is based on a Kessler-type bulk formulation where four categories of water substance are considered: water vapour, cloud water, rain and snow. Both the Bergeron-Findeisen process and the Seeder-Feeder mechanism are represented explicitly by this scheme through processes related to snow. The calculation of cloud water condensation and evaporation is based on instantaneous adjustment to water saturation. From the latter assumption, however, a number of major drawbacks result:

(a) Clouds will always exist at water saturation independent of temperature. That is, only water or mixed phase clouds but no ice clouds are simulated below freezing point.

(b) The cloud ice-phase is neglected by assuming a fast transformation from cloud water to snow. Thus, the glaciation of clouds cannot be simulated and cirrus will be at a wrong thermodynamic state. Also, the precipitation enhancement from the Bergeron-Findeisen mechanism may be overestimated.

(c) High-level clouds usually exist at or close to ice saturation. Since the scheme requires water saturation for cloud formation, the initial conditions must be artificially adapted to avoid long spin-up periods: In the analysis scheme, the specific humidity obtained from measurements is increased by the ratio of the saturation vapour pressure over water and over ice for temperature below $0°C$. This affects the high-level humidity structure in an unphysical way.

To overcome these problems, a new scheme including cloud ice (HYDCI) in addition to the other categories, namely water vapour, cloud water, rain and snow, has been developed.

2 Parameterization Concept and Microphysical Processes

Many ice-phase schemes used in NWP-models solve only one prognostic equation for cloud condensate and the distinction of the water and the ice phase has to be determined diagnostically by assuming a prescribed liquid fraction as function of temperature. Such schemes have a number of conceptional drawbacks and rely on strange thermodynamic assumptions. Thus, the new LM parameterization scheme was designed to take into account cloud ice by a separate prognostic budget equation (Doms and Schättler, 1999; Doms, 2002). Cloud ice is assumed to be in the form of small hexagonal plates that are suspended in the air and have no appreciable fall velocity.

As a novel feature of the scheme, we formulate the depositional growth of cloud ice as a non-equilibrium process and require, at all temperatures, saturation with respect to water for cloud liquid water to exist. Ice crystals which are nucleated in a water saturated environment will then grow very quickly by deposition at the expense of cloud droplets. Depending on local dynamic conditions, the cloud water will either evaporate completely, or will be resupplied by condensation. For strong dynamical forcings it is expected that water saturation will be maintained, resulting in a mixed phase cloud with efficient formation of precipitation due to the Bergeron Findeisen process. In case of a comparatively weak forcing, however, the cloud will rapidly glaciate to become an ice cloud existing at or near ice saturation (i.e. at subsaturation with respect to water). Figure 2 gives an overview on the hydrological cycle and the microphysical processes considered by the scheme.

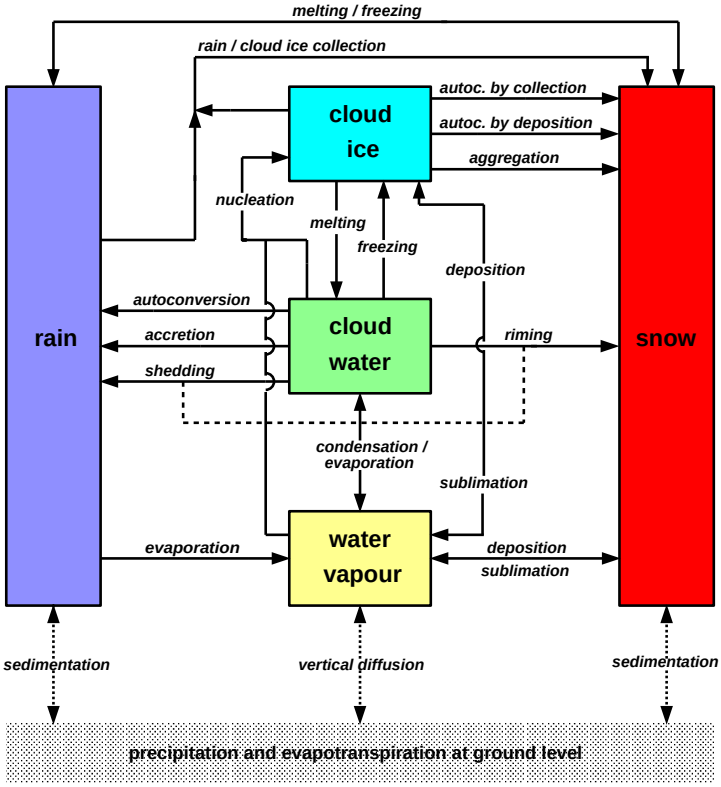

Figure 2: Hydrological cycle and microphysical processes in the LM cloud ice scheme

Since the Bergeron Findeisen process as well as cloud glaciation is described explicitly, no further parameterizations such as a liquid fraction are required and the cloud state will adjust freely to microphysical and dynamical forcings on a physical basis. Thus, the resulting cloud ice content will depend on the strength of the dynamical forcings maintaining ice supersaturation (mainly vertical ascent and radiative cooling) and the characteristic time scale of microphysical processes which decrease or increase cloud ice content. These time scales depend on details in the parameterizations of the microphysical conversion rates, and a variation of the rate coefficients within physical limits can be used to optimize the scheme for achieving a better cloud-radiation interaction. This type of tuning effort is described in the next section.

3 Some Modifications of the Scheme

The new cloud-ice scheme has been tested for a number of case studies as for extensive parallel suites of GME and LM during all seasons including data assimilation and forecasts. These test reveal a reasonable behaviour of the scheme with an improvement of the upper level humidity structure. Especially, the formation of high-level cirrus ice clouds due to vertical motion associated with fronts or due to deep convective forcing is represented explicitly. However, the test test suites with the GME/LM system indicated two major problems:

- The cloud ice content appears to be too high, especially in the tropics and in polar regions.
- There is substantial increase in high level cloudiness in LM, when compared to SYNOP observations.

A number of sensitivity experiments have been performed to cure these deficiencies. First, we focus on empirical parameters in microphysical conversion rates controlling the cloud-ice content. As a test case, we choose 8 September 2002, where high-level cirrus clouds related to a frontal system moved over France and Germany.

(a) Modification of Ice-Crystal Number Density

The depositional growth rate of specific cloud ice content q^i is calculated explicitly from

$$S^i_{dep} \;=\; c_i \, N_i \, m_i^{1/3} \, (q^v \,-\, q^v_{si}) \tag{1}$$

where N_i is the number density of cloud ice, $m_i = \rho q^i N_i^{-1}$ is the mean mass of ice crystals, c_i is a thermodynamic factor depending on the shape of the crystals, q^v is specific humidity and q^v_{si} is the specific humidity at ice saturation. The number density N_i is prescribed as a function of temperature according to

$$N_i(T) \;=\; N^i_0 \exp\{\, 0.2\,(T_0 \,-\, T)\}\;\; \textit{with}\; N^i_0 \;=\; 1.0 \cdot 10^2 m^{-3}\,. \tag{2}$$

N_i is a disposable empirical parameter, and Eq. (2) was derived by fitting data obtained by aircraft measurements in stratiform clouds (Hobbs and Rangno, 1985; Meyers et al., 1992). Other schemes often use the classical Fletcher relation (Fletcher, 1962)

$$N^F_i \;=\; N^F_0 \exp\{\, 0.6\,(T_0 \,-\, T)\}\,, \qquad N^F_0 \;=\; 0.01 m^{-3}\,, \tag{3}$$

which gives about 3 orders of magnitude higher values for the ice crystal number density at low temperatures of about -40 °C and about two orders of magnitude lower values at high temperatures of about -10 °C. Interestingly, the cloud ice content changes not very on much on average despite these large differences. Fig. 3 (middle) compares the vertical distribution of domain and time average cloud ice content for two formulations of the autoconversion rate. The impact of using Eq. (3) instead of (2) is relatively small, the Fletcher relation results in somewhat higher values a all model levels. Smaller values for N_i than from Eq. (2) would reduce the average cloud ice content somewhat, but smaller number densities can

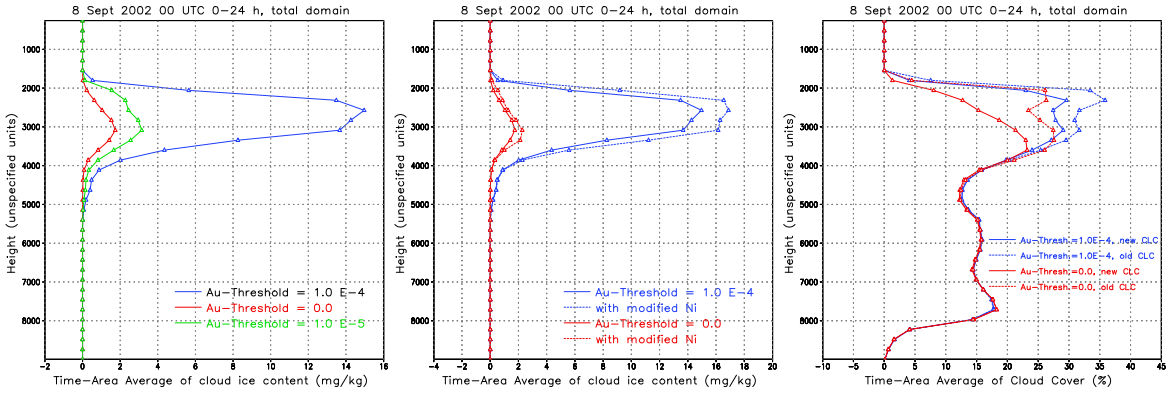

Figure 3: Left: Vertical distribution of domain and time averaged cloud ice content on model layers for three values of the autoconversion threshold value as indicated. Middle: Vertical distribution of domain and time averaged cloud ice content on model layers for two autoconversion threshold values as indicated, using the standard equation (2) for N_i and the modified equation (3). Right: Vertical distribution of domain and time averaged cloud cover, using the former and the modified diagnosis of cloud cover. All figures refer to a LM simulation starting on 8 September 2002 00 UTC, the time average is from 0 to 24 hours integration time.

hardly be justified from observations. We thus still rely on the Eq. (2) to parameterize N_i in the cloud ice scheme.

(b) Modification of Ice Autoconversion

Other disposable empirical parameters controlling the cloud-ice content are the coefficients in the autoconversion rate S^i_{au} of ice to snow (due to crystal aggregation):

$$S^i_{au} = \max\{c^i_{au}\,(q^i - q^i_0)\,,\,0\}\,. \tag{4}$$

Here, q^i_0 is a threshold value of specific cloud ice content which is set to 10^{-5} kg/kg by default. The rate coefficient is set to $c^i_{au} = 10^{-3}$ s^{-1} for cloud ice and corresponds to a decay time scale of 1000 s which gives a rather quick conversion of cloud ice into snow. Since we do not want to further decrease this time scale because of physical reasons, the threshold value was varied in sensitivity experiments. Increasing the default threshold to $q^i_0 = 10^{-4}$ kg/kg resulted in a dramatic increase of the average cloud ice content, whereas a reduction resulted in smaller ice contents. For $q^i_0 = 0$ kg/kg, the average cloud ice content is reduced by about a factor of two (see Fig. 3, left) on all model levels. Additional experiments with GME for various combinations of q^i_0 and c^i_{au} revealed best results with the standard value $c^i_{au} = 10^{-3}$ s^{-1} and $q^i_0 = 0$ kg/kg by evaluating the radiation balance at the top of the atmosphere and at the surface as well as the bias of near-surface temperatures. Thus we switched to a zero threshold value in the cloud-ice autoconversion rate for the operational application.

(c) Modification of Cloud-Cover Diagnosis

The problem of high-level cloudiness could be tackled by rescaling the cloud cover (both grid and sub-grid scale) which is diagnosed in terms of relative humidity and grid-scale cloud ice. Usually, the cloud cover is set to 100 % whenever cloud ice exists, otherwise a fractional cloud cover and a sub-grid scale cloud ice content are diagnosed. However, below a certain threshold value ($q^i_{min} = 0.1$ mg/kg) cirrus clouds are not detectable by a ground-based observer. If the cloud ice content exceeds $q^i_{max} = 10$ mg/kg, the impact on the visible part of the radiation spectrum is so large that the sky appears to be obscured by high clouds. In between these two values, the cloud cover obtained from standard diagnosis (clc_d) is now rescaled by an empirical function f_s which depends logarithmically on cloud ice content to

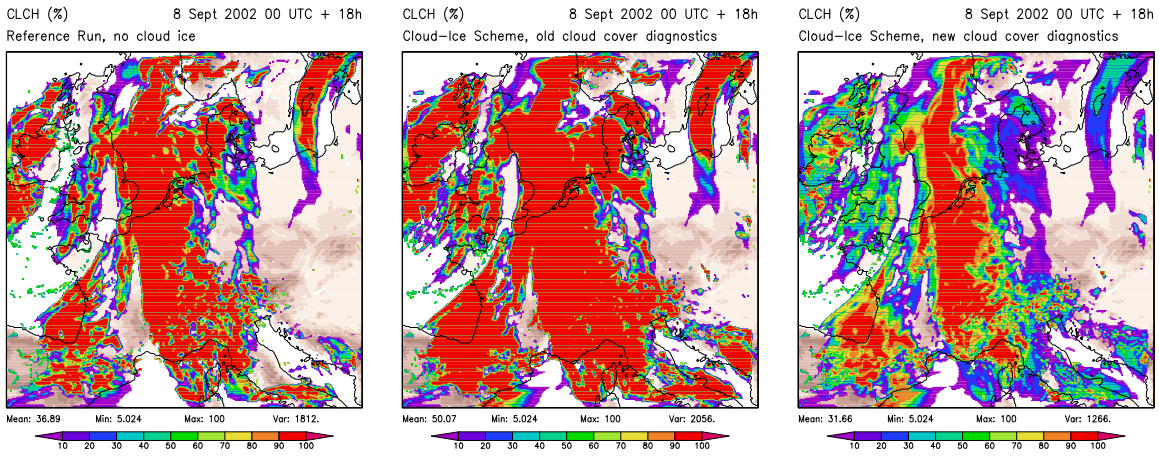

Figure 4: 18-h LM forecast of high cloud cover (%) valid at 18 UTC on 8 September 2002. Left: Reference run using the old cloud microphysics scheme (no cloud ice). Middle: Run using the cloud ice scheme but with standard cloud cover diagnosis. Right: Run using the cloud ice scheme but with modified cloud cover diagnosis.

give the final cloud cover clc:

$$clc = clc_d \cdot f_c\,, \quad f_c = \min\left(1\,,\ \max\left\{0.2\,,\ \frac{\ln q^i - \ln q^i_{min}}{\ln q^i_{max} - \ln q^i_{min}}\right\}\right) \tag{5}$$

The introduction of the scaling factor f_c results in significant reduction of high-level cloud cover when compared to the standard diagnosis (see Fig. 4, right). The spatial distribution now corresponds better to both the results from the old microphysics scheme and to ground based observations at SYNOP stations (see Section 4).

4 Verification Results of GME/LM Testsuites

The cloud-ice scheme has been tested in extensive parallel suites of GME and LM including data assimilation. The verification of this test suites generally showed only modest improvements of forecast accuracy over the operational model versions.

(a) Vertical Profiles

The verification of vertical profiles of LM forecasts for a test suite during May 2003 using the cloud ice scheme with modified ice-autoconversion reveals an almost neutral impact for wind and geopotential with a slightly reduced temperature bias. A more noticeable improvement

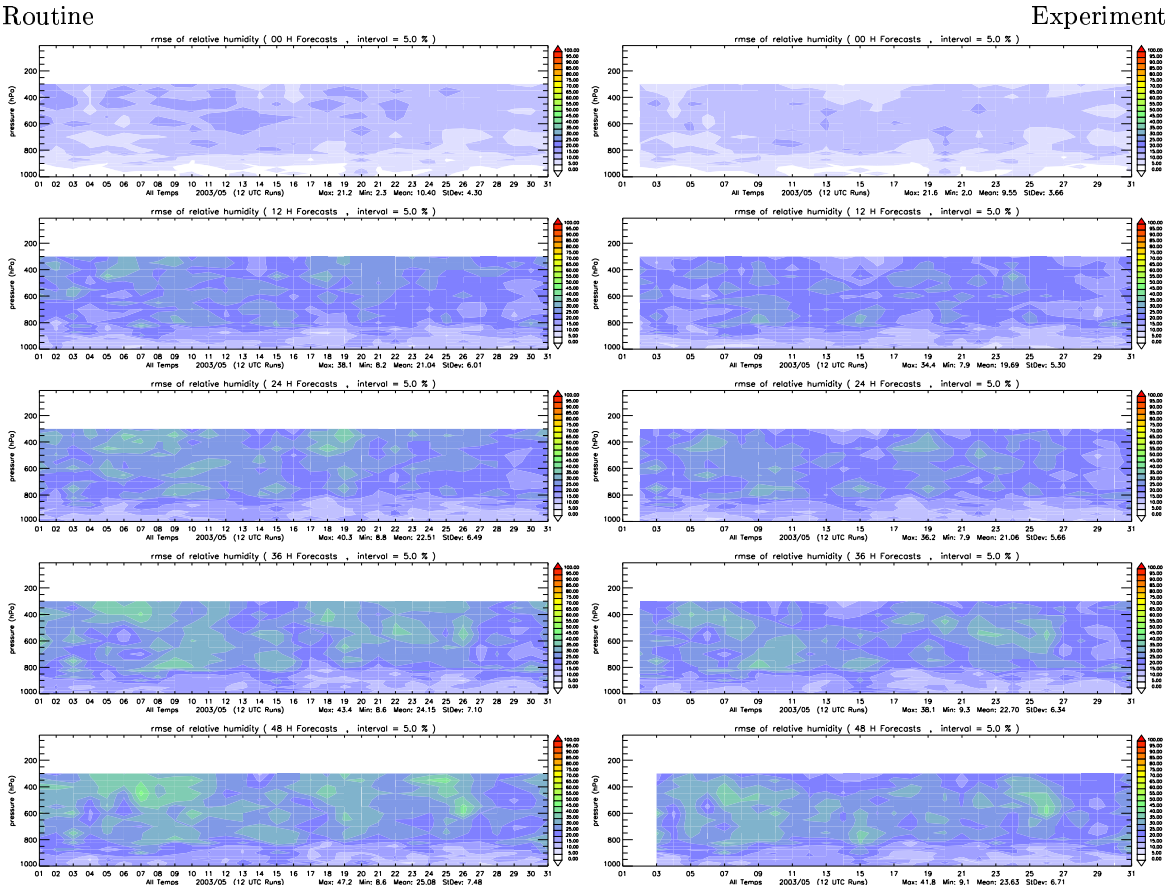

Figure 5: Time Series (1 - 31 May 2003) of relative humidity RMS errors for 12 UTC LM forecasts against radiosonde data. From top to bottom: Analysis, 12-h, 24-h, 36-h and 48-h forecast time. Left: operational runs at DWD without cloud ice. Right: Runs with cloud ice using the modified autoconversion rate with zero threshold.

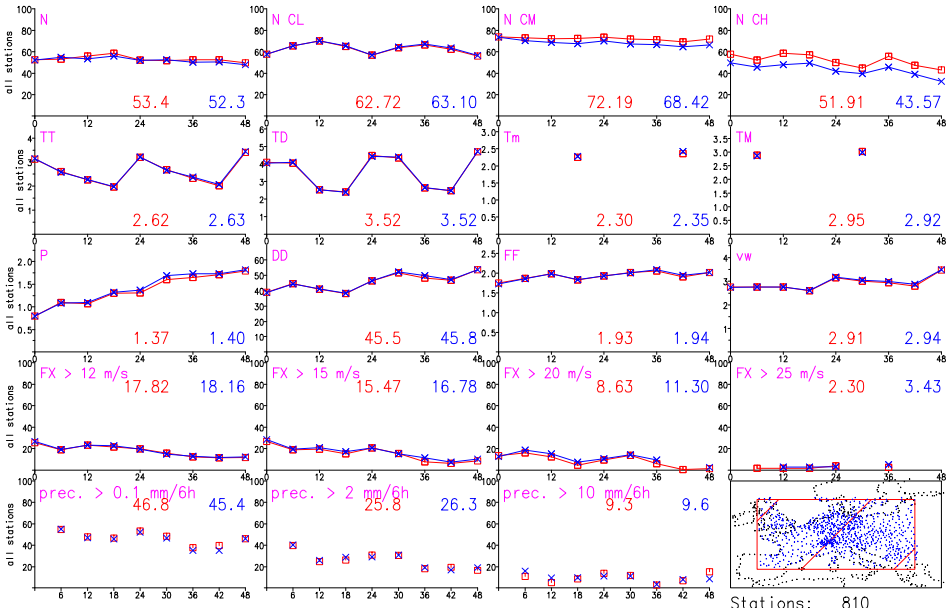

Figure 6: Verification of forecasts for local weather elements from operational LM 12 UTC runs (red) and from experimental runs with cloud ice (blue) using the modified autoconversion rate but the old cloud cover diagnosis, against SYNOP observations for 2 - 31 May 2003 as a function of forecast time. Percent correct for cloud covers (top row: total (N), low (NCL), medium (NCM) and high (NCH) cloud cover), TSS for precipitation (bottom row, for 6-h precipitation amounts above indicated thresholds), ETS for wind gusts (4th-row, for gusts (FX) above indicated thresholds), RMS errors for other elements (2nd row: 2m-temperature (TT), 2m dew-point (TD) , minimum 2m- (Tm) and maximum 2m-temperature (TM); 3rd row: mean sea-level pressure (P), 10m wind direction (DD), 10m wind speed (FF) and 10m wind vector (vw).

is found for relative humidity. Fig. 5 shows the root mean square (RMS) error for the test period for analysis and various forecasts times. Between 300 hPa and 600 hPa (i.e. for temperatures well below 0 °C), the RMS errors are significantly reduced in the analysis and for all forecast ranges when compared to the verification of the operational runs. Similar results are found from the GME verification.

(b) Surface Weather Elements

The verification of predicted surface weather elements of a test suite for May 2003 using the cloud ice scheme with modified ice-autoconversion and the standard (old) cloud cover diagnosis showed an almost neutral impact for all elements, except for high-level cloudiness (see Fig. 6): The percent correct value for high-level clouds decreases noticeable for all forecast ranges, from 51.9% to 43.6% on average. This result was the reason for introducing a modified cloud cover diagnosis as proposed by Eq. (5). Using this new diagnosis, another test suite for a period in September 2003 was run. The verification results shown in Fig. 7 reveal a significant improvement of the predicted high-level cloudiness, which now has a better score than from the operational runs. Interestingly, noticeable improvements are also achieved for 2m-temperature, 2m dew point temperature and precipitation.

5 Summary and Outlook

A new microphysics parameterization scheme including cloud ice has been developed and successfully tested in GME and LM. Since 16 September 2003, this new scheme is used operationally in both models at DWD, as well as in all LM applications at COSMO Centres

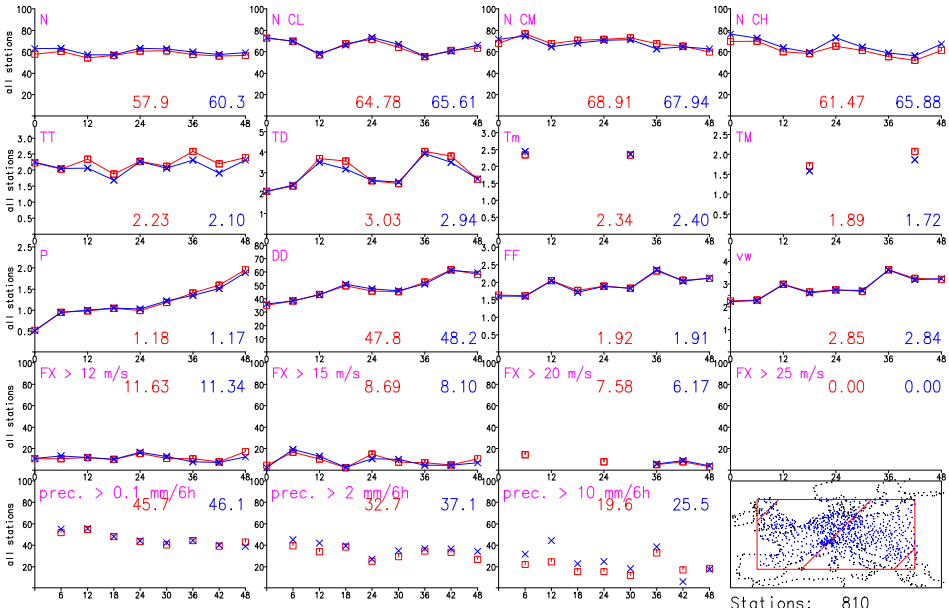

Figure 7: As in Fig. 6, but for a test period from 1 - 9 September 2003 using the new cloud cover diagnosis (5).

and in the HRM (High-resolution regional model) of DWD, which is used operationally at more than 13 national weather services world wide.

The main advantage of the scheme is a more physically based representation of ice and mixed-phase clouds, allowing for a direct simulation of cloud glaciation. The phase composition of high-level clouds appears to be well captured, which is important for a better cloud-radiation interaction. And in particular, the formation, growth and spreading of grid-scale anvil clouds can be simulated explicitly.

Further fine-tuning of the cloud-radiation interaction and the present interpretation of fractional cloudiness for low cloud ice content might be necessary. Also, further improvements or optimizations of cloud microphysical conversion rates are possible. Another issue for future work is the inclusion of sub-grid scale sources of cloud ice due to detrainment of ice from parameterized convective clouds. In context with the introduction of prognostic precipitation within the operational Leapfrog time-integration, the source terms have been reformulated with the mixing ratios instead of the precipitation fluxes and a stable numerical scheme for precipitation fallout has been formulated.

References

Doms, G., U. Schättler, 1999: The Nonhydrostatic Limited-Area Model LM (Lokal-Modell) of DWD. Part I: Scientific Documentation. Deutscher Wetterdienst (DWD), Offenbach (available at www.cosmo-model.org).

Doms, G., 2002: The LM cloud ice scheme. COSMO Newsletter No.2, 128-136.

Fletcher, N.H., 1962: The physics of rainclouds. Cambridge University Press, 390 pp.

Hobbs, P. V. and A. L. Rango, 1985: Ice particle concentrations in clouds. *J. Atmos. Sci.*, 42, 2523-2549.

Myers, M. P., P. J. DeMott and W. R. Cotton, 1992: New primary ice-nucleation parameterization in an explicit cloud model. *J. Appl. Meteor.*, 31, 708-721.

Numerical Simulation of Tropical Cyclogenesis with the Lokal-Modell

Thomas Frisius

Atmosphärische Wissenschaften
Institut für Meteorologie und Geophysik
der Universität Frankfurt a. M.

1 Introduction

Tropical cyclones are mesoscale phenomena. The inner structure of a tropical cyclone consists of an eye with warm dry air surrounded by an eyewall where a large amount of condensation takes place due to strong vertical motion. These structures can be assigned to the meso-β-scale. Therefore, the nonhydrostatic limited-area model "Lokal-Modell" (LM) of the German Weather Service would be an appropriate model for simulating the inner core of a tropical cyclone. However, convective clouds are also incorporated in such a storm, especially in the growth stage. Hence, convection must be parameterized or resolved explicitly. The use of a convective parameterization does not appear suitable since there is only a small gap between the scale of an individual convection cell and the scale of the tropical cyclone core. On the other hand the operational version of the LM uses a standard resolution of 6.95 km that is somewhat too coarse for simulating individual convective cells. However, other modelling studies of tropical cyclogenesis work with similar resolutions and found a reasonable reproduction of tropical cyclone structures (e. g. Liu et al. 1997 and Wang 2001). Therefore, it is not meaningless to attempt simulations of tropical cyclogenesis using the LM without a convective parameterization.

This study presents results of idealized tropical cyclone simulations in order to see how well the genesis event and the storm structures can be described with the LM. Furthermore, the sensitivity of the storm development to the use of a convective parameterization and various parameters is studied.

2 Description of Experiments

For all simulations the LM version 2.12 is used in which the effects of spherical geometry are neglected (f-plane geometry). The lower boundary is a sea surface with the constant temperature T_s. The experiments do not include effects of radiation. The model domain extends over a length of 1120 km in the zonal and in the meridional direction. The horizontal distance between two grid points amounts to 6.95 km so that each horizontal direction is divided into 161 grid points. In the vertical direction the 35 levels of the operational LM version (see Steppeler et al. 2003) are adopted. Near the lateral boundaries all variables are damped toward a horizontally uniform and motionless state with the Davies relaxation technique (Davies 1976). As in the operational LM version a four-category parameterization scheme for cloud microphysical processes is applied. The four categories of water are water vapor, cloud water, rain and snow. Turbulent exchange is parameterized with the operational scheme (see Steppeler et al. 2003).

Initially, a circular symmetric balanced cyclone is placed at the center of the model domain. The pressure p of this cyclone is prescribed by:

$$p(r,z) = p_0(z)(1 + \frac{\Delta p}{1000\text{hPa}})^{-} \exp(-r^2/r_0^2) \ , \tag{1}$$

where r denotes the distance from the center of the domain, z the height, $p_0(z)$ the pressure of the environment and r_0 a radius that determines the horizontal scale of the cyclone. The parameter Δp roughly measures the initial surface pressure difference between the center and the environment.

The initial temperature distribution only depends upon z and is given by:

$$T(z) = \begin{cases} T_s - \gamma z & z < H \\ \\ T_s - \gamma H & z \geq H \end{cases} \ , \tag{2}$$

where $H = 10000$ m is the height of the tropopause and $\gamma = 0.0065$ Km^{-1} the lapse rate. The initial relative humidity F is uniform and the pressure $p_0(z)$ is calculated from the hydrostatic balance equation using $p_0(0) = 1000$ hPa. The initial horizontal wind is in gradient wind balance.

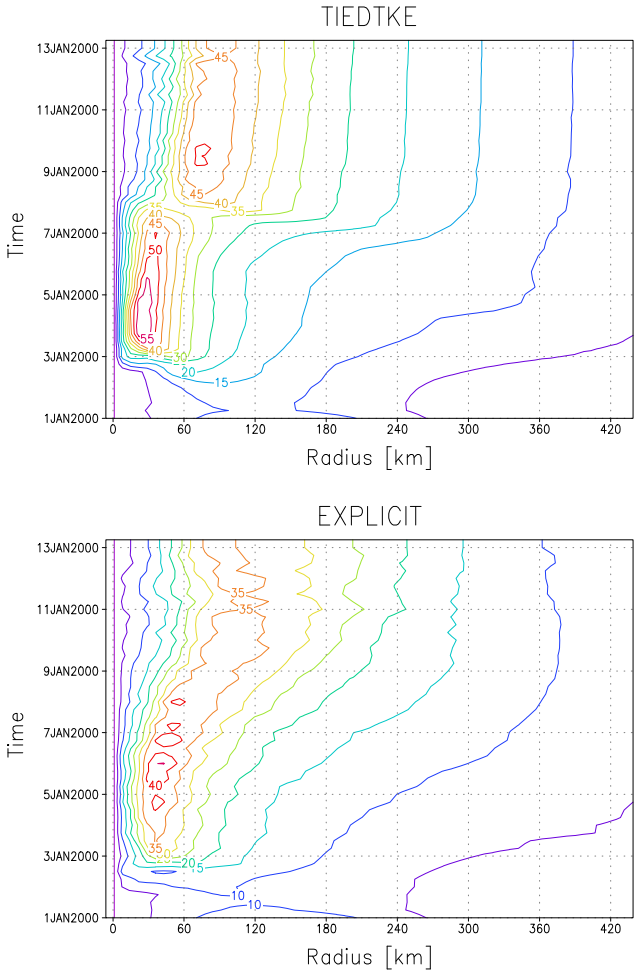

Figure 1: : Radius-time plot of the azimuthally averaged tangential wind at the lowest model level for the Tiedtke (upper panel) and Explicit (lower panel) run (contour interval 5m/s).

The parameters Δp, T_s and F are varied in the sensitivity experiments. For the reference runs the parameters are prescribed by Δp =5 hPa, r_0=150 km, T_s = 28°C, F = 0.7, $f = 0.729 \times 10^{-4}$ s^{-1}. Two categories of experiments are performed. In the first category the LM adopts the Tiedtke mass flux scheme for the parameterization of convection (Tiedtke 1989). In the second category convection is simulated explicitly without parameterization.

3 Reference experiment

In this section the results of the reference runs are presented. Fig. 1 shows the evolution of the azimuthal mean tangential wind at the lowest model level as a function of time and radius for both experiments. The azimuthal average has been applied with respect to the location of the minimum surface pressure. It can be seen that the initial wind increases and the radius of maximum wind shrinks until a mesoscale cyclone with hurricane force winds establishes. Compared to the explicit run the experiment with the Tiedtke closure reveals stronger maximum winds at a smaller radius. The magnitude and radius of maximum wind lie within the range observed in real tropical cyclones (e. g. Holland 1980). In the Tiedtke run the radius of maximum wind changes abruptly after 7 days due to the formation of a secondary wind maximum that replaces the inner one. Such a replacement has also been observed in real hurricanes (Willoughby et al. 1982) and in numerical simulations (Tenerelly and Chen 2002). In the explicit run the radius of maximum wind moves rather gradually outward. This seems to be related to asymmetries from the circular symmetry in the explicit run where spiral bands instead of convective rings induce the migration of the inner eyewall.

This suspicion is supported by Fig. 2 where snapshots of the vertically averaged temperature and vertical wind fields are displayed at $t = 108$ hours (the vertical average ranges from the surface to z =10000m). Obviously, the vertical wind pattern exhibits a ring-like eyewall in the Tiedtke run. In contrast, the explicit run reveals a spiral band rather than a closed eyewall. The temperature fields are in both cases nearly axisymmetric with a maximum at the storm center. The maximum of the temperature anomaly amounts to 12°C in the Tiedtke run and 9°C in the explicit run. Such magnitudes also arise in observed tropical cyclones

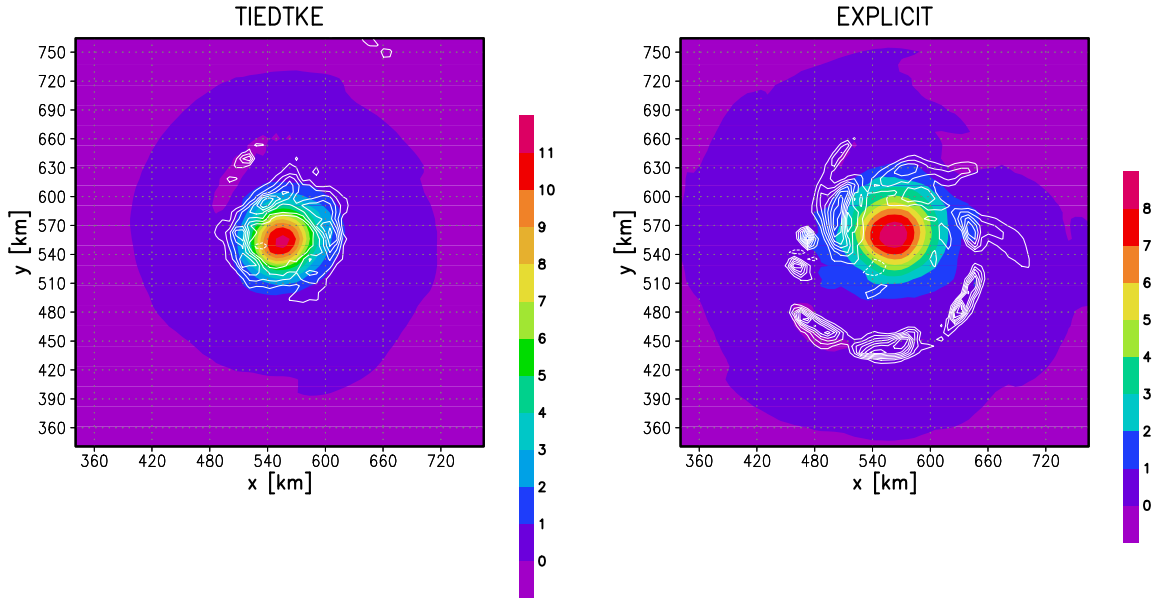

Figure 2: Snap-shot of the vertically averaged vertical wind (white isolines, contour interval 0.2m/s) and temperature (coloured shadings, in °C) at $t = 108$hours. Negative isolines are dashed.

a) TIEDTKE

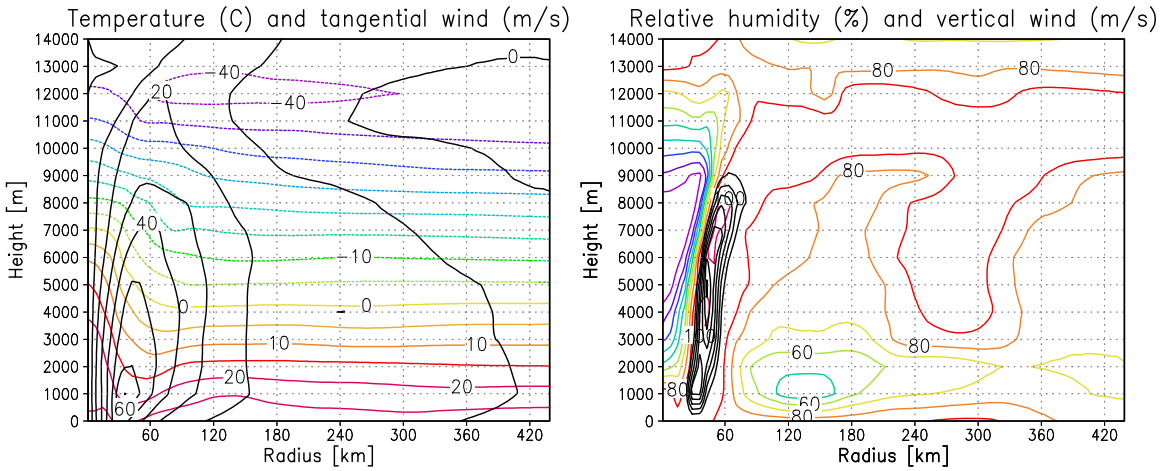

b) EXPLICIT

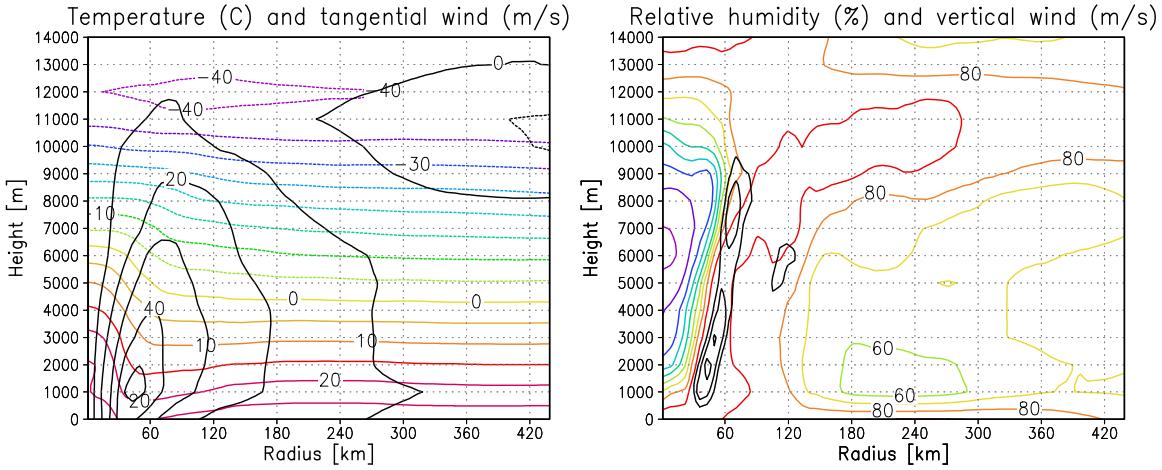

Figure 3: Azimuthal average of temperature (coloured isolines, left panel, contour interval 5°C), tangential wind (black isolines, left panel, contour interval 10m/s), relative humidity (coloured isolines, right panel, contour interval 10%), and vertical wind (black isolines, right panel, contour interval 0.2m/s) at t =108 hours for a) the Tiedtke run and b) the explicit run. Negative isolines are dashed.

(e. g. Anthes 1982). The center of the tropical cyclone moves only slightly and randomly in the horizontal plane. This result seems to be related to the simple f-plane geometry where no propagation of circular symmetric vortices occurs. The cyclone movement is a bit more pronounced in the explicit run than in the Tiedtke run.

Fig. 3 displays azimuthal averages of temperature, tangential wind, relative humidity and vertical velocity at t =108 hours. In both cases the cyclone has a warm and dry eye where the relative humidity is below 10%. This low value stems from adiabatic warming caused by the downward motion in the eye. Liu et al. (1997) also found such low values in their numerical simulations. The maximum of tangential wind appears at a height of z = 1000 m and inside of 50 km radius. The wind decreases with increasing height with an outward slope of the wind maximum. This can be understood by the thermal wind balance since the isotherms indicate a temperature front that also slopes outward with increasing height. The

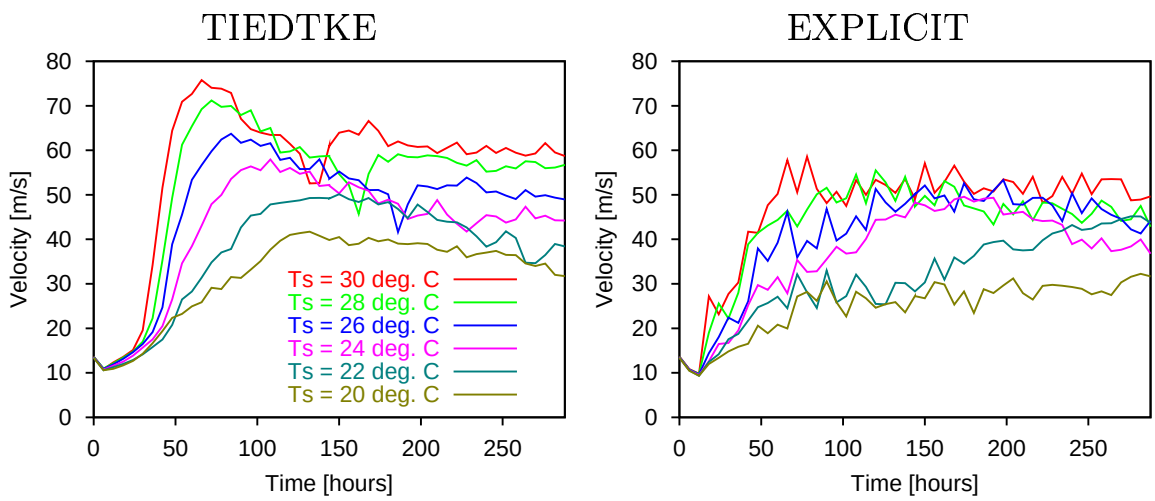

Figure 4: Maximum of wind at the lowest model level as a function of time for various sea surface temperatures. The left panel displays results for the Tiedtke runs and the right panel those for the explicit runs.

vertical wind has a maximum near the radius of maximum wind. Another maximum is seen in the explicit run which is associated with the spiral band detected in Fig. 2. Note that a substantial amount of the vertical velocity amplitude vanishes due to azimuthal averaging. In summary the basic structure of the azimuthally averaged cyclone in the Tiedtke run resembles that of the explicit run. However, the simulated cyclone of the explicit run has a larger eye and less strong tangential and vertical winds in the azimuthal mean.

4 Sensitivity to surface temperature, initial amplitude and humidity

In this section the sensitivity of tropical cyclogenesis to some model parameters is described. Fig. 4 displays the development of the maximum wind at the lowest model level for various surface temperatures. The maximum wind may be interpreted as a storm intensity. Obviously, the growth rate and the maximum storm intensity increases with increasing surface temperature in the Tiedtke experiments. This result coincides with the observational fact that tropical cyclones only occur over warm ocean surfaces. However, the LM with the Tiedtke closure exhibits the development of a cyclone with hurricane force winds even for $T_s = 20°\mathrm{C}$. In nature, tropical cyclogenesis is only observed for temperatures larger than 26.5°C. A gradual increase of maximum storm intensity to increasing surface temperature is not obvious in the explicit simulations. Until 150 hours the winds remain slightly below the lower limit of a hurricane (32.7 m/s) for $T_s = 20°\mathrm{C}$ and $T_s = 22°\mathrm{C}$ while the other simulations reveal the development of a tropical cyclone with strong surface winds of about 50 m/s. Until this time there seems to exist a threshold between 22°C and 24°C for the development of a hurricane. Later on, however, the vortex for $T_s = 22°\mathrm{C}$ also attains hurricane strength.

Fig. 5 shows the response to the initial vortex amplitude that is controlled by the parameter Δp. It is seen that the initial vortex amplitude acts to accelerate the development while the maximum storm intensity is relatively unaffected. In one case (explicit run with $\Delta P = 1\mathrm{hPa}$) no growth takes place at all. This can be explained by the missing ability of the initial cyclone to lift the air to the level of condensation. Indeed, condensation does not take place in this simulation. In contrast, the Tiedtke convection scheme can cause condensation even when no air parcel reaches the level of condensation.

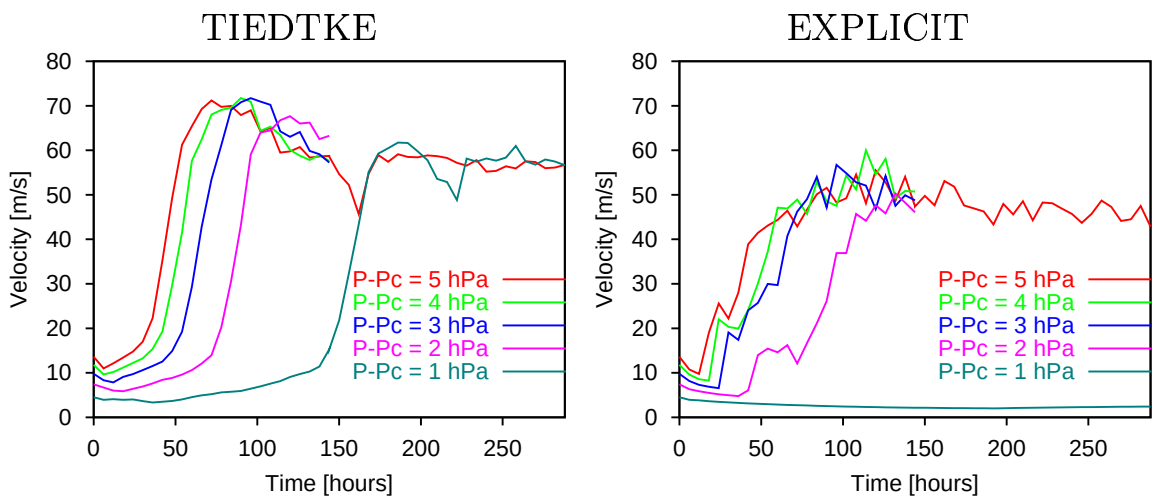

Figure 5: As in Fig. 4 but for various values of the initial surface pressure difference between vortex center and environment.

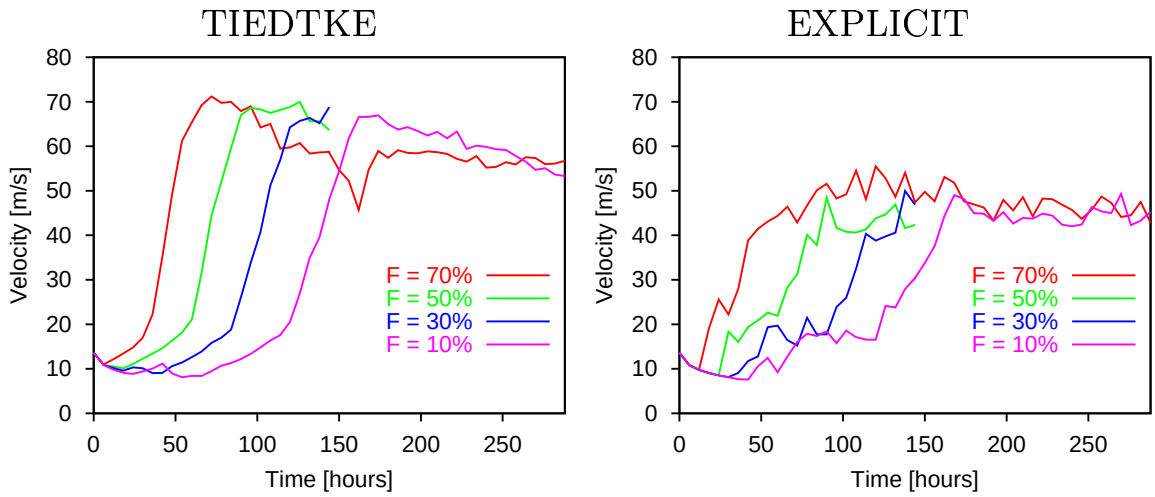

Figure 6: As in Fig. 4 but for various values of the initial relative humidity.

Fig. 6 displays the sensitivity of the development to initial relative humidity. A decrease in initial relative humidity leads to a delay of the development and again, the maximum intensity does not depend upon the varied parameter. Even in the very dry case of 10% initial relative humidity the model exhibits the development of a tropical cyclone. This fact can be explained by the evaporation from the sea surface that causes convective destabilization sooner or later.

5 Conclusion

The experiments reveal the ability of the LM to simulate the evolution and structures of a tropical cyclone realistically. The simulated mature cyclone has a warm and dry core which is surrounded by an eyewall with intense vertical motion. Asymmetries from the circular symmetry like spiral bands are more pronounced in the simulation with explicit convection than in the corresponding simulation involving the Tiedtke mass flux scheme. The intensity of the storm simulated with the Tiedtke closure is somewhat larger than without parameterization. Possibly, this can be explained by the larger degree of circular

symmetry leading to a better efficiency in converting the latent heat release to kinetic energy. Indeed, the maximum potential intensity theory for tropical cyclones (Emanuel 1995) is based on the assumption of axisymmety. Further experiments show that the maximum storm intensity increases with increasing surface temperature while it is relatively insensitive to the initial vortex strength and humidity except for one case in which condensation does not take place. On the other hand the development is accelerated with increasing initial strength and humidity. A threshold behaviour with respect to the surface temperature is only indicated in the explicit simulation results. However, the threshold value still seems to be too low when compared to statistics of observed tropical cyclones. In summary, it can be stated that the LM simulates the tropical cyclones somewhat more reasonably when no parameterization of convection is used. Possibly, a higher horizontal resolution may lead to more realistic results.

At a surface temperature of 28°C the occurrence of condensation and convective instability seems to be the only criterion for the development of a tropical cyclone in the idealized experiments presented here. In the real atmosphere, the criterions for the development are much more restrictive (see McBride and Zehr 1981). It is not clear so far wether this disagreement results from the unrealistic high degree of idealization in the experiments or from the weakness of the LM to forecast a non-developing tropical depression. This question remains as a prospect for future research.

Acknowledgments

The author thanks the DWD (Deutscher Wetterdienst) for making the LM available and the DKRZ (Deutsches Klimarechenzentrum) for the possibility to perform calculations on their NEC SX-6 high performance computer.

References

Anthes, R. A., 1982: Tropical cyclones - their evolution, structure, and effects. *Meteorol. Monogr.*, **41**, 208pp.

Davies, H., 1976: A lateral boundary formulation for multi-level prediction models. *Quart. J. R. Met. Soc.*, **102**, 405-418.

Emanuel, K. A., 1995: Sensitivity of tropical cyclones to surface exchange coefficients and a revised steady-state model incorporating eye dynamics. *J. Atmos. Sci.*, **52**, 3969-3976.

Holland, G. J., 1980: An analytic model of the wind and pressure profiles in hurricanes. *Mon. Wea. Rev.*, **108**, 1212-1218.

Liu, Y., D. L. Zhang and M. K. Yau, 1997: A multiscale numerical study of hurricane Andrew (1992). Part I: Explicit simulation and verification. *Mon. Wea. Rev.*, **125**, 3073-3093.

McBride, J. L., and R. Zehr, 1981: Observational analysis of tropical cyclone formation. Part II: Comparison of non-developing versus developing systems. *J. Atmos. Sci.*, **38**, 1132-1151.

Steppeler, J., G. Doms, U. Schättler, H. W. Bitzer, A. Gassmann, U. Damrath, 2003: Meso-gamma scale forecasts using the nonhydrostatic model LM. *Meteorol. Atmos. Phys.*, **82**, 75-96.

Tenerelli, J. E., and S. S. Chen, 2002: Intensity change and eyewall replacement in hurricane Floyd (1999). Extended Abstract, *25th Conference on Hurricanes and Tropical*

Meteorology, San Diego.

Tiedtke, M., 1989: A comprehensive mass flux scheme for cumulus parameterization in large-scale models. *Mon. Wea. Rev.*, **117**, 1779-1800.

Wang, Y., 2001: An explicit simulation of tropical cyclones with a triply nested movable mesh primitive equation model: TCM3. Part I: Model description and control experiment. *Mon. Wea. Rev.*, **129**, 1370-1394.

Willoughby, H. E., J. A. Clos and M. G. Shoreibah, 1982: Concentric eye walls, secondary wind maxima, and the evolution of the hurricane vortex. *J. Atmos. Sci.*, **39**, 395-411.

Evaluation of the Two-Way Nesting Version of LM at HNMS

E. Avgoustoglou and I. Papageorgiou

Hellenic National Meteorological Service, Athens, Greece

1 Introduction

Athens Olympics of 2004 provide with an outstanding opportunity for test, and consequently operational use, of local non-hydrostatic numeric weather prediction models of very high resolution (< 3 km). Based on the first version of the two-way nesting version of the Local Model (LM2WN) [Ref. 1], some representative cases are examined for the wider Attica area at the horizontal grid of 2.3 Km against the results of the latest operational version of LM at 7 Km horizontal grid as well as observations. All the runs were performed at ECMWF using the IBM supercomputing system based on the POWER 4 processor.

2 Code outline and results

The main idea of the LM2WN code is based on the parallel run of the LM both for one coarse and one (or more) horizontally finer grid domains "nested" within this coarse domain. A numerical feedback between the results enters after the finite number n of integration time steps t/n of the fine domain equals the integration time step t of the coarse grid domain. In our tests, we took $t = 30$ sec and $n = 3$. Also the horizontal grid size for the coarse domain was $x_{coarse} = 7$ Km and for the fine domain was $x_{fine} = 2.3$ Km. In Figure 1, we present the algorithm flowchart of the LM2WN following Rimann [Ref. 1] where a detailed description of the method is given. The numerical scheme is based on the MM5 two-way nesting option as described in [Ref. 2]. The coarse grid domain given in Figure 2a covers the wider area of

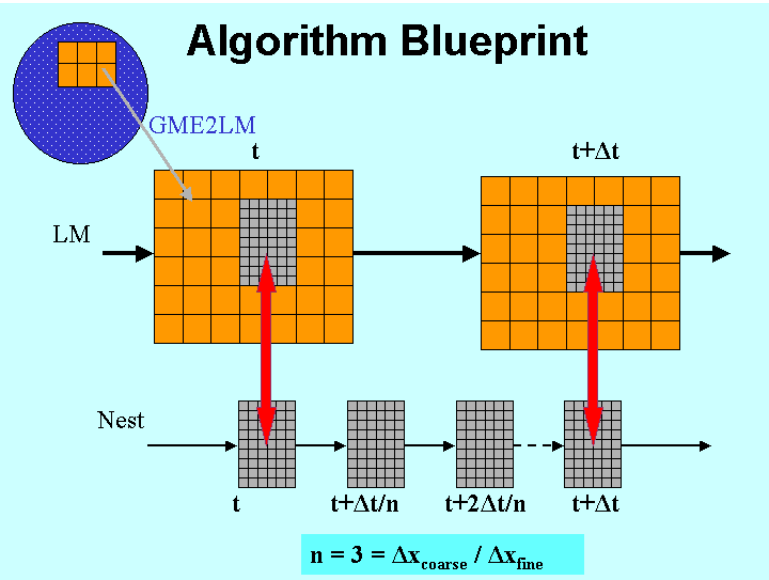

Figure 1: Algorithm flowchart

Greece as it stems from 7 Km horizontal grid. The blue frame defines the fine grid domain

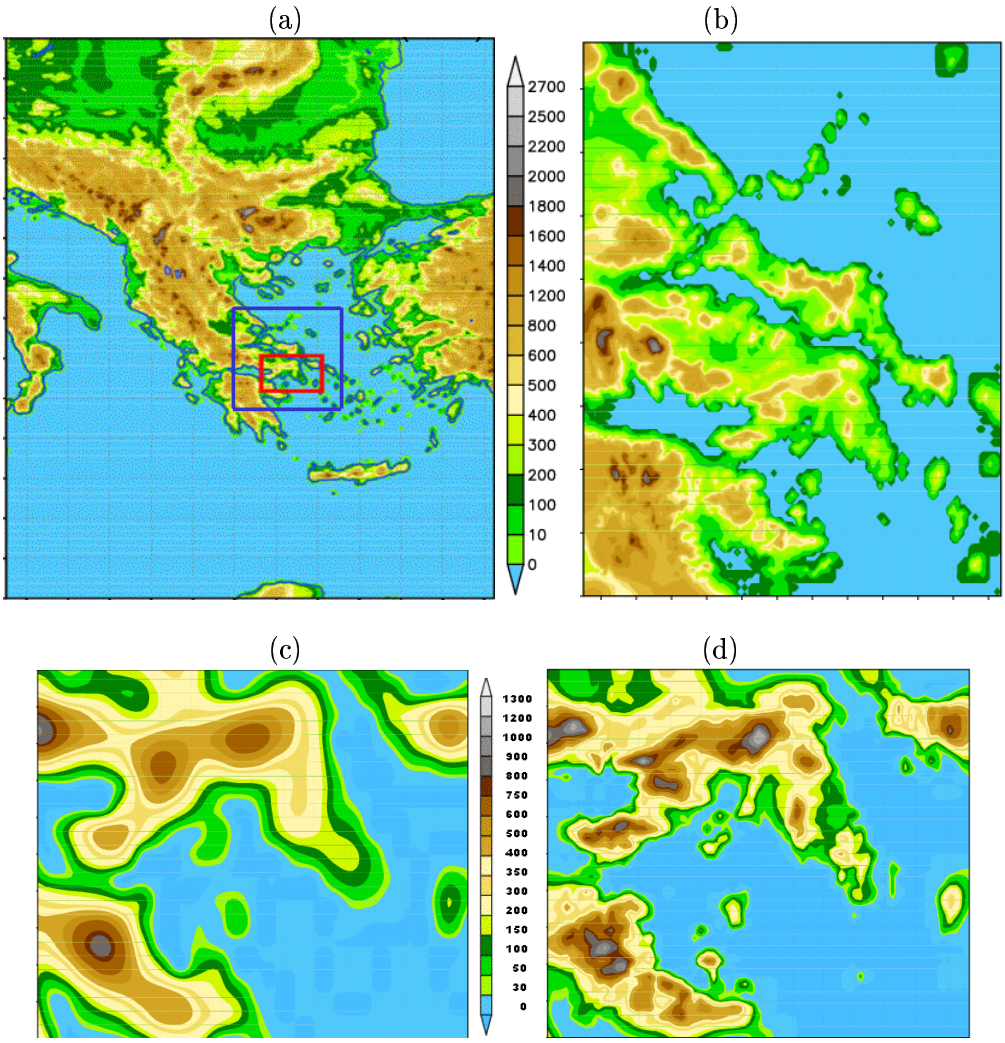

Figure 2: Domain orography for Greece (a), Attica (c) in 7 Km grid size and for Nest (b) and Attica (d) in 2.3 Km grid size.

that encloses Attica, which is the main area of interest and is enclosed with the red frame. In Figure 2b, the fine grid domain is given with orography at 2.3 Km horizontal grid size. In Figures 2c and 2d, we present the orography of Attica at 7 Km and 2.3 Km horizontal grid size respectively.

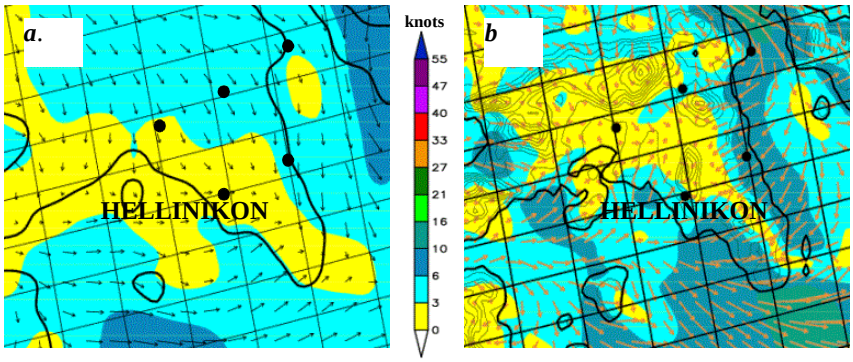

Figure 3: 10–meter winds for August 25 2003 in Attica, (a) coarse grib, (b) fine grid.

Although reservations have been raised regarding the status of LM2WN [Refs 4 and 6], it has been considered of interest to test the code under some weather patterns developed in

the area of Attica during the summer period. In Figures 3a and 3b, we show the 10-meter winds for August 25 2003 at 12 UTC from the regular LM at 7 Km and the LM2WN at 2.3 Km grid respectively (24 hours forecast). During this day see breeze conditions in the area of Hellinikon were developed. The hourly 10-meter wind sequence is presented in Figure 4.

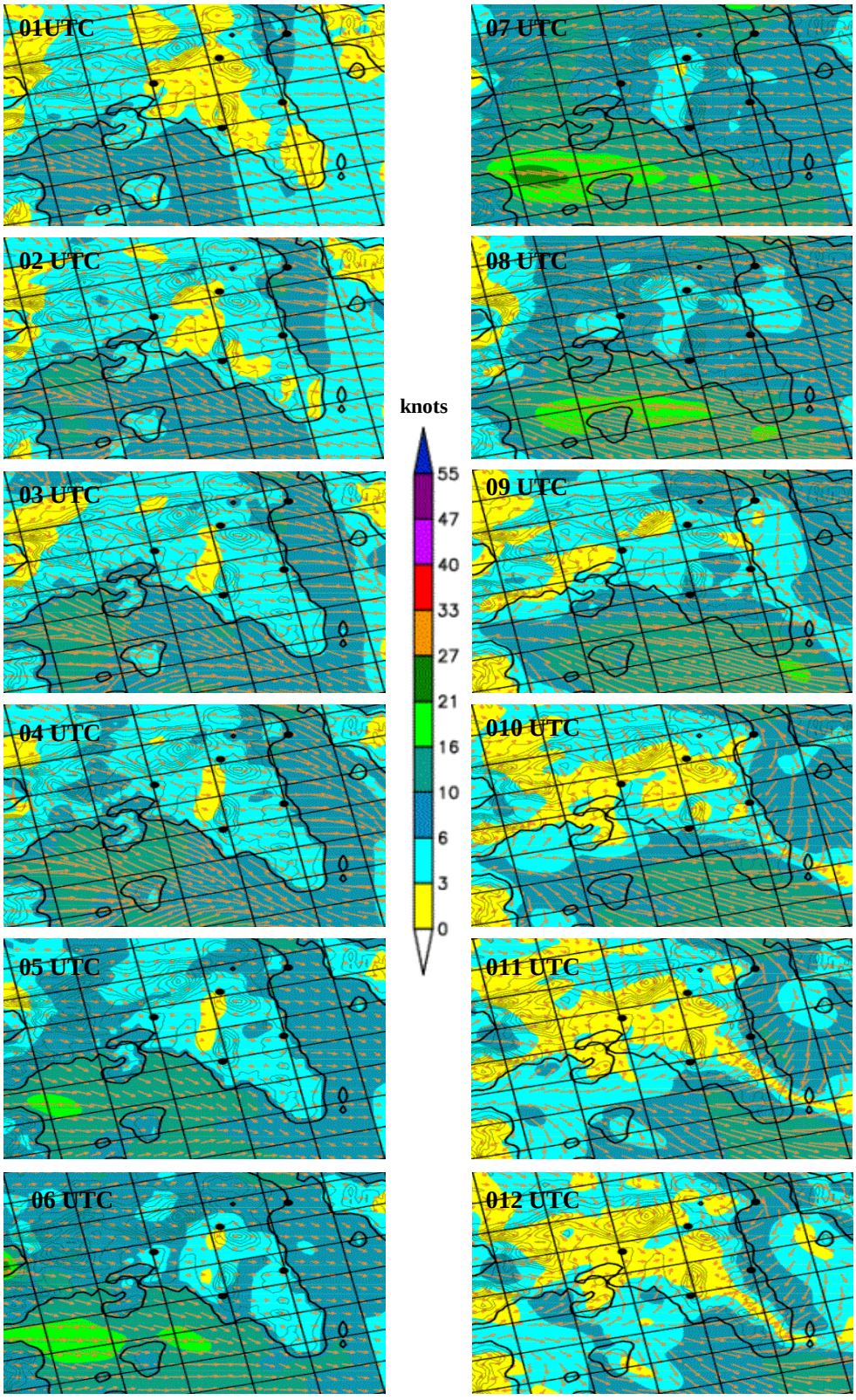

Figure 4: continued

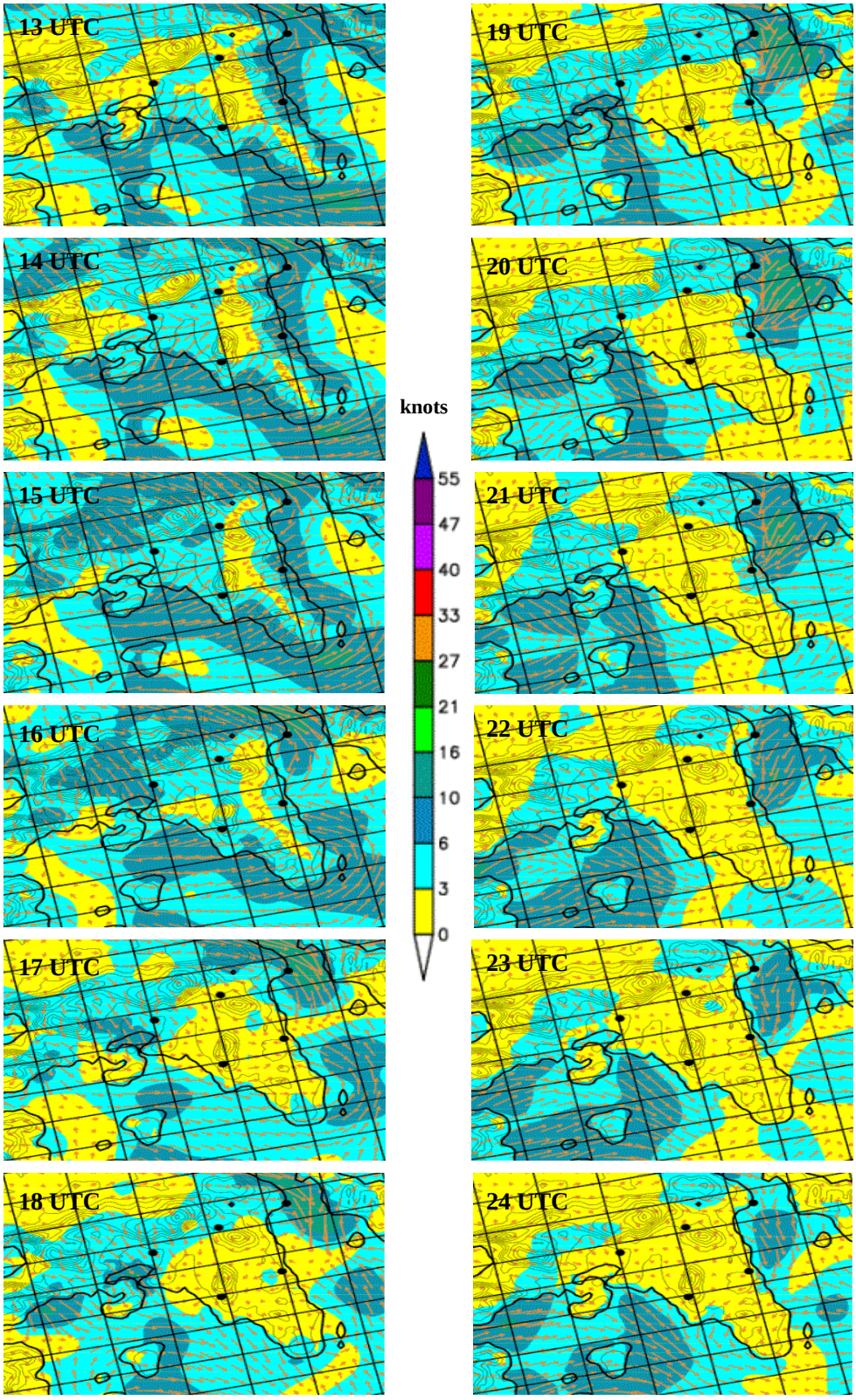

Figure 4: Hourly 10–meter wind development for Attica (fine grid) in August 25 2003.

In Figures 5a and 5b, we show the 10-meter winds for August 07 2003 at 12 UTC from regular LM at 7 Km and the LM2WN at 2.3 Km grids respectively (24 hours forecast). During this day, northern winds (Etesians) with range up to 20 knots prevailed over the whole Attica area. Comparisons of the nearest point results with METAR observations are

given in Tables 1 and 2 for Hellinikon and Schinias Meteorological Stations respectively and for 24 hour forecast. The parameters considered are 10-meter wind direction (DIR) and intensity (SPD) as well as 2m Temperature (2T). In each column forecasted/observed values are listed.

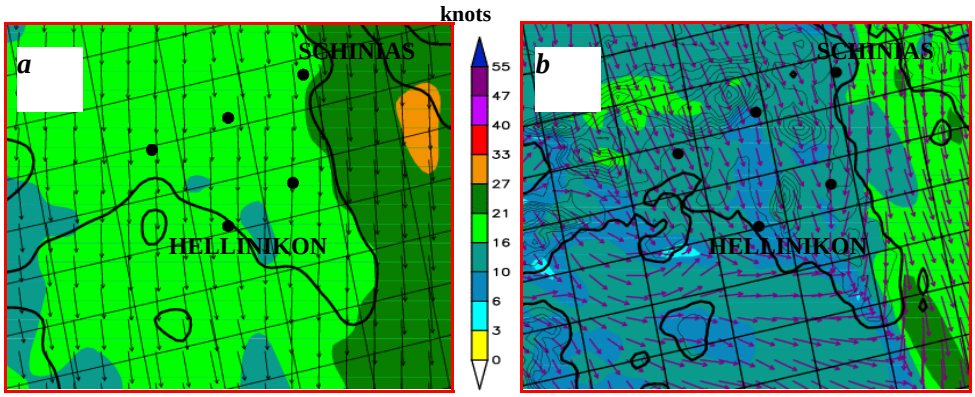

Figure 5: 10–meter winds for August 25 2003 in Attica, (a) coarse grid, (b) fine grid.

HELLINIKON 2003 AUGUST 07
00 UTC + HOUR

[HOUR]	[DIR(degs)]	[SPD(kts)]	[2T(°C)]
00	[335/360]	[08/11]	[25/27]
01	[340/360]	[06/16]	[22/27]
02	[355/360]	[05/13]	[20/27]
03	[345/360]	[04/11]	[19/27]
04	[350/360]	[04/12]	[17/26]
05	[355/010]	[05/14]	[18/27]
06	[345/010]	[05/12]	[22/28]
07	[335/360]	[07/18]	[26/30]
08	[335/020]	[07/15]	[29/31]
09	[330/020]	[07/18]	[31/32]
10	[320/010]	[07/20]	[34/32]
11	[325/020]	[07/18]	[35/33]
12	[335/360]	[09/16]	[35/33]
13	[340/360]	[09/15]	[35/33]
14	[340/030]	[09/12]	[34/33]
15	[340/020]	[08/14]	[32/32]
16	[350/020]	[07/14]	[30/31]
17	[360/360]	[06/15]	[27/30]
18	[005/010]	[06/13]	[23/29]
19	[005/350]	[07/11]	[21/28]
20	[360/360]	[07/12]	[20/28]
21	[360/360]	[06/13]	[19/28]
22	[005/360]	[06/17]	[18/27]
23	[005/360]	[06/15]	[17/27]

Table 1

SCHINIAS 2003 AUGUST 07
00 UTC + HOUR

[HOUR]	[DIR(degs)]	[SPD(kts)]	[2T(°C)]
00	[345/350]	[10/14]	[25/26]
01	[335/350]	[09/14]	[22/26]
02	[340/360]	[08/13]	[21/26]
03	[345/360]	[09/11]	[19/26]
04	[335/360]	[08/11]	[19/25]
05	[325/360]	[07/14]	[19/26]
06	[325/360]	[09/13]	[23/27]
07	[340/360]	[12/14]	[27/28]
08	[345/010]	[14/16]	[29/29]
09	[350/010]	[14/17]	[30/29]
10	[345/010]	[13/17]	[31/30]
11	[350/360]	[13/13]	[32/30]
12	[350/020]	[14/18]	[33/30]
13	[355/020]	[14/17]	[32/30]
14	[355/010]	[14/14]	[31/30]
15	[360/350]	[13/14]	[30/30]
16	[005/360]	[12/13]	[28/29]
17	[005/350]	[12/13]	[25/29]
18	[005/350]	[11/13]	[22/28]
19	[005/350]	[11/12]	[20/28]
20	[360/360]	[10/11]	[19/27]
21	[355/350]	[09/12]	[18/27]
22	[345/350]	[08/11]	[18/26]
23	[340/360]	[07/11]	[17/26]

Table 2

Finally, we present in Figures 6a and 6b the total accumulated precipitation 06-18UTC for August 18 2002 from regular LM at 7 Km and LM2WN at 2.3 Km grid size respectively (24 hours forecast) along with the observed values in mm.

3. Conclusions

From those cases as well as from several others that have been evaluated, mainly over the last year, LM2WN should be used cautiously for operational purposes. At this stage, from the test cases examined and from the issues raised in References 4 and 6, further insight needs to be gained both to the numerics and to the physics of the code.

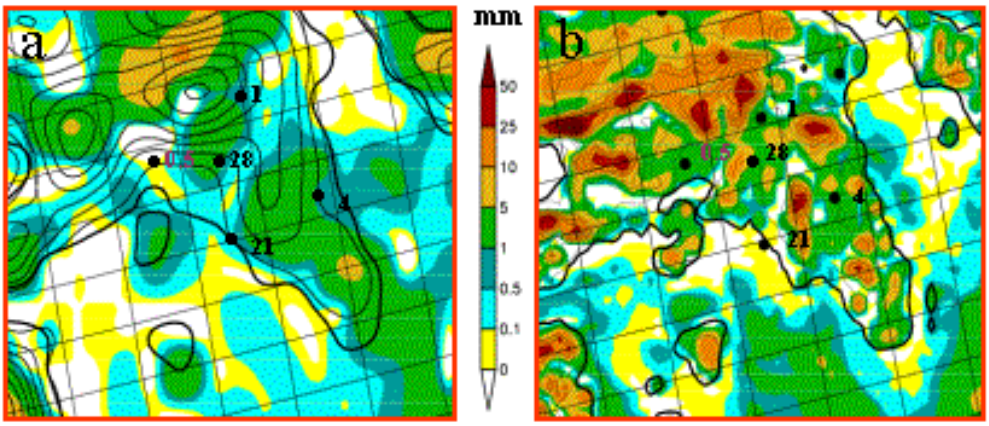

Figure 6: Accumulated precipitation (06–18) UTC for August 18 2002 in Attica, (a) coarse grid, (b) fine grid.

4. References

1. Jürgen Riβmann, Implementation of the two-way nesting option in the LM, DWD 2000 (unpublished) and references therein.

2. Grell, G. A. J. Dudhia and D. R. Stauffer. A description of the fifth-generation Penn/NCAR mesoscale model (MM5), NCAR Technical Note TN-398+STR 1994 122p.

3. E. Avgoustoglou and U. Schttler, The Two-Way Nesting Option in the LM, 3rd COSMO Meeting, Athens 3-5 October 2001 (Presentation).

4. E. Avgoustoglou, Status of the nesting option in the LM, LM-Users Seminar, BTZ Langen Germany, March 31 2003 (Presentation).

5. E. Avgoustoglou and I. Papageorgiou, Evaluation of the LM two-way nesting option during the recent Olympic Test Events in Greece, 5TH COSMO Meeting, Langen 24-26 September 2003 (Presentation).

6. M. Milelli, Analysis of the performance of the Two-Way Nesting Version of LM on Idealized Test Cases, 5TH COSMO Meeting, Langen 24-26 September 2003.

Real-Time Direct Link Between Meteorolocical- and Dispersion Models

Andrzej Mazur

Institute of Meteorology and Water Management,
Centre for Development of Numerical Weather Forecasts
61 Podlesna str., PL-01673 Warsaw, Poland

Introduction

Poland is one of the largest emitters of various pollutants in Europe. This leads to serious contamination of natural environment in this country. Moreover, more than ten large nuclear installations (reactors) are located in the closest vicinity of Poland (see Fig. 3). This situation requires a tool for decision-support in case of nuclear incident. The research presented here is a part of more general, long-term modelling project and its possible application to the problem of short-time emission incidents. Author attempted to establish the on-line link between meteorological model (COSMO-LM) and dispersion model (REMOTA - REgional MOdel for Atmospherical Transport of pollutants).

Models

1. Meteorological model is currently running in an operational manner at the Mesoscale Modelling Group at IMWM. It produces 72-hour forecasts of meteorological fields needed for the dispersion model, such as wind, precipitation intensity, cloud cover etc. The fields are two-dimensional (cloud cover or precipitation) or three-dimensional (e.g. wind or temperature) – from multiple levels [1]. For the dispersion model, also the eddy diffusivity coefficient is required. This is calculated using meteorological model results as input, with procedures developed by the Team for Modelling the Atmospheric Transport of Pollutants at IMWM, on the basis of PBL (Planetary Boundary Layer) Model from Washington University.

2. REMOTA is a simulation model, whish simulates the dispersion of multiple pollutants. The processes such as horizontal advection, vertical diffusion, dry deposition and wet removal are accounted for in the model. The governing equations are solved in the terrain-following co-ordinates. The numerical solution is based on the discretization applied on a staggered grid. Conservative properties are fully preserved by the discrete model equations. Advective terms in the horizontal directions are treated with the Area Flux Preserving method (Bott's type scheme) with boundary conditions assumed zero at incoming and "open" at outcoming flows; vertical turbulent diffusion – with the implicit Crank-Nicholson?s scheme. The bottom boundary condition is the dry deposition flux, while the top boundary condition is "open". Dry deposition velocity is postulated as a function of terrain roughness, friction velocity and diameter of a particle according to Sehmel's model, while washout ratio is assumed constant, but different for each pollutant.

Link Description

The meteorological (LM) and dispersion (DM) models are interacting via IMWM Intranet. The results from the LM model (meteorological fields) are available on separate server and

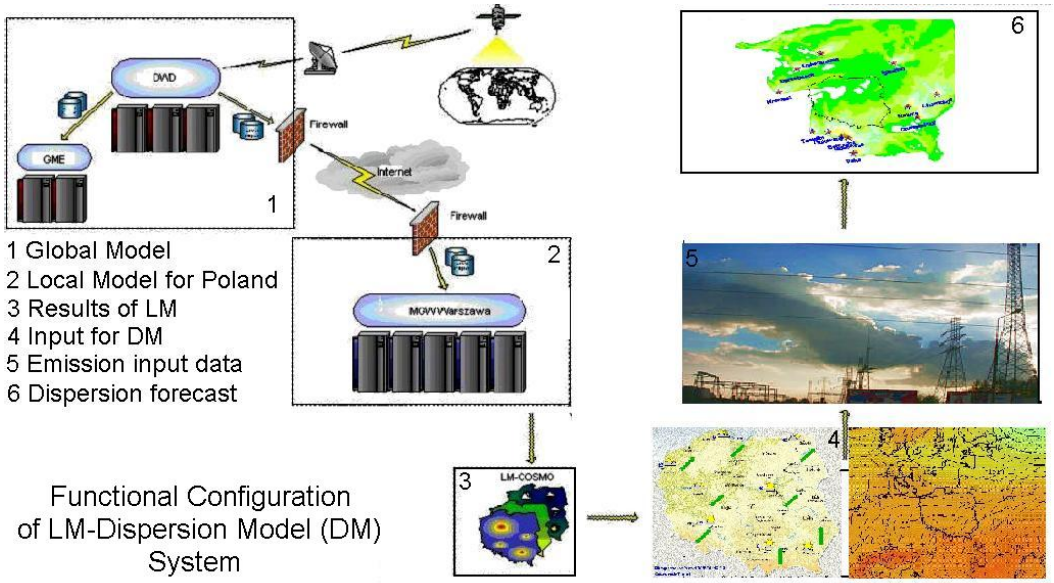

Figure 1: Functional configuration of LM-DM system.

path, accessible for DM preparation module. Once the results are ready (twice a day), it is possible to retract the necessary fields and to prepare meteorological input files for the DM. This retraction is fully automatic and depends only on the current date and time. Then, also in an automatic way, the full DM run (78 hours forecast with 27 output records) is performed.

Dispersion Model Description

The three-dimensional, Eulerian DM model is based on similar model for Europe [2, 3]. The numerical grid system for this particular study consists of 193×161 cells of the size of about 14×14 km and five vertical levels. The model is composed of three main modules; the first sets parameters of the model (i.e. local deposition coefficient, washout ratio, dry deposition velocity), the second solves the advection-diffusion equation, and the last prepares output files for graphical presentation and statistical analysis. During a simulation, the program reads user-defined parameters, then it begins the main loop of calculations: reads all necessary input data (emissions, meteorological fields etc.), performs computations (advection, diffusion, deposition) and stores the results (if required). The governing transport equation is solved using the Area Flux Preserving method (horizontal advection, [4]) and a Crank-Nicholson method (vertical diffusion). In each time step, current concentration field is computed followed by total deposition (sum of dry and wet).

Results

a)
The first model runs (tests in a small domain, 14-km grid, 57 × 51 nodes) produced concentration and deposition patterns for pollutant (chemically inert, for instance, primary dust) emitted from the high source located close to the centre of the model domain. This case represents the situation of short-term incident due to "emission catastrophe" of some sort. The patterns are shown in Figure 2.

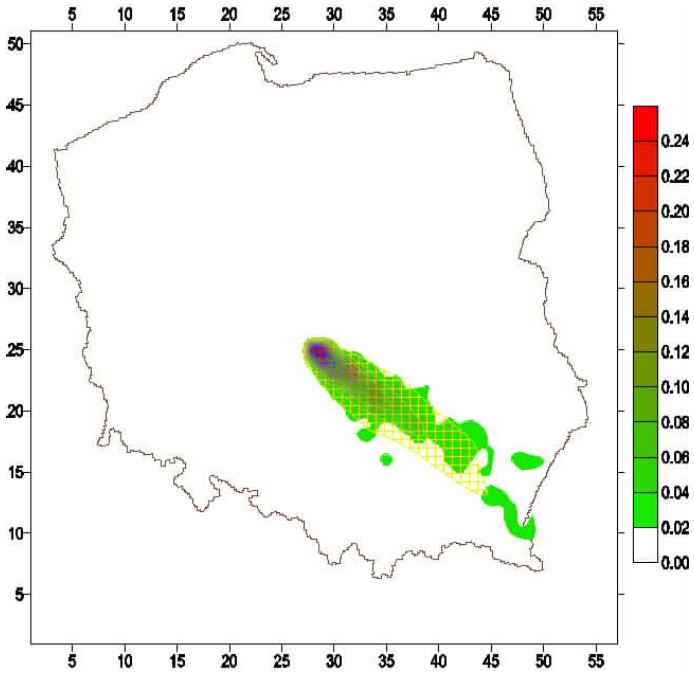

Figure 2: Model results - concentration and deposition (relative units) of test pollutant emission from February 9^{th}, 2003 until February 11^{th}, 2003.

b)
As it was mentioned earlier, more than ten large nuclear power plants (some build in the same manner as Chernobyl reactor) are located in the vicinity of Polish territory. Therefore, actual configuration for real-time, on-line link between models should include the full LM model domain, covering almost entire Europe. In this way more than 90% of all European nuclear installations are in taken into account in the computations.

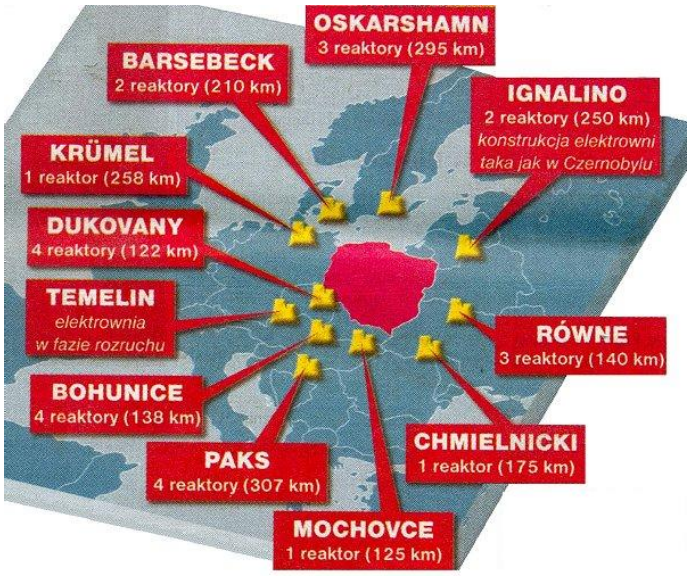

Figure 3: Nuclear installations in the vicinity of Poland (www.atomowe.kei.pl).

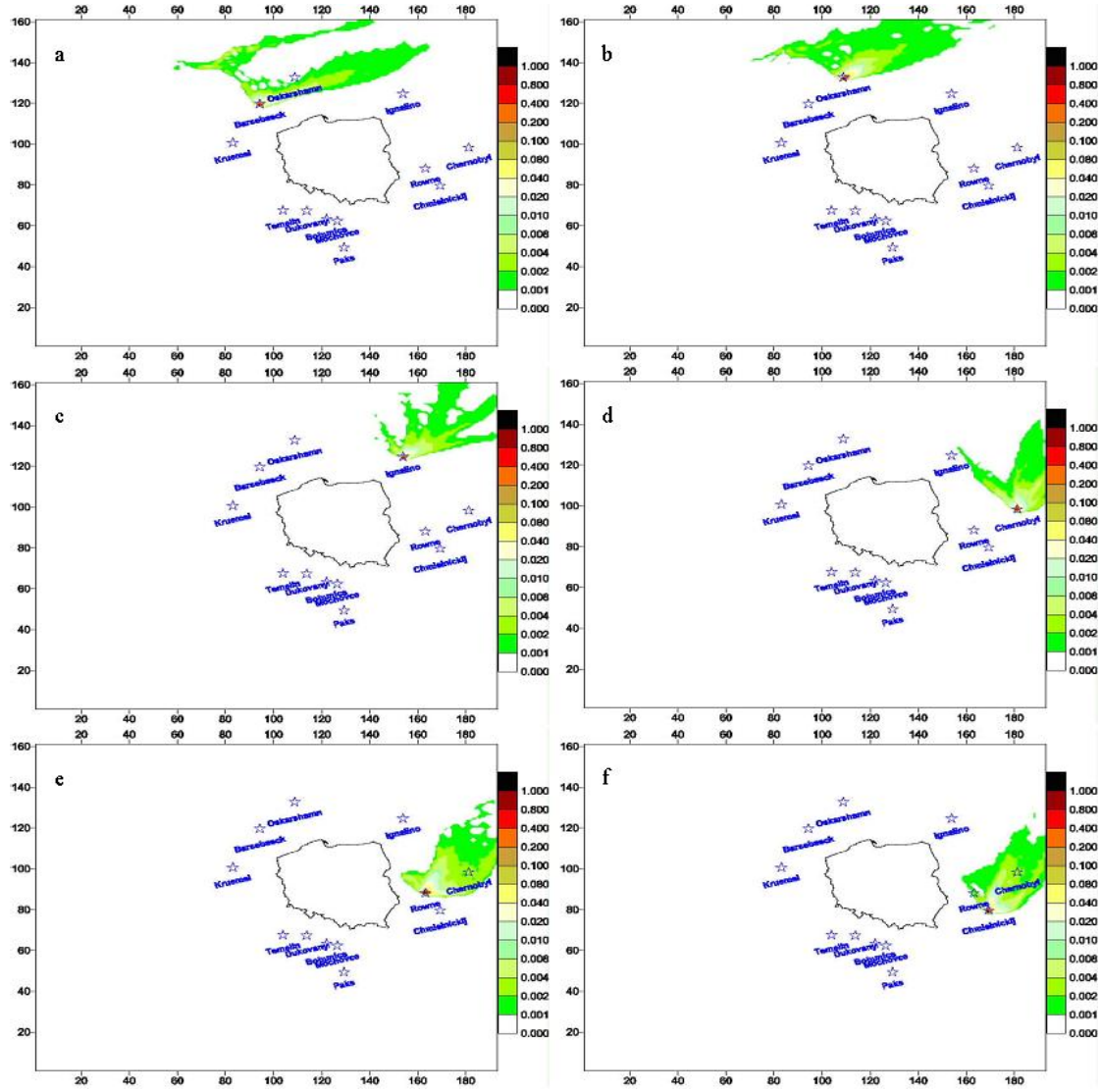

Figure 4: Dispersion of nuclear contamination in case of hypothetical accident in Barsebaeck (a), Oskarshamn (b), Ignalino (c), Chernobyl (d), Rowne (e) or Chmielnicki (f) Nuclear Power Plant. All forecasts valid for April 28^{th}, 2003 to May 1^{st}, 2003.

Following Figures 4 and 5 show the results of the simulations of hypothetical simultaneous accidents in all nuclear reactors in the closest vicinity of Poland. The results presented above were computed for rather symbolic date of April 28^{th}, but for 2003. They show that in the case of an accident even country without a nuclear power plant is not safe from serious contamination.

c)

Additional work has been done for implementation of ozone and acidifying agents, like NO, NO_2, PAN, HNO_3, NO_3, NH_4NO_3, NH_3, $(NH_4)_2SO_4$, SO_4 and SO_2 in the DM model. To cover all photochemical transformations that apply to ozone and NO_x/SO_x, one should use a chemical scheme with more than hundred reactions. So, as the first approximation of the problem, a simple scheme for the photochemistry (EMEP, 1993) was applied (EMEP, 1993) in DM (see Figure 6 below).

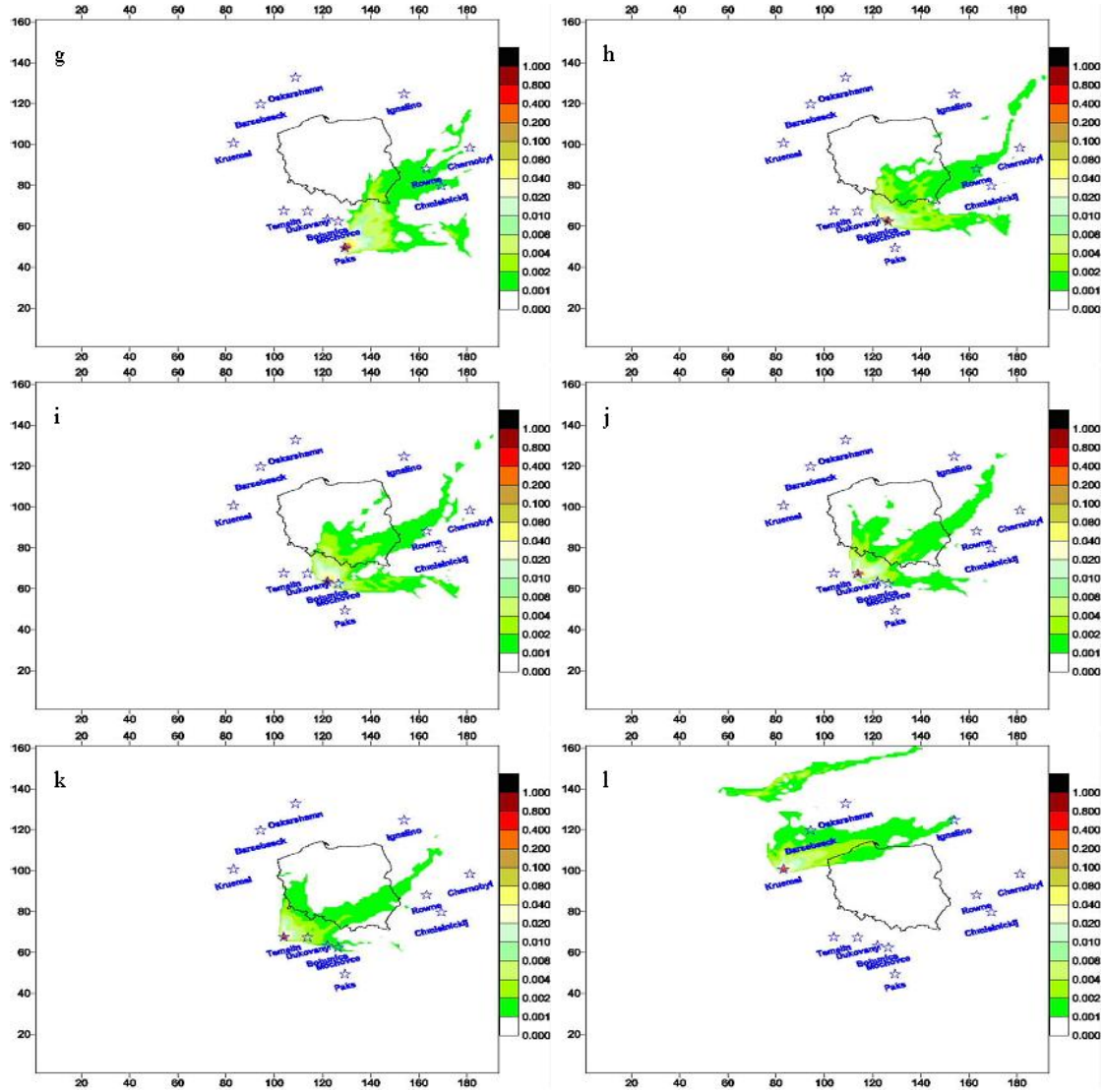

Figure 5: Dispersion of nuclear contamination in case of hypothetical accident in PAKS (g), Mochovce (h), Bohunice (i), Dukovany (j), Temelin (k) or Kruemel (l) Nuclear Power Plant. All forecasts valid for April 28^{th}, 2003 to May 1^{st}, 2003.

As an example of model performance concerning photochemical pollutants, the patterns of the deposition of nitrogen and sulphur and of concentration of ozone are presented in Figure 7. They are calculated for May 7^{th}, 2003 due to emission from fictitious source located in the centre of Poland.

Conclusions

The main results of this study can be summarized as follows:

- An operational link between meteorological model and dispersion model for Poland has been established and tested. It is efficient and seems to work well.
- An operational version of the dispersion model for atmospheric transport and deposition of pollutants emitted in short-term emission incidents or accidents. This model takes into account radioactive and photochemical pollutants.

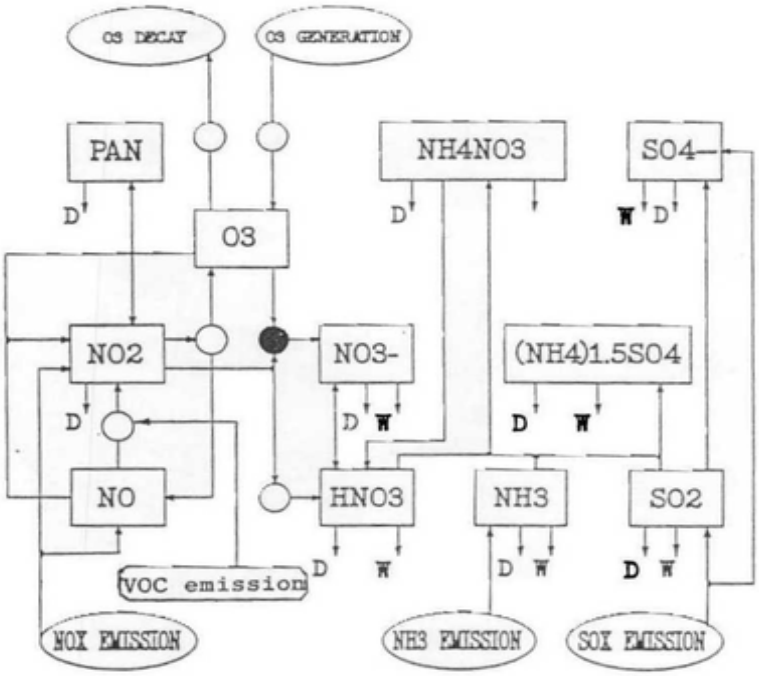

Figure 6: Physical- and chemical transformations for NO_x/SO_x cycle, combined with ozone formation and depletion. D - dry-, W - wet deposition, ∘ - photochemical- and • - dark phase reactions (EMEP, 1993).

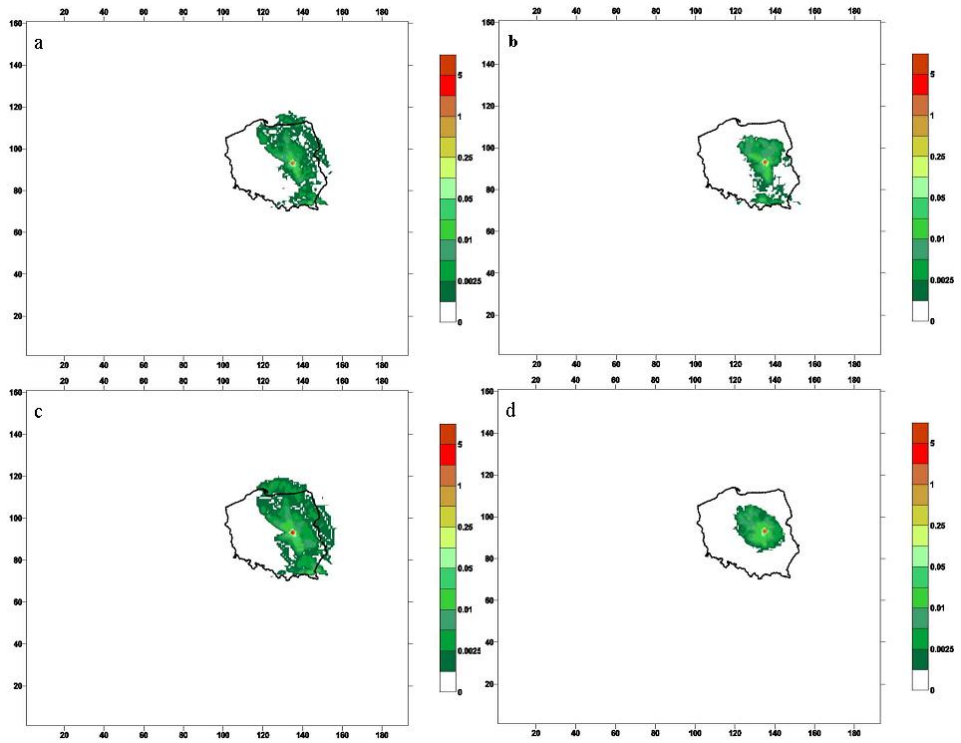

Figure 7: Deposition of oxidised (a) and reduced (b) nitrogen, deposition of sulphur (c) and concentration of ozone (d) due to emission from fictitious source located in the centre of Poland. Valid for: 07.05.2003 - 78 hours forecast. Deposition in relative units (mass deposited/mass emitted, %). Concentration units - ppbs over mean annual value of O_3 concentration.

This particular application of meteorological and dispersion (LM+DM) model, conneted online, can serve as a first estimate of a system simulating dispersion of dangerous pollutants emitted into the atmosphere during serious accidents. This system will be further improwed at IMWM.

References

1. Bartnicki J. (1986) An efficient positive definite method for the numerical solution of the advection equation. IIASA Working Paper WP-86-35, Institute for Applied Systems Analysis, Laxenburg, Austria.

2. Bartnicki J . (1991) Long range transport of heavy metals from Poland computed by an Eulerian model, in: van Dop H., Steyn D.G. (Eds.) *Air pollution modelling and its application VIII.* Plenum Press, pp. 339-348.

3. Bartnicki J., Modzelewski H., Bartnicka-Szewczyk H., Saltbones J., Berge E. and Bott A. (1993) *An Eulerian model for atmospheric transport of heavy metals over Europe: Model development and testing.* Techn. Report 117, Norwegian Meteorological Institute, Oslo, Norway.

4. Bott A. (1989) A Positive Definite Advection Scheme Obtained by Nonlinear Renormalization of the Advective Fluxes. *Mon. Wea. Rev.* 117, 1006-1015.

5. Hrehoruk J., Bartnicki J., Mazur A., Grzybowska A., Modzelewski H., Frydzinska B. and Bartnicka H. (1992) Modelling the Transport of Air Pollution. IMWM Tech. Report P-7 (in Polish).

6. Hrehoruk J., Grzybowska A., Mazur A., Frydzinska B., Bartnicki J., Modzelewski H. and Bartnicka H. (1993) Regional Model for Atmospheric Transport of Heavy Metals over Poland. IMWM News, 3.

7. Brashers, B. (1997) web page "readme" file (from pbl-lib@atmos.washington.edu)

8. Doms, G. and Schaettler, U. (2000) The Nonhydrostatic Limited-Area Model LM (Lokal-Modell) of DWD. Scientific Documentation. DWD documents.

9. Schaettler, U. and Doms, G. (2000) The Nonhydrostatic Limited-Area Model LM (Lokal-Modell) of DWD. Implementation Documentation. DWD documents.

10. Schaettler, U. and Doms, G. (2000) The Nonhydrostatic Limited-Area Model LM (Lokal-Modell) of DWD. User Guide. DWD documents.

11. EMEP, 1993: Annual Report (September 1992 - August 1993). EMEP, MSC-E, Moskwa, 1993.

12. Malik S., Simpson D., Hjellbrekke A.-G. and Simpson H., 1996: Photochemical model calculations over Europe for summer 1990. Model results and comparison with obserwations. EMEP/MSC-W Report 2/96, July 1996, Oslo, Norway.

10 Collaboration and External Users of LM

All national weather services of COSMO are members of EUMETNET, the network of meteorological services within Europe. EUMETNET provides a framework to organize co-operative programmes between the Members in the various fields of basic meteorological activities such as observing systems, data processing, basic forecasting products, research and development, and training (*www.eumetnet.eu.org*). COSMO's activities are embedded in this network and are especially related to EUMETNET programmes such as MAP-NWS (Mesoscale Alpine Programme - National Weather Services) and EUCOS (EUMETNET Composite Observing System).

Since the 1st of January 2000, EUMETNET provides a Coordinator for the SRNWP (Short Range Numerical Weather Prediction) Group. Representatives of the NWP branches of European National Meteorological Services meet in this group on a yearly basis to organize co-operative activities in development of numerical atmospheric models. The present SRNWP-coordinator is J. Quiby from MeteoSwiss. Within the SRNWP Group, Lead Centres have been selected for different topics. The Lead Centres have the responsibility to organize intercomparisons, workshops and to ensure the flow of information between participants. DWD has taken the role as the Lead Centre for Nonhydrostatic Modelling (responsible for this LC is Jürgen Steppeler from DWD). For more information on SRNWP and its Lead Centres see *http://srnwp.cscs.ch*.

All COSMO partners are also members of EWGLAM (European Working Group on Limited Area Modelling). This group meets once a year to exchange information on the current status and on recent developments in high-resolution numerical weather prediction.

Another type of collaboration with other European meteorological services is via COST, an intergovernmental framework for European *Co-operation in the field of Scientific and Technical Research*, allowing the co-ordination of nationally funded research on an European level (for more information about COST see *www.netmaniacs.com/cost*).

10.1 International Projects

This section lists the current participation of COSMO partners in international research projects which are related to LM. This list will be updated in the forthcoming issues.

- **COST 717** *Use of Radar Observations in Hydrological and NWP models.*
  Type: COST concerted research action
  MeteoSwiss contribution: *Chairmanship of COST 717 Action (A. Rossa).*
  DWD contribution: *Chairmanship of COST 717 Working Group 2: Using radar observations in parameterisation and validation of atmospheric models (D. Frühwald).*
  MeteoSwiss contribution: *Assimilation of three-dimensional radar reflectivities into a non-hydrostatic NWP model.*
  DWD contribution: *Development of an on-line adjustment scheme.*
  Information: www.smhi.se/cost717

- **COST 716** *Exploitation of Ground-Based GPS for Climate and Numerical Weather Prediction Applications.*
  Type: COST concerted research action
  MeteoSwiss/University of Berne contribution: : *Impact study with aLMo.*
  DWD contribution: *Validation of integrated water vapour from ground-based GPS observations and their assimilation in the LM of DWD.*

Information: www.oso.chalmers.se/geo/cost716.html

- **CLOUDMAP 2** *Validation and assimilation of cloud properties derived from ground based and satellite observations in NWP and climate models.*
  Type: EU project with funding
  MeteoSwiss contribution: *Use of cloud water content derived from 3-dim cloud observations in very high resolution LM runs.*
  Information: www.photogrammetry.ethz.ch/research/cloudmap/cloudmap.html

- **EFFS** *An European Flood Forecasting System.*
  Type: EU-project with funding.
  DWD contribution: *Hindcasting of flood events, input to flood forecasting models, analysis of precipitation (24-h totals) based on rain gauge data and radar estimates.*
  Information: http://effs.wldelft.nl

- **ELDAS** *Development of an European Land Assimilation System to Predict Floods and Droughts.*
  Type: EU-project with funding.
  DWD contribution: *Design and application of a variational assimilation scheme.*
  Information: http://www.knmi.nl/samenw/eldas

- **EUCOS** *EUMETNET composite observing system.*
  MeteoSwiss contribution: *Impact studies (OSE) with aLMo for SYNOP data.*
  Type: EUMETNET project
  Information: www.eucos.net

- **SEAROUTES** *Advanced Decision Support for Shiprouting Based on Full-Scale Ship Specific Responses as well as Improved Sea and Weather Forecasts Including Synoptic, High Precision and Realtime Satellite Data*
  Type: EU-project with funding.
  DWD contribution: *a) Supply of LM-data over the Baltic Sea for the development of a high-resolution sea wave model at GKSS (Geesthacht); b) Supply of sea-state information of the Mediterranean sea wave model (MSM) for verification against Altimeter data and for driving ship response models.*
  Information: www.tu-berlin.de/fb10/MAT/searoutes

Furthermore, a number of activities of COSMO members are related to the *Mesoscale Alpine Project* (MAP). For more information, see the MAP homepage at *www.map.ethz.ch.*

10.2 National Projects and Collaboration

This section lists LM-related projects and collaboration of COSMO members on a national level. At present, the list is by no means complete. Please inform the editors on such activities, especially those with national funding, in order to get a more complete list in the next COSMO newsletter.

- **DWD/University of Bonn**
  Special Investigations in Statistical Model Interpretation
  This is bilateral project which is partly funded by DWD.

- **MeteoSwiss/NCCR Climate**
  National Centre of Competence in Research - Climate.

Type: Nationally funded research project.
Information: www.meteoswiss.ch/nccr

- **MeteoSwiss/University of Berne**
  Extraction of snow-cover, lake-temperature, NDVI, LAI, land surface temperature and albedo from NOAA satellites, primarily for the data assimilation suite.
  Type: bilateral project, partially funded by MeteoSwiss

- **MeteoSwiss/EMPA**
  Determination of typical source regions of air pollutants for stations of the national air quality observing network.
  Type: BUWAL project with partial funding (EMPA only)
  Information: www.empa.ch > Organisation > Mobilität und Umwelt > Luftfremdstoffe / Umwelttechnik > Ausbreitungsmodellierung

- **MeteoSwiss/PMOD-WRC**
  Longwave radiation measurements compared to radiative transfer model and aLMo.
  Type: Swiss National Science Foundation Project "Greenhouse-effect in the Alps: by models and observations".
  Information: www.pmodwrc.ch/pmod.php?topic=asrb

- **MeteoSwiss/PartnerRe**
  High-resolution re-analysis of extreme weather events. Computation with LM [at the Swiss Center for Scientific Computing (CSCS)] of winter storms (1957-2002) over Europe based on initial and boundary fields from the ECMWF ERA-40 Project. Calculation of wind gusts with an alternative approach by Brasseur (2001) using the height of the balance between turbulent kinetic energy and the buoyancy force.

- **CLM**
  In autumn 2001, the German community on regional climate modelling decided to use the Lokal-Modell as a basis for a new regional climate model. The CLM (Climate Version of the LM) has been derived from the release 2.14 of LM. You find information on this modelling group and the related model developments at the CLM web-site *http://w3.gkss.de/CLM/index.html*.

- **ICON**
  The Max Planck Institute for Meteorology in Hamburg (MPI) and DWD have started a joint research project to develop ICON (ICOsahedral Nonhydrostatic), a unified global model to be used both for climate studies and operational short range weather forecasting. The model will employ finite volume numerical techniques to discretize the fully compressible nonhydrostatic equations on a geodesic, icosahedral grid. More information is available at the ICON web site *http://icon.enes.org*.

- **AFO2000**
  The German Atmospheric Research Programme 2000-2006 (AFO200) is funded by the Federal Ministry for Education and Research. It aims to improve the understanding of the atmospheric system including earth-surface interactions, chemistry, dynamics, radiation and their interactions, multiphase processes, and atmosphere-system analysis. DWD contributes with LM-based studies in various subprojects. More information is available at the web site *http://www.afo-2000.de*.

10.3 External Users of LM

The source code of the LM-package is available free of charge for scientific and educational purposes to third parties outside COSMO. Such external users, however, must register and sign a special agreement with a COSMO meteorological service. For questions about the request and the agreement, please contact M. Capaldo (massimo.capaldo@iol.it) or D. Frühwald (dieter.fruehwald@dwd.de) from the COSMO Steering Committee.

Meanwhile, a number of universities and research institutes have received the model software. Once a year, there is a *User Workshop on Scientific Applications of the LM* organized by J. Steppeler at DWD (contact: juergen.steppeler@dwd.de, see also Section 7.4). There is, however, not always a feedback on the activities or on results and problems. The following table lists the current registered users of the LM (outside the COSMO group).

Institution	**Country**	**Research Activities**
Academy of Science, Hydrometeorological Institute	Bulgaria	unknown
Academy of Science, Institute for Physics of the Atmosphere, Prague	Czech Republic	Clouds and precipitation at high resolution
Alfred Wegener Institut, Bremerhaven	Germany	Cloud physics
Frontier Research, Institute for Global Change Research	Japan	Tests on time-splitting methods
German Aerospace Centre, Institute of Atmospheric Physics, Oberpfaffenhofen	Germany	Turbulence studies, model intercomparison
GKSS Research Centre Geesthacht	Germany	Regional climate simulations,
Institute for Tropospheric Research (IFT), Leipzig	Germany	Z-coordinate model version, turbulence studies
Konrad-Zuse Institut, Berlin	Germany	Scientific visualization
Massachusetts Institute of Technology, Cambridge MA	USA	unknown
Meteorological Research Institute	Japan	Model intercomparison
Meteorological Research Institute	Korea	unknown
National Center for Atmospheric Research, Boulder CO	USA	unknown
National Institute of Meteorology and Hydrology	Romania	Test simulations
Norwegian Meteorological Institute (DNMI), Oslo	Norway	Model intercomparison
Potsdam Institute for Climate Impact Research (PIK), Potsdam	Germany	Regional climate studies, low Mach-number dynamics
Swiss Institute of Technology (ETH), Zürich	Switzerland	Regional climate studies High resolution experiments

Institution	Country	Research Activities
Turkish State Meteorological Service	Turkey	Coastal wind simulations
University of Berlin	Germany	unknown
University of Bern	Switzerland	Land use and regional climate
University of Bonn	Germany	Physical initialization, statistical postprocessing, regional evaporation and water resource management
University of Bremen	Germany	unknown
University of Cologne	Germany	unknown
University of Dresden	Germany	unknown
University of Frankfurt	Germany	Numerics and cloud physics
University of Hamburg	Germany	unknown
University of Hannover	Germany	Aircraft icing
University of Hohenheim	Germany	Assimilation of LIDAR data
University of Karlsruhe	Germany	Soil modelling, case studies
University of Leipzig	Germany	Cloud physics, hydrology
University of Ljubljana	Slovenia	Latent heat nudging
University of Munich	Germany	Model comparison, case studies
University of Trento	Italy	Numerics, shaved elements

References

Baldauf. M. and J.-P. Schulz, 2004: Prognostic precipitation in the Lokal-Modell (LM) of DWD. COSMO Newsletter No. 4.

Davies, H. C. and R. E. Turner, 1977: Updating prediction models by dynamical relaxation: An examination of the technique. *Quart. J. Roy. Meteor. Soc.*, 103, 225–245.

Doms, G., U. Schättler, 1999: The Nonhydrostatic Limited-Area Model LM (Lokal-Modell) of DWD. Part I: Scientific Documentation. Deutscher Wetterdienst (DWD), Offenbach. January 1999.

Doms, G., 2001: A scheme for monotonic numerical diffusion in the LM. *Cosmo Technical Report*, No.3 (available at www.cosmo-model.org).

Doms, G., 2002: The LM cloud ice scheme. *COSMO Newsletter*, No.2, 128–136 (available at www.cosmo-model.org).

Doms, G., Gassmann, A., Heis, E., Raschendorfer, M., Schraff, C. and R. Schrodin, 2002: Parameterization issues in the non-hydrostatic NWP-model LM. *ECMWF Seminar on Key Issues in the Parameterization of Subgrid Physical Processes*, 205-252.

Doms, G. and U. Schättler, 2002: A description of the nonhydrostatic regional model LM. Part I: Dynamics and numerics. Deutscher Wetterdienst (DWD), Offenbach. November 2002 (available at www.cosmo-model.org).

Dudhia, J., 1993: A nonhydrostatic version of the Penn State / NCAR mesoscale model: Validation tests and simulation of an Atlantic cyclone and cold front. *Mon. Wea. Rev.*, 121, 1493–1513.

Förstner, J. and G. Doms, 2004: Runge-Kutta time integration and high-order spatial discretization of advection: a new dynamical core for LM. COSMO Newsletter No. 4.

Gassmann, A., 2001: Filtering of LM-orography. *COSMO Newsletter*, No.1, 71–78 (available at www.cosmo-model.org).

Gassmann, A., 2002: 3D-transport of precipitation. *COSMO Newsletter*, No.2, 113–117 (available at www.cosmo-model.org).

Gassmann, A., 2002: A two timelevel integration scheme for the LM. *COSMO Newsletter*, No.2, 97–100 (available at www.cosmo-model.org).

Hess, R., 2001: Assimilation of screen-level observations by variational soil moisture analysis. *Meteor. Atmos. Phys.*, 77, 155–166.

Jacobsen, I. and E. Heise, 1982: A new economic method for the computation of the surface temperature in numerical models. *Contr. Atmos. Phys.*, **55**, 128–141.

Kessler, E., 1969: On the distribution and continuity of water substance in the atmospheric circulations. *Meteor. Monogr.*, 10, No. 32, Amer. Met. Soc., 84pp.

Klemp, J. B. and R. Wilhelmson, 1978: The simulation of three-dimensional convective storm dynamics. *J. Atmos. Sci.*, 35, 1070–1096.

Lorenc, A. C., R. S. Bell and B. Macpherson, 1991: The Meteorological Office analysis correction data assimilation scheme. *Quart. J. Roy. Meteor. Soc.*, 117, 59–89.

Louis, J.-F., 1979: A parametric model of vertical eddy fluxes in the atmosphere. *Bound. Layer Meteor.*, **17**, 187–202.

Lynch, P., D. Girard and V. Ivanovici, 1997: Improving the efficiency of a digital filtering scheme. *Mon. Wea. Rev.*, **125**, 1976–1982.

Majewski, D., 1998: The new global icosahedral-hexagonal grid point model GME of the Deutscher Wetterdienst. *ECMWF Seminar on Numerical Methods in Atmospheric Models.*

Majewski, D., D. Liermann, P. Prohl, B. Ritter, M. Buchhold, T. Hanisch, G. Paul, and W. Wergen, 2002: The operational global icosahedral-hexagonal gridpoint model GME: Description and high-resolution tests. *Mon. Wea. Rev.*, 130, 319–338.

Mellor, G. L. and T. Yamada, 1974: A hierarchy of turbulence closure models for planetary boundary layers. *J. Atmos. Sci.*, 31, 1791–1806.

Mellor, G. L. and T. Yamada, 1982: Development of a turbulence closure model for geophysical flow problems. *Rev. Geophys. and Space Phys.*, 20, 831–857.

Montani, A., M. Capaldo, D. Cesari, C. Marsigli, U. Modigliani, F. Nerozzi, T. Paccagnella, P. Patruno and S. Tibaldi, 2003: *ECMWF Newsletter Summer 2003*, 98, 2–7.

Raymond, W. H., 1988: High-order low-pass implicit tangent filters for use in finite area calculations. *Mon. Wea. Rev.*, **116**, 2132–2141.

Ritter, B. and J. F. Geleyn, 1992: A comprehensive radiation scheme for numerical weather prediction models with potential applications in climate simulations. *Mon. Wea. Rev.*, **120**, 303–325.

Schär, C., D. Leuenberger, O. Fuhrer, D. Lüthi and C. Girard, 2002: A new terrain-following vertical coordinate formulation for atmospheric prediction models. *Mon. Wea. Rev.*, 130, 2459–2480.

Schraff, C., 1996: Data assimilation and mesoscale weather prediction: A study with a forecast model for the Alpine region. Publication No. 56, Swiss Meteorological Institute.

Schraff, C., 1997: Mesoscale data assimilation and prediction of low stratus in the Alpine region. *Meteorol. Atmos. Phys.*, **64**, 21–50.

Schraff, C. and R. Hess, 2003: A description of the nonhydrostatic regional model LM. Part III: Data assimilation. Deutscher Wetterdienst (DWD), Offenbach. June 2003 (available at www.cosmo-model.org).

Schrodin, R. and E. Heise, 2001 : The multi-layer version of the DWD soil model TERRA_LM. *Cosmo Technical Report*, No.2 (available at www.cosmo-model.org).

Skamarock, W. C. and J. B. Klemp, 1992: The stability of time-split numerical methods for the hydrostatic and the nonhydrostatic elastic equations. *Mon. Wea. Rev.*, **120**, 2109–2127.

Sommeria, G. and J. W. Deardorff, 1977: Subgrid-scale condensation in models of non-precipitating clouds. *J. Atmos. Sci.*, 34, 344–355.

Stauffer, D. R. and N. L. Seaman, 1990: Use of four-dimensional data assimilation in a limited-area mesoscale model. Part I: Experiments with synoptic-scale data. *Mon. Wea. Rev.*, 118, 1250–1277.

Stauffer, D. R. and N. L. Seaman, 1994: Multiscale four-dimensional data assimilation. *J. Appl. Meteor.*, 33, 416–434.

Steppeler, J., G. Doms, U. Schättler, H.-W. Bitzer, A. Gassmann, U. Damrath and G. Gre-

goric, 2003: Meso-gamma scale forecasts using the non-hydrostatic model LM. *Meteorol. Atmos. Phys.*, 82, 75-96.

Thomas, S., C. Girard, G. Doms and U. Schättler, 2000: Semi-implicit scheme for the DWD Lokal-Modell. *Meteorol. Atmos. Phys.*, **75**, 105–125.

Tiedtke, M., 1989: A comprehensive mass flux scheme for cumulus parameterization in large-scale models. *Mon. Wea. Rev.*,**117**, 1779–1799.

Wicker, L. and W. Skamarock, 1998: A time-splitting scheme for the elastic equations incorporating second-order Runge-Kutta time differencing. *Mon. Wea. Rev.*, **126**, 1992–1999.

Wicker, L. and W. Skamarock, 2002: Time-splitting methods for elasic models using forward time schemes. *Mon. Wea. Rev.*, **130**, 2088–2097.

Appendix A: The GRIB Binary Data Format used for LM I/O

All input and output arrays of the LM and of the preprocessor programs providing interpolated initial conditions and the boundary values are stored in a compressed binary data format called GRIB-code. GRIB means "gridded binary" and is designed for the international exchange of processed data in the form of grid-point values expressed in binary form.

The GRIB-code is part of the FM-system of binary codes of the World Meteorological Organization (WMO). Currently, we use Edition 1 of the GRIB-code with number FM 92-VIII. For coding details, see the *Manual on Codes, International Codes, Volume 1.2* of WMO (WMO Publication No. 306, 1995). In this section, we describe only the basic features of the GRIB code which are relevant for the I/O of the LM-system.

A.1 Code Form

Each GRIB-coded record (analysis or forecast field) consists of a continuous bit-stream which is made up of a sequence of octets (1 octet = 8 bits). The representation of data by means of series of bits is independent of any particular machine representation. The octets of a GRIB messsage are grouped in sections (see Table 1, where the length of the record and the length of the sections are expressed in octets. Section 0 has a fixed length of 4 octets and section 5 has a fixed length of 4 octets. Sections 1, 2, 3 and 4 have a variable length which is included in the first three octets of each section.

Section number	**Name**	**Contents**
0	Indicator Section	"GRIB"; length of record; GRIB edition number
1	Product Definition Section	Length of section; identification of the coded analysis/forecast field
2	Grid Description Section (optional)	Length of section; grid geometry, as necessary
3	Bit-map Section (optional)	Length of section; the bit per grid-point, placed in suitable sequence
4	Binary Data Section	Length of section; data values
5	End Section	7777

Table 1: *Form of GRIB-code*

Octets are numbered 1, 2, 3, etc., starting at the beginning of each section. Bit positions within octets are referred to as bit 1 to 8, where bit 1 is the most significant bit and bit 8 is the least significant bit. Thus, an octet with only bit 8 set to 1 would have the integer value 1.

A.2 Indicator and End Section

The Indicator Section has a fixed length of 8 octets. The first four octets shall always be character coded as "GRIB" (according to the CCITT International Alphabet No.5). The remainder of the section shall contain the length of the entire GRIB-record (including the Indicator Section) expressed in binary form over the left-most 3 octets (i.e. 24 bits in octet 5-7), followed by the GRIB edition number (currently 1), in binary, in the remaining octet 8.

The End Section has a fixed length of 4 octets. These octets are character coded as '7777'

according to the International Alphabet No.5.

Thus, the beginning and the end of a GRIB-record can be identified by the character coded words "GRIB" and "7777". All other octets included in the code represent data in binary form. Each input or output array defined on the rotated lat/lon grid of the LM (e.g the surface pressure or the temperature at a specified model level) is coded as a GRIB-record. Various such records can be combined in a single GRIB-file.

A.3 Product Definition Section

The Product Definition Section (PDS) contains the necessary information to identify the binary coded field contained in the GRIB-record. The most important octet in this section is the indicator of the meteorological parameter. The indicator relates a specific meteorological element to an integer number. This indicator number is also referred to as GRIB-number or element-number and is defined in a separate code table. More than one indicator code tables may be used in GRIB-code. Thus, one can have the same element-number but different code table numbers for various fields. The element-numbers and code tables used by LM are described below.

The program `grbin1` of the supplementary GRIB-library `griblib` of the LM-system can be used to decode GRIB binary code. Besides the decoded data set, this program does also retrieve the contents of the octets of the PDS in an integer array `ipds`. To illustrate the structure of the PDS, Table 2 shows the contents of the product definition section of a binary coded LM output array, the total cloud cover (CLCT). The GRIB-record for this field is valid for 28.10.1998 00 UTC + 11 h and was created at 28.10.1998 7.04 UTC by an LM forecast.

Octet 4 (ipds(2)) assigns a table number to the parameter indicator number given in octet 9. Currently, we use 4 additional code tables besides the WMO-table (see Table 3), where table 205 is used to code synthetic satellite products (from LM version 3.7 and higher). A full list of variables defined by these tables is available from DWD.

Octet 6 (ipds(4)) indicates the process identification number which is allocated by the originating centre. Currently, we use only two different process numbers for forecasts or analyses (see Table 4).

The level or layer for which the data are included in the GRIB-record is coded in octets 10 - 12 (ipds(8) - ipds(10)), where octet 10 indicates the type of level and octets 11 and 12 indicate the value of this level. Table 5 shows the code figures used for LM. For reserved values, or if not defined, octets 11 and 12 shall contain zero.

All 3-D variables of LM except the vertical velocity are defined on terrain-following main levels. In GRIB, these main levels are coded as level-type 110: hybrid layers between two adjacent hybrid levels - which are the LM half levels, i.e the layer interfaces. In this case, octet 11 contains the level index of the upper half level and octet 12 contains the level index of the lower half level. The vertical velocity and the height of the half levels are coded as level type 109: hybrid levels, i.e. the LM half levels. In this case, octet 11 contains zero and octet 12 contains the level index of the model half level. Pressure levels (ipds(8) = 100) and height levels (ipds(8) = 105) are used when the interpolation from model to specified p- or z-surfaces is switched on for model output. For synthetic satellite images (table number 205 and level-type 222), the octets 11 - 12 are used to code the channel of a satellite: ipds(9) = 0 and ipds(10) contains the channel number.

array ipds(i)	Octet number	Contents of PDS Value	Remarks
1	1-3	54	Length of the PDS (in octets)
2	4	2	Version number of the GRIB indicator table (see Table 3)
3	5	78	Identification of originating/generating centre (DWD has WMO number 78)
4	6	132	Generating process identification number (allocated by originating centre, see Table 4)
5	7	255	Number of grid used - from catalogue defined by the originating centre. Octet 7 set to 255 indicates a non-cataloged grid, in which case the grid is defined in the grid description section.
6	8	128	Block-flag; the value 128 indicates that the grid description section is included.
7	9	71	Indicator of parameter (element number) from GRIB-table in ipds(2); see Section 3.7
8	10	1	Indicator of type of level, see Table 5
9-10	11-12	0	Value of level (height, pressure, etc.) for which the data are included (see Table 5)
11	13	98	Year (start time of forecast; analysis time)
12	14	10	Month (start time of forecast; analysis time)
13	15	28	Day (start time of forecast; analysis time)
14	16	0	Hour (start time of forecast; analysis time)
15	17	0	Minute (start time of forecast; analysis time)
16	18	1	Indicator of unit of time range (see Table 6)
17	19	11	P1 - period of time (number of time units);
			time units given by octet 18 (ipds(16))
18	20	0	P2 - period of time (number of time units);
			time units given by octet 18 (ipds(16))
19	21	0	time range indicator (see Table 7)
20	22-23	0	Number of forecasts included in average, when octet 21 (ipds(19)) indicates an average or accumulation of forecasts (or analyses); otherwise set to zero.
21	24	0	Number of forecasts missing from averages or accumulations.
22	25	20	Century of reference time of data given by octets 13- 17
23	26	255	Sub-centre identification, national use
24	27-28	0	Units decimal scale factor (D)
25-36	29-40	0	Reserved: need not to be present
37	41	254	Octets 41-54 are reserved for the originating centre. The integer value 254 indicates that additional data follow. We use this part as follows:
38	42	0	not used
39	43-45	0	not used
40	46	0	not used
41	47	0	Additional indicator for a GRIB element number
42	48	98	Year of production of GRIB-record
43	49	98	Month of production of GRIB-record
44	50	11	Day of production of GRIB-record
45	51	2	Hour of production of GRIB-record
46	52	0	Minute of production of GRIB-record
47	53-54	1	Version number, currently 1 for LM

Table 2: ***Contents of the Product Definition Section***

Version number of GRIB-table; ipds(2)	Comment
2	WMO-table of indicator parameters
201	national table of DWD for internal use
202	national table of DWD for internal use
203	national table of DWD for internal use
205	national table of DWD for internal use

Table 3: *GRIB-tables for parameter (element) indicator number*

process id-number; ipds(4)	Comment
131	LM-analyses from data assimilation cycle
132	LM-forecasts and initialized analyses

Table 4: *Process identification numbers*

level type ipds(8)	Meaning	ipds(9)	ipds(10)
1	Ground or water surface	0	0
2	Cloud base level	0	0
3	Level of cloud tops	0	0
4	Level of $0°C$ isotherm	0	0
8	Top of atmosphere	0	0
100	Pressure (isobaric) level	0	Pressure in hPa
102	Mean sea level	0	0
103	Specified height above mean sea level	0	Height in m
105	Specified height level above ground	0	Height in m
109	Hybrid level (half levels)	0	Level number (k)
110	Hybrid layer (main level) between two hybrid levels	Level number of top (k)	Level number of bottom (k+1)
111	Depth below land surface	0	Depth in cm
112	Layer between two depths below land surface	Depth of upper surface in cm	Depth of lower surface in cm
222	Satellite images	0	Satellite Channel

Table 5: *Types of fixed levels or layers used by LM*

Octets 13-17 contain the reference time of the data: the start of a forecast, the time for which an analysis is valid or the start of an averaging or accumulation period. The year of the century is coded in octet 13 and the century (100 years) in octet 25. For a reference time within the year 2000, octet 13 will contain the integer value 100 and octet 25 will contain the integer value 20.

The time or time interval for which the data are valid with respect to the reference time is coded in octets 18-21 (ipds(16)-ipds(19)). Octets 19 and 20 contain two periods of time, P1 and P2. The units of the values of P1 and P2 are defined in octet 18. Currently, we use hours as the time unit, but other values may be more appropriate for special applications of the model as the maximum integer number in an octet is 256. Thus, for long-term climate runs or short-term cloud simulations, other time units must be chosen. The WMO code-table for the unit of time in P1 and P2 is given in Table 6.

ipds(16)	Meaning	ipds(16)	Meaning	ipds(16)	Meaning
0	Minute	5	Decade	11	6 hours
1	Hour	6	Normal	12	12 hours
2	Day	7	Century	13-253	Reserved
3	Month	8-9	Reserved	254	Second
4	Year	10	3 hours		

Table 6: *Code table for unit of time*

The meaning of the time period P1 in octet 19 (ipds(17)) and of the time period P2 in octet 20 (ipds(18)) - given in the units coded in octet 18 - depends on the time-range indicator, which is contained in octet 21 (ipds(19)). The WMO code-table allows for a large number of indicators including averages and accumulation over a number of forecasts and analyses. For the LM-system, we use only a few standard indicators as shown in Table 7. In order to distinguish output from the nudging assimilation cycle from other external analysis products, as e.g. the sea surface temperature or snow depth, all nudging products will have a time-range indicator 13.

ipds(19)	Meaning
0	Forecast product valid for reference time + P1 (if P1 > 0) or uninitialized analysis product valid for reference time (P1 = 0)
1	initialized analysis product valid for reference time (P1 = 0)
2	Product with a valid time ranging between reference time + P1 and reference time + P2
3	Average from reference time + P1 to reference time + P2
4	Accumulation from reference time + P1 to reference time + P2; product valid for reference time + P2
13	Nudging analysis product, valid for reference time (P1 = 0) Note: All output from a nudging assimilation cycle will have time-range indicator 13, also fields which usually have ipds(19) = 2, 3 or 4.

Table 7: *Time range indicators used by LM*

A.4. Grid Description Section

Section 2 of a GRIB-record, the grid description section GDS, contains all information about the geometry of the grid on which the data are defined. For all input and output files of the LM, this section is coded completely for every field contained in the file. The program `grbin1` of the supplementary GRIB-library `griblib` retrieves the contents of the GDS in an integer array `igds`.

The contents of the grid description section of an LM GRIB-record is illustrated in Table 8 for the model domain used operationally at DWD. The octets corresponding to the integer array `igds` are numbered relative to this section.

array igds(i)	Octet number	Contents of GDS Value	Meaning
1	1-3	202	Length of GDS (in octets) including the vertical coordinate parameters. (here for $ke = 35$ layers, i.e. $ke + 1 = 36$ half levels)
2	4	40	NV: Number of vertical coordinate parameters (four base state parameters + $(ke + 1)$ values of the vertical coordinates of the half levels)
3	5	43	PV: Location (octet number) of the list of vertical coordinate parameters
4	6	10	Data representation type according to WMO code-table 6; '10' assigns a rotated latitude/longitude grid
5	7-8	325	Number of gridpoints in 'zonal' direction
6	9-10	325	Number of gridpoints in 'meridional' direction
7	11-13	-17000	Rotated latitude of the first gridpoint in millidegrees
8	14-16	-12500	Rotated longitude of the first gridpoint in millidegrees
9	17	0	Resolution flag according to WMO code-table 7; '0' means that the grid spacing is not given
10	18-20	3250	Rotated latitude of the last gridpoint in millidegrees
11	21-23	7750	Rotated longitude of the last gridpoint in millidegrees
12	24-25	0	Longitudinal direction increment (grid spacing in λ-direction, not given)
13	26-27	0	Meridional direction increment (grid spacing in ϕ-direction, not given)
14	28	64	Scanning mode flag according to WMO code-table 8 '64' means that points scan in +i and +j direction and adjacent points in i-direction are consecutive
15-19	29-32	0	Reserved (set to zero)
20	33-35	-32500	Geographical latitude of rotated southern pole in millidegrees
21	36-38	10000	Geographical longitude of rotated southern pole in millidegrees
22	39-42	0	Angle of rotation
26-65	43-202	.....	List of vertical coordinate parameters, each packed on 4 octets (length = 4 x NV octets). first the three parameters defining the base state: `igds(26)=p0sl`, `igds(27)=t0sl`, `igds(28)=dt0lp`; then the parameter `igds(29)=vcflat` of the hybrid coordinate system; and finally the $ke + 1$ values of the vertical coordinate $\eta(k)$ of the model half levels for $k = 1, \ldots, ke + 1$ in `igds(30)`,..., `igds(65)`.

Table 8: ***Contents of the Grid Description Section***

Appendix B: Available LM Output Fields

This appendix summarizes the GRIB parameter indicators (element numbers), the table numbers and the dimensions of the direct model output variables. Any changes will be updated in the next COSMO Newsletter.

B.1 General Remarks

For direct model output, we distinguish between so-called *multi-level fields* which are defined on model layers or levels or on fixed pressure or height levels, and *single level fields* which are defined at the surface or on another fixed level.

The fields contained in the model output GRIB-files can be freely chosen by the user: The names of the model variables to be written out have to be specified on the following NAMELIST input character arrays:

- `yvarml` for output on the model grid and for single level data,
- `yvarpl` for output on constant pressure levels
- `yvarzl` for output on constant height levels.

If latter two variables are empty, the model-internal interpolation to pressure and height levels is omitted. If they are set, the values of the corresponding pressure and height levels can be specified by the NAMELIST input arrays `plev` and `zlev`. By default, some multi-level variable are interpolated to 10 pressure levels and 4 height levels:

- p-levles: 1000, 950, 850, 700, 600, 500, 400, 300, 250, 200 hPa.
- z-levles: 1000, 2000, 3000, 5000 m (above sea level).

B.2 Element and Table Numbers used by LM

The name of an input/output field is specified as a CHARACTER variable (in capital letters, names must be 8 characters long, filled with blanks) in NAMELIST input. The model then relates this name internally to a corresponding GRIB element number and table number as well as the corresponding global model variable (which has usually the same name but with small letters). However, some names of output variables are not related to a globally defined model variable. In these cases, the output array is calculated locally only at the output time step.

Table 1 shows the GRIB-element numbers (ee) and table numbers (tab) for the multi-level fields available for LM output files. The level-types (lty) and the corresponding values in octet 11 (lvt) and octet 12 (lv) as well as the physical units (unit) are also included. For variables with level-types 109 and 110, the integer level numbers denoted by k (and k+1) are stored in octets 11 and 12. For pressure levels the constant pressure value in hPa is stored in octet 12 (denoted by pres), and for height levels the constant height level in m above sea level (denoted by z) is stored in octet 12.

Some of the multi-level fields in Table 1 can only be put on the output list if certain parameterization schemes are switched on. These variables are denoted as optional fields. All variables on the list for constant pressure and constant height levels are in the default output list.

Table 1: ***Multi-level fields of LM GRIB-output***

Name	Meteorological Element	ee	tab	lty	lvt	lv	unit
Multi-level fields on model layers/levels k							
U	Zonal wind component (rotated grid)	33	2	110	k	k+1	m/s
V	Meridional wind component (rotated grid)	34	2	110	k	k+1	m/s
W	Vertical wind component	40	2	109	-	k	m/s
P	Pressure	1	2	110	k	k+1	Pa
PP	Pressure perturbation	139	201	110	k	k+1	Pa
T	Temperature	11	2	110	k	k+1	K
QV	Specific humidity	51	2	110	k	k+1	kg/kg
QC	Specific cloud water content	31	201	110	k	k+1	kg/kg
CLC	Fractional cloud cover	29	201	110	k	k+1	%
HHL	Height of half levels (i.e. layer interfaces) constant with time, written only at t=0	8	2	109	-	k	m
Optional multi-level fields on model layers/levels k							
QI	Specific cloud ice content	33	201	110	k	k+1	kg/kg
QR	Specific water content of rain	35	201	110	k	k+1	kg/kg
QS	Specific water content of snow	36	201	110	k	k+1	kg/kg
QRS	Specific content of rain and snow	39	201	110	k	k+1	kg/kg
TKE	Specific turbulent kinetic energy	152	201	109	-	k	m^2/s^2
TKVM	Turbulent diffusion coefficient for vertical momentum transport	153	201	109	-	k	m^2/s
TKVH	Turbulent diffusion coefficient for vertical heat transport	154	201	109	-	k	m^2/s
Optional multi-level fields of soil layers m between depth z_m and z_{m+1}							
T_SO	Temperature of soil layer m	197	201	112	z_m	z_{m+1}	K
W_SO	Water content of soil layer m	198	201	112	z_m	z_{m+1}	kg/m^2
W_ICE	Ice content of soil layer m	199	201	112	z_m	z_{m+1}	kg/m^2
Multi-level fields interpolated on pressure levels pres (in hPa)							
U	Zonal wind component (rotated grid)	33	2	100	-	pres	m/s
V	Meridional wind component (rotated grid)	34	2	100	-	pres	m/s
OMEGA	Vertical motion	39	2	100	-	pres	Pa/s
T	Temperature	11	2	100	-	pres	K
RELHUM	Relative humidity	52	2	100	-	pres	%
FI	Geopotential	6	2	100	-	pres	m^2/s^2
Multi-level fields interpolated on height levels z (in m)							
U	Zonal wind component (rotated grid)	33	2	103	-	z	m/s
V	Meridional wind component (rotated grid)	34	2	103	-	z	m/s
W	Vertical wind component	40	2	103	-	z	m/s
T	Temperature	11	2	103	-	z	K
P	Pressure	1	2	103	-	z	Pa
RELHUM	Relative humidity	52	2	103	-	z	%

Table 2 shows the GRIB-element numbers (ee) and table numbers (tab) for the single-level forecast fields available for LM output files. As in the previous table, the level-types (lty) and the corresponding values in octet 11 (lvt) and octet 12 (lv) as well as the physical units (unit) of the fields are also included. See Table 5 in Appendix A for the units of the numbers stored in lvt and lv for the corresponding level-type.

Table 2: ***Single-level fields of LM GRIB-output***

Name	Meteorological Element	ee	tab	lty	lvt	lv	unit
Single-level fields: valid at output time							
PS	Surface pressure	1	2	1	-	-	Pa
PMSL	Mean sea level pressure	2	2	102	-	-	Pa
U_10M	Zonal 10m-wind	33	2	105	-	10	m/s
V_10M	Meridional 10m-wind	34	2	105	-	10	m/s
T_2M	2m-temperature	11	2	105	-	2	K
TD_2M	2m-dewpoint temperature	17	2	105	-	2	K
T_G	Temperature at the interface surface-atmosphere	11	2	1	-	-	K
T_SNOW	Temperature of snow surface (surface temperature if no snow)	203	201	1	-	-	K
T_S	Temperature below snow (surface temperature if no snow	85	2	111	-	0	K
T_M	Temperature at the bottom of first soil layer	85	2	111	-	9	K
QV_S	Specific humidity at the surface	51	2	1	-	-	kg/kg
W_SNOW	Water content of snow	65	2	1	-	-	kg/m^2
W_I	Water content of interception store	200	201	1	-	-	kg/m^2
W_G1	Water content of upper soil layer	86	2	112	0	10	kg/m^2
W_G2	Water content of middle soil layer	86	2	112	10	100	kg/m^2
TCM	Turbulent transfer coefficient for momentum at the surface	170	201	1	-	-	-
TCH	Turbulent transfer coefficient for heat and moisture at the surface	171	201	1	-	-	-
Z0	Roughness length (land and water)	83	2	1	-	-	m
ALB_RAD	Surface albedo (shortwave radiation)	84	2	1	-	-	%
CLCT	Total cloud cover	71	2	1	-	-	%
CLCH	High cloud cover (0 - 400 hPa)	75	2	1	-	-	%
CLCM	Middle cloud cover (400-800 hPa)	74	2	1	-	-	%
CLCL	Low cloud cover (800hPa-surface)	73	2	1	-	-	%
CLCT_MOD	Total cloud cover (modified for graphics)	204	203	1	-	-	-
CLDEPTH	Normalized cloud depth (modified for graphics)	203	203	1	-	-	-
HTOP_DC	Top height of dry convection (height above mean sea level)	82	201	1	-	-	m
HZEROCL	Height of $0°C$ isotherm (above mean sea level)	84	201	1	-	-	m
MFLX_CON	Massflux at convective cloud base	240	201	1	-	-	$kg/(m^2s)$
CAPE_CON	Convective available potential energy	241	201	1	-	-	J/kg
QCVG_CON	Moisture convergence below convective cloud base	242	201	1	-	-	1/s
TKE_CON	Convective turbulent kinetic energy	243	201	1	-	-	J/kg
TWATER	Total column water	41	201	1	-	-	kg/m^2
TQV	Total column water vapour	54	2	1	-	-	kg/m^2
TQC	Total column cloud water	76	2	1	-	-	kg/m^2
TQI	Total column cloud ice	58	2	1	-	-	kg/m^2
SNOWLMT	Height of Snow-fall limit	85	201	1	-	-	m

Name	Meteorological Element	ee	tab	lty	lvt	lv	unit
PRR_GSP	Grid-Scale surface rain flux	100	201	1	-	-	kg/(m^{2}s)
PRS_GSP	Grid-Scale surface snow flux	101	201	1	-	-	kg/(m^{2}s)
PRS_CON	Convective surface rain flux	111	201	1	-	-	kg/(m^{2}s)
PRS_CON	Convective surface snow flux	112	201	1	-	-	kg/(m^{2}s)
FRESHSNW	Indicator for age of snow	129	201	1	-	-	-
ZTD	Total zenith delay	121	202	1	-	-	-
ZWD	Wet zenit delay	122	202	1	-	-	-
ZHD	Hydrostatic zenith delay	123	202	1	-	-	-
Single-level fields: Accumulated since start of the forecast							
RAIN_GSP	Amount of grid-scale rain	102	201	1	-	-	kg/m^2
SNOW_GSP	Amount of grid-scale snow	79	2	1	-	-	kg/m^2
RAIN_CON	Amount of convective rain	113	201	1	-	-	kg/m^2
SNOW_CON	Amount of convective snow	78	2	1	-	-	kg/m^2
TOT_PREC	Total precipitation amount	61	2	1	-	-	kg/m^2
RUNOFF_S	Surface water run-off	90	2	112	0	10	kg/m^2
RUNOFF_G	Ground water run-off	90	2	112	10	100	kg/m^2
TDIV_HUM	Total column divergence of specific humidity	42	201	1	-	-	kg/m^2
AEVAP_S	Accumulated flux of surface moisture	57	2	1	-	-	kg/m^2
Single-level fields: Averaged over the forecast period							
AUMFL_S	Surface u-momentum flux	124	2	1	-	-	N/m^2
AVMFL_S	Surface v-momentum flux	125	2	1	-	-	N/m^2
ASHFL_S	Surface sensible heat flux	122	2	1	-	-	W/m^2
ALHFL_S	Surface latent heat flux	121	2	1	-	-	W/m^2
ASOB_S	Solar radiation budget at the earth surface	111	2	1	-	-	W/m^2
ASOB_T	Solar radiation budget at the top of the atmosphere	113	2	8	-	-	W/m^2
ATHB_S	Thermal radiation budget at the earth surface	112	2	1	-	-	W/m^2
ATHB_T	Thermal radiation budget at the top of the atmosphere	114	2	8	-	-	W/m^2
APAB_S	Budget of photosynthetic active radiation at the earth surface	5	201	1	-	-	W/m^2
Single-level fields: Extreme values over certain time intervals							
TMIN_2M	Minimum of 2m-temperature	16	2	105	-	2	K
TMAX_2M	Maximum of 2m-temperature	15	2	105	-	2	K
VMAX_10M	Maximum of 10m-wind speed	187	201	105	-	10	m/s
HTOP_CON	Top height of convective clouds (above mean sea level)	69	201	3	-	-	m
HBAS_CON	Base height of convective clouds (above mean sea level)	68	201	2	-	-	m
TOP_CON	Main-level index of convective cloud top	73	201	1	-	-	-
BAS_CON	Half-level index of convective cloud base	72	201	1	-	-	-
Single-level fields: Constant and climatological fields							
FIS	Geopotential of earth surface	6	2	1	-	-	m^2/s^2

Name	Meteorological Element	ee	tab	lty	lvt	lv	unit
HSURF	Geometrical height of surface	8	2	1	-	-	m
FR_LAND	Land fraction of a grid area	81	2	1	-	-	-
SOILTYP	Soil texture for land fraction (key number 1-8, over water =9)	57	202	1	-	-	-
RLAT	Geographical latitude	114	202	1	-	-	° N
RLON	Geographical longitude	115	202	1	-	-	° E
PLCOV	Fractional plant cover	87	2	1	-	-	-
LAI	Leaf area index of vegetation	61	2	1	-	-	-
ROOTDP	Root depth of vegetation	62	202	1	-	-	m
FC	Coriolis parameter	113	202	1	-	-	s^{-1}
T_CL	Temperature of the lowest soil layer (climatological value)	85	2	111	-	36	K
W_CL	Water content of the lowest soil layer (climatological value)	86	2	112	100	190	kg/m^2
VIO3	Vertically integrated ozone	65	202	1	-	-	Pa O3
HMO3	Height of ozone maximum	64	202	1	-	-	Pa
Single-level fields: Synthetic satellite products							
SYNME5	METEOSAT-5, MVIRI instrument	1	205	222	0	nc	-
SYNME6	METEOSAT-6, MVIRI instrument	2	205	222	0	nc	-
SYNME7	METEOSAT-7, MVIRI instrument	3	205	222	0	nc	-
SYNMSG	MSG, SEVIRI instrument	4	205	222	0	nc	-

With respect to synthetic satellite images, only the element numbers 3 and 4, i.e. the MVIRI instrument on METEOSAT-7 and the SEVIRI on MSG, respectively, are supported by LM at present. To each channel number 'nc' coded in octet 12 (ipds(10) or 'lv' in the table above) corresponds a physical channel with a specific wavelength, as shown in Table 3.

ee	Satellite/Instrument	lv	channel	wavelength (μm)
3	METEOSAT-7 / MVIRI	1	1	WV 6.4
3	METEOSAT-7 / MVIRI	2	2	IR 11.5
4	MSG / SEVIRI	1	4	IR 3.9
4	MSG / SEVIRI	2	5	WV 6.2
4	MSG / SEVIRI	3	6	WV 7.3
4	MSG / SEVIRI	4	7	IR 8.7
4	MSG / SEVIRI	5	8	IR 9.7
4	MSG / SEVIRI	6	9	IR 10.8
4	MSG / SEVIRI	7	10	IR 12.1
4	MSG / SEVIRI	8	11	IR 13.4

Table 3: ***Coding of channels for synthetic satellite products***

ipds(41)	Product	unit
1	Cloudy brightness temperature	K
2	Clear-sky brightness temperature	K
3	Cloudy radiance	$mW/(m^2$ sr cm)
4	Clear-sky radiance	mW/m^2 sr cm)

Table 4: ***Specific synthetic satellite products***

For each channel on a specified satellite instrument, four different fields are calculated. These products are distinguished by a value for the additional element number (ipds(41), octet 47) in the product definition section, as indicated in Table 4.

All variables required on the input and boundary data files use also the corresponding GRIB table and element numbers from the above tables. The preprocessor programs to interpolate initial and/or boundary conditions to the LM-grid require the GRIB-files containing the external parameter data sets. The table and element numbers of the external parameter fields are shown in Table 5.

Table 5: ***Single-level fields in the LM external parameter files***

Name	**Meteorological Element**	**ee**	**tab**	**lty**	**lvt**	**lv**	**unit**
FIS	Geopotential of earth surface	6	2	1	-	-	m^2/s^2
HSURF	Geometrical height of surface	8	2	1	-	-	m
FR_LAND	Land fraction of a grid area	81	2	1	-	-	-
Z0	Roughness length (land and water)	83	2	1	-	-	m
SOILTYP	Soil texture for land fraction (key number 1-8, over water =9)	57	202	1	-	-	-
PHI	Geographical latitude	114	202	1	-	-	° N
RLA	Geographical longitude	115	202	1	-	-	° E
PLCOV_MX	Plant cover, vegetation period	67	202	1	-	-	%
PLCOV_MN	Plant cover, rest period	68	202	1	-	-	%
LAI_MX	Leaf area index, vegetation period	69	202	1	-	-	-
LAI_MN	Leaf area index, rest period	70	202	1	-	-	-
ROOTDP	Root depth of vegetation	62	202	1	-	-	m

Appendix C: List of COSMO Newsletters and Technical Reports

All Newsletters and Technical Reports are available for download from the COSMO Website: www.cosmo-model.org (or the mirror site cosmo-model.cscs.ch).

COSMO Newsletters

Newsletter No.1, February 2001.

Newsletter No.2, February 2002.

Newsletter No.3, February 2003.

Newsletter No.4, February 2004.

COSMO Technical Reports

No. 1, Dmitrii Mironov and Matthias Raschendorfer (2001):
Evaluation of Empirical Parameters of the New LM Surface-Layer Parameterization Scheme. Results from Numerical Experiments Including the Soil Moisture Analysis.

No. 2, Reinhold Schrodin and Erdmann Heise (2001):
The Multi-Layer Version of the DWD Soil Model TERRA_LM.

No. 3, Günther Doms (2001):
A Scheme for Monotonic Numerical Diffusion in the LM.

No. 4, Hans-Joachim Herzog, Ursula Schubert, Gerd Vogel, Adelheid Fiedler and Roswitha Kirchner (2002):
LLM - the High-Resolving Nonhydrostatic Simulation Model in the DWD - Project LITFASS. Part I: Modelling Technique and Simulation Method.

No. 5, Jean-Marie Bettems (2002):
EUCOS Impact Study Using the Limited-Area Non-Hydrostatic NWP Model in Operational Use at MeteoSwiss.